GEMS & GEMOLOGY

SPRING 2022
VOLUME LVIII

THE QUARTERLY JOURNAL OF THE GEMOLOGICAL INSTITUTE OF AMERICA

Yellow Topaz from Saxony, Germany

History of Emerald Mining at Habachtal, Part II

New Regular Feature: Diamond Reflections

2022 Tucson Report

GEMS & GEMOLOGY®
Spring 2022
VOLUME 58, No. 1

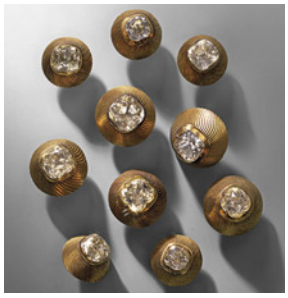
p. 3

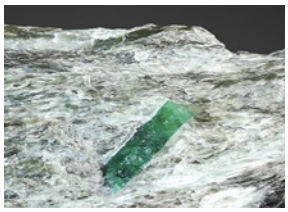
p. 40

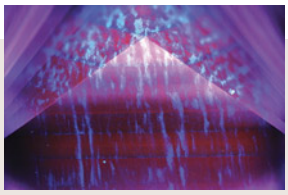
p. 55

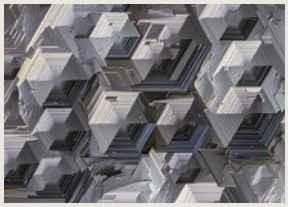
p. 71

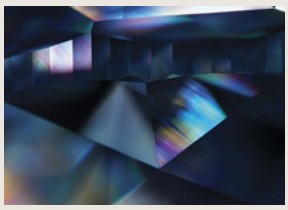
p. 72

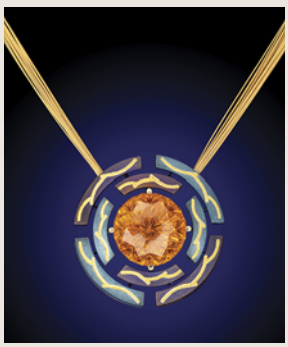
p. 99

Editorial

Feature Articles

Regular Features

GEMS & GEMOLOGY

gia.edu/gems-gemology

Customer Service
Amanda Perez
(760) 603-4200
gandg@gia.edu

Subscriptions
Copies of the current issue may be purchased for $29.95 plus shipping. Subscriptions are $79.99 for one year (4 issues) in the U.S. and $99.99 elsewhere. Canadian subscribers should add GST. Discounts are available for renewals, group subscriptions, GIA alumni, and current GIA students. To purchase print subscriptions, visit store.gia.edu or contact Customer Service. For institutional rates, contact Customer Service.

Database Coverage
Gems & Gemology's impact factor is 1.775, according to the 2020 Thomson Reuters Journal Citation Reports (issued June 2021). *G&G* is abstracted in Thomson Reuters products (Current Contents: Physical, Chemical & Earth Sciences and Science Citation Index—Expanded, including the Web of Knowledge) and other databases. For a complete list of sources abstracting *G&G*, go to gia.edu/gems-gemology, and click on "Publication Information."

Manuscript Submissions
Gems & Gemology, a peer-reviewed journal, welcomes the submission of articles on all aspects of the field. Please see the Author Guidelines at gia.edu/gems-gemology or contact the Managing Editor. Letters on articles published in *G&G* are also welcome. Please note that Field Reports, Lab Notes, Gem News International, Micro-World, Colored Stones Unearthed, Diamond Reflections, and Charts are not peer-reviewed sections but do undergo technical and editorial review.

Gems & Gemology is published quarterly by the Gemological Institute of America, a nonprofit educational organization for the gem and jewelry industry.

Postmaster: Return undeliverable copies of *Gems & Gemology* to GIA, The Robert Mouawad Campus, 5345 Armada Drive, Carlsbad, CA 92008.

Our Canadian goods and service registration number is 126142892RT.

About the Cover

This 9.5-inch knife crafted by Loren Feldman (Feldman Custom Knives) rests on top of a dinosaur bone specimen. With a Damascus steel blade, the knife also features a handle made of Jurassic-period gem dinosaur bone from nine different dinosaurs, accounting for the striking variation of colors. Feldman's knives were one of the highlights of the Tucson shows, which are reported on in this issue. Photo by Robert Weldon/GIA; courtesy of Loren Feldman.

Printing is by L+L Printers, Carlsbad, CA.

GIA World Headquarters The Robert Mouawad Campus 5345 Armada Drive Carlsbad, CA 92008 USA

ISSN 0016-626X

FSC www.fsc.org MIX Paper from responsible sources FSC® C006300

Yellow Topaz from Germany, Emerald Mining in Austria's Habachtal Region, a Return to Tucson, and More…

Welcome to the Spring 2022 issue of *Gems & Gemology*! For our industry, February is marked by the Tucson gem shows, and we're delighted to share content from our highly anticipated return to Tucson. With our two feature articles, our regular columns, the debut of a new regular feature, and the annual *G&G* Challenge, there's something for everyone in this issue.

In our lead article, Manuela Zeug and coauthors explore yellow topaz from the Schneckenstein crag in Saxony, Germany. The article provides a comprehensive summary of mineral, chemical, and spectroscopic investigations of Schneckenstein topaz, with an emphasis on luminescence studied by excitation-emission spectroscopy. This study offers a new perspective on previous mineralogical studies, which focused mainly on crystal forms and trace element geochemistry.

Our second feature article revisits the history of emerald mining in Austria's Habachtal region. In the second installment of his two-part series, Karl Schmetzer traces the history of the Habachtal mine during the era between World Wars I and II, using a variety of largely unpublished sources from Austrian and German archives.

Our regular features have much to offer, too. Among the variety of snapshots in *Lab Notes*, we report on two notable laboratory-grown diamonds recently examined by GIA: a new record-size CVD diamond and one with unusual laser drill holes. *Micro-World* offers a glimpse into the inner landscapes of gemstones, including a before-and-after comparison of an oiled apatite cabochon, a complex fluid inclusion in topaz, and a garnet crystal inclusion in aquamarine. Our *Gem News International* section features more than 30 pages of coverage from the 2022 Tucson shows, with market updates, interesting and noteworthy finds, and interviews with dealers, cutters, and designers. Other highlights from Gem News International include a study of irradiation treatment in amber and the discovery of davemaoite in a diamond from the earth's lower mantle.

"We're delighted to share content from our highly anticipated return to Tucson."

This issue also includes the debut of an exciting new section: *Diamond Reflections*. In his first installment, Evan M. Smith explores the potential role of modern-day deep-focus earthquakes on diamond growth.

Also in this issue: Be sure to take the annual *G&G* Challenge quiz, which offers the chance to test your gemological knowledge of our feature articles from 2021. And we congratulate the winners of this year's Dr. Edward J. Gübelin Most Valuable Article Award.

We hope you enjoy the Spring edition of *Gems & Gemology*!

Duncan Pay | Editor-in-Chief | dpay@gia.edu

Gem Topaz from the Schneckenstein Crag, Saxony, Germany: Mineralogical Characterization and Luminescence

Manuela Zeug, Lutz Nasdala, Chutimun Chanmuang N., and Christoph Hauzenberger

Yellow topaz from the Schneckenstein crag in Saxony, Germany, is a famous and historically important gemstone. Surprisingly, mineralogical studies of the material are comparably scarce and have focused mainly on crystal forms and trace element geochemistry. The present study provides a mineral-chemical and spectroscopic characterization of Schneckenstein topaz and its inclusions taking into consideration past and current research results. Particular emphasis lies on the photoluminescence (PL) behavior of the material. Schneckenstein topaz appears inert under common long-wave (~365 nm) and short-wave (~254 nm) UV light sources. In contrast, excitation wavelengths in the 400–440 nm range are much more efficient in exciting pinkish red emission that is assigned to trace levels (10–40 ppm) of Cr^{3+} incorporated at the six-coordinated Al^{3+} site.

For more than three centuries, the Schneckenstein crag in western Saxony, Germany, has been a source of gem-quality topaz. Gemstone mining at Schneckenstein had its short zenith in the second quarter of the eighteenth century. Professional exploitation started in 1727, by furrier and draper Christian Kraut of Auerbach, with permission of the impoverished landowner von Trützschler. Only a few months later, Augustus the Strong (1670–1733; as Friedrich August I Elector of Saxony, and as August II King of Poland and Grand Duke of Lithuania) purchased the property from von Trützschler and authorized Kraut to expand mining activities—with the precondition that Kraut would surrender the largest and most beautiful stones to him (Buchner, 1740). From then on, the Schneckenstein workings were called the *Königskrone* ("Kings Crown") mine. The finest topaz crystals were extracted during the following decade and a half. A lot of extraordinary quality had been ordered in 1732 by the late Augustus the Strong, but it was his son Friedrich August II (1696–1763; from 1733 Elector of Saxony and as August III concurrently King of Poland and Grand Duke of Lithuania) who commissioned their setting in *objets d'art*. Several of these items of enormous cultural and historical value are now in the collection of the Green Vault in Dresden (figure 1). Another significant historical piece is a crown containing 485 topaz gemstones from Schneckenstein, which was ordered by George III of Great Britain and Ireland (1738–1820) for his wife Charlotte, on the occasion of their mutual coronation in 1761 (Charpentier, 1778). This crown is presumed to be lost, supposedly disassembled for use for other jewelry (Vollstädt and Lahl, 1997).

In Brief

- Topaz from the Schneckenstein crag appears virtually inert under common short-wave and long-wave UV sources but shows fairly intense pink to red Cr^{3+}-related luminescence when illuminated with violet light.
- High F/OH ratio (F 84 at.%), high Ge (40–70 ppm), and low Ga (2–3 ppm) support late-stage topaz formation under hydrothermal conditions.
- Annealing leads to nearly complete bleaching. As color is not related to Cr^{3+} (10–40 ppm), the material hence is not "Imperial" topaz.
- Cr^{3+}-related photoluminescence is not a suitable means to distinguish between "Imperial" and other topaz.

Despite several attempts to resume mining in the second half of the eighteenth century, topaz production never again became as profitable as in the early days, and professional mining finally ceased in 1796. However, the decline of the Schneckenstein topaz

See end of article for About the Authors and Acknowledgments.
Gems & Gemology, Vol. 58, No. 1, pp. 2–17,
http://dx.doi.org/10.5741/GEMS.58.1.2

Figure 1. Historical objects containing Schneckenstein topaz, from the former possession of Friedrich August II (Elector of Saxony; and as Augustus III concurrently King of Poland and Grand Duke of Lithuania). All specimens were handcrafted in 1734 by Johann Heinrich Köhler in Dresden and are now in the collection of the Green Vault in Dresden. Left: Rattan walking stick with a 2.3-cm-tall topaz knob (inventory number VIII 253). Right: Selection of five (out of 48) coat buttons (2.1–2.2 cm diameter; inventory number VIII 248) and five (out of 36) cuff links (1.8 cm; inventory number VIII 249), all cushion-cut topaz set in gold. Photos by Jürgen Karpinski; courtesy of the board of the Green Vault in Dresden.

as a commercial gemstone coincided with increased interest in it as a mineralogical object, both in terms of scientific and collector's items.

One of the first descriptions of the occurrence was made by counselor of mines, chemist, and mineralogist Johann Friedrich Henckel in 1737 (Henckel, 1737), who was inspector of the Schneckenstein crag in 1739. A more detailed description, which included not only sketches of the crag seen from all four cardinal directions but also sketches of topaz crystals and specimens, was compiled in 1744 by Johann Gottlieb Kern, who worked until 1741 as an appraiser in Freiberg, Saxony, Germany (published posthumously; cf. Kern, 1776). Another early (and perhaps the first colored) drawing of a Schneckenstein topaz specimen was sketched by the French painter and draftsman François Louis Swebach-Desfontaines, published as plate LIV in *Histoire Naturelle – Règne Minéral* (Gautier D'Agoty, 1781; see also Wilson, 1995).

Soon thereafter, two publications of historical significance appeared. In his *Traité de Minéralogie*, the famed mineralogist René Just Haüy (1743–1822), often referred to as the "father of modern crystallography," illustrated and described in detail crystal forms of Schneckenstein topaz (Haüy, 1801). Results of thorough measurements of these crystals eventually contributed to the elaboration of Haüy's "law of rational indices." In 1817, another famous mineralogist, Carl Friedrich Christian Mohs (1773–1839), included the Schneckenstein topaz as a reference material for a hardness of 8 (Mohs, 1822) in what is today known as the Mohs hardness scale (e.g., Deer et al., 2013). In the more recent past, Schneckenstein topaz was studied mainly in terms of its geochemical peculiarities, in particular as a major host for germa-

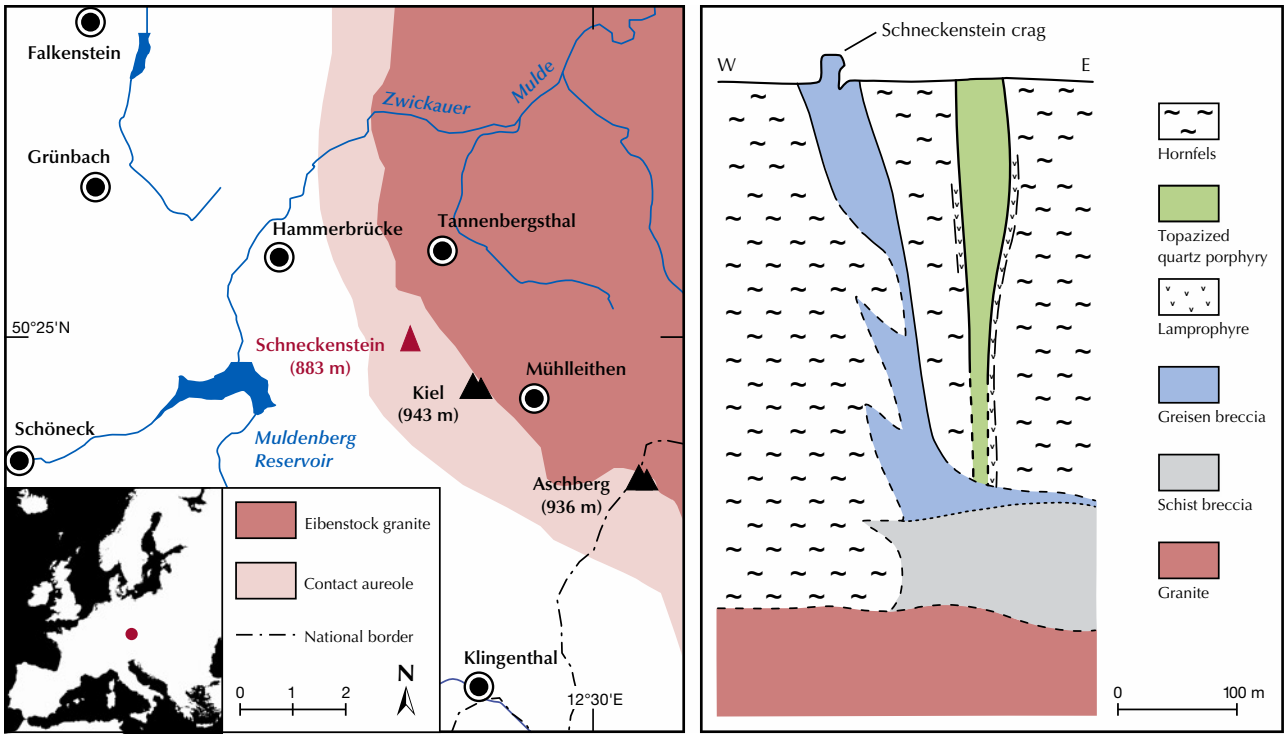

Figure 2. Left: Location of the Schneckenstein crag (marked by a solid red circle in the inset map) in the western contact aureole of the Eibenstock granite (modified after Jäschke and Unger, 2007, and Sebastian, 2013). Right: Cross-sectional profile of the Schneckenstein breccia (simplified after Baumann and Gorny, 1964).

nium (Schrön, 1968; Seim and Schweder, 1969; Breiter et al., 2013b).

Since 1938 the Schneckenstein crag has had the status of a natural monument. The area is fenced, and collecting and especially digging is strictly prohibited. Nevertheless, small topaz crystals of fairly good quality can still be found in the weathering debris. For additional historical information concerning Schneckenstein topaz, the reader is referred to the comprehensive descriptions of Vollstädt and Lahl (1997), Leithner (2008), and Lahl (2012).

GEOLOGICAL BACKGROUND

The Schneckenstein crag is located on the western slope of Kiel Mountain, about 10 km southeast of the town of Falkenstein/Vogtland (figure 2, left). Its formation is related to the Eibenstock tourmaline granite (part of the Nejdek-Eibenstock massif; Breiter, 2012), whose emplacement was about 319.8 ± 1.0 Ma (million years ago) (Tichomirowa and Leonhardt, 2010). The Schneckenstein crag is situated about 400 m away from the granite body, within its contact aureole (Förster et al., 1999; see again figure 2, left). During granite intrusion, several diatremes formed. These were filled with quartz porphyries or breccia that underwent pneumatolytic overprinting "greisenization" (Baumann and Gorny, 1964). The Schneckenstein crag represents the top of a breccious vent filling that resisted weathering (figure 2, right). Greisenization is assigned to a two-stage process: (1) tourmaline formation due to boron infiltration and (2) topaz formation—that included partial tourmaline replacement—from fluorine-rich solutions. The breccia consists of fist-sized fragments of a quartzite-schist-like rock cemented by topaz and quartz crystals. With increasing depth, the tourmaline content increases at the expense of topaz (Schröder, 1915; Baumann and Gorny, 1964). This is known because a lower level of the Schneckenstein breccia was drilled from a mining tunnel of the nearby Grube Tannenberg tin mine. Gem-quality topaz crystals worth cutting were mostly found in cavities and druses in the uppermost regions of the crag.

Topaz originates predominantly from granitic pegmatites (as in Brazil, the Ural Mountains, and Namibia) or from vapor cavities in rhyolite lava flows (as at the Thomas Range in the state of Utah and the Chivinar volcano in Argentina). By contrast, hydrothermal topaz formation in a late greiseniza-

tion stage is decidedly rare. To the best of our knowledge, only one genetic analogue of the Schneckenstein topaz exists worldwide, namely the topaz occurrence in the tin-bearing quartz porphyry of Mount Bischoff, Tasmania (Twelvetrees and Petterd, 1897; Wright and Kwak, 1989).

MATERIALS AND METHODS

Thirteen topaz crystals (0.47–3.86 g) were selected for the present study (figure 3). Seven of them were collected at the Schneckenstein crag during a field trip in 2014, three were provided from the museum collection of the Vogtländisch-Böhmisches Mineralienzentrum Schneckenstein, and three are from the mineral collection of the Institut für Mineralogie und Kristallographie (University of Vienna). Three of the specimens were embedded in araldite epoxy, ground, and polished for Raman spectroscopic and chemical analyses. After completion of Raman spectroscopy and trace element analysis, the mount was coated with carbon for electron probe microanalysis (EPMA). Two raw (i.e., unprepared) crystals that were particularly clear and virtually free of inclusions were used for photoluminescence (PL; including excitation-emission) spectroscopy. These two specimens were then placed in a platinum crucible subjected to dry annealing in air (at 550°C for 48 h), and PL analyses were repeated.

Figure 3. Topaz sample material investigated in the present study (height of the tallest crystal is 18 mm). The two colorless samples (lower left) were initially yellow and became bleached upon heat treatment at 550°C for 48 h. The one-inch sample mount in the background contains three doubly polished crystals embedded in epoxy; it was subjected to spectroscopy, EPMA, and LA-ICP-MS analysis. Photo by Manuela Zeug.

Mass densities were determined by weighing samples in air and in distilled water (a drop of liquid detergent was added to reduce surface tension). Refraction measurements were done using a Krüss ER601-LED refractometer equipped with a diode lamp emitting 589 nm light.

Major-element analyses were performed on a JEOL JXA-8530FPlus HyperProbe EPMA system operated at 15 kV and 10 nA. Counting times were 10 s for major and 30 s for minor elements. A topaz reference crystal was used for calibrating major elements (F-Kα, Si-Kα, and Al-Kα). For calibrating the instrument for minor elements, reference materials included diopside NMNH117733 (Mg-Kα and Ca-Kα), microcline NMNH143966 (K-Kα), albite (Na-Kα), garnet (Fe-Kα), ilmenite NMNH96189 (Ti-Kα), rhodonite (Mn-Kα), and tugtupite (Cl-Kα). The three NMNH reference materials are Smithsonian microbeam standards (Jarosewich, 2002; and references therein) and all others are in-house reference materials. Detection limits were determined according to Toya and Kato (1983) as the threefold background noise. Further EPMA details are described in Nasdala et al. (2021).

Trace element analysis was done by means of laser ablation–inductively coupled plasma–mass spectrometry (LA-ICP-MS) using an Agilent 7500cx quadrupole ICP-MS unit coupled with an ESI NWR193 laser ablation system. A 193 nm laser operated with 8 Hz repetition frequency was used, resulting in ~6.5 mJ/cm^2 energy density at the sample surface. The spot size was set to 75 µm and the dwell time was 20 ms per element. A gas blank was acquired for 25 s prior to 50 s of ablation time. The ablated material was transported with He (gas flow rate 0.75 L/min) to the spectrometer unit. NIST standard glasses SRM610 and SRM612 (Jochum et al., 2011) were used for external calibration, and Si was measured as the internal standard. SRM612 was used for data reduction of all elements. USGS reference glass BCR-2G (Jochum et al., 2016) served for monitoring possible beam drift and was reproduced within 10% relative error. GLITTER 4.0 software (Griffin et al., 2008) was used for data reduction. For more analytical details, see Kruzslicz et al. (2020).

Raman spectra were obtained at room temperature using a dispersive Horiba LabRAM HR Evolution system equipped with an Olympus BX-series optical microscope and a Peltier-cooled, Si-based charge-coupled device detector. Spectra were excited with the 473 nm emission of a diode-pumped solid-state laser (8 mW at the sample surface). A 100× objective (numerical aperture 0.90) was used. The scattered light was dispersed with an 1800 grooves/mm diffraction grating, resulting in spectral resolution of 1.2 cm^{-1}. Further experimental details are described elsewhere (Zeug et al., 2018).

Photoluminescence emission spectra, excitation spectra, and excitation-emission matrices were obtained from a crystal that was virtually free of major inclusions by means of a Horiba Fluorolog-3 system equipped with double-grating excitation and emission monochromator (gratings with 1200 grooves/mm) and R928P photomultiplier detector. Xe-lamp excitation (450 W) was used, and excitation correction was performed using an internal reference photodiode. Spectra and maps were obtained with an activated dark offset, resulting in noise reduction. With this system, excitation source, and settings, emission can be reliably obtained in the wavelength range 250–850 nm. Bandpass for excitation spectra of the 683 nm emission band was set to 1 nm. Excitation spectra were obtained in the wavelength range of 250–700 nm with a step width of 0.5 nm. Emission spectra (bandpass 1 nm and step size 0.2 nm) were excited with 407 nm excitation wavelength and obtained in the wavelength range 555–800 nm. For the excitation-emission map, step size and bandpass were set to 2 nm for excitation and 1 nm for emission, respectively.

RESULTS AND DISCUSSION

General Properties. All samples studied here showed different shades of pale yellow, which is the most typical color of Schneckenstein topaz. This color is rather low-grade for gemological uses; it is commonly referred to as "wine yellow" (figure 4). After annealing, samples were "bleached" and became nearly colorless. All samples were transparent and appeared inert under short-wave and long-wave UV lamps. The crystals had a short prismatic habit with well-developed terminations. Most of them contained diverse gaseous, liquid, and/or solid inclusions, with sizes of up to several hundred micrometers. SG values averaged 3.52 ± 0.01, and the RI was 1.607–1.616.

Chemical Composition. The chemical composition of Schneckenstein topaz is summarized in table 1. The samples had generally low levels of non-formula constituents. The calculated chemical formula is $Al_{1.99}Si_{1.01}O_{4.00}[F_{0.84}(OH)_{0.16}]_2$. Note that the F content measured here (17.4 ± 0.5 wt.%) is higher than the values of 14.4–14.5 wt.% reported by Bauer (1902) and lower than the value of 19.5 ± 0.6 wt.% reported by

Figure 4. Four specimens of vivid "wine yellow" topaz with quartz from the Schneckenstein crag. Top left: The largest topaz crystal is 18 mm tall. Top right: The crystal in the center is 17 mm tall. Bottom: Both large crystals are 14 mm tall. The top right specimen is from the private collection of L. Nasdala; the other three specimens are in the mineral collection of TU Bergakademie Freiberg (inventory numbers MiSa56852, MiSa59082, and MiSa57016, respectively). Photos by Andreas Massanek (top left and bottom right), Manfred Wildner (top right), and Jeff Scovil (bottom left).

Ribbe and Rosenberg (1971), but it coincides well with the results of Breiter et al. (2013b; 17.9–18.5 wt.%, or ~1.75 apfu). Based on the inverse correlation of OH/F ratio and formation temperature (Barton, 1982), the lower F content compared with pneumatolytic columnar topaz from the Erzgebirge ("pycnite" with F > 1.8 apfu) points to late-stage formation, presumably under hydrothermal conditions (Breiter et al., 2013b).

Ge concentrations of 40–70 ppm and Ga concentrations of 2–3 ppm determined herein correspond reasonably well with results of previous studies (~69

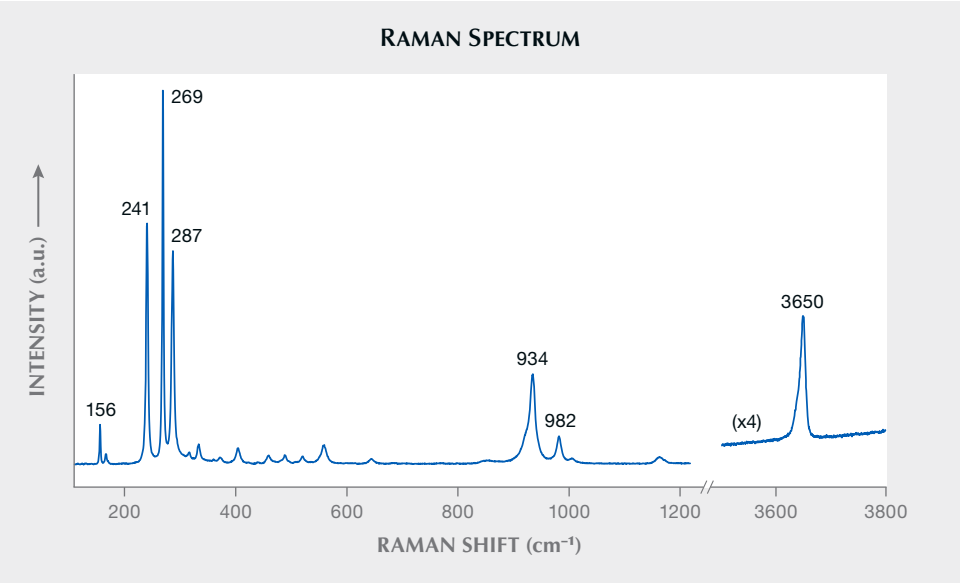

Figure 5. Raman spectrum of a topaz from Schneckenstein (second crystal from the left in figure 3, random sample orientation). The intensity of the hydroxyl-stretching region (between 3500 and 3800 cm^{-1}) has been increased four times for better recognizability.

ppm Ge by Goldschmidt and Peters, 1933; 50–86 ppm Ge by Seim and Schweder, 1969; 42–116 ppm Ge and 2–4 ppm Ga by Breiter et al., 2013b). Comparably high Ge but low Ga values again support low-temperature topaz formation: Greisenization leads to Ge enrichment due to the uptake in newly formed hydrothermal topaz, while Ga is dissipated by hydrothermal fluids (Breiter et al., 2013a).

Raman Spectroscopy. The Raman spectrum of Schneckenstein topaz (figure 5) shows the typical fingerprint pattern of this mineral's Raman-active vibrations (for band assignment, see Beny and Piriou, 1987). The OH stretching range is dominated by a clearly asymmetric band. This asymmetric band shape is due to an unresolved splitting of two bands, with a band at ~3650 cm^{-1} that corresponds mainly to "OH_B" of Pinheiro et al. (2002), and a low-intensity shoulder near ~3640 cm^{-1} that is assigned to "OH_A." Such an OH band pattern, along with the generally low OH band intensity, points to topaz with high F/OH ratio, with a fraction of OH at the (F,OH) site of about 15 mol.% (Pinheiro et al., 2002). The latter corresponds well with our chemical data (table 1).

Raman analyses of inclusions (often showing two or more phase assemblages; figure 6) yielded a range of phases, including gaseous CO_2, liquid H_2O, rutile, apatite, a xenotime-group mineral, clinochlore, and quartz. Fluid inclusions may be described as multiphase, vapor-rich two-phase or three-phase inclusions. We were unable to identify small opaque inclusions that probably consisted of one or more ore mineral(s). Colorless cubic-shaped crystals did not yield any Raman band pattern; it appears reasonable to assume they are halite.

Photoluminescence Spectroscopy. Results of PL spectroscopic analyses are presented in figure 7. A reasoning for why such data should preferably be plotted on an energy-equivalent scale such as the wavenumber, instead of on a wavelength scale (as is commonplace in gemological papers), is provided in box A, along with some additional remarks on luminescence terminology.

The emission spectrum (figure 7, top right) is dominated by a narrow doublet in the red range, at ~14632 and ~14720 cm^{-1} (~683.4 and ~679.4 nm, respectively), assigned to the split, spin-forbidden d–d transition $^2E \rightarrow {}^4A_2$ of trace Cr^{3+} (commonly referred to as R_1 and R_2 lines). This doublet is superimposed on a broad emission feature in the 12500–15500 cm^{-1} (approximately 800–645 nm) range, which is due to the spin-allowed $^4T_2 \rightarrow {}^4A_2$ transition of Cr^{3+} (Tarashchan et al., 2006). The broad band is modulated by lower-intensity bands at ~14080 cm^{-1} (~710 nm) and ~14400 cm^{-1} (~694 nm) whose assignment remains an open question. They have been interpreted as emissions of pairs and clusters of Cr^{3+} ions (Gaft et al., 2003) and phonon satellites (Tarashchan et al., 2006), respectively. The spectral positions of the two R lines correspond to Cr^{3+} in a fully fluorinated environment—that is, a $(CrO_4F_2)^{7-}$ site (O'Bannon and Williams, 2019)—which supports again the above interpretation of the sample as topaz with a low OH/F ratio. The emission spectrum remained virtually unchanged after sample annealing (figure 7). Differences with emission patterns

TABLE 1. Mean chemical composition of Schneckenstein topaz.

Major oxides and constituents (EPMA)

Constituent[a]	Concentration (wt.%)	Calculated formula[b] (apfu)		MDL[c] (wt.%)
SiO_2	32.95 ± 0.50	Si	1.01	0.114
Al_2O_3	55.07 ± 0.51	Al	1.99	0.111
H_2O[d]	1.52 ± 0.21	OH	0.31	
F	17.43 ± 0.48	F	1.69	0.085
–O=F	7.34 ± 0.20	O	4.00	
Total	99.64 ± 0.98	Σ anions	6.00	

Trace elements (LA-ICP-MS)

Element[e]	Isotope measured	Concentration (ppm)	MDL (ppm)
Mg	24	3.71 ± 1.34	0.441
Ti	49	34.3 ± 10.9	1.429
V	51	7.55 ± 3.34	0.054
Cr	53	23.4 ± 13.6	1.522
Ga	71	2.40 ± 0.42	0.113
Ge	74	65.1 ± 12.8	0.561

All errors are quoted at the 2σ level. EPMA, n = 18; LA–ICP–MS, n = 15 for Mg and Ge and n = 33 for all other trace elements.
[a]Constituents (with detection limits in wt.% in parentheses) CaO (0.013), K_2O (0.013), Na_2O (0.036), TiO_2 (0.019), FeO (0.037), MnO (0.36), MgO (0.019), and Cl (0.013) were also analyzed, but mean concentrations were below the EPMA detection limits.
[b]Calculated on the basis of 3 cations per formula unit.
[c]Minimum detectability limit = $(2\sqrt{2} \times \sqrt{NB} \times Cstd)/(NnP)$ according to Toya and Kato (1983); NB = background counts, Cstd = concentration in standard, and NnP = net peak counts.
[d]H_2O calculated from stoichiometry.
[e]The following elements were also analyzed (detection limits in ppm in parentheses), but mean concentrations were below the LA-ICP-MS detection limits: Li (0.301), Be (0.178), B (0.958), Mn (0.597), Co (0.049), Ni (0.234), Cu (0.782), Zn (1.014), Rb (0.117), Sr (0.021), Y (0.018), Zr (0.032), Nb (0.022), Sn (0.296), Cs (0.085), Ba (0.166), La (0.020), Ce (0.017), Pr (0.017), Nd (0.105), Sm (0.108), Eu (0.030), Gd (0.103), Tb (0.019), Dy (0.063), Ho (0.014), Er (0.051), Tm (0.016), Yb (0.070), Lu (0.017), Hf (0.067), Ta (0.018), Pb (0.289), Th (0.022), and U (0.020).

of other Cr^{3+}-bearing gem minerals are explained by different crystal-field effects (that is, distortion of electronic levels in a non-isotropic environment). For a more detailed discussion, see box B.

The Schneckenstein topaz is certainly not unique but perhaps somewhat special, because this material does not show noticeable Cr^{3+}-related absorption but fairly intense Cr^{3+}-related emission. The majority of

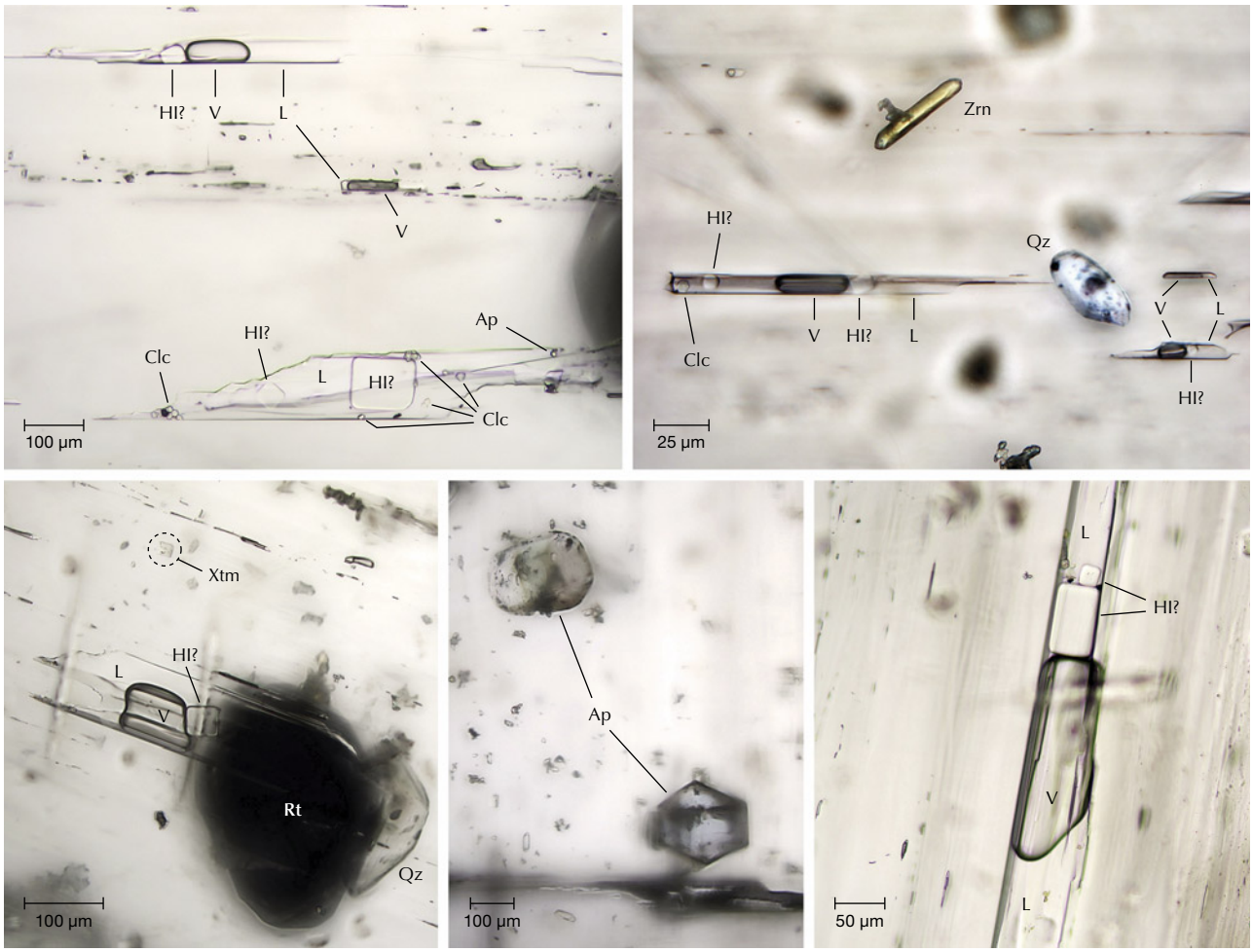

Figure 6. Plane-polarized transmitted-light photomicrographs showing the diversity of single- and multiphase inclusions in Schneckenstein topaz (bottom center crystal in figure 3). V—vapor (predominantly CO_2). L—liquid (predominantly H_2O). The occurrence of halite (colorless cubic-shaped crystals) is assumed but could not be confirmed, because crystals did not yield any Raman spectra. Abbreviations of names of minerals and mineral groups according to Whitney and Evans (2010): Ap—apatite; Clc—clinochlore; Hl—halite; Qz—quartz; Rt—rutile; Xtm—xenotime; Zrn—zircon. Photomicrographs by Manuela Zeug.

other pale gem topaz (originating from Namibia, Pakistan, and the Ural Mountains) that we tested did not show any luminescence. The PL characteristics of "Imperial" topaz with its much higher, coloration-affecting Cr^{3+} content—on the order of hundreds of ppm (Taran et al., 2003; Schott et al., 2003; Krzemnicki, 2017; Gauzzi et al., 2018)—is widely similar to that of the Schneckenstein topaz. High emission intensity of the Schneckenstein material in spite of its low Cr^{3+} content may in part be assigned to particularly low concentrations of luminescence "quenchers," such as Fe^{2+}.

Excitation Spectroscopy. The excitation spectrum (figure 7, bottom), obtained for the most intense PL signal at ~683.4 nm, shows two main broad signals in the ranges 16000–18800 and 22400–25800 cm^{-1} (approximately 625–530 and 445–390 nm). The spectrum is widely similar to that of a light violet topaz (300 ppm Cr) from Ouro Preto, Brazil, presented by Tarashchan et al. (2006). Already Hoover and Theisen (1993) had studied the excitation of Cr^{3+}-related emission of pink topaz; however, these authors did not present any excitation spectra but merely mentioned its wide similarity to that of ruby, emerald, red spinel, and green jade. The two broad bands correspond to the main electronic absorption levels and are assigned to intense PL following Cr^{3+}-related electronic excitation ($^4A_2 \rightarrow {}^4T_2$ and $^4A_2 \rightarrow {}^4T_1$ transitions, respectively). For detailed discussions of the energy difference ("Stokes shift") between $^4A_2 \rightarrow {}^4T_2$ absorption and $^4T_2 \rightarrow {}^4A_2$

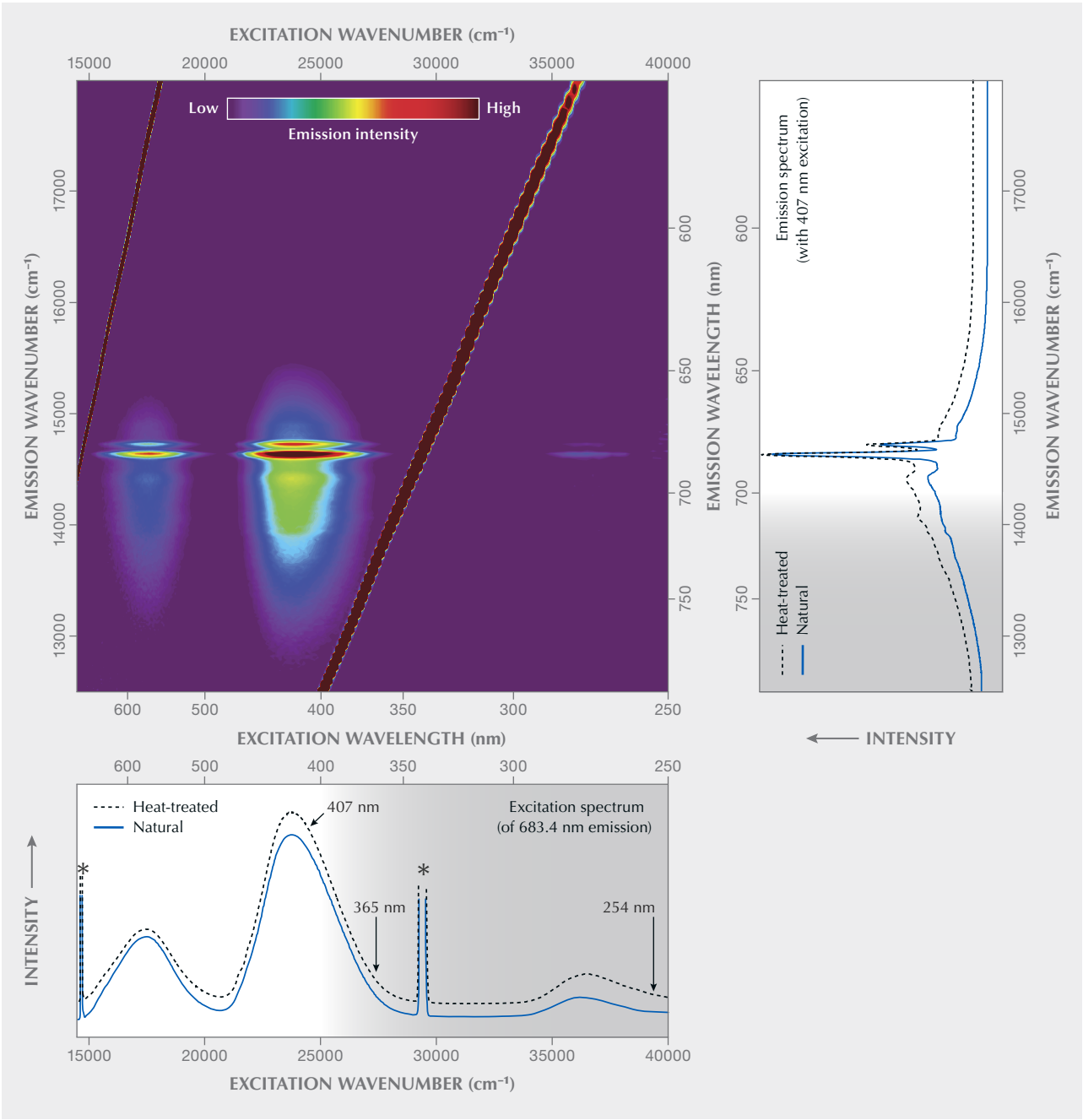

Figure 7. Top left: Color-coded excitation-emission matrix (visualizing the emission intensity at variable wavenumber/wavelength upon excitation with light of variable quantum energy, consisting of a total of 56,250 individual data points) for topaz from Schneckenstein. The matrix is presented along with selected emission spectra (emission intensity under 407 nm excitation obtained at variable wavelength; top right) and excitation spectra (intensity of the ~14632 cm^{-1} [~683.4 nm] emission under variable excitation; bottom). In the emission and excitation plots, spectra of a natural topaz specimen and its heat-treated analogue (bottom left crystal in figure 3) are shown. Spectral ranges that are not visible to the human eye are underlain in gray. Diagonal dark red lines in the main emission-excitation matrix, and corresponding narrow lines in the excitation spectra (here marked by asterisks), are analytical artifacts (emission = excitation, and emission = 1/2 × excitation energy). Note that the 407 nm laser used herein is much more efficient for exciting Cr^{3+} emission than common UV lamp sources (spectral positions marked with arrows in the bottom plot). Emission and excitation spectra of the annealed sample are shown with vertical offset for clarity.

BOX A: LUMINESCENCE—NOMENCLATURE AND SPECTRAL VISUALIZATION

Luminescence describes the general ability of minerals and other matter to emit UV, visible and/or IR light after valence electrons have experienced *energetic excitation*. If emission occurs upon spontaneous energy release from the excited state, the process is named according to the initial energetic excitation (such as *photoluminescence* after excitation by photons of electromagnetic radiation, *chemoluminescence* for emissions whose energy originated from a chemical reaction, or *cathodoluminescence* after excitation by electrons). In contrast, non-spontaneous release of excited electrons from so-called electron traps requires energetic *stimulation* (in addition to the initial energetic excitation); here the emission process is named according to the type of stimulation (such as *optically stimulated luminescence*).

It should be noted that there is general confusion of terms in the published literature. *Excitation* and *stimulation* are often used interchangeably, and even more often *fluorescence* is used when *luminescence* is meant. Fluorescence and phosphorescence are two terms that relate to different delay-time regimes caused by different types of electronic transitions. *Fluorescence* describes emission upon quick spontaneous decay of the energetically excited state, typically within less than 10 microseconds, due to spin-allowed electronic transitions. By contrast, *phosphorescence* is emission based on comparably slow spontaneous decay of the energetically excited state (between tens of microseconds and several hours), related to spin-forbidden electronic transitions. The subdivision into fluorescence and phosphorescence is applied mostly to photoluminescence. A non-PL example is the "glow" of white phosphorous, a permanently refreshed fluorescence-type chemoluminescence.

Emissions of ions of transition metals arise mostly from slow, spin-forbidden electronic transitions, and hence their common description as "fluorescence" is misleading. One of the most prominent examples is the Cr^{3+}-related emission of ruby (lifetime of the excited state is several milliseconds), which actually belongs to phosphorescence (Jones et al., 2020) but has mostly—and not quite correctly—been described as fluorescence (e.g., Brown, 1964; Tsai and D'Haenens-Johansson, 2021). The bottom line is that if the exact type of electronic transition causing the observed emission is unknown, or if an emission consists of several different components, the use of the general term *luminescence* is preferred.

Another issue, especially in the gemological literature, is how to visualize spectra whose signals are based on electronic transitions (this applies not only to luminescence but also to optical absorption). Most individual spectral signals that relate to electronic transitions are symmetric in energy. For this reason, spectra—especially in cases when data evaluation is intended—need to be plotted on a scale that is proportional to the quantum energy of the detected light, such as the wavenumber (in units of cm^{-1}). By contrast, wavelength (i.e., the inverse of the wavenumber) is a physical parameter that is *not* proportional to photon energy. Spectra that are plotted on the usual wavelength scale are therefore distorted—that is, compressed in their high-energy region (blue to UV) and stretched in their low-energy (red and near-infrared) region (see figure A-1). Consequently, fitting spectra that are plotted on the wavelength scale with the assumption of symmetric (Gaussian and/or Lorentzian) band shapes must yield biased fit results. For this reason, excitation and emission shown in figures 7 and B-1 are plotted on the wavenumber scale. However, we are well aware of the general preference for wavelengths in the gemological community, and we also provide the (not evenly spaced) wavelength scale on a second abscissa axis for convenience.

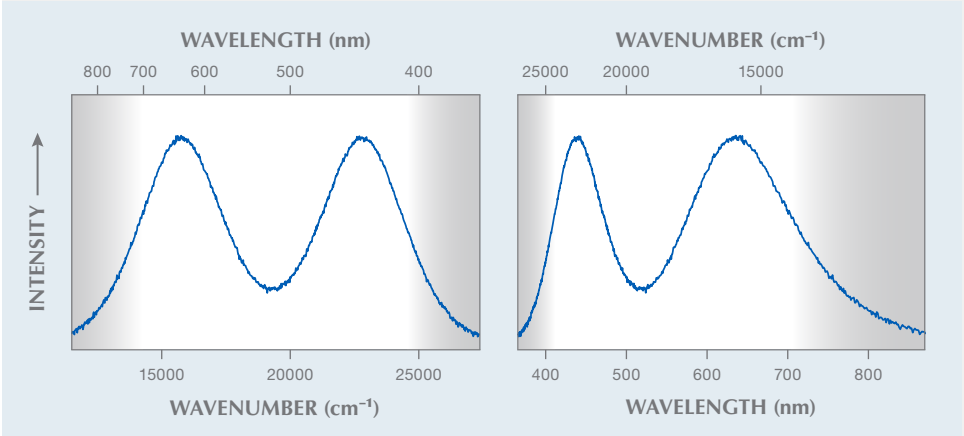

Figure A-1. A spectrum consisting of two perfectly symmetric bands of the same energy width (left) is significantly distorted when plotted on the wavelength scale (right).

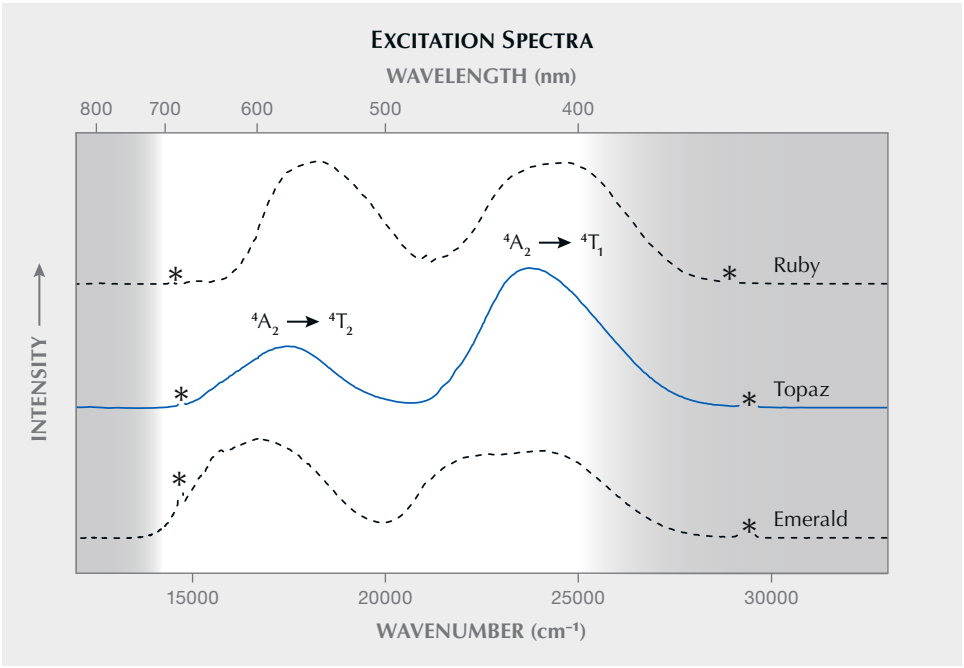

Figure 8. Excitation spectrum of Schneckenstein topaz (obtained from the bottom left crystal in figure 3 before annealing), visualizing the intensity of the Cr^{3+}-related emission at 14632 cm^{-1}/683.4 nm depending on the excitation energy. Spectra of ruby (14403 cm^{-1}/694.3 nm) and emerald (14620 cm^{-1}/684 nm) are shown for comparison. Spectra are shown with vertical offset for clarity. Breaks in the excitation spectra (marked by asterisks) are analytical artifacts (emission = excitation, and emission = ½ × excitation energy). Note the shift of the two main absorption bands among the three minerals. For band assignment, see Tarashchan et al. (2006).

emission, see for instance Kisliuk and Moore (1967) and Marfunin (1979).

The excitation spectrum is similar but not identical to absorption patterns of "Imperial" topaz (Petrov et al., 1977; Schott et al., 2003; Krzemnicki, 2017; Smith, 2020). The difference between absorption and excitation spectra is because a certain fraction of the absorption in natural, untreated topaz is due to defect-related color centers (Petrov, 1977, 1978). Note that annealing of such color centers causes significant color change after thermal treatment (Schott et al., 2003; Greenidge, 2018). The latter is especially true for the yellow Schneckenstein topaz that, after dry heating in air at 550°C for 48 h, was found to turn near-colorless (while retaining the Cr^{3+}-related PL).

The excitation spectrum indicates that common gemological UV lamps with ~365 nm and ~254 nm excitation wavelengths are decidedly inefficient sources to induce Cr^{3+}-related emission from topaz. In contrast, PL is readily excited by illumination by either orange to greenish yellow or by blue to violet light. For instance, a 407 nm laser (see again figure 7, bottom) or a 390 nm LED lamp emit light that is effectively absorbed by Cr^{3+}-bearing topaz and thus excite pink to red luminescence with relative ease, whereas a 385 nm LED was found to be less efficient.

The excitation characteristics of other Cr^{3+}-bearing gem minerals may be similar but not necessarily identical to that of topaz. This is due to their different crystal-field strengths that, among others, control the energetic difference of $^4T_2$ and ^2E levels (figure 8; see also box B).

Excitation-Emission Spectroscopy. The excitation-emission matrix of Schneckenstein topaz shown in figure 7 is the color-coded visualization of quantum energy and intensity of the emission with respect to the quantum energy of the excitation. Such a matrix is generated by measuring the emission intensity at variable spectral positions (potentially comprising the long-wave UV, visible, and NIR ranges) and at different excitation energies. Note that such plots have also been described as three-dimensional luminescence spectra (with excitation energy, emission energy, and intensity as the three dimensions) or as excitation-emission maps. We prefer not to use the latter term, to avoid possible confusion with hyperspectral maps where multiple point analyses are conducted at different x and y coordinates, whereas a matrix consists of multiple analyses obtained at the very same sample location. For the principle of the technique, the reader is referred to the fundamental description in Marfunin (1979); more specific elucidations are given in box B of Zhang et al. (2020).

The emission intensity of the Schneckenstein topaz varies strongly with the excitation energy, whereas the principal spectral pattern of the emission does not. Note that the coloration distribution in the excitation-emission matrix does not show significant diagonal features (for a contrasting example, see figure 4G of Zhang et al., 2020). This indicates that the emission does not

BOX B: LUMINESCENCE RELATED TO TRIVALENT CHROMIUM

Several gem minerals incorporate minor amounts of Cr^{3+} at a lattice site that is six-coordinated to O^{2-} (and possibly other anions). Examples include corundum, beryl, chrysoberyl, diopside, garnet, tourmaline, and topaz. However, absorption (i.e., coloration) and emission related to Cr^{3+} may vary appreciably (see also figure 8 in Tsai and D'Haenens-Johansson, 2021). This is because of so-called crystal-field effects: The six-coordinate octahedral Cr^{3+} site is variably distorted from its ideal octahedral symmetry, due to various arrangements of neighboring atoms, depending on the respective host mineral's crystal structure.

In contrast to optical absorption processes, only the two lowest-energy excited levels of six-coordinate octahedral Cr^{3+} (i.e., the narrow, split ^2E level and the broad, thermally populated $^4T_2$ level) are significant for the emission of light. In different host minerals, these levels have unequal energy differences relative to one another and relative to the electronic ground state ($^4A_2$), finally resulting in different emission characteristics. This is visualized (greatly simplified) in figure B-1.

For Cr^{3+} in corundum, the energy difference ΔE between ^2E and $^4T_2$ is comparably large. The two levels hence do not "overlap" at room temperature, and direct $^4T_2 \rightarrow {}^4A_2$ relaxation does not occur, but excited electrons undergo a so-called fast intersystem crossing (ISC) from the $^4T_2$ singlet to the energetically favorable ^2E triplet-excited state (Kisliuk and Moore, 1967). Emission of chromium-bearing corundum is therefore dominated by the two narrow R lines (spin-forbidden $^2E \rightarrow {}^4A_2$ transition). In contrast, ΔE is much smaller for Cr^{3+} in beryl, resulting in energetic preference and hence significant contribution of the spin-allowed $^4T_2 \rightarrow {}^4A_2$ relaxation at room temperature (Kisliuk and Moore, 1967). The latter is detected as an intense broad band underlying the two R lines (figure B-1). Chromium-bearing topaz has intermediate ΔE and therefore practically represents an intermediate state between the two former minerals. Here, $^4T_2$ and ^2E states are in virtual thermal equilibrium at room temperature (Gaft et al., 2003; Tarashchan et al., 2006). The Cr^{3+}-related emission of topaz therefore consists of nearly equal contributions of the two narrow R lines (and their vibrational satellites) related to the spin-forbidden $^2E \rightarrow {}^4A_2$ transition, and a broad band related to the spin-allowed $^4T_2 \rightarrow {}^4A_2$ transition (Gaft et al., 2003; Tarashchan et al., 2006; O'Bannon and Williams, 2019).

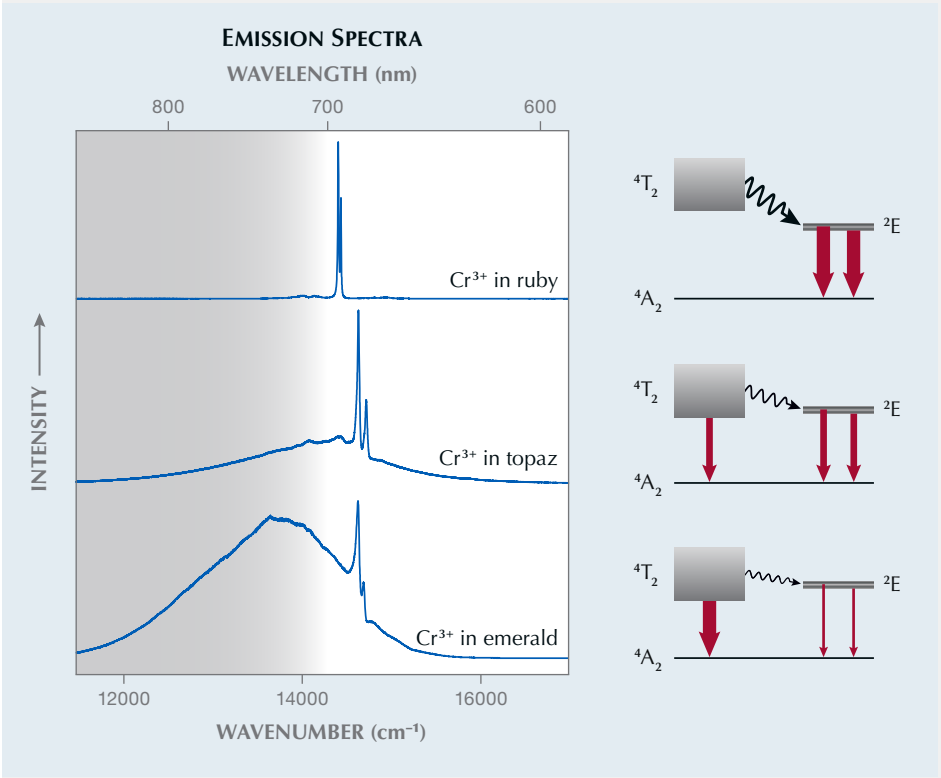

Figure B-1. Room-temperature emission spectra related to Cr^{3+} in three common gem minerals, along with greatly simplified sketches of the lowest electronic levels. Rather minor variations in energy differences among corresponding electronic levels result in apparently different PL patterns: In ruby, electrons are transferred non-radiatively from the $^4T_2$ to the split ^2E level (wavy black arrow), and the energy is released radiatively (that is, under emission of PL) only upon $^2E \rightarrow {}^4A_2$ transition (red arrows). In the other two minerals, increasing portions of electrons undergo a radiative $^4T_2 \rightarrow {}^4A_2$ transition and correspondingly fewer electrons are transferred to the ^2E level (visualized by varying thicknesses of lines).

Figure 9. Two photos of the second crystal from the left in figure 3 (1.6 g, 9.5 mm tall). Left: White-light photo showing the common pale yellow bodycolor. Right: The crystal emits pink to red luminescence under 407 nm illumination. Photos by Manfred Wildner.

consist of several components with different excitation characteristics. Rather, the emission is assigned solely to Cr^{3+} substituting for Al^{3+} (Gaft et al., 2003; Tarashchan et al., 2006; O'Bannon and Williams, 2019).

CONCLUSIONS

The present article provides a comprehensive summary of past and present mineral-chemical and spectroscopic investigations of the historical Schneckenstein topaz, with emphasis on luminescence studied by excitation-emission spectroscopy. It is, to the best of our knowledge, only the third excitation-spectroscopy study of topaz, and the first that was conducted on non-"Imperial" topaz. The Schneckenstein material is characterized by remarkably low contents of non-formula elements and a high F/OH ratio. The latter is also reflected in the Raman spectra by the OH-band pattern with its comparable low intensity. The PL spectra reveal the typical Cr^{3+}-luminescence pattern in topaz, and no additional luminescence bands are present. The determined values for Ge (40–70 ppm) and Ga (2–3 ppm) are mainly consistent with results from previous studies (Goldschmidt and Peters, 1933; Schrön, 1968; Seim and Schweder, 1969) and coincide with an assumed topaz formation in a late hydrothermal state following pneumatolytic greisenization (Breiter, 2013a). To the best of our knowledge, this is the first study that provides microscopic images of, and analytical data for, the manifold inclusions in Schneckenstein topaz. Inclusions identified by means of Raman spectroscopy were apatite, rutile, quartz, zircon, and a xenotime-group mineral. The assumed assignment of cubic crystals in multiphase inclusions as halite will require further study.

The excitation-emission spectroscopy technique is a rather recent advancement of excitation spectroscopy, which is becoming more important in the analysis of gemstones. Successful applications of excitation-emission spectroscopy include studies of Cr^{3+}-colored gem minerals (Hoover and Theisen, 1993); amber (Bellani et al., 2005; Jiang et al., 2020; Zhang et al., 2020); opal (Fritsch et al., 2015); and diamond (Luo and Breeding, 2013). In the present case, excitation-emission spectroscopy provides simple reasoning for the apparent luminescence inertness of yellow topaz observed under UV illumination. Excitation energies of Cr^{3+} electronic levels in topaz do not coincide with quantum energies of light that is emitted by short-wave and long-wave UV lamps used in conventional gem testing. By contrast, short-wavelength visible (i.e., violet) light is remarkably efficient in exciting readily visible pinkish PL (figure 9) that is caused by Cr^{3+} concentrations as low as ~25 ppm.

ABOUT THE AUTHORS

Dr. Manuela Zeug and Dr. Chutimun Chanmuang N. are researchers, and Prof. Dr. Lutz Nasdala is chairholder for Mineralogy and Spectroscopy, at the Institut für Mineralogie und Kristallographie, University of Vienna. Prof. Dr. Christoph Hauzenberger is chairholder for Petrology and Geochemistry at the Institute of Earth Sciences - NAWI Graz Geozentrum in Graz, Austria.

ACKNOWLEDGMENTS

Three of the topaz crystals investigated were kindly made available by Steffen Gerisch, and sample preparation was done by Andreas Wagner. Gerald Giester, Michael Loitzenbauer, and Roland Seitz are thanked for experimental help. Alexander Repstock and Wolfgang Zirbs assisted in acquiring literature. Michael Gaft is thanked for helpful discussions. We are indebted to Dirk Weber for providing images of historical objects, and the board of the Green Vault in Dresden for permission to use the images herein. Andreas Massanek, Jeff Scovil, and Manfred Wildner are thanked for photographs of topaz specimens. Constructive comments and suggestions of three anonymous reviewers are gratefully acknowledged.

REFERENCES

Barton M.D. (1982) The thermodynamic properties of topaz solid solution and some petrologic applications. *American Mineralogist*, Vol. 67, pp. 956–974.

Bauer M. (1902) Hermann Albert Weber: Ueber die Aufschliessung der Silikate durch Borsäureanhydrid und über eine neue Methode zur Bestimmung des Fluors im Kryolith. Review of inaugural dissertation (Heidelberg 1900, 38 pp.). *Centralblatt für Mineralogie, Geologie und Paläontologie*, pp. 504–507.

Baumann L., Gorny S. (1964) Neue tektonische und petrographische Untersuchungsergebnisse in der Zinnerzlagerstätte Tannenberg-Mühlleiten. *Freiberger Forschungshhefte C*, Vol. 181, pp. 89–118.

Bellani V., Giulotto E., Linati L., Sacchi D. (2005) Origin of the blue fluorescence in Dominican amber. *Journal of Applied Physics*, Vol. 97, No. 1, article no. 016101, http://dx.doi.org/10.1063/1.1829395

Beny J.M., Piriou B. (1987) Vibrational spectra of single-crystal topaz. *Physics and Chemistry of Minerals*, Vol. 15, No. 2, pp. 148–154, http://dx.doi.org/10.1007/BF00308777

Breiter K. (2012) Nearly contemporaneous evolution of the A- and S-type fractionated granites in the Krušné hory/Erzgebirge Mts., Central Europe. *Lithos*, Vol. 151, pp. 105–121, http://dx.doi.org/10.1016/j.lithos.2011.09.022

Breiter K., Gardenová N., Kanický V., Vaculovič T. (2013a) Gallium and germanium geochemistry during magmatic fractionation and post-magmatic alteration in different types of granitoids: A case study from the Bohemian Massif (Czech Republic). *Geologica Carpathica*, Vol. 64, No. 3, pp. 171–180, http://dx.doi.org/10.2478/geoca-2013-0018

Breiter K., Gardenová N., Vaculovič T., Kanický V. (2013b) Topaz as an important host for Ge in granites and greisens. *Mineralogical Magazine*, Vol. 77, No. 4, pp. 403–417, http://dx.doi.org/10.1180/minmag.2013.077.4.01

Brown G.C. Jr. (1964) Fluorescence lifetimes of ruby. *Journal of Applied Physics*, Vol. 35, pp. 3062–3063, http://dx.doi.org/10.1063/1.1713175

Buchner J.G. (1740) Lapidibus pretiosis in Voigtlandia reperiendis. *Acta Physico-Medica Academiae Caesareae Leopoldino-Carolinae Naturae Curiosorum Exhibentia*, Vol. 5, pp. 101–105.

Charpentier J.F.W. (1778) *Mineralogische Geographie der Chursächsischen Lande*. Siegfried Leberecht Crusius, Leipzig.

Deer W.A., Howie R.A., Zussman J. (2013) *An Introduction to the Rock-Forming Minerals*, 3rd ed. Berforts Information Press, Stevenage, UK, 510 pp.

Förster H.-J., Tischendorf G., Trumbull R.B., Gottesmann B. (1999) Late-collisional granites in the Variscan Erzgebirge, Germany. *Journal of Petrology*, Vol. 40, No. 11, pp. 1613–1645, http://dx.doi.org/10.1093/petroj/40.11.1613

Fritsch E., Megaw P.K.M., Spano T.L., Chauviré B., Rondeau B., Gray M., Hainschwang T., Renfro N. (2015) Green-luminescing hyalite opal from Zacatecas, Mexico. *Journal of Gemmology*, Vol. 34, No. 6, pp. 490–508.

Gaft M., Nagli L., Reisfeld R., Panczer G., Brestel M. (2003) Time-resolved luminescence of Cr^{3+} in topaz $Al_2SiO_4(OH,F)_2$. *Journal of Luminescence*, Vol. 102–103, pp. 349–356, http://dx.doi.org/10.1016/S0022-2313(02)00532-X

Gautier D'Agoty F. (1781) *Histoire naturelle ou exposition générale de toutes ses parties, gravées et imprimées en couleurs naturelles. 1. Règne minéral*. Paris (self-published).

Gauzzi T., Graça L.M., Lagoeiro L., Mendes I.C., Queiroga G.N. (2018) The fingerprint of imperial topaz from Ouro Preto region (Minas Gerais state, Brazil) based on cathodoluminescence properties and chemical composition. *Mineralogical Magazine*, Vol. 82, No. 4, pp. 943–960, http://dx.doi.org/10.1180/minmag.2017.081.078

Goldschmidt V.M., Peters C. (1933) Zur Geochemie des Germaniums. *Nachrichten von der Gesellschaft der Wissenschaften zu Göttingen. Mathematisch-Physikalische Klasse, Fachgruppe IV*, Vol. 33, pp. 141–166.

Greenidge D. (2018) Investigations of color center phenomena in topaz and quartz through electron spin resonance with reference to optical absorption and nuclear magnetic resonance: Implications for extended mineral applications. *Malaysian Journal of Fundamental and Applied Sciences*, pp. 142–149, http://dx.doi.org/10.11113/mjfas.v14n1-2.958

Griffin W.L., Powell W., Pearson N.J., O'Reilly S.Y. (2008) GLITTER: Data reduction software for laser ablation ICP-MS. In P. Sylvester, Ed., *Laser Ablation ICP-MS in the Earth Sciences: Current Practices and Outstanding Issues*. Mineralogical Association of Canada, Québec, pp. 308–311.

Haüy R.J. (1801) *Traité de Minéralogie*. Chez Louis, Paris.

Henckel J.F. (1737) De Topasio vera Saxonum, orientali non inferiore. *Acta Physico-Medica Academiae Caesareae Leopoldino-Carolinae Naturae Curiosorum*, Vol. 4, pp. 316–320.

Hoover D.B., Theisen A.F. (1993) Fluorescence excitation-emission spectra of chromium-containing gems: An explanation for the effectiveness of the crossed filter method. *Australian Gemmologist*, Vol. 18, No. 6, pp. 182–187.

Jarosewich E. (2002) Smithsonian microbeam standards. *Journal of Research of the National Institute of Standards and Technology*, Vol. 107, No. 6, pp. 681–685, https://doi.org/10.6028/jres.107.054

Jäschke U., Unger B. (2007) *Der Vogtlandatlas. Regionalatlas zur Natur, Geschichte, Bevölkerung, Wirtschaft, Kultur des sächsischen Vogtlands*. Klaus Gumnior, Chemnitz, Germany.

Jiang X., Zhang Z., Wang Y, Kong F. (2020) Gemmological and spectroscopic characteristics of different varieties of amber from the Hukawng Valley, Myanmar. *Journal of Gemmology*, Vol. 37, No. 2, 144–162.

Jochum K.P., Weis U., Stoll B., Kuzmin D., Yang Q., Raczek I., Jacob D.E., Stracke A., Birbaum K., Frick D.A., Günther D., Enzweiler J. (2011) Determination of reference values for NIST SRM 610–617 glasses following ISO guidelines. *Geostandards*

and Geoanalytical Research, Vol. 35, pp. 397–429, http://dx.doi.org/10.1111/j.1751-908X.2011.00120.x
Jochum K.P., Weis U., Schwager B., Stoll B., Wilson S.A., Haug G.H., Andreae M.O., Enzweiler J. (2016) Reference values following ISO guidelines for frequently requested rock reference materials. *Geostandards and Geoanalytical Research*, Vol. 40, No. 3, pp. 333–350, http://dx.doi.org/10.1111/j.1751-908X.2015.00392.x
Jones Z., Hinds J., Woznichak S., Calamai A. (2020) Revisiting the room-temperature metastable ^2E lifetime in ruby for an upper division phosphorescence laboratory experiment. *Journal of Undergraduate Reports in Physics*, Vol. 30, No. 100004, http://dx.doi.org/10.1063/10.0002044
Kern J.G. (1776) *Vom Schneckensteine oder dem sächsischen Topasfelsen*. Edited and published by I.E. von Born. Wolfgang Gerle, Prague.
Kisliuk P., Moore C.A. (1967) Radiation from the $^4T_2$ state of Cr^{3+} in ruby and emerald. *Physical Review*, Vol. 160, No. 2, pp. 307–312, http://dx.doi.org/10.1103/PhysRev.160.307
Kruzslicz Á.B., Nasdala L., Wildner M., Škoda R., Redhammer G.J., Hauzenberger C., Wanthanachaisaeng B. (2020) Black spinel – a gem material from Bo Phloi, Thailand. *Journal of Gemmology*, Vol. 37, No. 1, pp. 66–79.
Krzemnicki M.S. (2017) Rarities and collector stones recently tested at SSEF. *Facette*, No. 23, pp. 8–10.
Lahl B. (2012) *Königliche Topase vom Schneckenstein – Edelsteine aus dem Vogtland*. Chemnitzer Verlag, 144 pp.
Leithner H. (2008) Famous mineral localities: The Königskrone topaz mine, Schneckenstein, Saxony, Germany. *Mineralogical Record*, Vol. 39, No. 5, pp. 355–367.
Luo Y., Breeding C.M. (2013) Fluorescence produced by optical defects in diamond: measurement, characterization, and challenges. *G&G*, Vol. 49, No. 2, pp. 82–97, http://dx.doi.org/10.5741/GEMS.49.2.82
Marfunin A.S. (1979) *Spectroscopy, Luminescence and Radiation Centers in Minerals*. Springer, Berlin, 352 pp.
Mohs F. (1822) *Grund-Riß der Mineralogie. Erster Theil: Terminologie, Systematik, Nomenklatur, Charakteristik*. Arnold'sche Buchhandlung, Dresden.
Nasdala L., Wildner M., Giester G., Chanmuang N. C., Scicchitano M.R., Hauzenberger C. (2021) Blue dravite ("indicolite") from the Elahera gem field, Sri Lanka. *Journal of Gemmology*, Vol. 37, No. 6, pp. 618–630.
O'Bannon E.F., Williams Q. (2019) A Cr^{3+} luminescence study of natural topaz $Al_2SiO_4(F,OH)_2$ up to 60 GPa. *American Mineralogist*, Vol. 104, No. 11, pp. 1656–1662, http://dx.doi.org/10.2138/am-2019-7079
Petrov I. (1977) Farbuntersuchungen an Topas. *Neues Jahrbuch für Mineralogie, Abhandlungen*, Vol. 130, No. 3, pp. 288–302.
——— (1978) Farbe, Farbursachen und Farbveränderungen bei Topasen. *Zeitschrift der Deutschen Gemmologischen Gesellschaft*, Vol. 27, pp. 3–11.
Petrov I., Schmetzer K., Eysel H.H. (1977) Absorptionsspektren von Chrom in Topas. *Neues Jahrbuch für Mineralogie Monatshefte*, Vol. 8, pp. 365–372.
Pinheiro M.V.B., Fantini C., Krambrock K., Persiano A.I.C., Dantas M.S.S., Pimenta M.A. (2002) OH/F substitution in topaz studied by Raman spectroscopy. *Physical Review B*, Vol. 65, pp. 1–6, http://dx.doi.org/10.1103/PhysRevB.65.104301
Ribbe P.H., Rosenberg P.E. (1971) Optical and X-ray determinative methods for fluorine in topaz. *American Mineralogist*, Vol. 56, pp. 1812–1821.
Schott S., Rager H., Schürmann K., Taran M. (2003) Spectroscopic study of natural gem quality "Imperial"-topazes from Ouro Preto, Brazil. *European Journal of Mineralogy*, Vol. 15, No. 4, pp. 701–706, http://dx.doi.org/10.1127/0935-1221/2003/0015-0701
Schröder M. (1915) *Erläuterungen zur geologischen Spezialkarte des Königsreiches Sachsen, Nr. 144, Blatt Falkenstein*. Wilhelm Engelmann, Leipzig, 81 pp.
Schrön W. (1968) Ein Beitrag zur Geochemie des Germaniums. *Chemie der Erde*, Vol. 27, pp. 193–251.
Sebastian U. (2013) *Die Geologie des Erzgebirges*. Springer Spektrum, Berlin, Heidelberg, 270 pp.
Seim R., Schweder P. (1969) Untersuchungen zum Germaniumgehalt im Topas. *Chemie der Erde*, Vol. 28, pp. 83–90.
Smith C.P. (2020) ColorCodex™ – A new tool for the gemstone and jewelry industry. *InColor*, No. 45, pp. 84–90.
Taran M.N., Tarashchan A.N., Rager H., Schott St., Schürmann K., Iwanuch W. (2003) Optical spectroscopy study of variously colored gem quality topazes from Ouro Preto, Minas Gerais, Brazil. *Physics and Chemistry of Minerals*, Vol. 30, No. 9, pp. 546–555, http://dx.doi.org/10.1007/s00269-003-0356-9
Tarashchan A.N., Taran M.N., Rager H., Iwanuch W. (2006) Luminescence spectroscopic study of Cr^{3+} in Brazilian topazes from Ouro Preto. *Physics and Chemistry of Minerals*, Vol. 32, No. 10, pp. 679–690, http://dx.doi.org/10.1007/s00269-005-0042-1
Tichomirowa M., Leonhardt D. (2010) New age determinations (Pb/Pb zircon evaporation, Rb/Sr) on the granites from Aue-Schwarzenberg and Eibenstock, Western Erzgebirge, Germany. *Zeitschrift für Geologische Wissenschaften*, Vol. 38, No. 1–2, pp. 99–123.
Toya T., Kato A. (1983) *JEOL Practical techniques for microprobe analysis*. JEOL Training Center, Tokyo, 193 pp.
Tsai T.-H., D'Haenens-Johansson U.F.S. (2021) Rapid gemstone screening and identification using fluorescence spectroscopy. *Applied Optics*, Vol. 60, No. 12, pp. 3412–3421, http://dx.doi.org/10.1364/AO.419885
Twelvetrees W.H., Petterd W.F. (1897) On the topaz quartz porphyry or stanniferous elvan dykes of Mount Bischoff. *Papers and Proceedings of the Royal Society of Tasmania*, pp. 119–128.
Vollstädt H., Lahl B. (1997). Der Schneckenstein. In M. Glas, Ed., *Topas – Das prachtvolle Mineral, der lebhafte Edelstein*. extraLapis, No. 13, pp. 26–37.
Whitney D.L., Evans B.W. (2010) Abbreviations for names of rock-forming minerals. *American Mineralogist*, Vol. 95, No. 1, pp. 185–187, http://dx.doi.org/10.2138/am.2010.3371
Wilson W.E. (1995) Fabien Gautier d'Agoty and his 'Histoire Naturelle Regne Mineral' (1781). *Mineralogical Record*, Vol. 26, No. 4, pp. 65–76.
Wright J.H., Kwak T.A.P. (1989) Tin-bearing greisens of Mount Bischoff, northwestern Tasmania, Australia. *Economic Geology*, Vol. 84, No. 3, pp. 551–574, http://dx.doi.org/10.2113/gsecongeo.84.3.551
Zeug M., Nasdala L., Wanthanachaisaeng B., Balmer W.A., Corfu F., Wildner M. (2018) Blue zircon from Ratanakiri, Cambodia. *Journal of Gemmology*, Vol. 36, No. 2, pp. 112–132.
Zhang Z., Jiang X., Wang Y., Kong F., Shen A.H. (2020) Fluorescence characteristics of blue amber from the Dominican Republic, Mexico, and Myanmar. *G&G*, Vol. 56, No. 4, pp. 484–496, http://dx.doi.org/10.5741/GEMS.56.4.484

History of Emerald Mining in the Habachtal Deposit of Austria, Part II

Karl Schmetzer

Published information about the history of the Habachtal emerald mine in the era between World War I and World War II is limited and superficial. Subsequent to the departure of Emerald Mines Limited, the English company that had owned the property since 1896, the Habachtal mine was owned or controlled by Austrian, Swiss, Italian, or German companies or citizens. The names of various companies and individuals who were actively mining for some time in the Habach Valley are mentioned in numerous papers, books, or newspapers. The relationships between them and the property owners mentioned in files of the Mittersill land registry office are frequently unknown and the reasons for numerous transitions of ownership, followed by changes of the mining entities that operated the deposit, are not clearly seen. Using a wide selection of materials from Austrian and German archives, largely unpublished, the author seeks to trace the history of the Habachtal mine through this period and to fill the gaps left by existing publications. Activities and events after 1945 and the present situation are also briefly described.

In the first part of this article, it has been shown that no regular mining occurred in the Habach Valley up until the end of the eighteenth century. After the secondary deposit in Habachtal was described in 1797, emeralds were collected in the valley, and regular mining commenced in the early 1860s after the discovery of the primary deposit. For several decades, from about 1865 to 1895, only minor activities took place in the primary and secondary parts of the deposit. In contrast, major activities with up to 30 miners are seen under English guidance and ownership by Emerald Mines Limited, from 1896 to 1913. Thereafter, the ownership reverted to three Austrian citizens: Alois Kaserer, Johann Blaikner, and Peter Meilinger, all landowners and farmers in the area. However, the outbreak of World War I prevented them from starting any regular mining on a larger scale and prompted them to sell the property. This is the starting point for part two of the Habachtal investigation.

The first half of the twentieth century brought numerous transitions in ownership and various mining activities (see figure 1) that also have, until now, not been described in detail with regard to the unpublished original documents preserved mainly in Austrian and German archives. In part two, the focus is laid upon this era. It will illustrate the problems that occurred in emerald mining, the individuals involved, and their success or failure in emerald recovery in Austria.

MINING HISTORY OF THE HABACHTAL EMERALDS (1916–1939)

Property Under Anton Hager and Peter Staudt (1916–1927). In October 1916, landowners Kaserer, Blaikner, and Meilinger resold the property for 15,000 Kronen (approximately US$1,900 at the time) to Anton Hager (figure 2), an Austrian citizen then residing in Traunstein, Germany.[1] Prior to that transaction, Hager had already applied for several exploration permits in the area.[2] Circa 1917, an

See end of article for About the Author and Acknowledgments.
Gems & Gemology, Vol. 58, No. 1, pp. 18–46,
http://dx.doi.org/10.5741/GEMS.58.1.18

[1]Notarized contract between Alois Kaserer/Johann Blaikner/Peter Meilinger and Anton Hager, October 26, 1916, Mittersill land registry office, Archive of Salzburg Federal State; Habachtal emerald mine file, entry January 5, 1917, Mittersill land registry office. Anton Hager (1872–1940) was a timber merchant involved in his stepfather's company at Traunstein, originally hailing from the area of Zell am See in the Pinzgau and then living in Traunstein from 1900 to 1926. He moved in 1926 to the community of Gnigl (which in 1935 became part of Salzburg). Franz Haselbeck, Traunstein City Archive, pers. comm., 2020; Brigitte Leitermann, granddaughter of Peter Staudt, pers. comm., 2020.

[2]File Bezirkshauptmannschaft Zell am See, BH Zell 1936 A1 – 7587, Archive of Salzburg Federal State.

Figure 1. The Madonna emerald, on permanent display at Bramberg Museum, is an exceptional specimen found at the Habachtal deposit in 1970. It measures approximately 30 cm tall. Photo by K. Schmetzer; courtesy of Alois Steiner.

Figure 2. In October 1916, the Habachtal mine was purchased by timber merchant Anton Hager, an Austrian citizen residing in Traunstein, Germany. Photo circa 1925; courtesy of B. Leitermann.

anonymous memorandum was written, likely by Hager, describing the history of the Habachtal emerald mine and its current condition.[3] Certain comments hinted at a possible intent for future emerald mining, and it was noted that the adit to the D gallery was still blocked by rocks and needed to be reopened.

In July 1918, Hager began efforts to restore the property with five laborers, and that work continued in the following years.[4] Additional exploration permits were sought by Hager in 1918, and he also applied that same year for permits for talc production near the emerald deposit.[5] During that era, talc was mined for various applications such as cosmetics, pharmaceutical products, glass, specialized papers, leather, textiles, and soap.[6] Mining engineer Heinrich Stuchlik (figure 3) of Traunstein provided Hager with estimates for a supply of 200 wagons per year with a reserve for 100 years, even speculating as to whether the talc occurrence might extend over the mountain ridge to allow economic mining for talc in the adjacent Hollersbach Valley as well.[7]

Beginning in August 1918, Hager searched for a chemist and/or a partner to invest alongside him in the Habachtal venture.[8] A figure of 800,000 Kronen was proposed as the amount necessary for mining and transport of the rough talc downhill.[9] Finding no takers, in September 1920 Hager sold a one-half interest in the property to his half-brother Peter Staudt (figure 4) from Traunstein for 31,000 Kronen[10] (approximately US$100 at the time). An entity under the name Talk- und Edelsteinbergwerk Habachthal (Talc and Gemstone Mine Habachthal) was founded in 1920 for purposes of the venture.[11] Hager and Staudt resumed emerald mining that same year[12] and continued to consider activities in the area not related to gemstones, such as the extraction of talc and even asbestos from the schistose rocks.[13]

Investigation of mining prospects proceeded in 1920 and 1921. Inspection reports of the area were pre-

[3]Anonymous, Das Smaragd-Bergwerk im Habachthale, Archive of the Municipality of Bramberg, circa 1917, 6 pp. The exposé was prepared on stationery from the desk of "Carl Staudt, Holzhandlung, Traunstein" and likely written by Hager.

[4]File "Beryll Bramberg," mining documents collected by W. Günther, Archive of the Bergbau- und Gotikmuseum Leogang.

[5]File Bezirkshauptmannschaft Zell am See, BH Zell 1936 A1 – 7587, Archive of Salzburg Federal State.

[6]Wenzel, 1921.

[7]Letters from Heinrich Stuchlik to Anton Hager (dated December 5, 1918, August 7, 1919, and August 12, 1921), Archive of the Municipality of Bramberg. Stuchlik was born in the Austrian part of Silesia near Troppau, now in the Czech Republic, and studied at the Imperial and Royal School of Mining in Leoben. Early in life, Stuchlik focused on coal, publishing in 1887 about the deposit in his home village of Schönstein. In the late 1880s, he moved to Bavaria and worked at the coal deposit in the Peissenberg area, serving from 1897 to 1905 as head of the mining administration. From 1905 to 1912, he was the administrator for the saltworks of Traunstein. During World War I, Stuchlik was involved in mining in Romania. See Haselbeck, 2019.

[8]*Salzburger Volksblatt*, Vol. 48, No. 179, August 7, 1918, p. 5.

[9]Letter from unknown sender (signature illegible) to Anton Hager, August 19, 1919, Archive of the Municipality of Bramberg.

[10]Notarized contract between Anton Hager and Peter Staudt, September 27, 1920, Mittersill land registry office, Archive of Salzburg Federal State; Habachtal emerald mine file, entry December 4, 1920, Mittersill land registry office. Peter Staudt (1883–1948) was a timber merchant in Traunstein, leading a large company with up to 20 workers that had been founded by his father Carl Staudt in 1897 and remained in existence until 1928. Franz Haselbeck, Traunstein City Archive, pers. comm., 2020; Brigitte Leitermann, granddaughter of Peter Staudt, pers. comm., 2020.

[11]File "Beryll Bramberg," mining documents collected by W. Günther, Archive of the Bergbau- und Gotikmuseum Leogang; Compass, Industrielles Jahrbuch – Österreich, Vol. 61, 1928, p. 388.

[12]File Bezirkshauptmannschaft Zell am See, BH Zell 1936 A1 – 7587, Archive of Salzburg Federal State; *Salzburger Volksblatt*, Vol. 58, No. 240, October 18, 1928, p. 7; Grundmann, 1979; Lausecker, 1986; Lewandowski, 1997; Düllmann, 2009.

[13]*Salzburger Volksblatt*, Vol. 54, No. 174, July 31, 1924, p. 7.

Figure 3. In the late 1910s and early 1920s, mining engineer and administrator Heinrich Stuchlik evaluated the Habachtal property for Hager, focusing in particular on the use of the deposit for industrial recovery of talc. He also prepared a subsequent report in 1928 during the mine's ownership by the Swiss firm Aktiengesellschaft für modernen Bergbau. Photo circa 1910; courtesy of the Historical Archive of the City of Traunstein.

Figure 4. Following an unsuccessful search for a partner to invest in the Habachtal venture, Hager sold a one-half interest in the property to his half-brother Peter Staudt (pictured), also a timber merchant from Traunstein. Photo circa 1925; courtesy of B. Leitermann.

pared by engineer Ludwig Autzinger of the firm Abihag in Linz and Graz[14] (who also published his results in 1922) and by mine foreman Johann Hanisch (figure 5),[15] and chemical analyses of talc were commissioned from laboratories in Salzburg, Vienna, and Munich. Besides noting that the mine was well maintained and all entries to the four galleries were accessible, Autzinger focused on potential production.[16] For talc, he calculated 400 railway wagons (with 10,000 kg per wagon) per year by open-pit mining, with reserves for 200 years. For emerald, Autzinger used a wildly optimistic yield reported to him for the period of the English ownership of 5 kg (25,000 carats) of clean emeralds per week and projected similar totals. (Note that this figure was never reached even during one complete season, and such a weekly yield would have made selling the mine financially irrational.) Hanisch's report centered on the mine's condition and recent efforts to prepare it for operation, advising that the previously decrepit galleries had been renovated in 1920 and that safety measures had been undertaken.[17] Also in 1920, H. Obpacher of the Mineralogical-Geological Laboratory at the Munich Technical University examined

[14]Ludwig Autzinger (1890–1964) studied civil engineering at the Technical University of Vienna from 1908 to 1915 and served as an assistant at the school in 1917. He subsequently worked in various industrial capacities, including director of a fertilizer factory. In 1939 he emigrated to the United States.

[15]Johann Hanisch (b. 1885) was a foreman at the Mitterberg copper mine (owned by Mitterberger Kupfer-Aktiengesellschaft) near Mühlbach at the Höchkönig from 1916 to 1924. The deposit had been known since the Bronze Age.

[16]Autzinger L., Über das Talk- und Smaragdbergwerk in Habach, Post Bramberg im Pinzgau, July 1920, 4 pp. + map, Archive of the Municipality of Bramberg; see also Autzinger, 1922.

[17]Hanisch J., Bericht über den Smaragdbergbau oberhalb der Söllalpe im Habachtal, January 20, 1921, 2 pp., Archive of the Municipality of Bramberg.

Figure 5. In 1920 Johann Hanisch, foreman at the Mitterberg copper mine near Mühlbach, prepared one of the reports commissioned by Hager and Staudt in view of resuming mining operations after World War I. Photo circa 1920; archive of W. Günther at Mining and Gothic Museum Leogang.

the talc-bearing rocks. Petrographic thin sections were prepared to determine the mineral assemblage, and methods for processing and cleaning the talc and asbestos were evaluated.[18]

Based on the production figures provided by Autzinger, a detailed business plan was developed by K.E. Moldenhauer from the Institute for Chemical Technology at the Munich Technical University and presented to Hager and Staudt in December 1920.[19] The cost for open-pit mining of talc, underground mining of emeralds, and transportation of the ore downhill was estimated, as was the outlay for recommended supporting facilities. An electric power plant was to be built, along with facilities for separating emeralds from host rock, grinding and sieving talc ore, magnetic separation of iron-bearing components, and drying, weighing, packing, and transporting the refined talc powder to the railway station. The emerald and talc business lines were said to require a combined investment in the range of 8,500,000 German marks (approximately US$150,000 at the time). Nonetheless, the enterprise was expected to be profitable based on the unrealistic estimated 5 kg per week yield and value of 250,000 marks per kilogram of emerald rough, amounting to weekly revenue of 1,250,000 marks (approximately US$22,000) from the emerald line alone.

In Brief

- The Habachtal property was purchased in 1916 by the Austrian Anton Hager, who mined it with his German half-brother Peter Staudt until 1927.
- In 1927, the mine was sold to the Swiss company Aktiengesellschaft für modernen Bergbau.
- Beginning in 1932, control of the Habachtal mine became a subject of ongoing legal controversies between different parties. Against that backdrop, the mine was leased to an Italian citizen. Ownership was then transferred in 1933 to three German and Swiss individuals: Max Gaab, Meta Geist, and Florian Prader.
- After the conflicts were resolved, the Swiss firm Smaragd Aktiengesellschaft, formed in 1934, took over mining activities from 1935 to 1939.
- German lawyer Max Gaab acquired another part of the mine in 1941, and ownership has remained with Gaab's descendants since his death in 1953.

In 1921, Hager and Staudt applied for and received the requisite working permits for the mine, and an application for permission to install the plant and transport facilities for the talc production was filed by Hager the same year. Operations on site in 1921 were supervised by Austrian mining engineer Josef Gerscha (1864–1941, figure 6), who was forced to deal with the lack of proper maintenance of the galleries for more than a decade following the activities of the English proprietors.[20]

While talc production seems never to have advanced beyond preliminary or experimental stages, and the intended facilities were never constructed,

[18]Obpacher H., Begutachtung von Gesteins- und Mineralproben (vorgelegt von Dipl. Ing. Moldenhauer) aus dem Talk-Asbest- und Smaragdvorkommen im Habachtal am Grossvenediger, December 18, 1920, 9 pp., Archive of the Municipality of Bramberg.

[19]Moldenhauer K.E., Das Talkum-, Asbest- und Smaragd-Vorkommen im Habachtal (Oberpinzgau) und seine Verwertung, December 1920, 36 pp, Archive of the Municipality of Bramberg.

[20]File Bezirkshauptmannschaft Zell am See, BH Zell 1936 A1 – 7587, Archive of Salzburg Federal State; Schiffner, 1940; File "Beryll Bramberg," mining documents collected by W. Günther, Archive of the Bergbau- und Gotikmuseum Leogang.

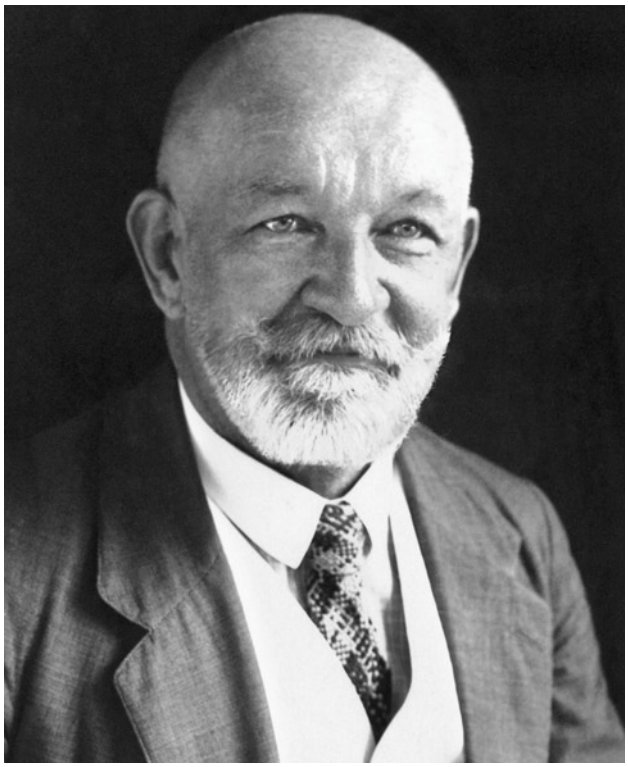

Figure 6. Efforts in 1921 to return the Habachtal mine to production were overseen by Austrian mining engineer Josef Gerscha, who had to contend with the fact that the tunnels had not been maintained for several years. Undated photo; archive of the TU Bergakademie Freiberg, Germany.

emerald mining was undertaken on a larger scale.[21] An unknown number of workers was employed in the enterprise, and Anton Hager Jr. (figure 7), son of the owner, joined in the effort.[22] Between 1923 and 1926, extensions were added to the extremities of the D gallery tunnel system (figures 7 and 8) and German

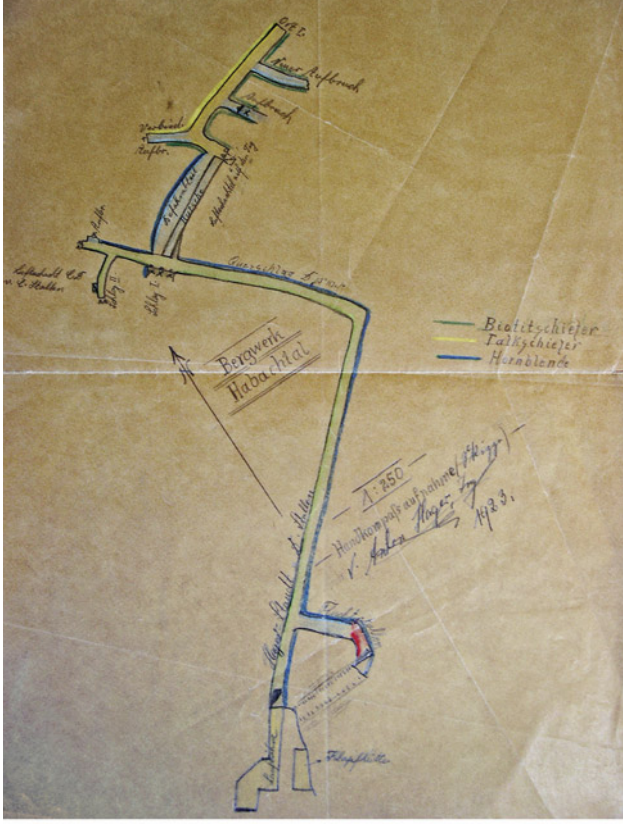

Figure 7. Top: This map of the D gallery drawn by Anton Hager Jr. in 1923 shows that the far reaches of tunnel system intersected the targeted emerald-bearing talc- and biotite-schists (light blue and yellow). Courtesy of E. Burgsteiner. Bottom: Engineer Anton Hager Jr. was the son of the mine owner. Photo circa 1927 in front of the adit to the mine; courtesy of B. Leitermann.

Dr. Max Brennekam (figure 9) took over responsibility as mining engineer for operations.[23] The record indicates that Hager and Staudt experienced solid emerald production in some years but that market-

[21]See Fritz, 1972.

[22]Anton Hager Jr. (1902–1980) was born in in Traunstein. He later studied mechanical engineering at the engineering school in Mittweida, Saxony, from 1921 to 1923.

[23]Dr. Max Brennekam (1870–1954) studied at the universities of Tübingen, Halle, and Greifswald and wrote a dissertation on the philosophy of Immanuel Kant (1895). In the following years, he worked as a schoolteacher in the Berlin region. After World War I, Brennekam shifted his focus to mining, spending a period from 1921 to 1928 in Austria. Together with his son Otto Brennekam (1899–1960), he served on the board of directors of the firm Kohle und Erz Aktiengesellschaft, which was founded in 1923 in Berlin and operated several gold mines in Austria. The 1940s found Brennekam as the owner of a feldspar mining company in Tirschenreuth, Bavaria. *Montanistische Rundschau*, Vol. 15, No. 22, 1923, p. 525; letter from K. Martius to W. von Seidlitz, June 21, 1938, Lagerstättenarchiv Österreichische Geologische Bundesanstalt Wien; Eberl, 1972; Beate Heinrich, Archive of the Municipality of Tirschenreuth, pers. comm., 2020.

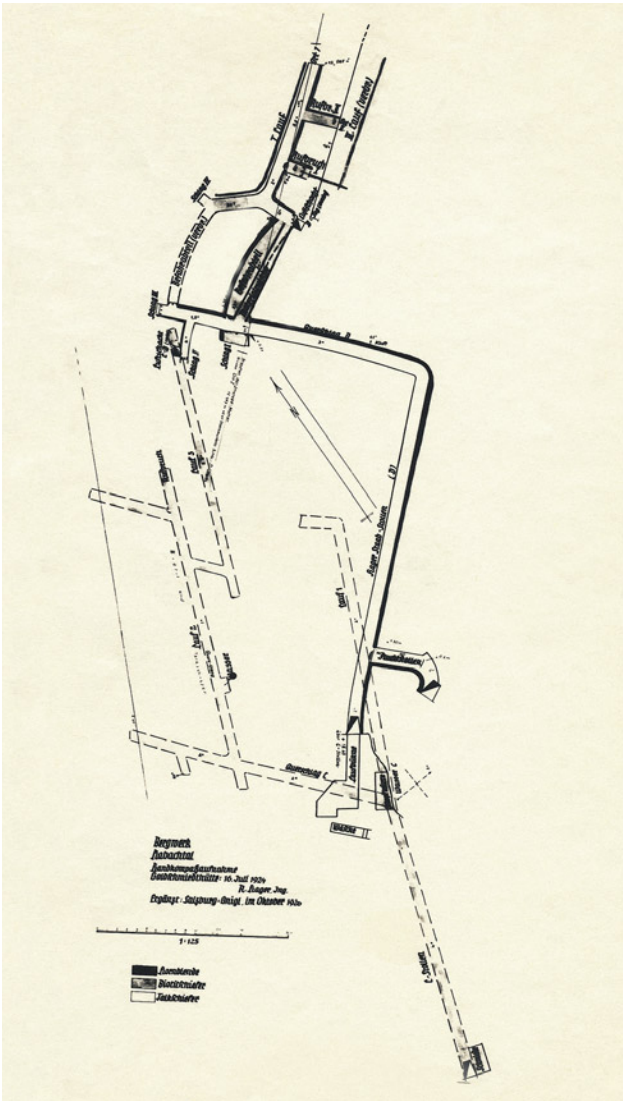

Figure 8. Map of the C and D galleries of the Habachtal emerald mine, the oldest known sketch showing both galleries, drawn by Anton Hager Jr. in 1924 and updated in 1926. Archive of the municipality of Bramberg.

ing and sales were ineffective.[24] Meanwhile, in February 1924 an option to purchase the property was recorded with the Mittersill land registry by Hager and Staudt in favor of Adolf Eichmann, an investor and merchant of electrical devices from Linz, but it terminated the same year without exercise.[25]

Conflicts Over Interests in the Property (1927–1934). The property was eventually sold in October 1927, and ownership transferred along with several exploration permits held by Hager to the Swiss firm Aktiengesellschaft für modernen Bergbau, located in Chur.[26] This company had been registered in October 1927, with a stated capital of 100,000 Swiss francs (approximately US$19,000 at the time) and an initial board of directors consisting of Alfred Mannesmann (president) and Hermann Hoesch, both German industrialists; Hans Nipkow (vice president), Emil Frey, Bartholome Jeger, and Florian Prader (figure 10),[27] all Swiss engineers or bankers; Conde de Santa Maria de la Sisla, a Spanish citizen and member of parliament representing Madrid; and Christian Buol, a lawyer from Zurich. A German banker named Justus H. Vogeler replaced Buol in 1929.[28] A local office was set up in the Senningerbräu, an inn in Bramberg.[29] The purchase price was 66,000 Swiss francs, to be paid in two equal installments by January 1 and May 1, 1928, respectively,[30] and liens were recorded against the property to ensure full payment.

After the sale, mining resumed for approximately four weeks in the name of the new owner. Brennekam and Anton Hager Jr. stayed on, providing operational guidance for a team of eight miners.[31] The emerald-bearing rocks were hauled in containers from the mine down to the valley in Bramberg for washing and crystal separation, the same procedure that had been utilized by Hager and Staudt for some time.[32]

Such efforts notwithstanding, regulatory and financial problems quickly intervened. Brennekam, serving as local representative for the mine owner, was directed to apply for a working permit for the Swiss Aktiengesellschaft für modernen Bergbau, but

[24]Eberl, 1972.

[25]Option declaration given by Anton Hager/Peter Staudt in favor of Adolf Eichmann, February 24, 1924, Mittersill land registry office, Archive of Salzburg Federal State; Grundmann, 1979.

[26]Notarized contract between Anton Hager/Peter Staudt and Aktiengesellschaft für modernen Bergbau, October 13, 1927, Mittersill land registry office, Archive of Salzburg Federal State; Habachtal emerald mine file, entry November 30, 1927, Mittersill land registry office; *Montanistische Rundschau*, Vol. 20, No. 9, 1928, p. 278.

[27]Florian Prader (1883–1946), a Swiss engineer from Zurich, owned several construction companies engaged in the building of railways, bridges, and power plants. *Schweizerische Bauzeitung*, Vol. 127, No. 12, March 23, 1946, pp. 148–149.

[28]*Schweizerisches Handelsamtblatt*, Vol. 45, No. 249, October 24, 1927, p. 1874; Vol. 47, No. 257, November 2, 1929, p. 218.

[29]Lausecker, 1986.

[30]Notarized contract between Anton Hager/Peter Staudt and Aktiengesellschaft für modernen Bergbau, October 13, 1927, Mittersill land registry office, Archive of Salzburg Federal State; Habachtal emerald mine file, entry November 30, 1927, Mittersill land registry office.

[31]File Bezirkshauptmannschaft Zell am See, BH Zell H1 2286-1933, Archive of Salzburg Federal State.

[32]Ibid. See also Leitmeier, 1929/1930 (recounting a presentation given in March 1929 but adding observations from summer 1929 at the locality prior to final publication in 1930).

Figure 9. Dr. Max Brennekam guided mining operations on site during the 1920s, when the property was owned by Anton Hager and Peter Staudt. After the mine was sold to the Swiss entity Aktiengesellschaft für modernen Bergbau, he stayed on for several weeks at the end of 1927, but he left Austria in mid-1928. Brennekam is shown with a group of miners at the entrance to one of the galleries during the 1920s. The inset portrait of Brennekam is circa 1927. Photos courtesy of E. Burgsteiner.

Figure 10. The Swiss engineer Florian Prader served as one of the directors of Aktiengesellschaft für modernen Bergbau, which purchased the Habachtal property in 1927. He later loaned money to the company and subsequently joined with Max Gaab and Meta Geist in purchasing the Habachtal property out of foreclosure in 1933. Undated photo from Schweizerische Bauzeitung *(1946).*

he was unable to do so in the absence of consent from Switzerland, which was not forthcoming over several months. Brennekam left Bramberg and moved back to Berlin in June 1928.[33]

The company also failed to pay the second installment of the purchase price, leading Hager and Staudt to initiate foreclosure proceedings.[34] The property was valued at 67,000 Austrian shillings, and the lowest acceptable purchase price was deemed to be 44,354 shillings (equivalent to the unpaid 33,000 Swiss francs).[35] The auction scheduled for December 1, 1928, was averted, however, when Aktiengesellschaft für modernen Bergbau was able to obtain a loan of 50,000 reichsmark (equivalent to about US$11,900 at the time) on November 6 from Hans (Johann) Streubert, a mine owner and entrepreneur from Munich who also held interests in the neighboring Hollersbach Valley.[36]

Hager and Staudt were paid the remaining purchase price, and their liens against the property were released on November 9, 1928,[37] while a new lien in favor of Streubert was recorded at the Habachtal emerald mine file of the Mittersill land registry office. Considering all the information available, Staudt had lost a substantial amount of money operating the Habachtal mine.[38] Approximately two weeks later, on November 21, 1928, Streubert transferred his interest in the three-year loan in equal parts to Max Gaab (figure 11) and Meta Geist (figure 12).[39]

In December 1928, Smaragd-Bergbau Habachtal GmbH was founded in Mittersill to serve as the Austrian operating entity for the Swiss owner. Streubert, working from Munich, led the new firm.[40] However, no regular mining took place from 1928 through the

[33]File Bezirkshauptmannschaft Zell am See, BH Zell H1 2286-1933, Archive of Salzburg Federal State.

[34]*Salzburger Volksblatt*, Vol. 58, No. 240, October 18, 1928, p. 7; Vol. 58, No. 243, October 22, 1928, p. 8; Vol. 58, No. 244, October 23, 1928, p. 8.

[35]*Reichspost*, Vol. 35, No. 293, October 20, 1928, p. 7; *Linzer Volksblatt*, Vol. 60, No. 246, October 23, 1928, p. 9.

[36]Notarized contract between Hans Streubert and Aktiengesellschaft für modernen Bergbau, November 6, 1928, Mittersill land registry office, Archive of Salzburg Federal State; see also *Salzburger Chronik*, Vol. 64, No. 275, November 30, 1928, p. 4; *Reichspost*, Vol. 35, No. 335, December 2, 1928, p. 7. Hans (Johann) Streubert (1866–1941) was born in Regenstauf, near Regensburg, Bavaria. He later resided in Munich and was active in mining operations at various localities in Austria. Between 1925 and 1929, he was one of the owners of the company Hollersbacher Zink- und Bleibergwerke. *Grazer Volksblatt*, Vol. 47, No. 69, February 21, 1914, p. 6; *Montanistische Rundschau*, Vol. 11, No. 6, 1919, p. 182; Vol. 15, No. 7, 1923, p. 115; Vol. 15, No. 16, 1923, p. 352; *Salzburger Volksblatt*, Vol. 55, No. 295, December 30, 1925, p. 7; *Compass, Industrielles Jahrbuch - Österreich*, Vol. 60, 1927, p. 410; *Salzburger Volksblatt*, Vol. 58, No. 186, August 14, 1928, p. 9.

[37]Notarized contract between Anton Hager/Peter Staudt and Aktiengesellschaft für modernen Bergbau, November 9, 1928, Mittersill land registry office, Archive of Salzburg Federal State.

[38]Peter Staudt thereafter closed his timber company in Traunstein in December 1928 and subsequently worked for the administration of the city of Traunstein. Company registration file, entry December 6, 1928, Archive of the City of Traunstein (Stadtarchiv Traunstein); Brigitte Leitermann, granddaughter of Peter Staudt, pers. comm., 2020.

[39]Notarized contract between Hans Streubert and Max Gaab/Meta Geist, November 21, 1928, Mittersill land registry office, Archive of Salzburg Federal State. Max Gaab (1866–1953) was a lawyer from Munich. Meta Geist (1879–1966), residing in Munich and Fischbachau, Bavaria, was the daughter of food and coffee merchant Adolph Brougier and the widow of Theodor Geist, owner of Geist & Breuninger, a grain wholesaler in Munich. Gaab's private apartment and the office of his law firm, both in Munich, were destroyed during World War II, leaving no documentation regarding events before 1945. Ingrid von Klitzing, granddaughter of Max Gaab, pers. comm., 2020.

[40]Although Hans Streubert worked from a Munich office, the company was registered only in Austria and not in Germany.

Figure 11. At the end of the 1920s, Munich lawyer Max Gaab acquired a one-half interest in a loan that had been extended to Aktiengesellschaft für modernen Bergbau, the Swiss owner of the mine, and also made an additional loan to the company. In the ensuing years, Gaab and his family would become the sole owners of the Habachtal property. Photo from the 1920s; courtesy of Ingrid von Klitzing.

Figure 12. The remaining one-half interest in the 1928 loan to Aktiengesellschaft für modernen Bergbau was transferred to the wealthy widow Meta Geist, living in Munich and Fischbachau, Bavaria, who supported Max Gaab in his efforts and investments. Photo circa 1940; courtesy of Ingrid von Klitzing.

remaining period of Aktiengesellschaft für modernen Bergbau's ownership.[41] Instead, only limited exploration, maintenance of the tunnels, and trial mining ensued.[42] In June 1929, Gaab loaned a further 5,000 reichsmark (equivalent to about US$1,900 at the time) to Aktiengesellschaft für modernen Bergbau,[43] and mining expert Wilhem Müller was hired for trial mining and evaluation, which he did that month with seven workers.[44] On the basis of 1,800 emeralds totaling 3,600 carats recovered during his time on site, with 2% of the crystals (72 carats) of facet quality, Müller compiled a report calculating annual income of 61,500 reichsmark, enough for profitability. He also prepared a map of the different galleries (figure 13) and offered

[41]File Bezirkshauptmannschaft Zell am See, BH Zell H1 2286-1933, Archive of Salzburg Federal State; Leitmeier, 1929/1930.

[42]*Salzburger Volksblatt*, Vol. 58, No. 294, December 24, 1928, p. 9; File Bezirkshauptmannschaft Zell am See, BH Zell H1 2286-1933, Archive of Salzburg Federal State; Letter from E. Klein to W. Müller, August 1, 1929, File "Beryllium," Österreichische Geologische Bundesanstalt, Vienna.

[43]Notarized contract between Aktiengesellschaft für modernen Bergbau and Max Gaab, June 4, 1929, Mittersill land registry office, Archive of Salzburg Federal State.

[44]Wilhelm Müller (born 1885) was educated at the mining school in Diedenhofen (now Thionville), Lorraine. He worked in the mining field in Lorraine and elsewhere and was involved in diamond recovery in the German colony of South-West Africa (now Namibia) before World War I. From 1920 to 1930, he was a manager of the Kappel/Schauinsland lead-zinc mine near Freiburg in southwest Germany, which had a staff of more than 200 miners. Müller lived in the Freiburg area during the 1950s. File "Akten des Bergmeisters Erzbergwerke Schauinsland," 1920, Landesbergdirektion Freiburg; http://www.freiburg-postkolonial.de/Seiten/personen.htm; Heiko Wegmann, pers. comm., 2020; Helge Steen, pers. comm., 2020; B. Steiber, pers. comm., 2020.

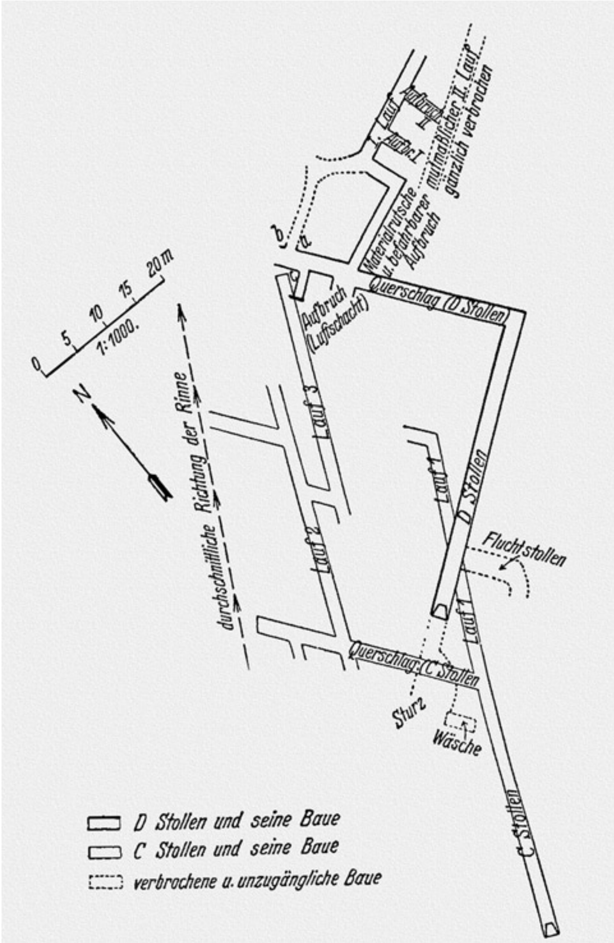

Figure 13. In June 1929, German mining expert Wilhelm Müller examined the mine upon request of the Swiss owner Aktiengesellschaft für modernen Bergbau. Müller prepared a report including this map, which was redrawn and published by Leitmeier (1937).

detailed suggestions for how to target exploration for emerald-bearing schist in the C and D galleries.[45] After his departure, exploration was led by E. Klein, who even then continued to communicate with Müller for counsel and expertise.[46]

In 1930, the Habachtal mine apparently became caught up in yet another financial scandal. A purported company under the name Deutsch-Österreichische Edelsteinbergwerks Gesellschaft was allegedly established in Munich to collect capital and issue shares in support of the "owner" of the mine, which was incorrectly referred to as the operating entity Smaragd-Bergbau Habachtal GmbH.[47] Both a memorandum and a related business plan were prepared in service of those aims.[48] The anonymous memorandum listed a board consisting of four directors of the Swiss parent company—namely Hoesch, Buol, Vogeler, and Conde de Santa Maria de la Sisla—as well as three German citizens (Friedrich Ritter von Heinzelmann, Heinrich Paxmann, and Friedrich Graf Larisch). The business plan offered a glowing picture of the mine's potential and commercial relevance.

Emphasizing that the mines in Colombia were closed and those in the Urals completely exploited, the business plan considered the possibility of economic production not only of gem-quality emeralds but also beryllium-bearing minerals and talc. The plan cited earlier reports by mining engineer Emil Sporn from 1928,[49] by Stuchlik also from 1928, and by Müller from 1929, somehow arriving at a property value of 684,000 reichsmark (or approximately US$163,000 at the time), an emerald yield of 60,000 carats in 1930, and a profit of 267,000 reichsmark in 1932, despite the obvious disparity with the more realistic figures tabulated by Müller.

Whether these missives had any impact on the investors targeted is unknown, but an examination by the Munich Chamber of Commerce in June 1930 revealed that no such company was legally registered there.[50] It was later suggested that the alleged entity was linked to several individuals involved in other mining swindles in Germany who were sentenced to prison in 1932.[51]

Subterfuges aside, the actual mine owner Aktiengesellschaft für modernen Bergbau spent much of the 1930s enmeshed in a web of litigation and admin-

[45]Müller, W., Smaragdvorkommen Habachtal – Salzburg, June 1929, 7 pp., File "Beryllium," Österreichische Geologische Bundesanstalt Wien; Letter from W. Müller to A. Cissarz, December 25, 1939, Lagerstättenarchiv Österreichische Geologische Bundesanstalt Wien; Müller, W., Smaragd – Beryll – Vorkommen Habachtal, March 26, 1940, 2 pp., Lagerstättenarchiv Österreichische Geologische Bundesanstalt Wien; File "Beryll Bramberg," mining documents collected by W. Günther, Archive of the Bergbau- und Gotikmuseum Leogang.

[46]Letter from E. Klein to W. Müller, August 1, 1929, File "Beryllium," Österreichische Geologische Bundesanstalt Wien.

[47]File "Beryl-Emerald-Habachtal" (Beryll-Smaragd-Habachtal), Bundesministerium für Landwirtschaft, Regionen und Tourismus, Montanbehörde West, Salzburg (containing multiple documents from the period 1930 to 1978, hereinafter cited as File "Beryl-Emerald-Habachtal," Montanbehörde West, Salzburg).

[48]File "Beryl-Emerald-Habachtal," Montanbehörde West, Salzburg.

[49]Emil Sporn (b. 1869) studied at the Imperial and Royal School of Mining in Leoben and worked for the Austrian mining administration for several decades from 1896 until 1919. Beginning in 1920, he resided in or near Salzburg and worked for several mining companies. He was last referenced in the Archive of the City of Salzburg as of January 1945.

[50]File "Deutsch-Österreichische Edelsteinbergwerks Gesellschaft," 1930, Munich Chamber of Commerce.

[51]*Innsbrucker Nachrichten*, Vol. 79, No. 181, August 8, 1932, pp. 5–6.

TABLE 1. Parties involved in the legal dispute over the Habachtal mine, 1932–1933.

Interested individual or entity	Lawyer or representative	Engineer or other supporting personnel
Aktiengesellschaft für modernen Bergbau (Chur, Switzerland)	Dr. Karl Sender (Zurich) and Dr. Max Duschl (Salzburg)	Othmar Kelb, mining engineer
Christian Schad (Berlin)	Julius Burger, engineer (Munich)	Josef Köstler, mining engineer
Rudolf Nocker (Bramberg, Austria) and Habach Weggenossenschaft (Bramberg)	Dr. Gustav Freytag (Mittersill, Austria)	
Hugo Ullhofen (Mittersill) and Angelo De Marchi (Milan and Rome)	Dr. Gustav Freytag	Gottfried Förster, "geologist"
Max Gaab (Munich) and Meta Geist (Fischbachau, Germany)	Dr. Max Duschl	
Florian Prader (Zurich)	Dr. Max Duschl	
Gottfried Förster (Innsbruck, Austria)	Dr. Felix Friedrich (Innsbruck)	

istrative proceedings, one in Switzerland and several in Austria. The opening salvo occurred when both Gaab and Geist, as creditors, filed separate lawsuits in Austria against the company for nonpayment of debts and interest.[52] Those were apparently resolved through loans extended to the company by board member Prader and a Munich bank, which also resulted in further lien encumbrances against the property.[53] This offered minimal respite, however, because a Swiss bankruptcy proceeding was opened in October 1931 but was then terminated three days later, without dissolution of the company, on account of a lack of any assets of value in Switzerland for distribution.[54]

Aktiengesellschaft für modernen Bergbau remained the owner of the mine, and ensuing controversies shifted to Austria. The early years of the decade saw in particular several different groups of associates seeking to establish or pursue interests in the property (see table 1).[55] Beginning in the 1930s, exploration permits were registered for the Habachtal area by Munich mining engineer Julius Burger[56] in the name of Christian Schad (figure 14, left) and as directed by his father, Dr. Carl Schad (figure 14, right).[57] Existing permits held by others were also purchased by and transferred to Christian Schad. At that time, technical progress had developed several lucrative applications for beryllium ore and metal (e.g., for X-ray tube windows and metallurgic processes), rendering Habachtal an increasingly in-

[52]*Max Gaab v. Aktiengesellschaft für moderenen Bergbau* and *Meta Geist v. Aktiengesellschaft für moderenen Bergbau*, Bezirksgericht Mittersill, May 21, 1930, Mittersill land registry office, Archive of Salzburg Federal State.

[53]Notarized contract between Florian Prader and Aktiengesellschaft für modernen Bergbau, June 26, 1931, Mittersill land registry office, Archive of Salzburg Federal State.

[54]*Schweizerisches Handelsamtsblatt*, Vol. 49, No. 254, October 31, 1931, p. 2318.

[55]File "Beryl-Emerald-Habachtal," Montanbehörde West, Salzburg; File "Status of Beryl as Ore Mineral" (Vorbehaltener Charakter des Berylls), Bundesministerium für Handel und Verkehr, 166.786 – O.B. – 1932, Austrian State Archive, Vienna (Österreichisches Staatsarchiv, Vienna); *Florian Prader v. Habach Weggenossenschaft*, Bezirksgericht Mittersill, C 145/1932, Archive of Salzburg Federal State; *Gottfried Förster v. Angelo De Marchi*, Bezirksgericht Mittersill, C 132/1933, Archive of Salzburg Federal State.

[56]Julius Burger (1893–1977) was an engineer from Munich who had been involved in multiple mining projects in Austria, including coal mining near Lechaschau, Tyrol. He moved from Munich to Kitzbühel, Austria, in 1934 and later returned to Munich in 1947. Contemporaneous with his involvement with Christian Schad in the Habachtal emerald project, Burger remained engaged in several other mining ventures in Austria, such as one in Rettenbach, during the 1930s and 1940s. Assisting with the work in Habachtal was Austrian mining engineer Josef Heinrich Köstler (1878–1935). *Mitteilungen über den Österreichischen Bergbau*, Vol. 1, 1920, p. 44; Schmidegg, 1955; City Archive of Kitzbühel, pers. comm., 2020; City Archive of Munich, pers. comm., 2020.

[57]Christian Schad (1894–1982), a painter from Berlin, was apparently never active on site in Habachtal and is thus considered an investor in the undertaking. The investment in Habachtal emerald mining was initiated by his father Dr. Carl Schad (1866–1940), a notary from Munich, using Christian's name mainly for tax reasons. Carl also invested large sums in various other mining projects, especially in Italy, which eventually led to substantial losses. Archive of Salzburg Federal State; Richter, 2020.

Figure 14. In the early 1930s, multiple exploration permits in the Habachtal area were registered in the name of the painter Christian Schad (left, circa 1930) from Berlin. The investments were initiated by his father, Dr. Carl Schad (right, circa 1934–1935), a notary from Munich. Photos courtesy of Christian Schad Stiftung Aschaffenburg, Museen der Stadt Aschaffenburg.

teresting target.[58] Reports were prepared in 1931 and 1932 by Professor Hans Leitmeier (figure 15) from Vienna University, at the request of Aktiengesellschaft für modernen Bergbau and the Schad/Burger team, with a possible joint venture in view.[59] Leitmeier concluded that although the emeralds (figure 16) were not of a sufficient quality for economical mining, the extraction of beryl for metallic ore would be.

However, before further steps could be taken by Schad, Burger, or Aktiengesellschaft für modernen Bergbau, the Swiss company was sued in the court in Mittersill by Rudolf Nocker and the entity Habach Weggenossenschaft, both of Bramberg, to recover alleged liabilities of 625 Austrian shillings arising in 1930 and 1931. When initial attempts to resolve the matter by leasing the property for 500 shillings per year were unsuccessful,[60] the court named Hugo Ullhofen (1886–1973), a schoolteacher from Mittersill, receiver of the property. Ullhofen, in turn, leased the Habachtal emerald mine to Angelo De Marchi, a farmer and landowner from Milan,[61] via a contract dated July 27, 1932, and running from August 1932 to October 1933.[62] De Marchi had become aware of the property through Gottfried Förster, a self-described geologist active throughout Austria in searching for mining deposits and familiar with Habachtal since approximately 1930.[63]

As noted in materials prepared by De Marchi's rep-

[58]Waagen, 1936.

[59]File "Beryl-Emerald-Habachtal," Montanbehörde West, Salzburg (with only the 1932 report remaining available in the file). Hans Leitmeier (1885–1967) was a professor of mineralogy and petrography at Vienna University who dedicated a substantial percentage of his scientific research to alpine mineralogy and deposits. In addition to the 1931 and 1932 reports, Leitmeier in 1938 published a history of the Habachtal deposit, based largely on personal communication with Ernst Brandeis, grandson of Samuel Goldschmidt. However, such recollections were premised on memories some 35 years after the fact and not necessarily consistent with what can be derived from contemporaneous documentation. A further historical summary published by Leitmeier (1946) suffers from similar discrepancies, particularly as relates to the era between 1918 and 1939. See Hammer and Pertlik, 2014.

[60]*Salzburger Chronik*, Vol. 68, No. 112, May 17, 1932, p. 6; *Salzburger Volksblatt*, Vol. 62, No. 112, May 17, 1932, p. 6.

[61]Angelo De Marchi was born in 1882 in the municipality of Amatrice northeast of Rome. For the 1932 and 1933 period, addresses in both Milan and Rome are noted, and references can be found to the "De Marchi group of investors from Rome," suggesting that De Marchi maintained both landholdings in Milan and business connections in Rome. File Bezirkshauptmannschaft Zell am See, BH Zell H1 2286-1933, Archive of Salzburg Federal State; File "Beryl-Emerald-Habachtal," Montanbehörde West, Salzburg.

[62]Ullhofen, H., undated report covering 1930–1953, Archive of E. Burgsteiner, 2 pp.

[63]*Gottfried Förster v. Angelo De Marchi*, Bezirksgericht Mittersill, C 132/1933, Archive of Salzburg Federal State. Gottfried Förster (1882–1942) was born in Bozen (Bolzano), then part of the Austro-Hungarian Empire and now part of Italy. Förster was a painter by training but characterized himself as a geologist. The year 1924 saw him active in the Hollersbach Valley, east of Habachtal. By the 1930s, he had been operating as a purported exploration geologist for more than two decades in various parts of Austria, searching primarily for gold, copper, lead, and zinc deposits. Förster also applied for exploration permits and tried to sell the mining rights; some of his efforts were apparently deemed fraudulent. See *Innsbrucker Nachrichten*, Vol. 56, No. 152, July 8, 1909, p. 5; *Tiroler Volksblatt*, Vol. 49, No. 3, January 8, 1910, p. 8; *Der Tiroler*, Vol. 30, No. 36, March 25, 1911, p. 5; *Tiroler Anzeiger*, Vol. 10, No. 11, January 9, 1917, p. 6; *Meraner Tagblatt*, Vol. 38, No. 67, April 13, 1920, p. 1; *Tiroler Anzeiger*, Vol. 15, No. 57, March 10, 1922, p. 4; *Salzburger Volksblatt*, Vol. 54, No. 50, February 29, 1924, p. 4; *Der Landsmann*, Vol. 25, No. 106, May 8, 1924, p. 2.

Figure 15. Professor Hans Leitmeier of Vienna University authored various reports concerning the Habachtal mine in the early 1930s. Their premise was that although emerald mining at Habachtal was not economical, the extraction of beryl for beryllium ore could be. Photo at the entrance to D gallery circa 1935. Archive of Peter Lausecker.

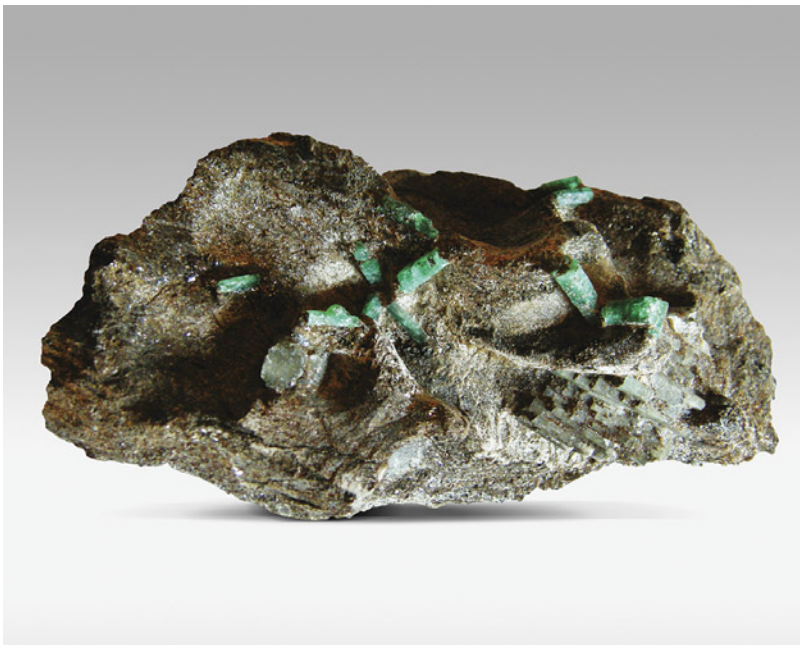

Figure 16. Habachtal emeralds often display a bright green coloration but are fractured and heavily included. For that reason, only a small fraction of prismatic rough crystal material is of facetable quality. Shown here are emerald crystals with lengths of up to 15 mm from the Habachtal deposit, on a matrix of biotite schist measuring approximately 19 × 6 cm, accompanied by light bluish gray aquamarines (lower right). Photo by K. Schmetzer; private collection.

resentative, attorney Dr. Gustav Freytag from Mittersill, the condition of the mine in 1932 was very poor. The mine had not been maintained for several years, and the galleries had been rendered nearly inaccessible by illegal mining activities and uncontrolled blasting (figure 17).[64] De Marchi invested 25,000 Austrian shillings (equivalent to approximately US$1,790 at the time) and employed 15–20 miners to recommence operations, with Förster serving as mine manager.[65] Authorization for recovery operations pursuant to the Trade, Commerce and Industry Regulation Act was sought through a September 1932 application.[66] While that was pending, their first season's efforts enabled the transport in October 1932 of 16 boxes of rough material with a total weight of 500 kg over the Alps to Italy.[67]

Not surprisingly, Schad and Burger were disquieted by the turn of events. Only two weeks into the De Marchi lease, Burger—again acting on behalf of Schad—instigated a regulatory proceeding at the mining administration in Wels that would protect their rights by:[68]

1. Ensuring unrestricted access in accordance with the existing exploration permits, thus allowing for further development activities in the galleries (§ 100-103 of the mining law).

[64]*Gottfried Förster v. Angelo De Marchi*, Bezirksgericht Mittersill, C 132/1933, Archive of Salzburg Federal State. Dr. Gustav Freytag (1881–1947) was a judge in Salzburg before starting his own law firm there in 1925. In 1931 he moved to Mittersill in Pinzgau, where he continued to work as a lawyer.

[65]Ibid. See also Leitmeier, 1938; Lausecker, 1986; Hönigschmid, 1993; Lewandowski, 1997.

[66]File "Beryl-Emerald-Habachtal," Montanbehörde West, Salzburg.

[67]*Gottfried Förster v. Angelo De Marchi*, Bezirksgericht Mittersill, C 132/1933, Archive of Salzburg Federal State.

[68]File "Beryl-Emerald-Habachtal," Montanbehörde West, Salzburg.

Figure 17. One piece of evidence introduced in legal proceedings in 1932 was a map of the Habachtal mine apparently prepared by copying and coloring the map drawn by Anton Hager Jr. in 1924 and updated in 1926. The C gallery (red) was not accessible at the time, while the D gallery (blue) could be accessed. File "Beryl-emerald-Habachtal," Montanbehörde West, Salzburg.

2. Granting mining titles for the property, as would be feasible if beryl were declared to be an ore mineral of economic value covered by the mining law (§ 40-44).

Aktiengesellschaft für modernen Bergbau was involved in that proceeding, represented by attorney Dr. Max Duschl from Salzburg.[69] Following negotiations, a preliminary ruling was made by the head of the mining administration (or *Berghauptmann*). On September 13, 1932, Dr. Franz Aigner (figure 18)[70] deemed beryl to be covered by the mining law, a reversal of the administration's earlier stance. The victory was short lived, however. An inspection at the mine the next day found only limited quantities of beryl, such that mining could not be considered of

[69]Dr. Max Duschl (1870–1949) began his career as a lawyer in 1903 and continued in that field in Salzburg for nearly five decades. He was assisted by the Austrian mining engineer Othmar Kelb (1871–1947).

[70]Dr. Franz Aigner (1872–1962) studied law in Vienna and mining in Leoben. He began his career at the Austrian mining administration in 1903, serving as staff member in Wels from 1910 and as head of the department from 1913 to 1936, responsible for mining activities in the Habach Valley. Werneck, 1988; Günther and Lewandowski, 2002.

Figure 18. In 1932, Dr. Franz Aigner was the head of the Austrian mining administration located at Wels. Dr. Aigner was responsible for overseeing and ruling in the regulatory controversies targeting the Habachtal emerald mine. 1930s photo from Montanistische Rundschau *(1935).*

economic value and no mining privileges could be granted. De Marchi and his workers had apparently hidden some locations in the galleries where the tunnels crossed rocks with high concentrations of beryl and emerald. As a result, Schad and Burger maintained only a right of admission to the property for further development, in hopes of proving the mine to be economically viable for the extraction of beryl as beryllium ore.[71]

Yet another tactic was pursued by the lien holders Gaab, Geist, and Prader, the latter of whom also held exploration permits in the area. All were represented by Duschl. Seeking to maximize options, Duschl instigated litigation on behalf of Gaab and Geist at the court in Salzburg and on behalf of Prader at the court in Mittersill, with both suits seeking to overturn the Mittersill court's decision to appoint Ullhofen as receiver.[72] Although neither suit achieved greater rights for the petitioning lien and permit holders, given the nature of their interests, a procedural error identified by Duschl did cause the Mittersill court on November 20, 1932, to revoke Ullhofen's appointment as receiver, which rendered invalid the contract between Ullhofen and De Marchi.[73]

In light of these developments, De Marchi appealed the decisions of both the Wels mining administration and the Mittersill court, while continuing his efforts to obtain a working permit for emerald recovery under the Trade, Commerce and Industry Regulation Act.[74] Complicating such attempts were multiple additional lawsuits that entangled De Marchi during the same timeframe. His former mine manager Förster sued in May 1933, claiming inadequate compensation and a right under a June 1932 agreement to at least 25% of the mine's profit.[75] De Marchi was also involved in actions pending in Italy. For reasons beyond the scope of this study, after he had returned to Italy in October 1932, De Marchi risked imprisonment if he reentered Austria.[76] Pursuit of the Austrian proceedings was not curtailed, however, as they could be handled locally by his attorney Freytag. A measure of success in his appeal of the Mittersill court's ruling was achieved when the Supreme Court in Vienna reinstated the lease contract with Ullhofen in April 1933. De Marchi also finally obtained a working permit in July 1933.[77] His appeal of the administrative ruling, on the other hand, was dismissed in September 1933 by the Ministry for Trade and Traffic on procedural grounds, and no final decision about the coverage of beryl under the mining law was made.[78]

[71]File "Beryl-Emerald-Habachtal," Montanbehörde West, Salzburg.

[72]Ibid.; *Florian Prader v. Habach Weggenossenschaft*, Bezirksgericht Mittersill, C 145/1932, Archive of Salzburg Federal State.

[73]File "Beryl-Emerald-Habachtal," Montanbehörde West, Salzburg; File "Beryll Bramberg," mining documents collected by W. Günther, Archive of the Bergbau- und Gotikmuseum Leogang.

[74]File "Beryl-Emerald-Habachtal," Montanbehörde West, Salzburg.

[75]*Gottfried Förster v. Angelo De Marchi*, Bezirksgericht Mittersill, C 132/1933, Archive of Salzburg Federal State.

[76]Ibid.

[77]File Bezirkshauptmannschaft Zell am See, BH Zell H1 2286-1933, Archive of Salzburg Federal State; File "Beryll Bramberg," mining documents collected by W. Günther, Archive of the Bergbau- und Gotikmuseum Leogang. Notably, even the Austrian embassy in Rome and the Italian consulate in Innsbruck had become involved in the proceedings.

[78]File "Status of Beryl as Ore Mineral" (Vorbehaltener Charakter des Berylls), Bundesminsterium für Handel und Verkehr, 166.786 – O.B. – 1932, Austrian State Archive, Vienna. This action also saw intervention by the Italian Embassy in Vienna.

Figure 19. View from the Habachtal mine downhill to the large boulder field serving as a secondary deposit where emeralds were also found. Undated photo from Mühlviertler Nachrichten *(1935).*

Nonetheless, all of De Marchi's legal machinations eventually came to naught as a result of the foreclosure of the property instigated by Gaab and Geist in May 1933.[79] A foreclosure auction was held on August 31, 1933, and creditors Gaab, Geist, and Prader purchased the property for 12,806 Austrian shillings (approximately US$770 at the time), an amount less than the total outstanding liabilities.[80] Because the other pending legal actions had precluded De Marchi from taking any practical steps to work the mine between the time his lease was formally reinstated in April and the August sale, any rights were effectively vitiated before they could be acted upon in practice.

The next several years saw a shifting of applicable exploration permits among interested parties, as well as the formation of a new entity. Certain existing permits held by De Marchi, Schad, Freytag, and Förster were terminated, while others held by Schad were extended. New permits were applied for by and/or granted to De Marchi, Schad, Freytag, and Förster.[81]

Property Under the Swiss Smaragd Aktiengesellschaft (1934–1939). By June 1934, the company Smaragd Aktiengesellschaft had been established in Schaffhausen, Switzerland, with a stated capital of 35,000 Swiss francs (approximately US$11,000 at the time) in 35 equal shares.[82] The initial shareholders consisted of one Swiss citizen and four Germans: Prader, Geist, Gaab, Schad, and Burger.[83] Schad contributed nine exploration permits in exchange for 14 shares, becoming a major holder, and the property was leased to Smaragd Aktiengesellschaft by owners Gaab, Geist, and Prader for a 30-year term.

In 1935, Prader's construction company from Zurich led endeavors to recommence operations at the Habachtal site (figure 19) on behalf of Smaragd Aktiengesellschaft. That year he requested from Müller a copy of the 1929 report[84] and employed 10–12 workers to safeguard the property and form a plan for further activities.[85] Subsequent years saw mining by Smaragd Aktiengesellschaft continued on a low

[79]Ibid.

[80]*Schweizerisches Handelsamtsblatt*, Vol. 52, No. 46, February 24, 1934, p. 503; Order, Bezirksgericht Mittersill, March 26, 1934, Mittersill land registry office, Archive of Salzburg Federal State; Habachtal emerald mine file, entry November 13, 1933, Mittersill land registry office. Smaragdbergbau Habachtal GmbH, the Austrian operating entity of the Swiss Aktiengesellschaft für modernen Bergbau, was formally dissolved in 1937. *Salzburger Volksblatt*, Vol. 67, No. 142, June 24, 1937, p. 8.

[81]Reported frequently in *Montanistische Rundschau*, Vols. 25–27, 1933–1935.

[82]*Schweizerisches Handelsamtsblatt*, Vol. 52, No. 150, June 30, 1934, p. 1811; *Montanistische Rundschau*, Vol. 35, No. 44, 1935, T.Mo. 44.

[83]File "Beryl-Emerald-Habachtal," Montanbehörde West, Salzburg; File Bezirkshauptmannschaft Zell am See, BH Zell 1937 J5 – 5423, Archive of Salzburg Federal State; File Bezirkshauptmannschaft Zell am See, BH Zell 1938 H1 – 12261, Archive of Salzburg Federal State.

[84]Letter from W. Müller to A. Cissarz, December 25, 1939, Lagerstättenarchiv, Österreichische Geologische Bundesanstalt Wien.

[85]File Bezirkshauptmannschaft Zell am See, BH Zell 1936 A1 – 7587, Archive of Salzburg Federal State; File "Beryll Bramberg," mining documents collected by W. Günther, Archive of the Bergbau- und Gotikmuseum Leogang; *Salzburger Chronik*, Vol. 71, No. 202, September 3, 1935, p. 9; *Alpenländische Rundschau*, No. 621, September 7, 1935, p. 10.

Figure 20. Left: Entrance to the D gallery in the second half of the 1930s. Right: Processing of emerald-bearing rocks in the second half of the 1930s. Photos courtesy of E. Burgsteiner.

level, led by Burger from 1936 to 1938 with five to seven miners mentioned in various documents for the 1936 to 1938 seasons.[86] Local press from the period reported recovery of emeralds as gemstones (figure 20), with the permits contributed by Schad allowing Smaragd Aktiengesellschaft to pursue simultaneous exploration and development for the type of beryl mining that would be regulated by the mining law.[87] Leitmeier published two additional studies during the era, focusing on geology and the genesis of emerald formation (figure 21).[88] By 1939, Burger was no longer employed by the company. Operations that year, the final year of the firm's work on site, amounted only to one engineer, one foreman, and several miners searching exclusively for emeralds.[89] Freytag at that point served as legal representative for the company in Austria.[90]

Meanwhile, in 1937 the mine's former owner Anton Hager had filed a lawsuit against Smaragd Aktiengesellschaft and Christian Schad, with Gaab, Burger, and Dr. Carl Schad also becoming involved.[91] Details are vague, however, and no tangible substan-

[86]File Bezirkshauptmannschaft Zell am See, BH Zell 1936 A1 – 7587, Archive of Salzburg Federal State; File Bezirkshauptmannschaft Zell am See, BH Zell 1938 H1 – 12261, Archive of Salzburg Federal State; File "Beryll Bramberg," mining documents collected by W. Günther, Archive of the Bergbau- und Gotikmuseum Leogang; *Salzburger Chronik*, Vol. 73, No. 147, July 1, 1937, p. 6; *Der Wiener Tag*, Vol. 16, No. 5047, July 3, 1937, p. 5; Leitmeier, 1938.

[87]File Bezirkshauptmannschaft Zell am See, BH Zell 1938 H1 – 12261, Archive of Salzburg Federal State; *Völkischer Beobachter*, Wiener Ausgabe, No. 169, September 2, 1938, p. 12.

[88]Leitmeier, 1937, 1938.

[89]Hanke, 1939.

[90]*Montan-Handbuch für die Ostmark und die Südost-Länder*, Vol. 20, 1940, Verlag Rudolf Bohmann, Vienna, p. 20.

[91]See *Dr. Max Duschl v. Christian Schad, et al.*, Salzburg court, March 5, 1943, File CSSA 4826-2018, Christian Schad Stiftung Aschaffenburg, Museen der Stadt Aschaffenburg (a related suit over nonpayment of legal fees). The file for the primary case before the Salzburg court, characterized as "extremely complicated," is no longer preserved in the archive of Salzburg Federal State. Land Salzburg, Landesarchiv, pers. comm., 2020.

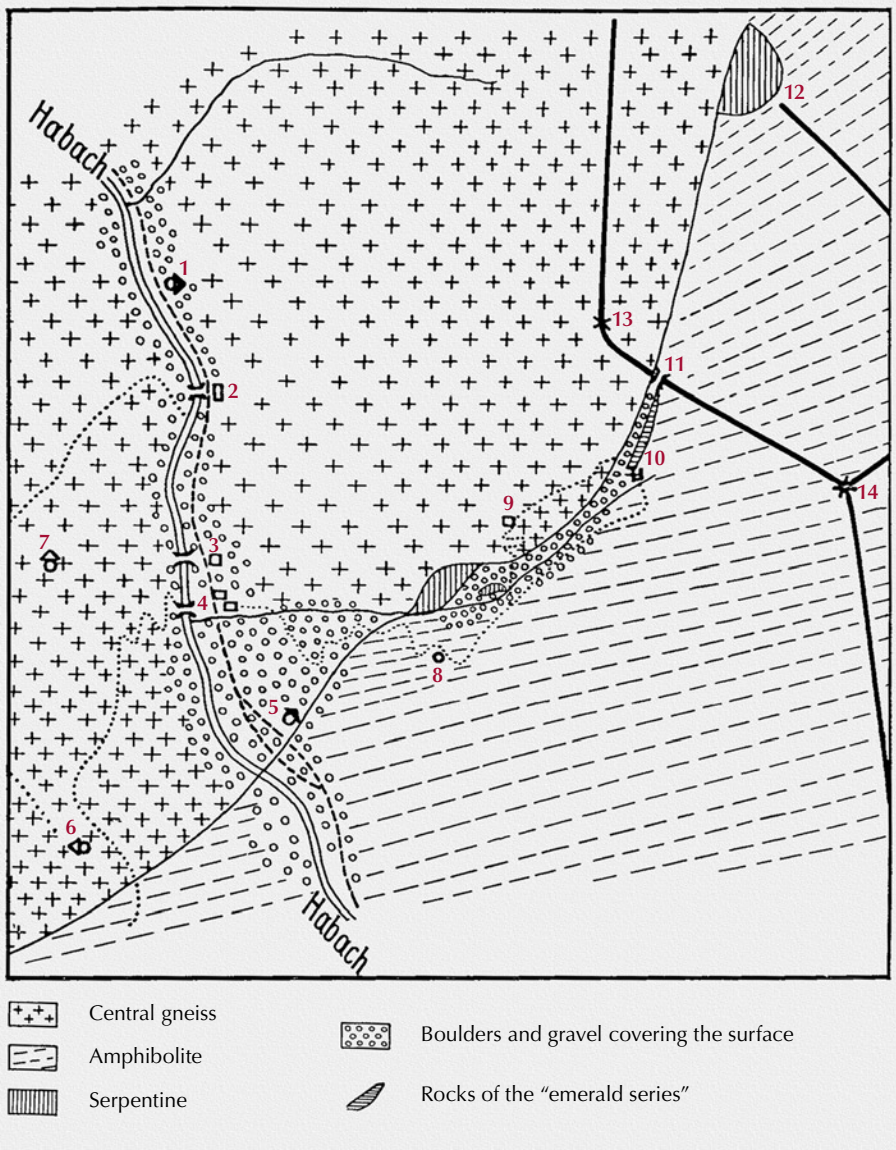

Figure 21. Geological map of the rocks found in the vicinity of the Habachtal deposit located east of the Habach Creek, after Leitmeier (1937). Indicated features include: the Alpenrose guest house (4), grazing pasture (8), Goldschmidthütte (9), the mining area (10), Legbachscharte (11), schwarze Wand (12), Nasenkogel (13), Graukogel (14), and various agricultural areas or guesthouses (1–3 and 5–7). Numbers are reproduced in red. The solid line represents the mountain ridge of the Habach Valley.

tive impact on the status of the mine or those connected thereto is apparent.

HABACHTAL IN THE MODERN ERA (1940 TO PRESENT)

As the decade turned, recovery of beryl as an ore mineral was discussed several times between 1939 and 1941 at the Reichsstelle für Bodenforschung in Vienna, now controlled from Berlin,[92] but no practical mining operations were undertaken.[93] Burger now evaluated for Frankfurt-based Gold- und Silberscheideanstalt[94] on the feasibility of mining for beryllium ore and even initiated efforts in 1940 to gain control of the mine, although those led to no tangible result either.[95]

In December 1940, the shareholders decided to dissolve Smaragd Aktiengesellschaft, and the process was finalized approximately one year later, rendering the shares worthless.[96] During the 1941 to 1942 period, Gaab then purchased the third of the Habachtal property owned by Prader for 4,000 Swiss francs (ap-

[92]Danner, 2015.
[93]Danner, 2014.
[94]Later known as Degussa AG.
[95]File "Beryl-Emerald-Habachtal," Montanbehörde West, Salzburg; File "Beryll Bramberg," mining documents collected by W. Günther, Archive of the Bergbau- und Gotikmuseum Leogang.
[96]*Schweizerisches Handelsamtsblatt*, Vol. 59, No. 23, January 28, 1941, p. 186; Vol. 60, No. 12, January 17, 1942, p. 129; Richter, 2020.

Figure 22. In the period shortly after World War II, Hans Zieger (left) served as an administrator at Habachtal, overseeing limited activity and assisted primarily by only one miner. Photo from 1948; courtesy of A. Lahnsteiner.

proximately US$930 at the time), raising his share to two-thirds.[97]

No minining activities were documented during the rest of World War II. After the war, only limited mining was performed by a few individuals during the summer months. The mine was administered primarily by the pianist Hans Zieger (1892–1953, figure 22), who began working in Habachtal in late 1945 under a contract with Gaab.[98] Zieger was also named administrator of the property by the U.S. Allied Commission for Austria, and he operated for many years with only one miner.[99]

Details of developments and activities at Habachtal after World War II are generally beyond the scope of this study and have been well covered by other authors.[100] Various individuals or groups of individuals were involved on a temporary basis, and the possibility of mining the property for beryllium ore continued to come up for discussion in several forums, but nothing was pursued.[101]

Meanwhile, upon Gaab's death in 1953, his interest was split between his son Karl Gaab (1901–2000, figure 23), a Munich lawyer, and daughter Irma Sauter. Karl Gaab later bought his sister's one-third

[97]Notarized contract between Florian Prader and Max Gaab, October 29, 1941 (Munich) and May 22, 1942 (Zurich), Mittersill land registry office, Archive of Salzburg Federal State; Habachtal emerald mine file, entry November 25, 1942, Mittersill land registry office.

[98]Contract between Max Gaab, Franz Mayböck, Leo Weiss, and Hans Zieger, October 4, 1945, Archive of Erwin Burgsteiner, Bramberg.

[99]USACA 1945–1950, Records of the Property Control Branch of the U.S. Allied Commission for Austria, File Sch 398, Property of Meta Geist and Max Gaab, 24 pp. https://www.fold3.com/image/306445403?terms=Gaab and Hausmann, 1950.

[100]See Eberl (1972), Pech (1976), Lausecker (1986), Grundmann (1991), Exel (1993), Lewandowski (1997), and Burgsteiner (2002).

[101]See File "Beryl-Emerald-Habachtal," Montanbehörde West, Salzburg; Kirnbauer, F., Gutachten über das Beryllvorkommen Habachtal einschl. Aufschlußplanung, October 1, 1955, 18 pp.; File "Beryllium," Österreichische Geologische Bundesanstalt Wien; Smaragdbergwerk für Atomindustrie, 1956.

Figure 23. After the death of his father in 1953 and various purchase transactions over the ensuing years, Munich lawyer Karl Gaab became the sole owner of the Habachtal property from 1964 until his death in 2000. Photo from the 1970s; courtesy of Ingrid von Klitzing.

Figure 25. The Habachtal emerald mine has been maintained since 1985 by the Steiner family from Bramberg. Andreas Steiner is seen here at the entrance to the D gallery. Photo from 2009 by E. Burgsteiner.

share in 1962 and the final one-third held by Geist in 1963 (transactions formally registered in 1963 and 1964, respectively).[102] Until his death, Karl Gaab remained the sole owner, attempting to protect the property to the extent possible. A comparison of maps prepared between the 1920s and the 1980s shows that as the decades passed, certain sections of the mine collapsed and additional areas were dug (figure 24, opposite page).

At present, the Habachtal emerald mine is still in private possession and since 1985 has been maintained by the Steiner family from Bramberg. Since 2001, Alois Steiner and his son Andreas (figure 25) have overseen operations. Three to four individuals work in the D gallery from mid-June to September or October. The finds have included emeralds in matrix sold to mineral collectors (figures 26 and 27), as well as limited quantities of material used in both faceted (figure 28) and rough form to produce Habachtal emerald jewelry pieces.[103]

[102]Habachtal emerald mine file, Mittersill land registry office, Archive of Salzburg Federal State.

[103]Andreas Steiner, pers. comm., 2019; Claudia Steiner, pers. comm., 2019.

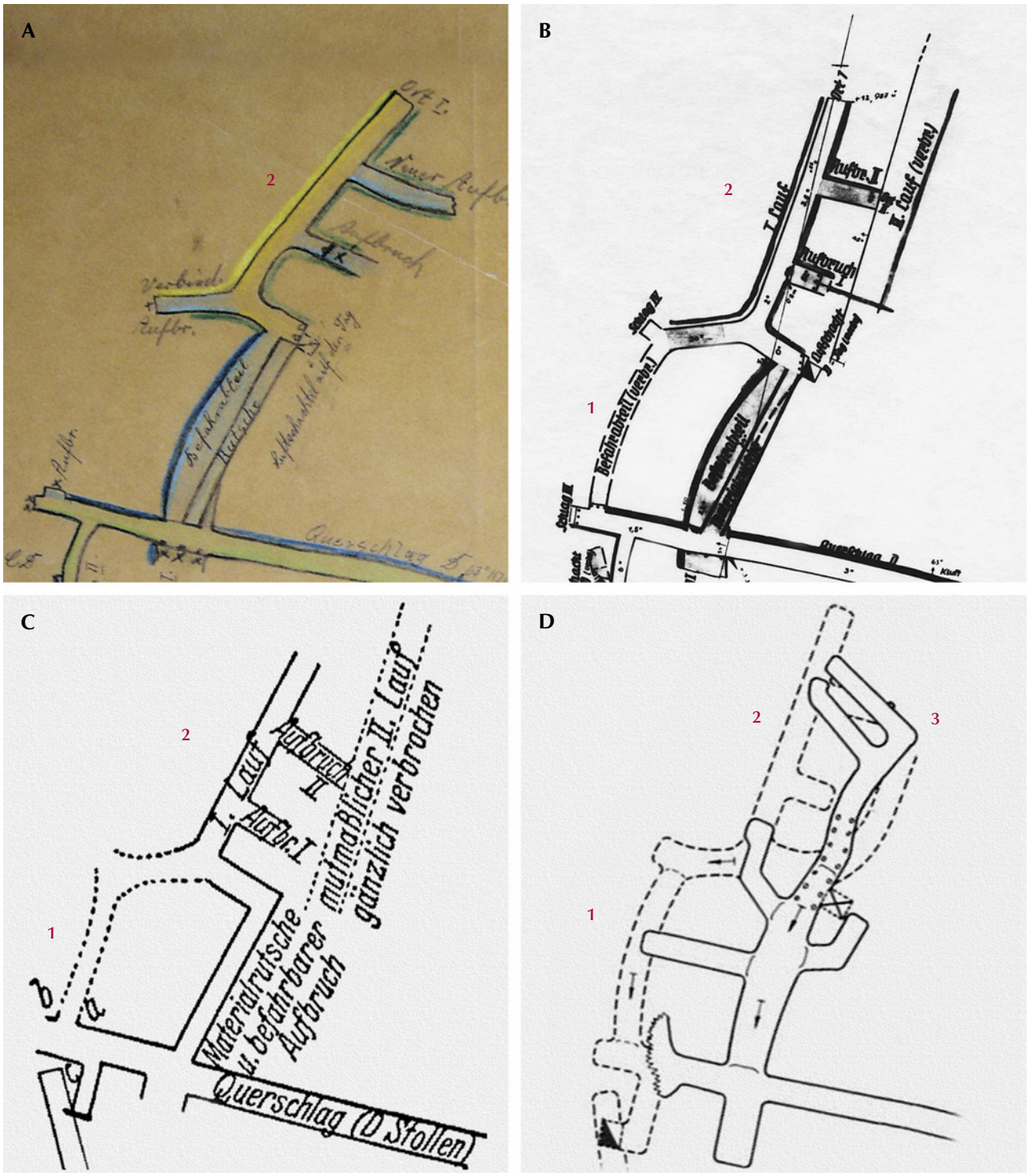

Figure 24. Four maps of a portion of the D gallery at the Habachtal mine, in the area where the emerald-bearing talc and biotite schists were reached, illustrate developments over the course of approximately seven decades: A: Hager (1923). B: Hager (1924/1926). C: Leitmeier (1937) after Müller (1929). D: Grundmann (1991). Solid lines represent accessible areas, while dashed lines indicate collapsed, inaccessible sections. Comparison reveals that early parts of the tunnels worked by Hager and Staudt (1) soon collapsed. After World War II, the main access to the end of the gallery (2) collapsed and a new tunnel (3) was prepared.

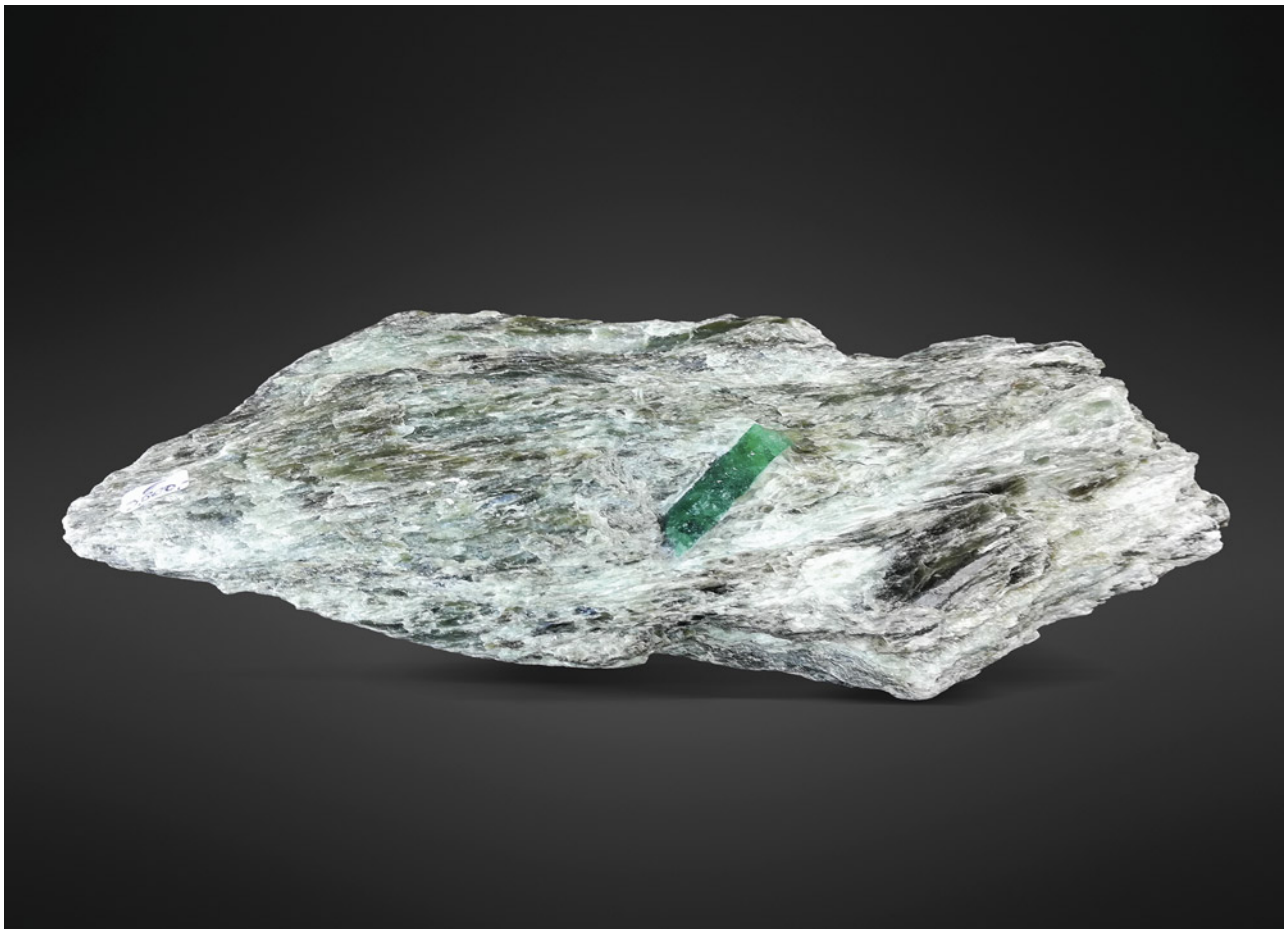

Figure 26. An emerald crystal 22 mm in length on a matrix of talc schist, mined in 2019 at the Habachtal deposit under the Steiner family. Photo by K. Schmetzer; courtesy of Andreas Steiner.

Figure 27. At the Habachtal emerald deposit, gray or blue beryl (aquamarine) is also found occasionally. Even rarer are color-zoned crystals such as those shown here on a biotite schist matrix (see arrow for the color zoning). The sample on the left measures 20 × 8 cm; the length of the two color-zoned crystals (right) is approximately 1 cm. Photos by K. Schmetzer; courtesy of private collection.

Figure 28. Faceted Habachtal emeralds from the H.A. Hänni collection at SSEF in Basel, Switzerland. The largest gem measures 9.4 mm in length and weighs 2.9 ct. Photo by H.A. Hänni.

DISCUSSION AND CONCLUSIONS

Contemporary thinking about the history of emerald mining at Habachtal during the sixteenth to eighteenth centuries has been based largely on perpetuated misinterpretation of several early references. Some look to the report by Aulitzky (1973) that mistook a 1593 landslide as an event destroying assumed emerald mines on the eastern slope of the valley, when in fact the disaster buried adits to the silver mines at Gamskogel on the western slope. Others rely on a 1727 mining chronicle by Brückmann, which in turn was based on editions of a booklet by Lehner (1669, 1702, 1718), all of which erroneously referred to green and violet fluorites from the Bach mining area near Donaustauf as emeralds and amethysts. Even aside from the mineralogical mistake, to connect Bach and Donaustauf in Bavaria to Habachtal in Austria is geographically baseless. However, this did not stop a number of well-known twentieth-century authors from repeating the error (see Scherz, 1955; Gübelin, 1956a,b), which is still found in more recent texts.[104]

Yet another misinterpretation, albeit more subtle, derives from the first known written but unpublished reference to Habachtal emeralds in a 1669 letter by Anna de' Medici, which mentions Danish-Italian scientist Niels Stensen's journey to the region. For some to have stretched mention of an *occurrence* in the original language to imply *mining* is unjustified. Only limited collection by locals during the era seems supportable. The first publication on the occurrence was written by Schroll (1797) as part of a geological and mineralogical description of Salzburg, and the primary source was identified some decades later in the 1820s.

Thereafter began the mining history at Habachtal, a saga fraught with twists, turns, starts, stops, hopes,

[104]Stehrer, 2000.

TABLE 2. History of emerald mining in Habachtal.

Date	Event
June 1669	Danish-Italian scientist Niels Stensen travels to the emerald occurrence, an event memorialized in a letter from Anna de' Medici of Innsbruck to her brother in Florence.
1797	The first published description of the Habachtal emerald occurrence is presented in a scientific treatise by Kaspar Melchior Schroll.
1816	Magnus von Petersen reports having visited the secondary deposit in 1815.
1821	Jakob Frischholz, a mineral dealer from Munich, authors a detailed description of the emerald material.
Summer 1861	Jeweler Samuel Goldschmidt undertakes an excursion to the Habachtal locality, assisted by Bergrath M.V. Lipold from the Austrian geological survey.
February 1862	Samuel Goldschmidt purchases from the government the parcel containing the Habachtal occurrence.
Starting in 1862	For several years under Goldschmidt's ownership, emerald recovery is pursued, first using open-pit methods and later digging three tunnels.
1871	Goldschmidt dies. Ownership of the Habachtal property transfers to his daughters Jeanette and Friederike, and the site is leased for a few years to third-party operators.
March 1894	Albert Brandeis, Jeanette's husband, purchases Friederike's half of the property.
1894	After being contacted by Albert Brandeis, representatives of Leverson, Forster & Co. from London visit the Habachtal site in view of a possible investment.
1895	Preliminary mining activities at Habachtal are undertaken on behalf of Leverson, Forster & Co.
May 1896	The Habachtal property is purchased by the London-based Emerald Mines Limited, an entity established earlier that year with a board of directors comprising members of the Leverson and Forster families, as well as Albert Brandeis. The purchase price is paid in shares of the new company.
1896–1902	Under the control of Leverson, Forster & Co., Emerald Mines Limited exploits the emerald deposit for several years via four tunnels, with on-site operations guided by English and Austrian mining engineers.
1902–1906	Administrative and legal proceedings are instigated by Austrian authorities questioning the regulatory propriety of Emerald Mines Limited's activities at Habachtal.
1905	Spargo & Sons from Liverpool investigates the Habachtal property at the behest of the Manchester-based Northern Mercantile Corporation, which is considering an acquisition.
1906	Northern Mercantile Corporation purchases the shares of Emerald Mines Limited, with all members of the Leverson and Forster families ceasing involvement and only Albert Brandeis formally remaining a director.
1906 and possibly 1907	Mining activities are renewed and pursued on a limited basis under the control of Northern Mercantile Corporation.
1909–1911	Certain transactions involving shares of Emerald Mines Limited and purported Habachtal emeralds, an Austrian prince, and directors William King and Leslie Clark erupt in financial scandal and litigation.
January 1913	The Habachtal property is transferred by the court in Mittersill to the municipality of Bramberg, as a consequence of outstanding liabilities.
December 1913	The Habachtal property is purchased by a group of three farmers and municipal leaders from Bramberg (Alois Kaserer, Johann Blaikner, and Peter Meilinger).
October 1916	Austrian citizen Anton Hager purchases the Habachtal property.
1917–1919	Hager considers mining for both emerald and talc, searching for a partner to invest alongside him in the Habachtal property.
September 1920	Hager sells a one-half interest in the property to his half-brother Peter Staudt.
1921–1927	Investigation of mining prospects proceeds, with inspection reports, chemical analyses, and a business plan being prepared to target not only emerald but also industrial talc production. However, the extensive investment for the talc operations is never made and only emerald mining occurs, with Max Brennekam responsible for activities on site. Anton Hager Jr. draws the first detailed maps of the C and D galleries.
October 1927	Ownership of the Habachtal property is transferred to the Swiss firm Aktiengesellschaft für modernen Bergbau, located in Chur, with the price to be paid in two installments. Max Brennekam stays on, working for the company in 1927 and 1928.

TABLE 2 (continued). History of emerald mining in Habachtal.

Date	Event
October–November 1928	Hager and Staudt initiate foreclosure proceedings because the second installment of the purchase price remained unpaid, but auction is avoided when Aktiengesellschaft für modernen Bergbau receives a loan from Hans Streubert of Munich. Streubert then transfers his interest in the loan to Max Gaab and Meta Geist from Munich.
December 1928	Smaragd-Bergbau Habachtal GmbH is founded in Austria to serve as the local operating entity for the Swiss Aktiengesellschaft für modernen Bergbau. Streubert, working from Munich, leads the new firm.
1928–1931	Wilhelm Müller is initially hired for trial mining and evaluation, and the period sees a dubious call for investors, consideration of mining for three targets (emeralds, beryllium ore, and talc), further loans from Max Gaab and Florian Prader, and limited actual mining activities. Aktiengesellschaft für modernen Bergbau also becomes the subject of a Swiss bankruptcy proceeding that terminates after three days without dissolution.
1930–1934	Multiple exploration permits are registered and later prolonged in the Habachtal area by Julius Burger from Munich in the name of the painter Christian Schad from Berlin.
1932	Hugo Ullhofen is named receiver of the Habachtal property by the Mittersill court, and he in turn leases the mine to the Italian Angelo De Marchi.
1932–1933	A web of litigation and administrative proceedings ensues in the wake of efforts by several groups of associates seeking to pursue interests in and control over the Habachtal mine, with prominent names being Schad/Burger, De Marchi/Ullhofen, Gaab/Geist, and Prader.
August 1933	Gaab, Geist, and Prader become owners of the Habachtal property upon purchase at a foreclosure auction.
June 1934	A new Swiss entity Smaragd Aktiengesellschaft is established in Schaffhausen, with initial shareholders consisting of Schad, Burger, Gaab, Geist, and Prader. Gaab, Geist, and Prader lease the Habachtal property to the company.
1935–1939	Smaragd Aktiengesellschaft undertakes limited mining activities.
December 1940	The shareholders of Smaragd Aktiengesellschaft dissolve the company.
1946	With Gaab having acquired Prader's one-third interest in the Habachtal property in the early 1940s, Hans Zieger starts limited mining activities under a contract with Gaab. Zieger is also named administrator of the property by the U.S. Allied Commission for Austria.

For a summary of ownership transitions after 1950 and an overview of present mining activities, see the article text.

and disappointments (see table 2). The property was held by the state in the first half of the nineteenth century and sold in 1861 to jeweler Samuel Goldschmidt from Vienna, who was the first to undertake systematic recovery of emeralds. Open-pit activities began in 1862, followed by tunneling, but efforts were canceled after a few years of limited success. In 1896, Goldschmidt's heirs sold the Habachtal property to the British firm Emerald Mines Limited, which in turn was owned or controlled by a succession of two different British groups. The first, from 1896 to 1906, was the London-based diamond merchant Leverson, Forster & Co. and individuals connected therewith. Mining was performed in the summer months for seven or eight years, with some intervening inactive seasons. Legal troubles led to the transfer of shares in 1906 to the Northern Mercantile Corporation Limited of Manchester. Under new leadership, only limited mining without great success was pursued in 1906 and possibly 1907. By 1913, mounting liabilities, particularly to the municipality of Bramberg, resulted in the mine being returned to public ownership before being resold in the ensuing decades to a series of Austrian, German, and Swiss private individuals and entities.

After World War I, mining recommenced under Hager, an Austrian citizen, and his half-brother Staudt, a German citizen, with the production of talc for industrial purposes also being considered. Detailed geological reports of the locality and business plans were prepared, but the requisite investment for actualization never materialized. In late 1927, the property was purchased by the Swiss firm Aktiengesellschaft für modernen Bergbau. The outcome, however, was just one month of mining in 1927 and a few weeks in 1928 and 1929 before liabilities and legal troubles overtook any hope of a sustainable business. Rivalries between multiple groups interested in the property and its prospects, not only for emeralds but also for beryllium as an ore mineral, erupted in a welter of litigation and regulatory proceedings. Key players included the team of Schad and Burger, who were

particularly active in seeking exploration permits; Gaab, Geist, and Prader, who held liens in the property as a consequence of extending loans to Aktiengesellschaft für modernen Bergbau; and the Italian investor De Marchi, to whom the property had been leased in 1932 by the court-appointed receiver Ullhofen. In the midst of the litigation and administrative actions, De Marchi was only able to engage in active mining for the single 1932 season.

Eventually, a foreclosure initiated by Gaab and Geist resulted in a public auction in 1933, where the property was purchased by Gaab, Geist, and Prader, with ownership thereafter held in three equal shares. Another Swiss entity, Smaragd Aktiengesellschaft, was established in 1934 in Schaffhausen, with the majority of those individuals pursuing mining at Habachtal joining together as shareholders. Notably, Schad contributed a number of exploration permits, while Gaab, Geist, and Prader leased the property to the company. Nonetheless, only limited production efforts were undertaken between 1935 and 1939, terminating in 1940 with the common refrain of insolvency and the dissolution of Smaragd Aktiengesellschaft. Control of the property narrowed down to the three owners Gaab, Geist, and Prader, before subsequently being consolidated in the Gaab family. The Habachtal property finally ended up as private German property, maintained today by the Steiner family from Bramberg.

In summary, it appears that from 1862 to 1939, active mining took place at Habachtal only during a series of relatively brief and disjointed periods:

1. For a few years starting in 1862 by Goldschmidt via open-pit methods and later tunneling
2. In the 1870s by lessees contracting with Goldschmidt's heirs
3. From 1896 to 1902 by the British entity Emerald Mines Limited under the control of Leverson, Forster & Co., which worked underground using four galleries
4. In 1906 and possibly into 1907 by the Emerald Mines Limited under the control of Northern Mercantile Corporation Limited
5. Intermittently between 1920 and 1927 by Hager and Staudt
6. Briefly in 1927 and 1928 or 1929 by the Swiss firm Aktiengesellschaft für modernen Bergbau
7. In 1932 by De Marchi
8. From 1935 to 1939 by the Swiss entity Smaragd Aktiengesellschaft

The success of any of the eras, and the broader question of the value of the Habachtal property for mining purposes, are difficult to intuit from the historical record left behind. Problems in that regard derive both from the backgrounds of the principals and from the disparate purposes underlying different reports or appraisals. As to the participants, it is notable that only Goldschmidt and the London-based diamond merchants had deep roots in and knowledge of the gemstone market. Later owners and directors were merchants hailing from other fields—bankers, civil engineers, and attorneys—who in turn were assisted by civil, technical, and mining engineers, geologists, and mine foremen. Notably absent were any skilled gem merchants truly able to assess the commercial value of the mined rough.

Concerning the different purposes of reports and appraisals, there is a marked divergence between figures or values offered in a regulatory sphere versus an investment setting. For example, Emerald Mines Limited reported to the mining administration that material was nearly worthless to minimize payment of taxes and fees. Mining administrator Aigner took a similar view, commenting that emerald mining in Habachtal had never been profitable. Leitmeier reported the same, but his remarks might have been biased toward starting commercial production of beryl as an ore mineral. The counterpoint provided by figures aimed at drawing investment is dramatic. By way of examples, in 1920 Autzinger estimated production of 5 kg of export-quality emeralds per week, and in 1930 Deutsch-Österreichische Edelsteinbergwerks Gesellschaft calculated profitability at several hundred thousand marks per year. Such inflated figures led to repeated financial failures for both companies and individuals, with perhaps only Müller's 1929 report having identified the real problem—only 2% of the emeralds recovered were of facet quality.

In the final analysis, it seems that between 1862 and 1939, emerald mining at Habachtal was only economical, at least in part, for brief periods under Leverson, Forster & Co. and De Marchi. That said, it is likely that even with the limited quantity of gem-quality rough, small-scale mining guided by experienced mining engineers or geologists, combined with distribution of emeralds in matrix for collectors and facet-quality rough for gem cutters by trade experts through the right channels, could have been profitable. That is the state of affairs at Habachtal today.

ABOUT THE AUTHOR

Dr. Schmetzer is an independent researcher residing in Petershausen, near Munich, Germany.

ACKNOWLEDGMENTS

Gratitude is expressed to countless individuals who helped to provide information concerning local conditions, photos, references, etc., many of whom are referenced in the figure captions. Highlighted in particular are Maureen Mary Brett (Bromley, UK); Erwin Burgsteiner (Bramberg, Austria); Peter Danner (Salzburg, Austria); Günter Grundmann (Detmold, Germany); Ingrid von Klitzing (Munich); Alfred Lahnsteiner (Hollersbach, Austria); Peter Lausecker (Kirchhundem, Germany); Brigitte Leitermann (Traunstein, Germany); Josef Seifriedsberger (Bramberg); Peter Semrád (Bergen, The Netherlands); Claudia and Andreas Steiner (Bramberg); Norbert E. Urban (Salzburg); and Heiko Wegmann (Freiburg).

Likewise acknowledged are the following archives, both public and private, as well as their leadership and staff members who searched through files for original documents and biographical data upon request from the author: Archive of the Jewish Community in Vienna; Archive of the TU Bergakademie Freiberg, Germany; Bayerisches Wirtschaftsarchiv, Industrie- und Handelskammer, Munich; Bergbaumuseum, Mühlbach am Hochkönig, Austria; Bergbau- und Gotikmuseum, Leogang, Austria; Bischöfliches Zentralarchiv, Regensburg, Germany; Christian-Schad-Stiftung, Museen der Stadt Aschaffenburg, Aschaffenburg, Germany; Fürst Thurn und Taxis Hofbibliothek und Zentralarchiv, Regensburg; Geologische Bundesanstalt, Vienna; Kresen Kernow, Redruth, Cornwall, UK; Landesamt für Geologie, Rohstoffe und Bergbau, Freiburg; Landesarchiv Baden-Württemberg, Freiburg; Landesarchiv, Land Salzburg, Salzburg, Austria; Montanbehörde West, Bundesministerium für Landwirtschaft, Regionen und Tourismus, Salzburg; Natural History Museum, London; Österreichisches Staatsarchiv, Vienna; Salzburg Museum, Salzburg; Staatsarchiv des Kantons Zürich, Switzerland; Tiroler Landesarchiv, Innsbruck, Austria; University Archive and Mineralogical Collection of Friedrich-Schiller-University Jena, Germany; Wiener Stadt- und Landesarchiv, Magistratsabteilung 8, Vienna. The author would also like to thank the archives of the cities or municipalities of Bramberg, Kitzbühel, Mittersill, Mühlbach am Hochkönig, and Salzburg (Austria); Fischbachau, Freiburg, Miesbach, Munich, Tirschenreuth, Traunstein, Windischeschenbach, and Würzburg (Germany); Bolzano (Italy); Chur, Schaffhausen, and Zurich (Switzerland); and Bromley (UK).

Josef Seifriedsberger and Erwin Burgsteiner (both of Bramberg, Austria) critically reviewed the manuscript. Andrea R. Blake (Chevy Chase, Maryland) assisted with editing the final version of the English text.

REFERENCES

Aulitzky H. (1973) *Hochwasser, Muren, Lawinen: Information über Wasserwirtschaft und Katastrophenschutz*, 2nd ed. Bundesministerium für Land- und Forstwirtschaft, Vienna, 272 pp.

Autzinger L. (1922) Das Talkum-und Smaragdbergwerk in Habach, Post Bramberg, im Pinzgau. *Montan-Zeitung für Österreich-Ungarn und die Balkanländer*, Vol. 29, No. 24, pp. 232–233.

Burgsteiner E. (2002) *Kristallschätze zur Geschichte der Steinsammler im Oberpinzgau.* Bode Verlag GmbH, Haltern, Germany, 248 pp.

Danner P. (2014) Geowissenschaftliche Forschungen in Salzburg 1938-1945. *Berichte der naturwissenschaftlich-medizinischen Vereinigung in Salzburg*, Vol. 17, pp. 43–148.

——— (2015) Görings Geologen in der Ostmark. "Bodenforschung" in Österreich für den Vierjahresplan von 1936 bis 1939 – eine Archivstudie. *Berichte der Geologischen Bundesanstalt*, Vol. 109, pp. 1–139.

Düllmann L. (2009) *Smaragdsuche(r) im Habachtal – Historie und Histörchen*. Pro BUSINESS GmbH, Berlin, 81 pp.

Eberl R. (1972) *Smaragde – Segen und Fluch*. Publ. by the author, Vienna, 105 pp.

Exel R. (1993) *Die Mineralien und Erzlagerstätten Österreichs*. Publ. by the author, Vienna, 447 pp.

Frischholz J. (1821) Über den Salzburger Smaragd. *Neue Jahrbücher der Berg- und Hüttenkunde*, Vol. 4, pp. 382–385.

Fritz E. (1972) Talk- und Talkschiefer-Vorkommen in Österreich. *Montan-Rundschau*, Vol. 20, No. 3, pp. 78–85, No. 4, pp. 95–100.

Grundmann G. (1979) Geologisch-Petrologische Untersuchung der Smaragd-führenden Gesteinsserien der Leckbachscharte, Habachtal (Land Salzburg, Österreich). Diploma thesis, Technische Universität Berlin, pp. 20–24.

——— (1991) Smaragd. *extraLapis No.1*, Christian Weise Verlag, Munich, 93 pp.

Gübelin E.J. (1956a) Emerald from Habachtal. *Journal of Gemmology*, Vol. 5, No. 7, pp. 342–361.

——— (1956b) The emerald from Habachtal. *G&G*, Vol. 8, No. 10, pp. 295–309.

Günther W., Lewandowski K. (2002) Montanbehörden und Montaninstitutionen in Salzburg. *Mitteilungen der Gesellschaft für Salzburger Landeskunde*, Vol. 142, pp. 267–290.

Hammer V.M.F., Pertlik F. (2014) Hans Leitmeier (1885-1967). Akademischer Lehrer, Dekan, Forscher und Sammler an der Wende von der analytischen zur experimentellen Mineralogie. *Mitteilungen der Österreichischen Mineralogischen Gesellschaft*, Vol. 160, pp. 73–108.

Hanke H. (1939) Das einzige Smaragdbergwerk Europas. *Das Werk, Monatsschrift der "Vereinigte Stahlwerke Aktiengesellschaft,"* Vol. 19, pp. 195–198.

Haselbeck F. (2019) Eine einleitende Betrachtung zur Stadtgeschichte. In F. Haselbeck, Ed. *Traunstein ohne Salz*? Stadt Traunstein, Traunstein, Germany, pp. 7–40.

Hausmann F. (1950) Ein Zweimannbergwerk in den Hohen Tauern. Die einzige Smaragdfundstelle Europas. *Große Österreich Illustrierte Wien*, Vol. 2, November 18, p. 8–9.

Hönigschmid H. (1993) *Bramberg am Wildkogel*. Gemeinde Bramberg, Bramberg, Austria, 656 pp.

Lausecker P. (1986) *Smaragdfundstelle Habachtal – Geschichte, Geologie, Bergbau*. Hof/Saale, PHL-Verlag, 104 pp.

Lehner J. (1669) *Balnei Abacensis in Bavaria inferior nova descriptio. Das ist: Kurze Beschreibung des Wildbads zu Abach in nieder Bayrn*. C. Fischer, Regensburg, Germany, 106 pp.

——— (1702) *Balnei Abacensis in Bavaria inferior nova descriptio. Das ist: Kurze Beschreibung des Wildbads zu Abach in nieder Bayrn*. J.C. Haam, Straubing, Germany, 87 pp.

——— (1718) *Balnei Abacensis in Bavaria inferior nova descriptio. Das ist: Kurze Beschreibung des Wildbads zu Abach in nieder Bayrn*. J.B. Lang, Regensburg, Germany, 106 pp.
Leitmeier H. (1929/1930) Das Smaragdvorkommen im Habachtal. *Mitteilungen der Wiener Mineralogischen Gesellschaft*, No. 92, pp. 11–17; published as supplement to *Mineralogische und Petrographische Mitteilungen, Neue Folge*, Vol. 40, 1930.
——— (1937) Das Smaragdvorkommen im Habachtal und seine Mineralien. *Mineralogische und Petrographische Mitteilungen, Neue Folge*, Vol. 49, No. 4-5, pp. 245–368.
——— (1938) Smaragdbergbau und Smaragdgewinnung in Österreich. *Berg- und Hüttenmännische Monatshefte*, Vol. 86, No. 1/2, pp. 3–12.
——— (1946) Die Smaragde vom Habachtal. *Die Presse*, No. 44, November 24, pp. 3–4.
Lewandowski K. (1997) *Der Smaragdbergbau in der Leckbachrinne im Habachtal*. Museumsverein, Heimatmuseum Bramberg, Bergbauforschung, Bramberg, Austria, 23 pp.
Pech H. (1976) *Smaragde – Gauner und Phantasten*. Pinguin-Verlag, Innsbruck, Austria, 123 pp.
Richter T. (2020) *Christian Schad. Künstler im 20. Jahrhundert - Bausteine zur Biographie*, Vol. 1. Stadt Aschaffenburg and Michael Imhof Verlag, Petersberg, Germany, 479 pp.
Scherz G. (1955) Niels Stensens Smaragdreise. *Centaurus*, Vol. 4, No. 1, pp. 51–57.
Schiffner C. (1940) Aus dem Leben alter Freiberger Bergstudenten. Band 3. Verlag E. Mauckisch, Freiberg, Germany, pp. 75–77.
Schmidegg O. (1955) Gips und andere Bodenschätze um Reutte. *Schlern-Schriften*, Vol. 111, pp. 53–59.
Schroll K.M. (1797) Grundriss einer Salzburgischen Mineralogie. *Jahrbücher der Berg- und Hüttenkunde*, Vol. 1, pp. 95–196.
Smaragdbergwerk für Atomindustrie (1956) *Der Aufschluss*, Vol. 7, No. 3, pp. 69–70.
Stehrer S. (2000) Rätsel um Smaragd geklärt. *Salzburger Nachrichten*, Vol. 56, April 11, 2000, p. 11.
Von Petersen M. (1816) Brief aus Regensburg vom 20. Nov. 1815. *Taschenbuch für die gesammte Mineralogie mit Hinsicht auf die neuesten Entdeckungen*, Vol. 10, pp. 591–593.
Waagen L. (1936) Bergbau Bramberg, Österreichs Smaragdgrube. *Wiener Zeitung*, Vol. 233, No. 188, July 10, p. 10.
Wenzel E. (1921) Die Talk-Gewinnung in Deutsch-Österreich. *Steinbruch und Sandgrube*, Vol. 20, No. 9, pp. 224–226.
Werneck W.L. (1988) Das k.k. Revierbergamt in Wels 1872-1942. *Jahrbuch des Museal-Vereins Wels*, Vol. 27, 1987/88, pp. 169–176.

The
Dr. Edward J. Gübelin
Most Valuable Article AWARD

Most Valuable Article

First Place

Measurement and Characterization of the Effects of Blue Fluorescence On Diamond Appearance

Summer 2021

Yun Luo, David Nelson, Troy Ardon, and Christopher M. Breeding


Yun Luo


David Nelson


Troy Ardon


Christopher M. Breeding

Yun Luo is director of metrology and quality control at GIA in Carlsbad, California, where she studies the science of measurements and instrumentation related to diamond grading. She earned her bachelor's degree from the Gemmological Institute, China University of Geosciences in Wuhan, and her PhD in environmental mineralogy from Miami University in Ohio. **David Nelson** is a senior metrologist at GIA in Carlsbad, focusing on developing new technologies and measurement systems. **Troy Ardon** is a senior research associate at GIA in Carlsbad specializing in diamond color origin and software development related to spectral processing. He received his bachelor's degree in physics at the University of Illinois, Chicago, and his master's degree in diamond science and technology from the University of Warwick. **Christopher M. Breeding** is a senior manager of analytics at GIA in Carlsbad, where he investigates origin of color in diamond and other gems. Dr. Breeding, who is a co-editor of *G&G*'s Gem News International section, holds a PhD in geology from Yale University.

Second Place

Internal Structures of Known *Pinctada maxima* Pearls: Natural Pearls from Wild Marine Mollusks

Spring 2021

Artitaya Homkrajae, Areeya Manustrong, Nanthaporn Nilpetploy, Nicholas Sturman, Kwanreun Lawanwong, and Promlikit Kessrapong


Left to right: Kwanreun Lawanwong, Nanthaporn Nilpetploy, Nicholas Sturman (seated), Promlikit Kessrapong, Areeya Manustrong, and Artitaya Homkrajae

Artitaya Homkrajae is a senior staff gemologist at GIA in Carlsbad. She earned her bachelor's degree in earth science from Kasetsart University in Bangkok. **Areeya Manustrong** is a staff gemologist at GIA in Bangkok. She holds a bachelor's degree in material science (gems and jewelry) from Srinakharinwirot University in Bangkok. **Nanthaporn Nilpetploy** is a senior staff gemologist at GIA in Bangkok. She obtained her bachelor's degree in geology from Chulalongkorn University in Bangkok. **Nicholas Sturman** is a consultant to GIA and its former senior manager of global pearl services. With more than 25 years of detailed experience in the examination of pearls, he oversaw GIA's pearl testing operations in Bangkok, New York, Carlsbad, and Hong Kong. **Kwanreun Lawanwong** is an analytics technician at GIA in Bangkok. She obtained a bachelor's degree in physics from Kasetsart University. **Promlikit Kessrapong** is a former analytics technician for GIA in Bangkok. He obtained his bachelor's degree in biological science from Kasetsart University and his master's degree in biotechnology from Coventry University, United Kingdom.

Third Place

Blue Sapphires from Mogok, Myanmar: A Gemological Review

Winter 2021

Wasura Soonthorntantikul, Ungkhana Atikarnsakul, and Wim Vertriest


Wasura Soonthorntantikul


Ungkhana Atikarnsakul


Wim Vertriest

Wasura Soonthorntantikul is a research scientist at GIA in Bangkok. She received a PhD in analytical chemistry from Chulalongkorn University in Thailand. **Ungkhana Atikarnsakul** is a staff gemologist of colored stone identification at GIA in Bangkok. She holds a master's degree in analytical chemistry science from Chulalongkorn University in Thailand. **Wim Vertriest** is manager of field gemology at GIA in Bangkok, where he also curates GIA's colored stone research collection. He obtained a master's degree in geology (geodynamics and geofluids) from KU Leuven in Belgium.

Many thanks to the members of G&G*'s Editorial Review Board for voting this year.*

Lab Notes

Editors
Thomas M. Moses | Shane F. McClure

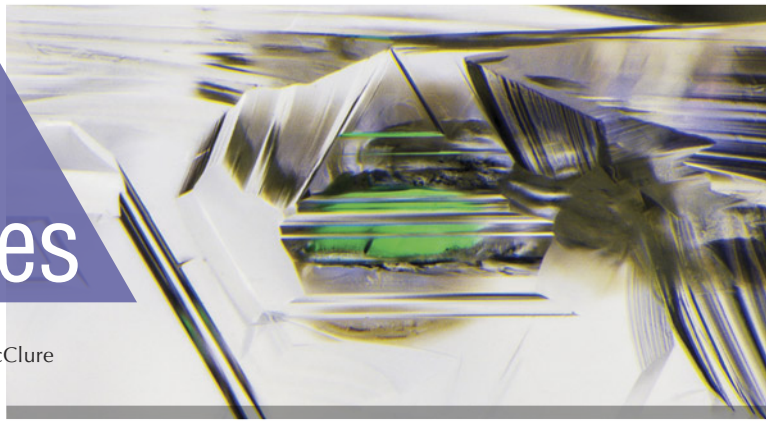

DIAMOND

HPHT-Processed Natural Type Ia Diamond

There are two types of high-pressure, high-temperature processes related to diamond: HPHT treatment and HPHT diamond growth. HPHT laboratory-grown diamonds were developed in the mid-1950s, with the first gem-quality production in the early 1970s and extensive production beginning in the 1990s.

HPHT treatment to change the color of natural diamonds was discovered as a byproduct of annealing natural diamond anvils. The General Electric Company (GE) and Lazare Kaplan International marketed the first commercial HPHT-treated color diamonds in March 1999 (K. Schmetzer, "Clues to the process used by General Electric to enhance the GE POL diamonds," Winter 1999 *G&G*, pp. 186–190). The same machines, such as a hydraulic press that produces extremely high pressure and temperature environments, are also used to treat both mined and laboratory-grown diamonds. HPHT treatment can change the color of diamonds or make them colorless.

A natural 5.20 ct type Ia SI_2 Fancy Dark yellowish brown diamond with natural anhedral crystal inclusions was submitted to the New York laboratory for grading services and returned. After being treated, it was resubmitted as a 5.17 ct type Ia SI_2 Fancy Deep yellow-orange diamond (figure 1), with the disclosure that it had been HPHT processed. After

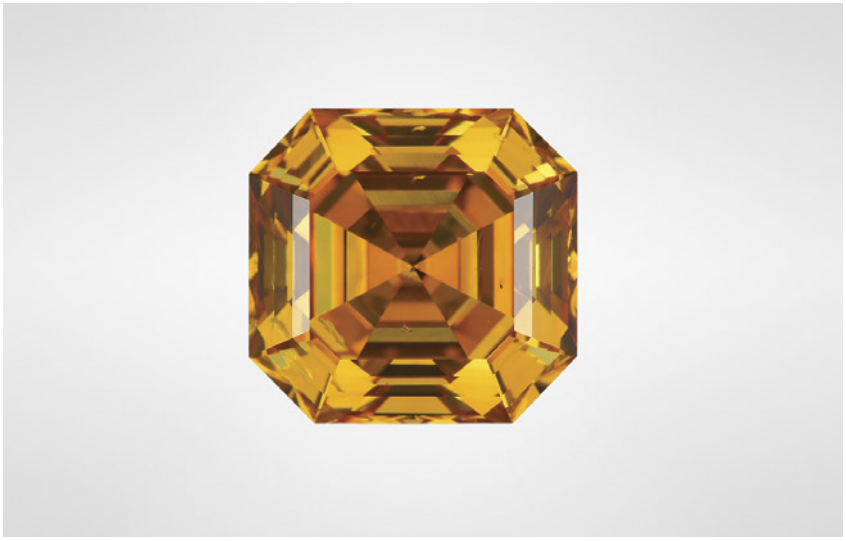

Figure 1. This 5.17 ct Fancy Deep yellow-orange HPHT-treated diamond was resubmitted to the New York laboratory.

Figure 2. Table-down images showing the diamond before HPHT treatment (left) and after (right).

Editors' note: All items were written by staff members of GIA laboratories.

Gems & Gemology, Vol. 58, No. 1, pp. 48–58.

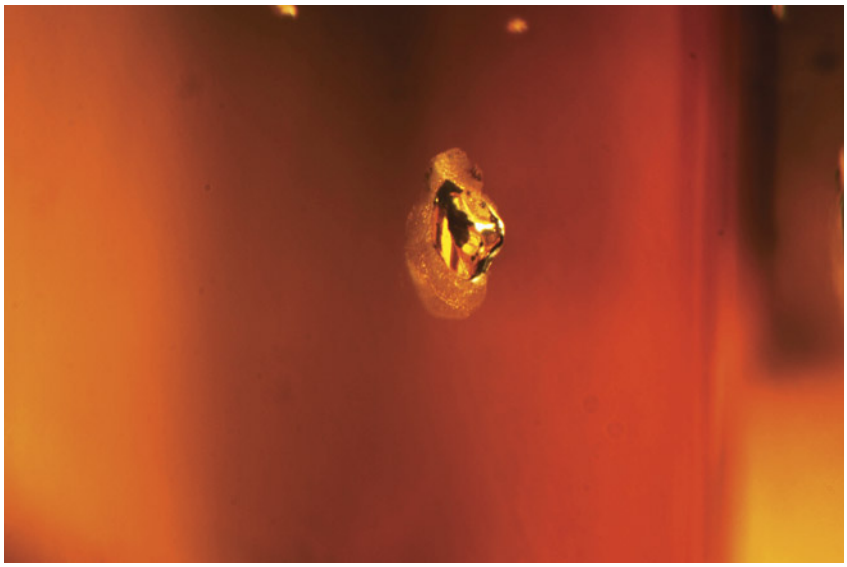

Figure 3. This natural anhedral crystal was formed during diamond growth and acquired a graphitized halo after HPHT treatment. Field of view approximately 1.26 mm.

analysis, the diamond was confirmed to have been treated using an HPHT process that changed the color from a dark yellowish brown to a deep yellow-orange (figure 2). After the HPHT process, each of the natural anhedral crystal inclusions developed a graphitized halo (figure 3). In the natural diamond, the visible/near-infrared (Vis-NIR) absorption spectrum showed a slight 550 nm band—a feature that may impart a pinkish color component depending on its absorbance and other features present within the diamond. After HPHT treatment, there is instead an increase in absorption from ~500 nm toward the lower wavelengths; this absorption rise is due to the creation of single, isolated nitrogen (figure 4).

As expected (I.M. Reinitz et al., "Identification of HPHT-treated yellow to green diamonds," Summer 2000 *G&G*, pp. 128–137), FTIR data from after the HPHT treatment showed that a peak associated with isolated nitrogen at 1344 cm^{-1} was introduced, the ~1363 cm^{-1} platelet peak was diminished, and the natural amber center at ~4165 cm^{-1} was destroyed (figure 5). Since the spectroscopic data changed after treatment, crystal inclusions plotted on the original grading diagram for this diamond confirmed it was the same stone. The 550 nm band in the Vis-NIR absorption spectrum related to a pink or brown diamond is stable at lower temperatures of HPHT treatment. Since the 550 nm band was not detected after the process, we believe this diamond was treated at the higher end of the HPHT regime or for a prolonged duration that required repolishing, which caused it to lose three points of carat weight.

While there are many different treatments that can be performed on diamonds, HPHT treatments are permanent and require a stable and controlled environment. In this stone, the treatment resulted in some of the nitrogen aggregates being split apart into single, isolated nitrogen that introduced new color centers and altered the color of the treated stone. The treatment also graphitized inclusions; however, this change was not sufficient to lower the clarity grade. As technology advances, HPHT treatments are becoming more common for both natural and laboratory-grown diamonds.

Sally Ruan

Figure 4. Vis-NIR spectra show the untreated natural diamond with the 550 nm band (orange line). After HPHT treatment (blue line), the 550 nm band is not apparent. Instead, there is an increase in absorption from 500 nm toward the lower wavelengths (higher energy). Spectra are offset for clarity.

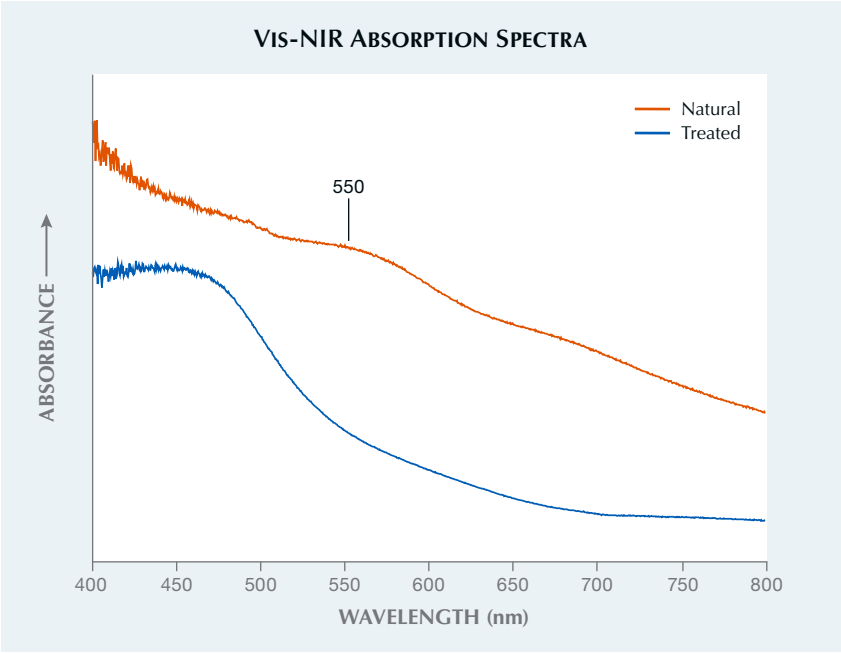

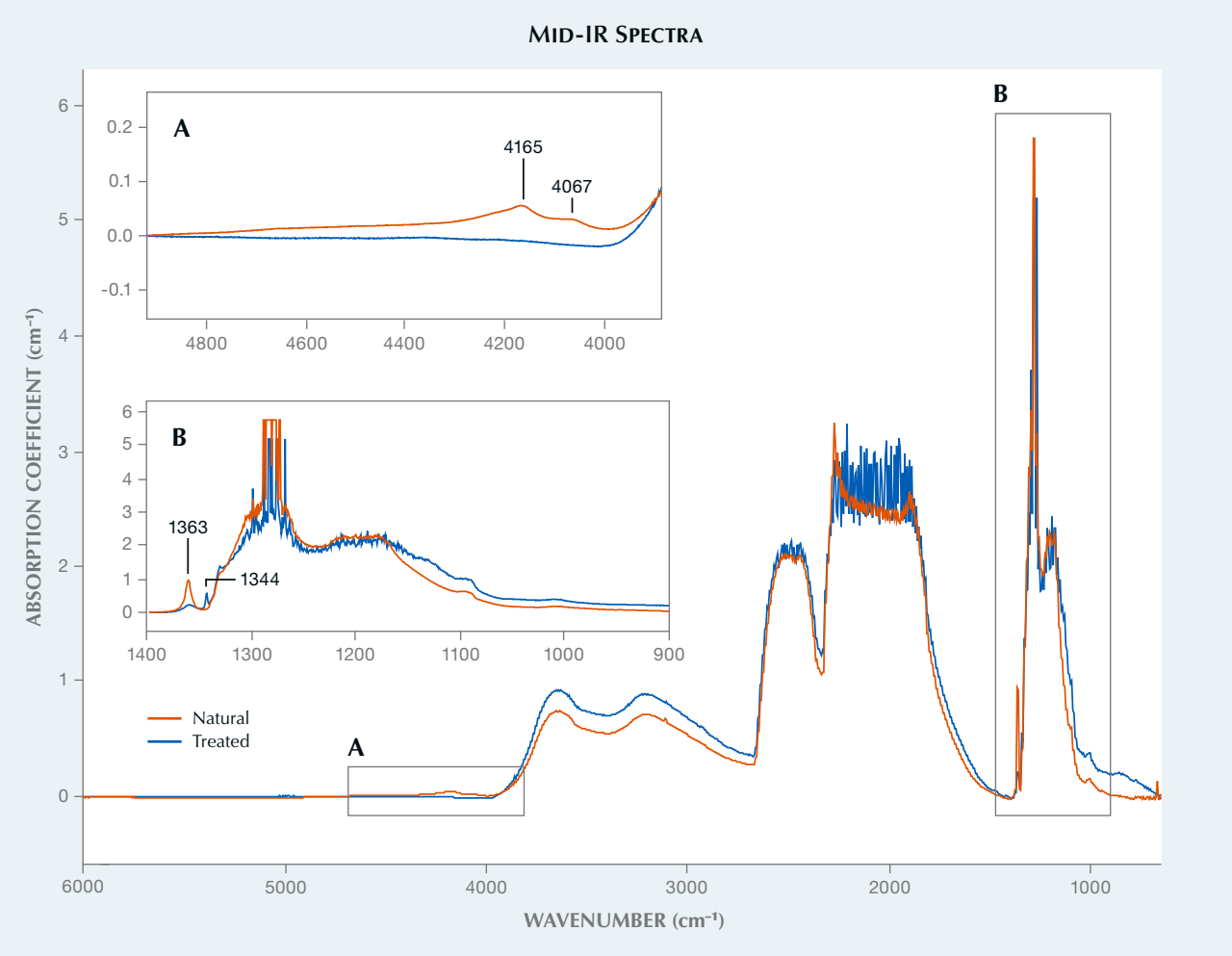

Figure 5. The B region of the mid-infrared spectrum shows a new isolated nitrogen peak at 1344 cm^{-1} and a diminished ~1363 cm^{-1} platelet peak after HPHT processing (orange line). The A region of the mid-infrared shows that the natural amber center at ~4165 cm^{-1} (shown in orange) was destroyed after HPHT processing. The spectra are baseline corrected.

Large Green and Yellow Diamonds Colored by Nickel Impurities

Diamonds colored by nickel impurities were previously thought to only occur in lower carat weights and with weaker color saturations. However, the Carlsbad laboratory recently received several large examples with strongly saturated color. Among the stones examined, a Fancy Intense green-yellow cushion weighing 5.02 ct, a Fancy yellow-green pear weighing 5.03 ct, and a Fancy Intense green-yellow pear weighing 5.06 ct were the most notable (figure 6).

Gemologically, these diamonds were mostly free of inclusions except for faint internal graining and small reflective platelets. Along with natural inclusions, FTIR spectra showed that all three stones were type IaA, confirming that these are naturally mined diamonds and not of synthetic origin. Vis-NIR spectra revealed an asymmetrical absorption band around 670 nm and a notable peak at 883 nm for all three (figure 7). These features in the UV-Vis-NIR strongly suggest that the color is caused by the presence of nickel-related defects.

Previously, the largest and most intensely colored gem diamonds reported to have been colored by nickel defects were a 2.54 ct Fancy Light greenish yellow diamond (see Fall 2013 Lab Notes, pp. 173–174) and a 2.81 ct Fancy Intense yellowish green diamond (W. Wang et al., "Natural type Ia diamond with green-yellow color due to Ni-related defects," Fall 2007 *G&G*, pp. 240–243).

The stones described in the present report are nearly twice as large and have significantly more sat-

Figure 6. Large gem diamonds with strong color saturations resulting from nickel-related impurities. Top: 5.02 ct Fancy Intense green-yellow cushion. Bottom left: 5.03 ct Fancy yellow-green pear. Bottom right: 5.06 ct Fancy Intense green-yellow pear.

urated hues. Therefore, it appears that nickel-colored diamonds can occur over a wider range of sizes and color saturations than previously suspected.

Jamie Price

Figure 7. Vis-NIR spectra collected from each diamond show a strong asymmetrical absorption band around 670 nm along with a distinct peak at 883 nm. These defects together, with the lack of any other color-causing defects, indicate that nickel is the main cause of color.

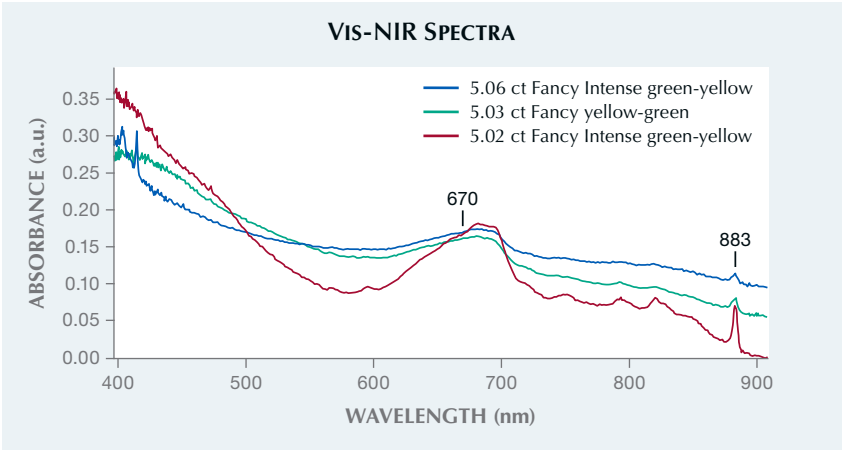

Nail-Head Spicule in a Russian EMERALD

Recently, a 1.86 ct transparent green pear mixed cut (figure 8) was submitted for identification to the Carlsbad laboratory. Initial testing produced the following results: refractive index values of 1.582–1.590, birefringence of 0.008, doubly refractive, and a hydrostatic specific gravity of 2.73. The long-wave UV reaction was red with a blue fluorescence in surface-reaching fractures from the clarity enhancement. These results were consistent with natural emerald. Trace element chemistry of the host emerald collected via laser ablation–inductively coupled plasma–mass spectrometry (LA-ICP-MS) matched well with GIA's Russian emerald chemistry reference data.

Figure 8. A 1.86 ct transparent green pear mixed-cut emerald.

While the identification of any gem requires further testing with a variety of instruments, in most cases the stone's natural or synthetic origin can be determined conclusively by features seen under magnification. Nail-head spicules are typically associated with synthetic hydrothermal (and occasionally flux-grown) emerald and synthetic quartz, but they are also occasionally found in natural gems such as beryl, sapphire, spinel, tourmaline, and quartz (G. Choudhary and C. Golecha, "A study of nail-head

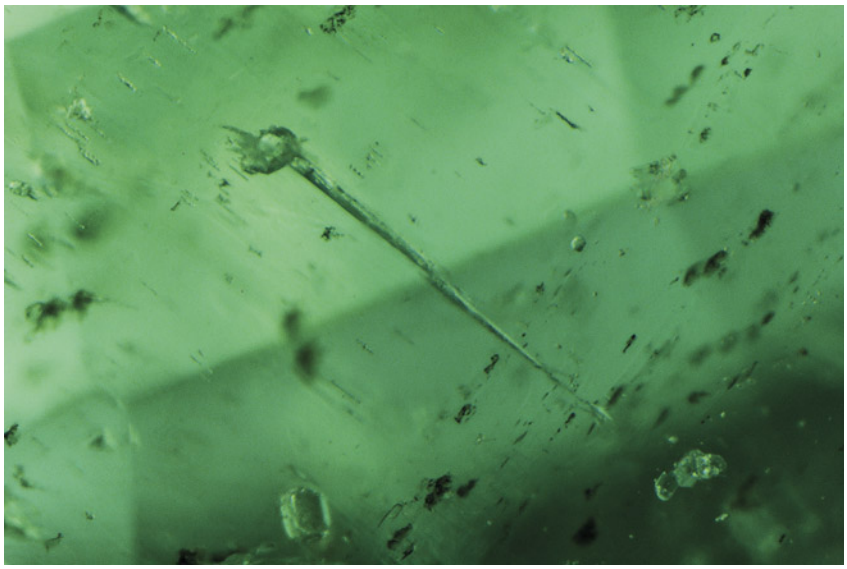

Figure 9. Nail-head spicule in the natural emerald from figure 8. Field of view 2.01 mm.

spicule inclusions in natural gemstones," Fall 2007 *G&G*, pp. 228–235; K. Schmetzer et al., "Multicomponent inclusions in Nacken synthetic emeralds," *Journal of Gemmology*, Vol. 26, No. 8, 1999, pp. 487–500). Nail-head spicules are wedge-shaped two-phase (liquid and gas) inclusions capped by crystals that act as growth obstacles (figure 9). During growth of the host crystal, a small crystal or platelet is deposited on its surface. As the crystal continues to grow past the inclusion, a tapered void is created, which traps the hydrothermal growth medium such that, upon cooling, it becomes two phases consisting of liquid and a gas bubble (Choudhary and Golecha, 2007).

Maxwell Hain

Dyed FLUORITE

Two pieces of green rough weighing 358.03 and 454.27 ct (figure 10) were recently sent to the Carlsbad laboratory for an emerald identification and origin report. Standard gemological testing could not be performed due to the rough surfaces and size of the stones. Raman spectroscopy was used to aid in the identification (figure 11), and the Raman spectra were consistent with the mineral fluorite.

Internally and externally, both pieces showed typical massive habit fluorite features. Small octahedral crystals were scattered along the surfaces, and perfect cleavage in four di-

Figure 10. These two rough pieces weighing 454.27 and 358.03 ct were identified as dyed fluorite.

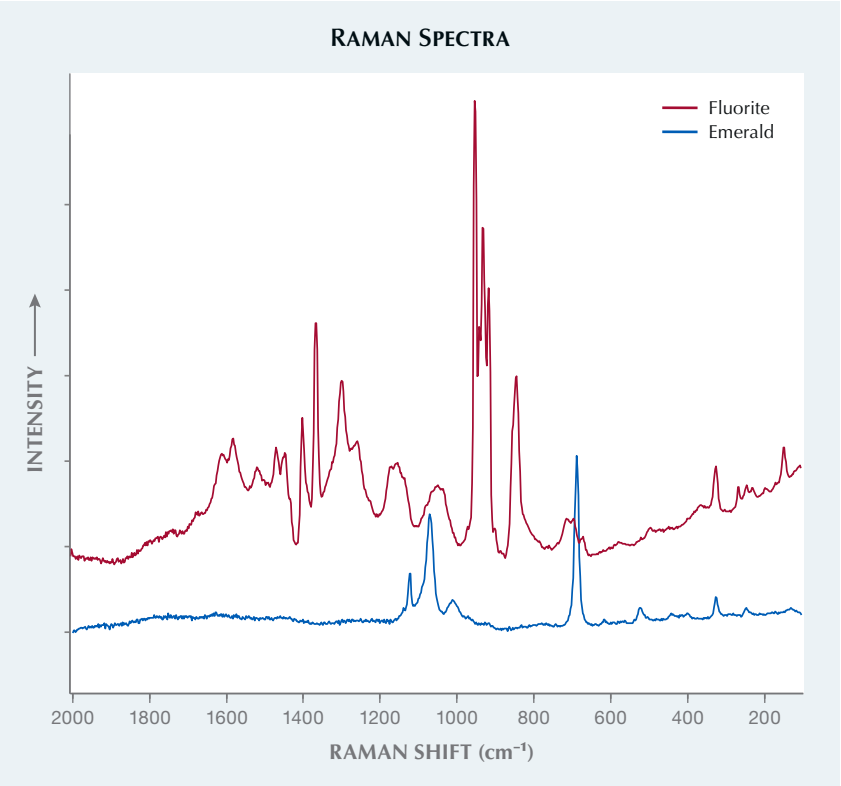

Figure 11. Overlay of the Raman spectra of one of the dyed fluorite samples and a known emerald sample.

rections was documented. Cleavage is not a gemological property of emerald, and octahedral cleavage is a key identifying feature for fluorite. Weak color banding could be seen with diffused lighting, but the most abnormal observation with both of these stones was the presence of obvious dye concentrations along their fractures (figure 12).

Fluorite naturally comes in a wide range of colors and can have multiple colors in a single crystal. These stones are a careful reminder to analyze every stone thoroughly for proper identification and to detect the most uncommon of treatments.

Nicole Ahline

Repaired GRANDIDIERITE

Recently the Carlsbad laboratory received for identification services a transparent bluish green stone weighing 1.43 ct and measuring 7.47 × 6.31 × 4.06 mm (figure 13). Standard gemological testing revealed a refractive index of 1.58–1.62 on both the crown and pavilion, suggesting that both the crown and pavilion were grandidierite. This was confirmed using FTIR and Raman spectroscopy. Microscopic examination showed a very large fracture that broke continuously around the entire stone. Closer inspection revealed that the fracture was filled (figure 14), and this filling was holding the stone together, indicating that the stone was likely broken into two pieces and then repaired with a resin or glue.

Figure 12. Obvious dye concentrations within surface-reaching fractures. Field of view 7.26 mm.

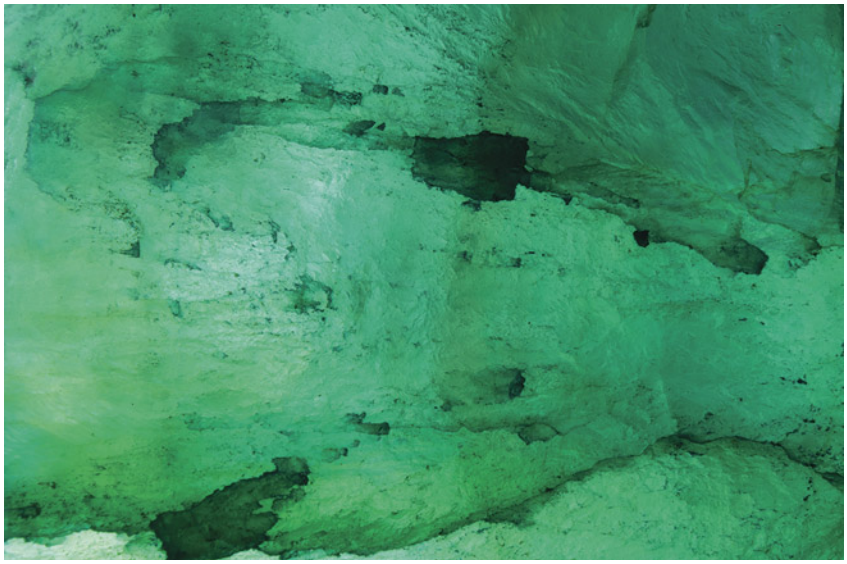

Figure 13. Flattened gas bubbles caught in the break of a filled fracture are visible face up in this 1.43 ct repaired grandidierite.

Figure 14. Flattened gas bubbles caught in the filling of the large fracture that breaks continuously through the entire pavilion and some of the crown. Field of view 4.79 mm.

Grandidierite is a very rare mineral, and transparent gem-quality material was not found in the market until 2015 (Winter 2015 Gem News International, pp. 449–450). Named after French naturalist Alfred Grandidier (1836–1912), grandidierite was first discovered in 1902 at the cliffs of Andrahomana on the southern coast of Madagascar (D. Bruyere et al., "A new deposit of gem-quality grandidierite in Madagascar," Fall 2016 *G&G*, pp. 266–275). This is the first repaired grandidierite GIA has seen to date.

Michaela Stephan

LABORATORY-GROWN DIAMOND

New Record Size for CVD Laboratory-Grown Diamond

Growth technology of single-crystal diamond has advanced significantly in the last two decades for both the high-pressure, high-temperature (HPHT) and chemical vapor deposition (CVD) methods. In addition to many other applications, laboratory-grown diamonds have become an expanding segment of the jewelry industry. Records for crystal size and quality are frequently broken. In this note, GIA's New York laboratory reports on a new record for CVD laboratory-grown diamond.

This square modified brilliant diamond produced by Shanghai Zhengshi Technology Co. Ltd. (figure 15) weighed 16.41 ct and measured 13.97 × 13.87 × 9.56 mm, with G color and VVS_2 clarity. The strong graining distributed throughout it created a "wavy" appearance (see the video at www.gia.edu/gems-gemology/spring-2022-lab-notes-new-record-size-CVD). In addition, a few tiny pinpoints were present. Absorption spectroscopy in the infrared region revealed this was a typical type IIa diamond. Except for absorptions from the diamond itself, no other defect-related absorption was detected in this region. Photoluminescence spectroscopy collected at liquid nitrogen temperature with 514 nm laser excitation (figure 16, left) showed emissions from NV centers with zero-phonon lines (ZPL) at 575.0 and 637.0 nm with moderate intensities. Clear emissions from SiV^- at 736.6 and 736.9 nm were detected. Weak emissions at 596 and 597 nm, which are specific to CVD diamond and also unstable at high temperature, were recorded overlapping with sidebands of the NV^0.

Figure 15. The new record size for CVD laboratory-grown diamond—16.41 ct, with G color and VVS_2 clarity—has been achieved by Shanghai Zhengshi Technology Co. Ltd. This is an as-grown diamond; no post-growth treatment was applied for color improvement, either before or after faceting.

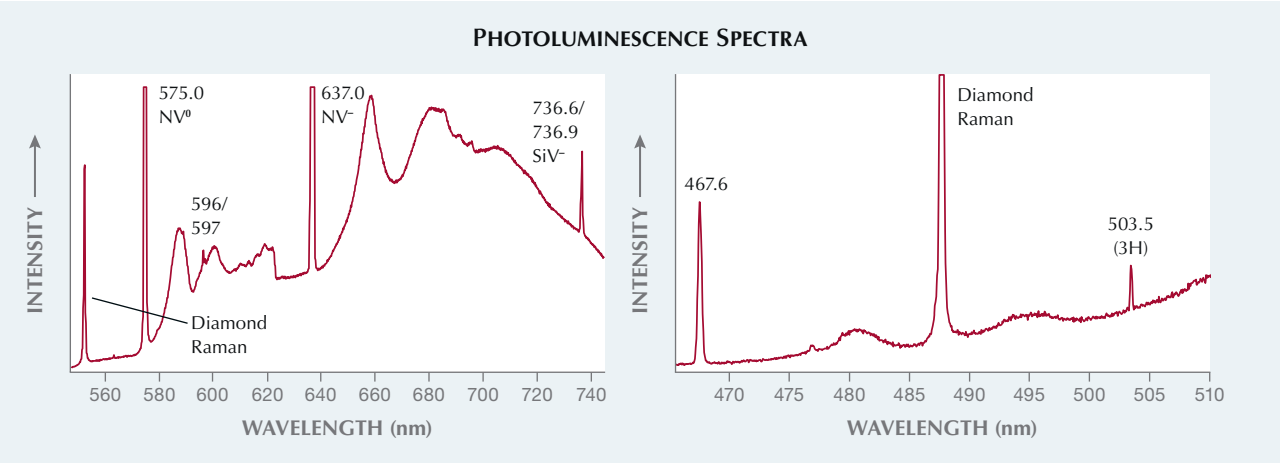

Figure 16. Left: The photoluminescence spectrum with 514 nm laser excitation under liquid nitrogen temperature showed typical features of as-grown CVD diamond. Right: In the photoluminescence spectrum with 457 nm laser excitation under liquid nitrogen temperature, weak emissions from the 3H defect and from the 467.6 nm center were recorded.

Photoluminescence spectroscopy with 457 nm laser excitation (figure 16, right) detected weak emissions at 503.5 nm (3H) and 467.6 nm. Similar to the emission at 596 and 597 nm, the 467.6 nm center is CVD-specific and would be annealed out at very high temperature. No emission from the H3 defect was observed. All these spectroscopic features confirmed this was a CVD diamond with no post-growth treatment to improve the color.

Images collected under deep short-wave UV excitation showed strong orange-red fluorescence with banded blue regions (figure 17). The blue "columns" were nearly perpendicular to the table and extended almost continuously to the pavilion and culet. This feature was consistent with both the strong lattice dislocations observed under the microscope with crossed polarizers (figure 18) and its observable graining. Up to seven growth steps were revealed in the fluorescence and cathodoluminescence images (figure 19), with each layer of similar thickness. This square modified brilliant diamond was faceted with its table face parallel to these layers for maximum weight retention, while keeping excellent proportions and symmetry.

For CVD growth, this 16.41 ct diamond broke the record previously held by a 14.60 ct diamond (emerald cut, F color, VS_2 clarity) produced in India, which surpassed the previous record of 12.75 ct (round brilliant, F

Figure 17. Fluorescence imaging with deep short-wave UV excitation showed the typical orange-red fluorescence of as-grown CVD diamond with irregular blue "banding." Up to seven growth layers were revealed.

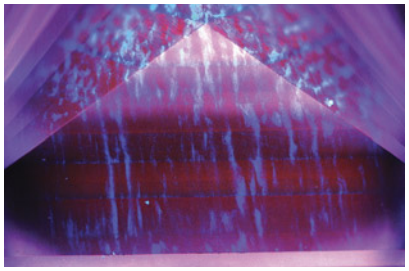

Figure 18. The large CVD diamond showed very strong dislocations under crossed polarizers, the main cause of its wavy appearance.

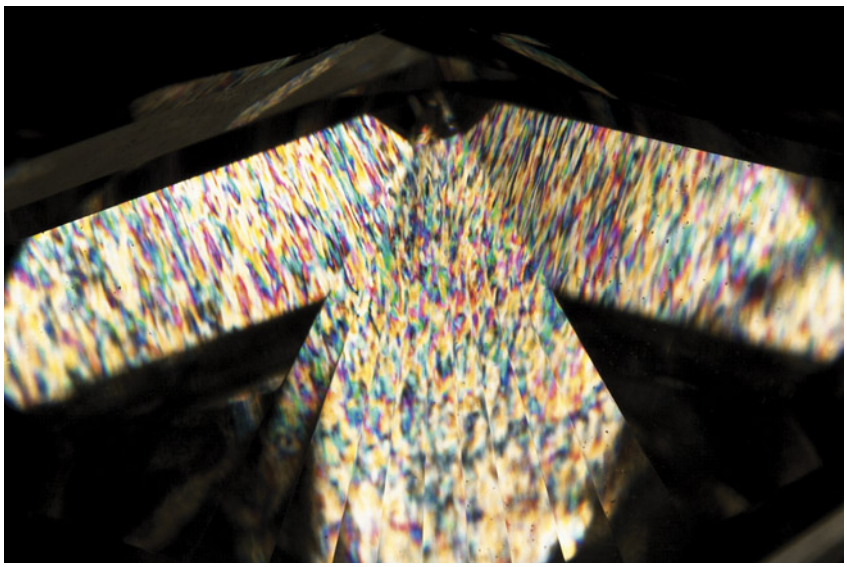

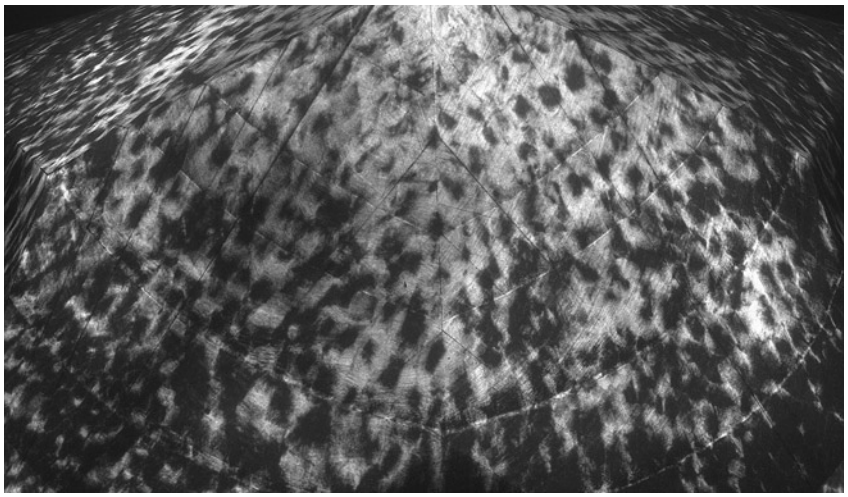

Figure 19. Cathodoluminescence imaging also revealed the seven growth steps. The dark dots in this image are related to the lattice dislocations.

color, VVS_2 clarity), both reported last year ("IGI certifies world record 14.60 ct lab grown diamond," *IGI GemBlog,* August 31, 2021). In comparison, the largest colorless or near-colorless HPHT laboratory-grown diamond is 15.32 ct (cushion cut, H color, I_1 clarity); see Summer 2018 Lab Notes, pp. 217–218. The largest laboratory-grown diamond of any kind tested by GIA so far is a 20.23 ct cushion cut (Fancy Vivid yellowish orange, VS_2) produced using the HPHT method in 2019. GIA will continue to follow the development of laboratory-grown diamonds to ensure that all are properly identified.

Wuyi Wang, Stephanie Persaud, and Elina Myagkaya

Unusual Laser Drill Holes in a Laboratory-Grown Diamond

Diamonds with dark inclusions have been laser drilled to enhance their clarity for more than 60 years. The internal inclusion is drilled from the diamond surface and then acid-boiled to bleach it out. GIA has identified many natural diamonds treated by this technique, but the Carlsbad laboratory recently received for a colored diamond identification and origin report an undisclosed laboratory-grown diamond with unusual laser drill holes.

The diamond was a Fancy yellow cushion modified brilliant weighing 2.02 ct. Gemological and spectroscopic analysis confirmed it was an HPHT-grown synthetic diamond. The diamond was attracted to a small magnet due to the numerous metallic inclusions. No strain was visible under crossed polarizers, and DiamondView imaging showed the typical cuboctahedral HPHT growth pattern.

Clarity was low due to the presence of numerous large flux inclusions, so laser drilling was likely done to enhance the appearance and clarity. One of the laser drill holes connected to a large flux inclusion can be seen in figure 20. A metallic flux inclusion cannot be bleached as some mineral inclusions can and so it must be dissolved out, which could pose additional challenges to improving the clarity. It appears there was an unsuccessful attempt to remove the flux, as the inclusion was still eye visible.

Three clusters of intersecting laser drill tubes resembling corals were observed (figures 21 and 22). We could see numerous roundish openings on the surface filled with dark materials. Raman spectroscopy confirmed they were all non-diamond carbon materials. Here the laser beam was likely reflected off a flux inclusion and refocused to a new point farther than intended, resulting in the unusual branching pattern. Other flux inclusions could have been successfully dissolved by acid because they were smaller than the one in figure 20 or because there were more drilled tubes for the acid to enter. This may have

Figure 20. Flux inclusion in a laboratory-grown diamond connected to a laser drill hole. Field of view 3.57 mm.

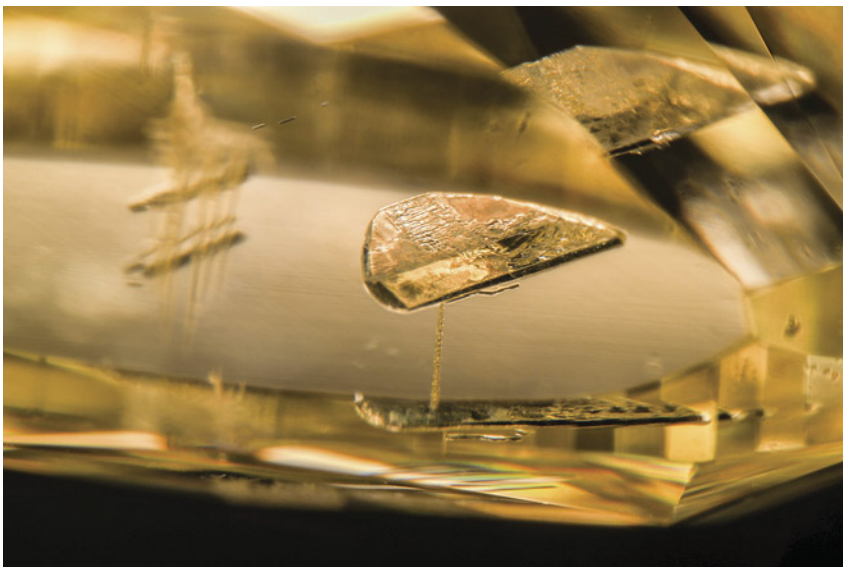

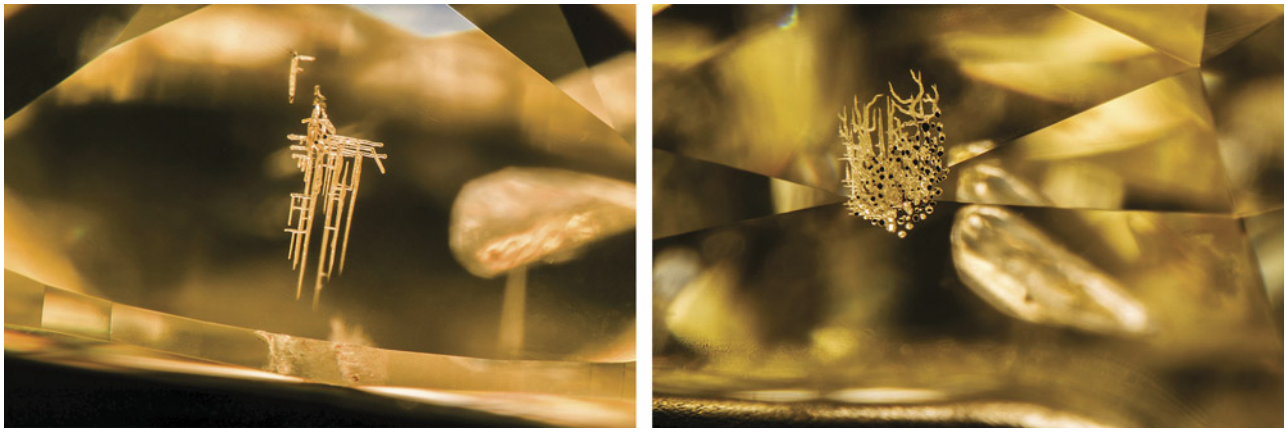

Figure 21. Clusters of unusual laser drill holes in a laboratory-grown diamond. Fields of view 3.57 mm (left) and 2.61 mm (right).

caused the unique crossed tubes inside the stone. Burn marks on the surface next to some of the laser drill holes might have been due to the heat generated by the laser beam (figure 22).

This diamond was identified as a laboratory-grown diamond. It was issued a laboratory-grown colored diamond report stating, "Laser drill holes are present."

Najmeh Anjomani and Troy Ardon

Hydrothermal SYNTHETIC RUBY

Hydrothermal synthetic ruby was first introduced to the market in the 1960s (A. Peretti and C.P. Smith, "An in-depth look at Russia's hydrothermal synthetic rubies," *JewelSiam*, April-May 1993, pp. 96–102). The hydrothermal process is very slow and requires high heat and very high pressure (400–600°C, 5,000–30,000 psi), mimicking the conditions deep in the earth that result in the formation of natural ruby. In this method, the corundum seed plates are suspended inside the growth chamber and nutrients are placed in the bottom. Slowly the nutrients dissolve and form a solution which deposits new synthetic corundum growth onto the seed crystal. The size of the synthetic crystal depends on the size of the seed, amount of nutrient solution, and time.

The Carlsbad laboratory recently received a 4.55 ct transparent cushion-cut hydrothermal synthetic ruby for an identification report (figure 23). This type of laboratory-grown ruby is seldom submitted to the laboratory today, though they were more prevalent in the 1980s. Gemological testing yielded an RI of 1.761–1.769 and a specific gravity of 3.99. Its fluorescence reaction was strong red to long-wave and medium red to short-wave UV radiation, and its pleochroism was orangy red to purplish red. These properties are typical of most rubies, natural or laboratory grown.

Chemical analysis was done by EDXRF and showed a high amount of chromium (1550 ppma), low iron (153 ppma), titanium (25.5 ppma), no gallium, and very low vanadium (2.24 ppma), which matches the synthetic corundum chemistry.

Magnification showed characteris-

Figure 22. Burn mark on the surface next to laser drill holes. Field of view 2.01 mm.

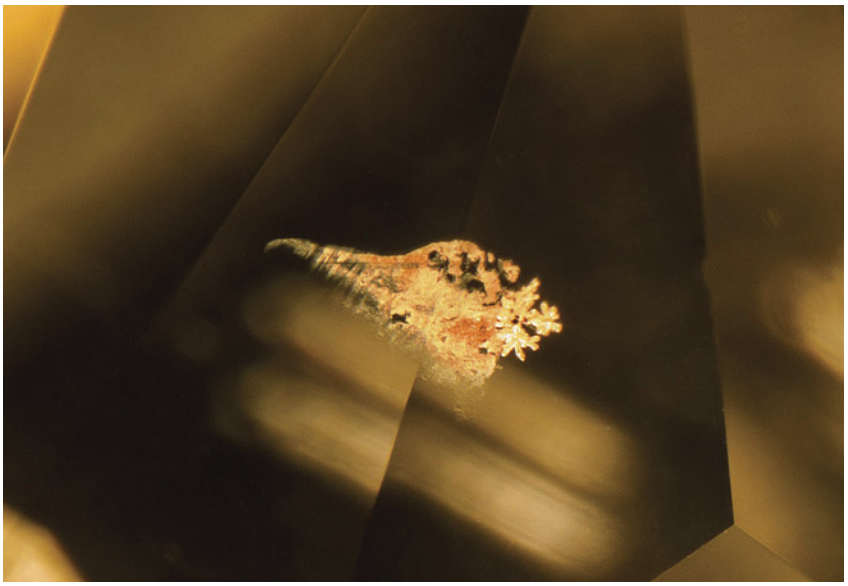

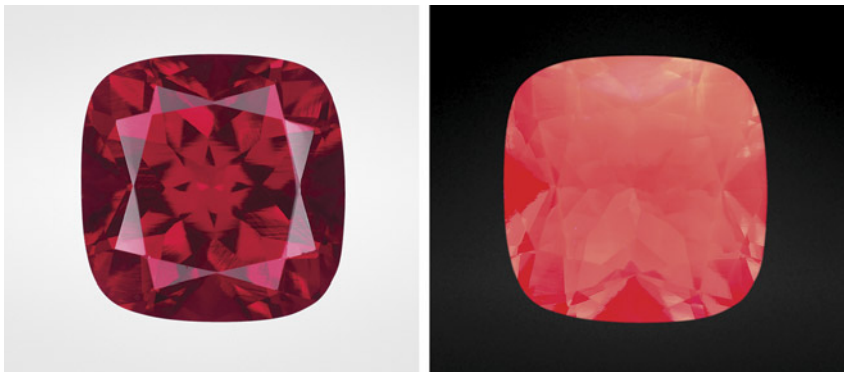

Figure 23. Photos of the hydrothermal synthetic ruby in daylight and short-wave UV light.

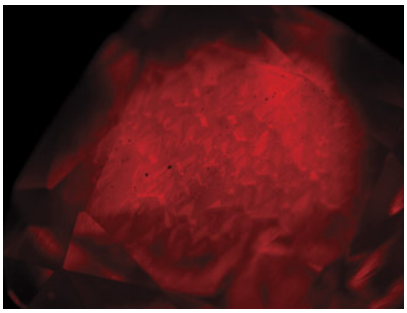

Figure 25. The DiamondView image of the chevron growth pattern in the hydrothermal synthetic ruby. Field of view 8.63 mm.

tic internal features of hydrothermal synthetic corundum such as subparallel striations and angular/zigzag (chevron) graining using a standard gemological microscope in conjunction with fiber-optic light or diffused light (figure 24).

The baseline-corrected spectra showed very strong water peaks in the region between 3200 and 3600 cm^{-1}, which is strongly indicative of hydrothermal synthetic origin. (The instrument was baseline corrected to remove the water signal from the atmosphere as well as having the sample chamber purged with dry air to minimize the detection of water from the atmosphere.) Luminescence images in an ultra-short-wave UV radiation DiamondView showed an interesting chevron growth pattern as well with red fluorescence, further confirming hydrothermal synthetic origin (figure 25).

While hydrothermal synthetic rubies are not as common in the gem trade today, it is helpful to review the distinctive features and characteristics that make them identifiable.

Figure 24. The chevron growth structure observed in the hydrothermal synthetic ruby. Field of view 4.79 mm.

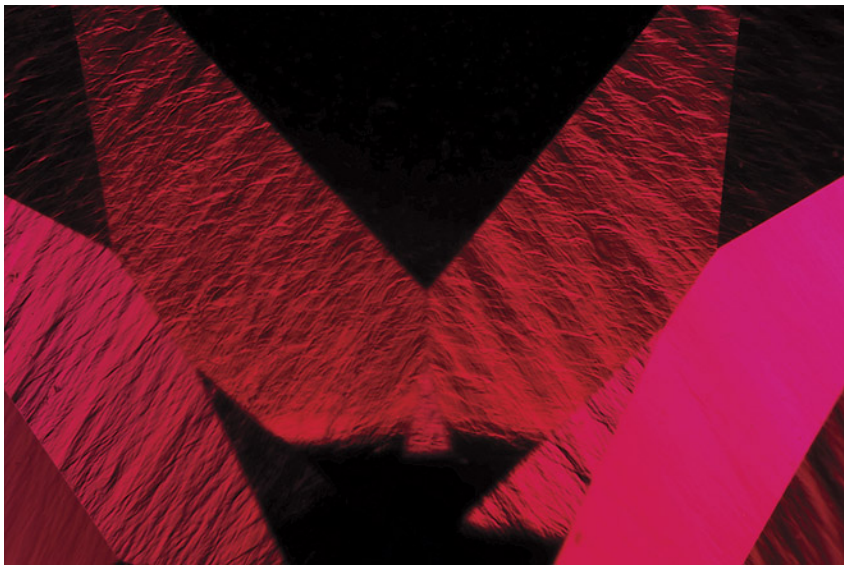

Shiva Sohrabi and Najmeh Anjomani

PHOTO CREDITS

Towfiq Ahmed—1, 15; Sally Ruan—3; Diego Sanchez—6, 8, 23; Nathan Renfro—9; Annie Haynes—10, 13; Nicole Ahline—12; Michaela Stephan—14; Stephanie Persaud—17, 18; Elina Myagkaya—19; Najmeh Anjomani—20–22; Shiva Sohrabi—24, 25

KNOW EVERY FACET OF YOUR
LABORATORY-GROWN DIAMOND

Get brilliant about your laboratory-grown diamonds with GIA's digital Laboratory-Grown Diamond Report, including full color and clarity specifications.

LGDR by GIA®

LEARN MORE
GIA.edu/GIALGDR

The following 25 questions are from the four 2021 issues of *G&G*. Please refer to the feature articles in those issues to find the single best answer for each question.

Visit gia.edu/gems-gemology to take the Challenge online. Entries must be received no later than **Monday, August 1, 2022**. All entries will be acknowledged with an email.

Score 75% or better, and you will receive a certificate of completion. Earn a perfect score, and your name also will be listed in the Fall 2022 issue of *Gems & Gemology*.

1. Distinguishing natural from cultured pearls
   - A. can always be accomplished with RTX and μ-CT.
   - B. relies upon trace element chemical analysis.
   - C. is never possible by visual examination.
   - D. is not always possible.

2. Which chromophore has the highest molar absorptivity in spinel?
   - A. Co^{2+}
   - B. Cr^{3+}
   - C. Fe^{2+}
   - D. V^{3+}

3. Haziness in colorless diamonds
   - A. results exclusively from strong fluorescence.
   - B. results exclusively from nano-inclusions.
   - C. is directly proportional to fluorescence.
   - D. can be evaluated by contrast loss.

4. Sapphires from Mogok
   - A. characteristically show orange fluorescence to long-wave UV.
   - B. were considered too dark about a century ago.
   - C. are found mainly in primary deposits.
   - D. generally show strong color zoning.

5. Linear structures in pearls
   - A. are generally regarded as indicative of non-bead cultured pearls.
   - B. are exclusive to saltwater non-bead cultured pearls.
   - C. are always found with organic-rich material.
   - D. are common in natural freshwater pearls.

6. Non-bead cultured pearls
   - A. are carefully planned with tissue grafting.
   - B. are all known as "Tokki pearls."
   - C. only form in wild mollusks.
   - D. are formed unintentionally.

7. Sudoite is a green mineral
   - A. used extensively throughout the Early Ceramic age.
   - B. that occurs as massive nodules in the Caribbean.
   - C. identified in ancient Amerindian carvings.
   - D. commonly used to imitate jadeite.

8. Color-treated freshwater pearls exhibit
   A. weaker SWUV fluorescence than untreated pearls.
   B. high background fluorescence with Raman.
   C. unusually strong aragonite Raman peaks.
   D. strong LWUV fluorescence.

9. Resin filling of turquoise
   A. is only performed on non-matrix-containing material.
   B. improves appearance by reducing porosity.
   C. is accomplished within several hours.
   D. does not increase stability.

10. Which of the following is diagnostic of peridot from Mogok?
   A. Protogenetic olivine inclusions
   B. Chromite crystal inclusions
   C. "Lily pad" inclusions
   D. Olive green color

11. Saturated purple spinel
   A. can be colored by combinations including iron, chromium, vanadium, and cobalt.
   B. is found only in the Luc Yen district of Vietnam.
   C. is more valuable than saturated purple diamond.
   D. does not contain iron.

12. Purple Chinese freshwater pearls
   A. fluoresce intensely to both long-wave and short-wave UV.
   B. always show strong pigment peaks.
   C. can be color-treated or untreated.
   D. are always optically brightened.

13. Chlorite-group minerals
   A. are commonly used as gem materials.
   B. have high hardness and toughness.
   C. are generally transparent.
   D. are sheet silicates.

14. The Namak Mandi gem market
   A. is primarily for the trading of faceted stones.
   B. has rigid pricing guidelines for goods.
   C. used to be a trading center for salt.
   D. is exclusive to Pakistani traders.

15. Peridot from Pyaung-Gaung
   A. is almost never found in sizes over five carats.
   B. was found to be comparatively sodium-poor.
   C. is generally found in secondary deposits.
   D. is generally bright apple green in color.

16. Of the turquoise deposits in Iran, what is unique about Neyshabur?
   A. Only recently has it produced the majority of Iranian turquoise.
   B. It is the only one dedicated to the production of turquoise.
   C. It is the only one producing turquoise with fine color.
   D. Its material is treated before leaving the mine.

17. For a uniaxial crystal, the E⊥c (o-ray) absorption spectrum corresponds to light traveling through the crystal
   A. in a direction halfway between parallel and perpendicular to the c-axis (optic axis).
   B. perpendicular to the c-axis (optic axis).
   C. parallel to the c-axis (optic axis).
   D. in any direction.

18. The *angoora* is
   A. part of a hand-operated faceting apparatus.
   B. a local authority in Namak Mandi.
   C. a tool for evaluating gem clarity.
   D. a highly mechanized device.

19. Mining of emerald from the Habachtal deposit in Austria
   A. involved large groups of miners working year-round.
   B. is clearly documented back to the Roman Empire.
   C. was very profitable in the nineteenth century.
   D. is very dangerous from the primary source.

20. Which of the Neyshabur tunnels produces turquoise with a greenish color?
   A. Chah Abdar in the Main tunnel
   B. Sabz in the Main tunnel
   C. Dom
   D. Zakh

21. A spindle-shaped core in a pearl indicates it
   A. could be non-bead cultured or natural.
   B. is non-bead cultured.
   C. is bead cultured.
   D. is natural.

22. Mogok sapphire inclusion scenes
   A. almost always contain zircon crystals.
   B. are distinct and diagnostic.
   C. are dominated by silk.
   D. never contain apatite.

23. Fluorescence in colorless diamonds
   A. can occur with a light source labeled as UV-free.
   B. always improves the color grade of a diamond.
   C. is only stimulated by ultraviolet light.
   D. increases transparency.

24. To generate an accurate unpolarized spectrum of a uniaxial polished crystal of known orientation with a given light source, one must use
   A. weighted combinations of the o-ray and e-ray visible transmission spectra.
   B. weighted combinations of the o-ray and e-ray visible absorption spectra.
   C. a polariscope and dichroscope.
   D. the Beer-Lambert law.

25. Habachtal emeralds
   A. were widely available in the eighteenth century.
   B. are easily confused with Colombian emeralds.
   C. are mainly suitable for mineral collectors.
   D. are generally clean and facetable.

To take the Challenge online, please scan the QR code.

Rare Blue Apatite Inclusion in Smoky Quartz

A natural smoky quartz with an obvious mineral inclusion at the center of the stone (figure 1) was recently observed by the author. Raman analysis confirmed that this mineral was apatite. The apatite had very light blue color and a hexagonal twinned morphology. Under cross-polarized light, the inclusion showed interference colors, confirming its doubly refractive nature (figure 2).

Apatite is a phosphate mineral with the chemical formula of $Ca_5(PO_4)_3(Cl/F/OH)$. Generally, smoky quartz and apatite can occur under the same geologic conditions, including pegmatitic hydrothermal environments. Apatite is commonly a protogenetic inclusion, but it can occasionally result from a later stage and be considered a syngenetic inclusion in quartz. The rounded shape of this apatite example suggests a protogenetic inclusion, one that would be a welcome sight for any gemologist examining stones in a microscope.

Nattapat Karava
GIA, Bangkok

Figure 1. A hexagonal apatite inclusion in smoky quartz. Photomicrograph by Nattapat Karava; field of view 6.3 mm.

Apatite Oiling: Before and After

Fissure filling of gemstones is an age-old treatment that can improve a stone's clarity (Fall 2020 Gem News International, pp. 443–444). By introducing oil or other fillers such as resin into the stone, the treater can minimize the appearance of fissures.

Recently we had the opportunity to observe this treatment up close in an apatite cabochon brought to our laboratory for photography while it was still untreated. Then the sample was oiled by Jeffery Bergman and returned to the laboratory for observation and photography.

Figure 2. A hexagonal apatite inclusion with interference colors in smoky quartz, viewed in cross-polarized illumination. Photomicrograph by Nattapat Karava; field of view 6.3 mm.

About the banner: Dark exsolution stringers of magnetite show vivid interference colors using reflected light in this yellow scapolite from Tanzania. Photomicrograph by Nathan Renfro; field of view 4.08 mm. Courtesy of Arsaa Gems and Minerals.

Gems & Gemology, Vol. 58, No. 1, pp. 62–71.

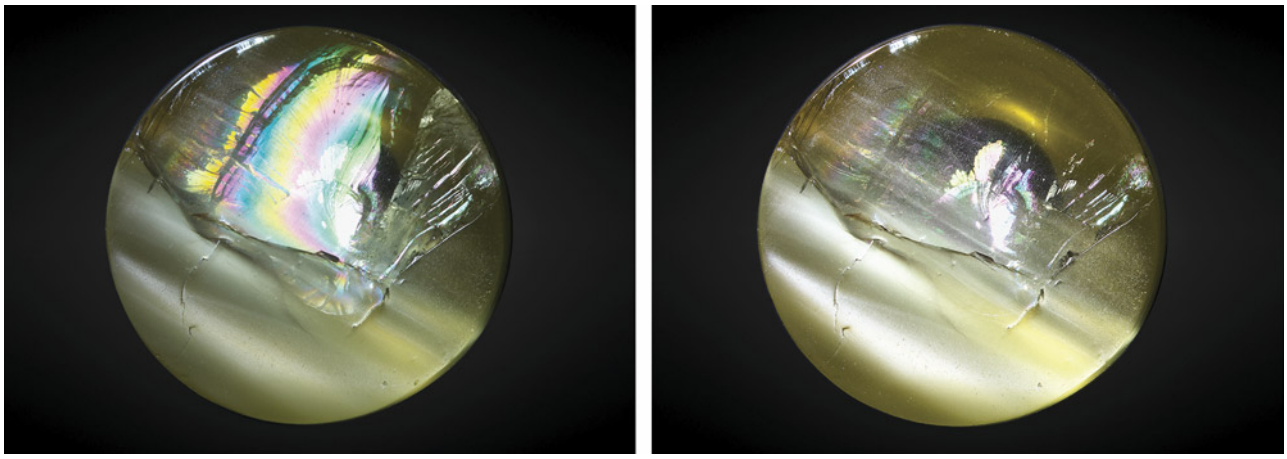

Figure 3. Left: On the base of this apatite cabochon (15 × 15 × 13 mm), a large, reflective fissure can be observed with fiber-optic illumination. Right: After the oil filling, the same fissure is much less noticeable and the iridescent reflective area is considerably smaller, enhancing the sample's clarity. Photos by E. Billie Hughes.

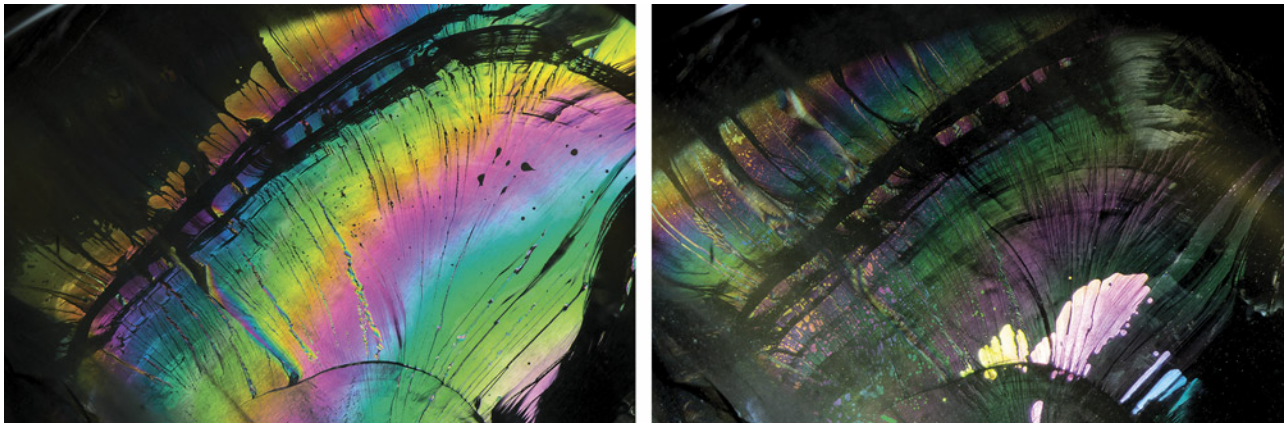

Figure 4. A close-up of the fissure before and after oil treatment, shown in diffuse fiber-optic illumination. Left: Before oiling, the fissure is easily visible and highly reflective. Right: After oiling, the reflection is more muted and less noticeable, with only a small highly reflective area remaining. Photomicrographs by E. Billie Hughes; field of view 10 mm.

Upon examination before and after, the effects of the treatment were clear. On the base of the cabochon, a large, reflective fissure became less visible after oiling (figure 3). Using fiber-optic illumination, it was apparent that the filler had diminished the reflective appearance of the fissure, with only small highly reflective areas remaining (figure 4). Darkfield illumination also revealed a stark difference in appearance: The filler had rendered large dark areas filled with air nearly invisible (figure 5).

This microscopic observation serves as a reminder of the significant impact clarity enhancement can have on gems of all types.

E. Billie Hughes
Lotus Gemology, Bangkok

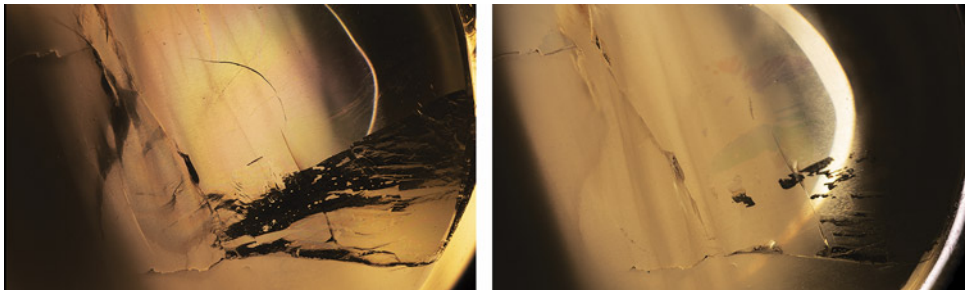

Figure 5. Left: Before filling, transmitted light shows dark areas where air has become trapped in the fissure, making it more visible. Right: Treatment with oil minimizes the dark areas, enhancing clarity. Photomicrographs by E. Billie Hughes; field of view 27 mm.

Acicular Troughs Coincident with Green Stains on Rough Diamond Surface

The author acquired an alluvial rough diamond from Guyana showing unique surficial features that do not appear to have been documented elsewhere. The specimen was a twinned crystal consisting of two intergrown octahedral crystals, ~0.12 ct in weight, with numerous flat-bottomed hexagonal etch features and trigons and a nearly pervasive green skin (figure 6). Most interesting were fine, linear, and randomly oriented features on the diamond surface that were spatially associated with the green stains (figure 7). Radiation stains are known to cause localized expansion in diamond (L. Nasdala et al., "Radio-coloration of diamond: A spectroscopic study," *Contributions to Mineralogy and Petrology*, Vol. 165, 2013, pp. 843–861; S.C. Eaton-Magaña and K.S. Moe, "Temperature effects on radiation stains in natural diamonds," *Diamond and Related Materials*, Vol. 64, 2016, pp. 130–142). These features also cross-cut trigons, implying that they post-date the diamond's growth in the earth's mantle and its surface dissolution within the kimberlite magma (figure 8). These features may be the result of localized dissolution caused by proximal acicular, radioactive, and as yet unknown minerals, leaving behind a cast impression. Green color in diamond can be produced by natural irradiation of the crystal lattice by exposure to radiation from proximal and adjacent radioactive grains (e.g., zircon, monzonite, uraninite, and K-feldspar) or salts dissolved in percolating fluids surrounding the diamond (C.M. Breeding et al., "Natural-color green diamonds: A beautiful conundrum," Spring 2018 *G&G*, pp. 2–27). Gamma, alpha, or beta radiation emanating from these sources are thought to cause collections of defects and impurities within the diamond. Gamma and beta radiation have low energies and long penetration depths producing green bodycolors. Due to its high energy, alpha radiation has the shortest penetration depth and only within the first 25 µm of the diamond surface, creating green skins, stains, and spots.

Figure 6. A ~0.12 ct green-skinned diamond from Guyana. Photo by Roy Bassoo.

Figure 7. Left: A magnified view of green radiation stains on an unpolished diamond surface in transmitted light. Right: An image of the same surface in reflected light with the radiation staining (outlined in red) and preserved acicular troughs. Photomicrographs by Roy Bassoo; field of view 0.5 mm.

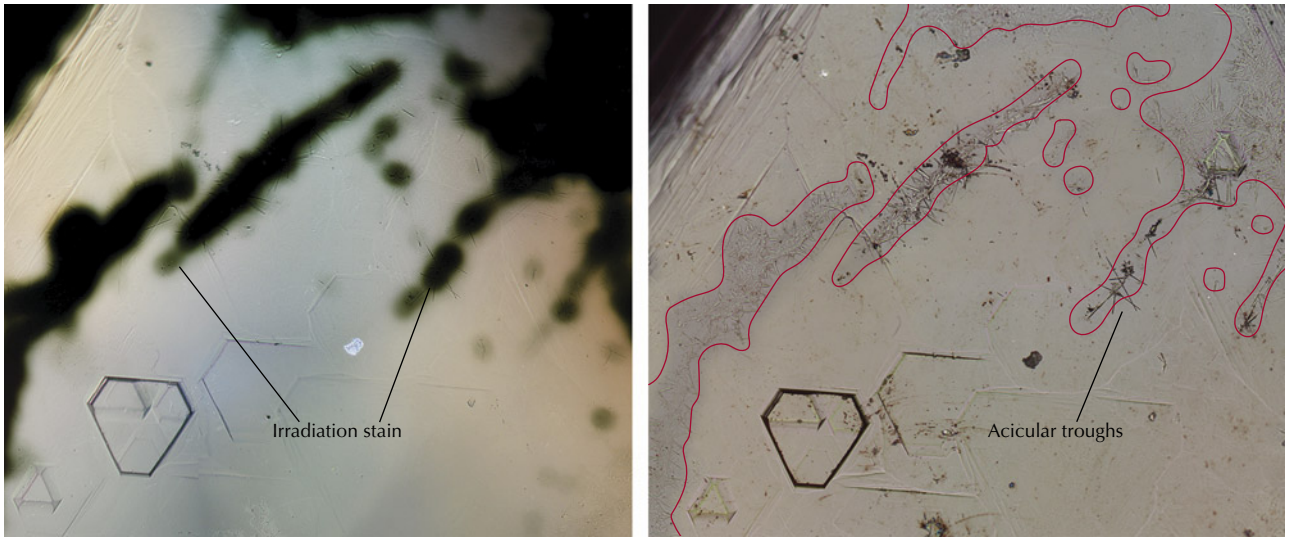

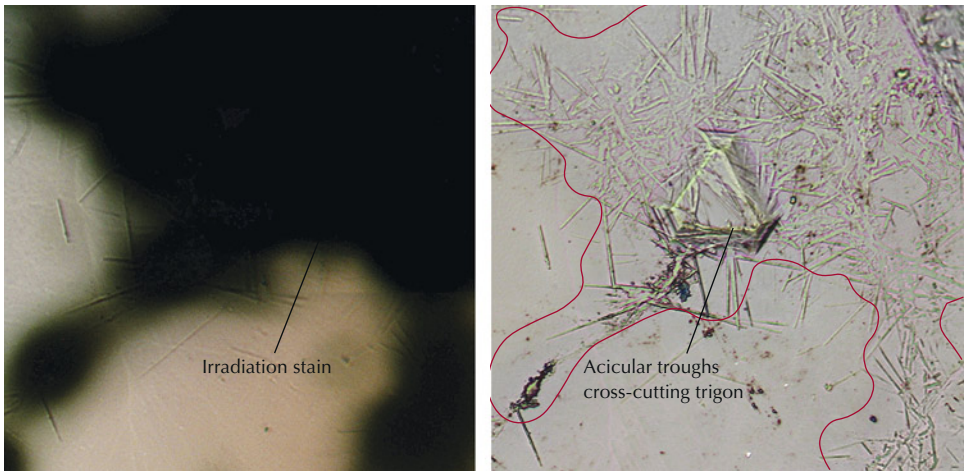

Figure 8. A further magnified view of the green radiation stains on an unpolished diamond surface in transmitted light (left) and an image of the same surface in reflected light with the radiation staining outlined in red and preserved acicular troughs which cross-cut a flat-bottomed trigon (right). Photomicrographs by Roy Bassoo; field of view 0.25 mm.

Although unusual, radiation-related surface features have been previously documented (e.g., Spring 2021 *G&G* Micro-World, pp. 66–67). The ones seen in this diamond from Guyana appear to be unique, however. It is quite likely that these features are pervasive in placer diamonds but have not been studied in detail.

Roy Bassoo
GIA, Carlsbad

Figure 9. A 7.98 ct blue aquamarine faceted by the author to display the garnet crystal within. Photo by Jessa Rizzo.

Spessartine Garnet in Aquamarine

The author recently had the opportunity to examine and facet a sample of aquamarine rough. The aquamarine, reportedly from Pakistan, was acquired from gemstone dealer Ali Shad of Shad Fine Minerals (Gilgit-Baltistan, Pakistan). The rough was specifically selected for the large red garnet inclusion within. In preparation for faceting, the stone was oriented with the garnet inclusion as the primary focus. After careful planning and execution, a 7.98 ct modified emerald cut was achieved, highlighting the garnet crystal under the table facet (figure 9). Oblique fiber-optic illumination was used to observe the internal features of the aquamarine, revealing a well-formed red spessartine garnet crystal with iridescent colors along the garnet and aquamarine interface (figure 10). This is one of the most

Figure 10. The red spessartine garnet showed vibrant interference colors along the interface with the aquamarine host. Photomicrograph by Nathan Renfro; field of view 5.63 mm.

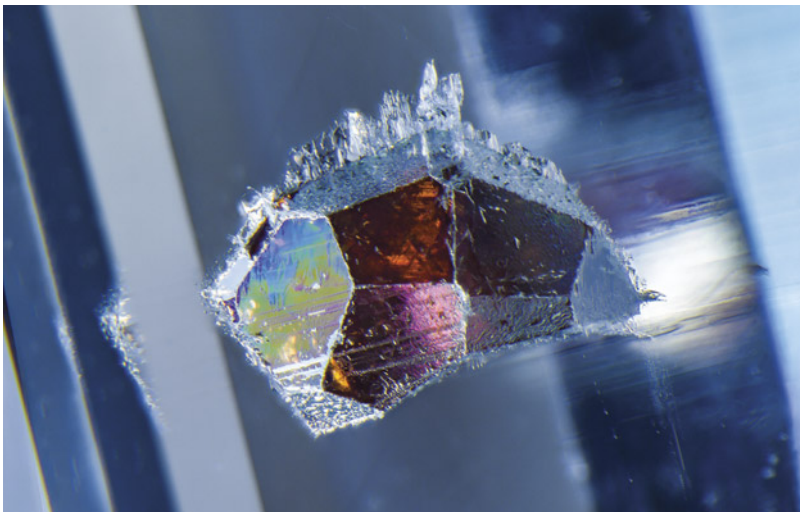

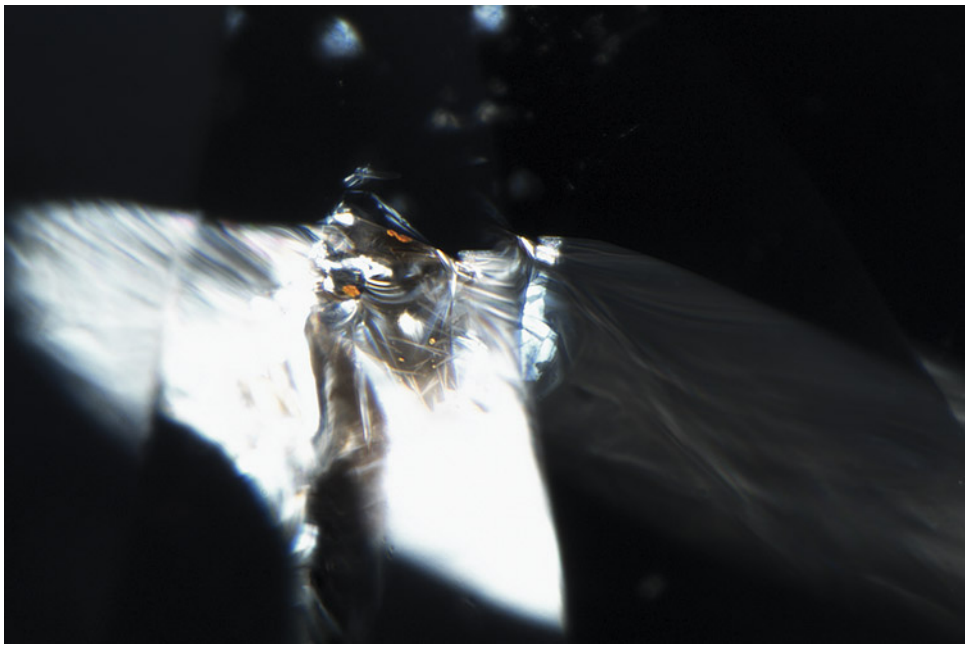

Figure 11. Several small brownish orange crystals found within the fracture of a diamond were identified as hematite. Photomicrograph by Abadie Ludlam; field of view 1.26 mm.

beautiful inclusions the author has seen in an aquamarine, and it is noteworthy as the gem was faceted to display the inclusion rather than to conceal or remove it.

Jessa Rizzo
GIA, Carlsbad

Hematite Crystals in Diamond

A 1.51 ct G-color diamond with I_2 clarity recently caught the authors' attention due to several brownish orange inclusions. These tiny crystals, only a few nanometers in size, were concentrated along two fractures in the stone (figure 11). They were identified using Raman spectroscopy as hematite (Fe_2O_3). Although it is common to find oxide staining within fractures in diamond, crystalline oxide inclusions such as these are a rarity. The concentration of the hematite crystals along the cracks suggests that, rather than being syngenetic inclusions, these are secondary (epigenetic) minerals. They likely precipitated inside the fractures when the diamond interacted with fluids while being stored in the crust. This rare sight offers a glimpse into the long and unique journey each diamond takes to the earth's surface.

Abadie Ludlam, Tingyen Yeh, and David Kondo
GIA, New York

Hyalite with Magnificent Internal Features

The Laboratoire Français de Gemmologie (LFG) received for analysis a 1.83 ct hyalite, also known as opal-AN: an amorphous (A) opal containing hydrated silica molecules that are network forming (N) (E. Fritsch et al., "Green-luminescing hyalite opal from Mexico," *Journal of Gemmology*, Vol. 34, No. 5, 2015, pp. 490–508). This is one of the rarest varieties of gem-quality opal. The gem fluoresced green under long-wave ultraviolet (365 nm) and, with more intensity, under short-wave UV (254 nm), due to U^{6+} in the form of uranyl $(UO_2)^{2+}$ (E. Gaillou et al., "Luminescence of gem opals: A review of intrinsic and extrinsic emission," *Australian Gemmologist*, Vol. 24, No. 8, 2011, pp. 200–201). A purple fluorite (identified by a micro-Raman spectrometer; figure 12) and a series of cube-shaped cavities were visible (figure 13) in the hyalite, which appear to be all interconnected. Sometimes these cavities also contain small crystals of fluorite relics detected by Raman. Thus, these cavities may be the result of the partial dissolution

Figure 12. Purple fluorite cube, identified by micro-Raman spectroscopy, in a hyalite. Photomicrograph by U. Hennebois; field of view 1.2 mm.

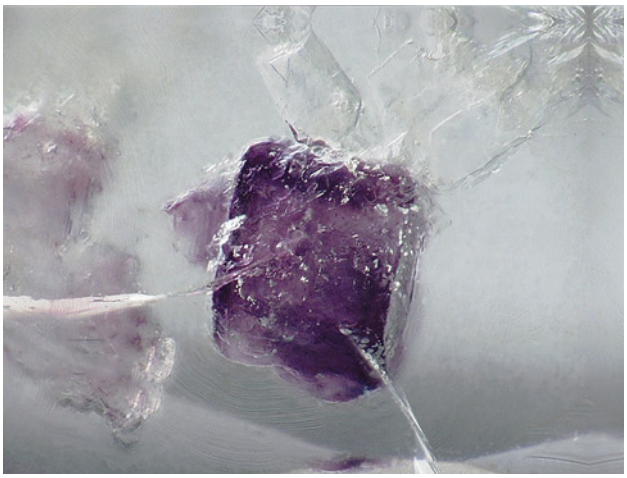

Figure 13. Interconnected cavities observed in a hyalite containing partially dissolved fluorite relics identified by Raman spectroscopy. Curved growth layers are also observed in the background. Photomicrograph by A. Delaunay; field of view 2 mm.

Figure 14. This fluid inclusion contains mostly a gaseous phase. It is trapped at the intersection of curved botryoidal growth zones and presents high-order interference colors obvious between crossed polarizers. Photomicrograph by U. Hennebois; field of view 1 mm.

of fluorite crystals. This would explain their cubic morphology, which cannot be explained by the dissolution of amorphous hyalite.

Between crossed polarizers, high-order interference colors were observed (figure 14), as expected for this gem. This is due to anomalous birefringence linked with the strain present between the curved growth layers of hyalite. Also, a fluid inclusion was observed in the intersection of the botryoids (again, see figure 14). This inclusion is composed mostly of gas, suggesting that this hyalite was deposited from a gaseous phase. Although some of these features have been previously observed in hyalite, it is rare to see them all in the same sample. To the best of our knowledge, this is the first reporting of pronounced cubic cavities in hyalite.

Ugo Hennebois, Aurélien Delaunay, and Stefanos Karampelas (s.karampelas@lfg.paris)
LFG, Paris

Emmanuel Fritsch
University of Nantes, CNRS-IMN, France

"Fishbone" Inclusion in a Burmese Peridot from Mogok

Recently, an 83.25 ct cushion faceted peridot with medium dark yellowish green color and good clarity was sent to the Taiwan Union Lab of Gem Research (TULAB) for identification service. This peridot, reported by the owner as from Mogok, Myanmar, was relatively rare in the Taiwanese market because of its impressive size, color, and clarity. Microscopic examination revealed a few short needle inclusions and a fishbone-shaped inclusion (figure 15), the latter of which is common in peridot from this origin. The backbone appeared to be a long prismatic crystal with some vertical cleavage planes along it, while the smaller branches were composed of parallel tabular inclusions that might result from epitaxial exsolution. Due to peridot's strong birefringence, brightfield illumination and plane polarized light were adopted to reduce the interference and obtain clear microscopic images.

Shu-Hong Lin
Institute of Earth Sciences,
National Taiwan Ocean University
Taiwan Union Lab of Gem Research, Taipei

Figure 15. The fishbone-like inclusion in the Burmese peridot. Photomicrograph by Shu-Hong Lin; field of view 1.32 mm.

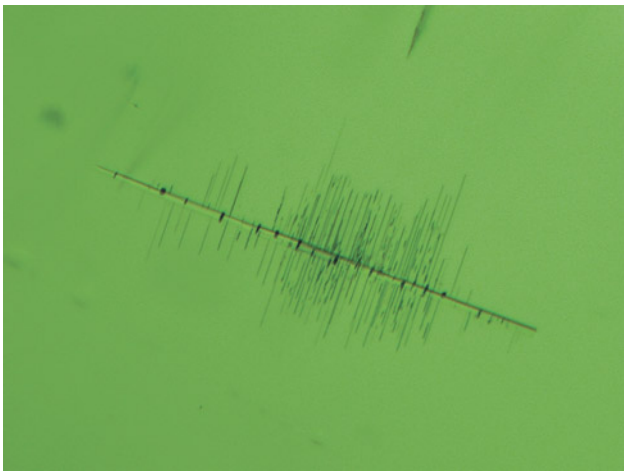

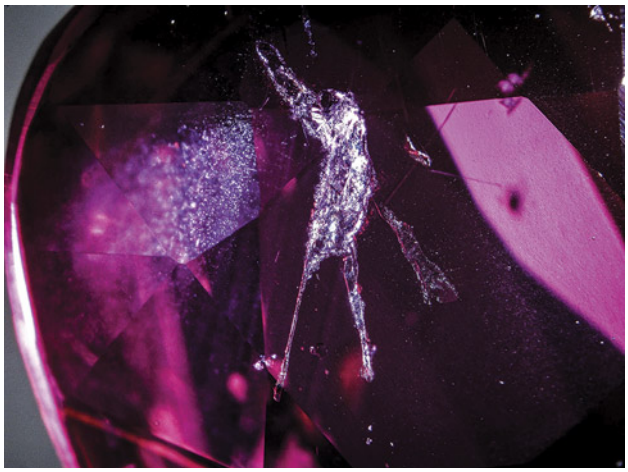

Figure 16. An extraterrestrial-like inclusion with iridescent color observed in a Mozambique ruby using fiber-optic illumination. Photomicrograph by Nattapat Karava; field of view 6.3 mm.

Extraterrestrial-Like Inclusion in Mozambique Ruby

A 3.03 ct stone submitted to GIA's Bangkok laboratory was identified as a ruby from Mozambique with no indication of heating. Microscopic examination revealed a hypnotizing inclusion that resembled an extraterrestrial standing among specks of nebulae and waving its hand (figure 16). It had a large head and very thin legs, with two outstretched hands. This large, eye-visible inclusion was a colorless crystal among the particulate clouds. It showed iridescent color using fiber-optic illumination and was identified by Raman analysis as mica. Mica inclusions in Mozambique rubies usually have a pseudo-hexagonal shape with fringes (small expansion fractures) and can be found with a rosette pattern around them ("Rubies from the Montepuez area [Mozambique]," *GIA Research News*, 2013). This is another example of pareidolia observed in gems, the tendency to interpret an inclusion as some other object.

Nattapat Karava

An A-maze-ing Fingerprint in Spinel

Of the variety of inclusions that can be seen in spinel, perhaps the most familiar are angular octahedral crystals. In many cases, we even see these crystals arranged in neat rows, forming delicate "fingerprint" inclusions.

However, spinel fingerprints can also take on other appearances, as observed in a Vietnamese sample that recently passed through our laboratory (figure 17). This stone contained a partially healed fissure with a maze-like pattern that was evident when lit with darkfield illumination. With the addition of diffuse fiber-optic illumination, small angular areas of the channels seemed to light up with a highly reflective appearance. Myriad inclusion scenes make spinel a fascinating gem to observe.

E. Billie Hughes

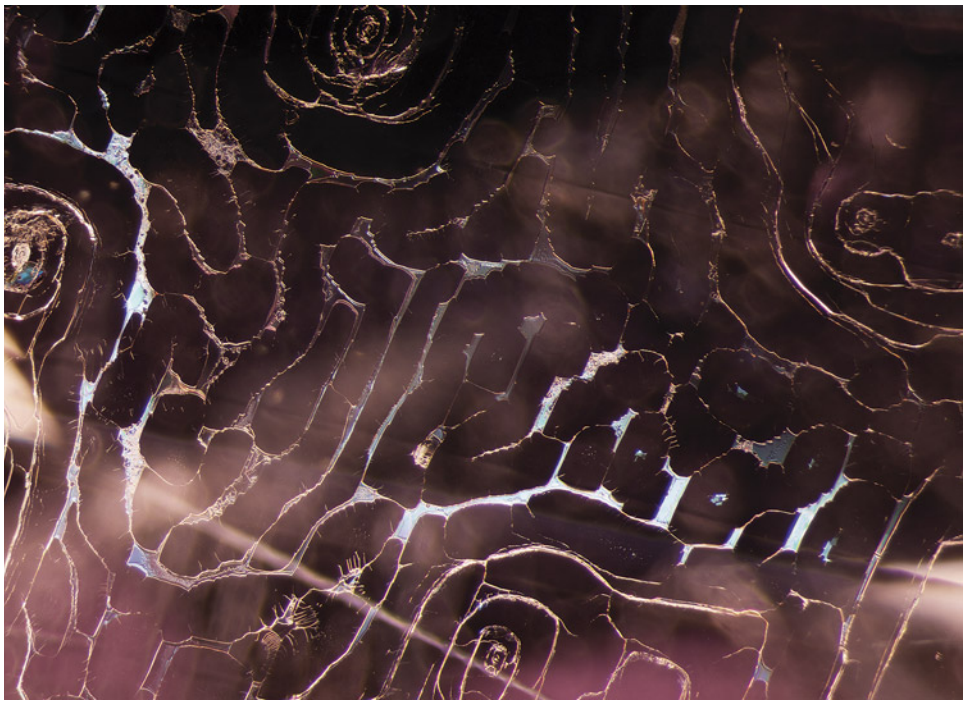

Figure 17. A web-like fingerprint creates a maze-like pattern in this spinel from Vietnam, observed with darkfield and diffuse fiber-optic illumination. Photomicrograph by E. Billie Hughes; field of view 5 mm. Courtesy of Vitalit Gems.

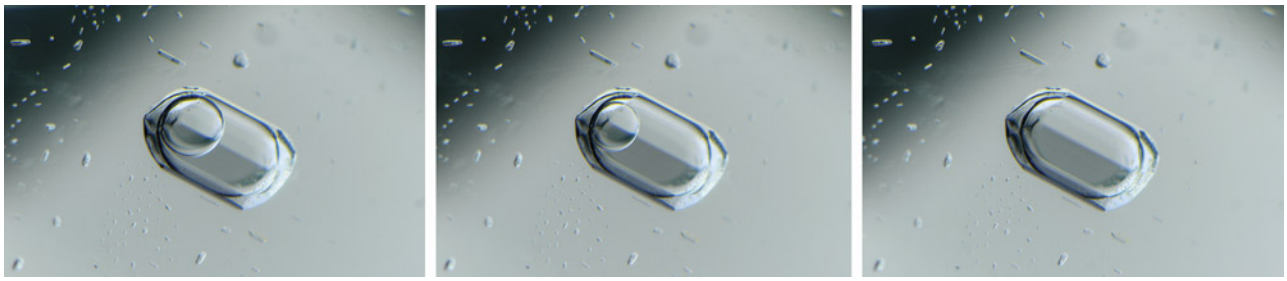

Figure 18. This complex fluid inclusion in topaz is composed of minute solid crystals, an aqueous liquid, and an immiscible CO_2 fluid. When cooled below 31.5°C, the CO_2 is in a liquid state with a vapor bubble trapped in the CO_2 liquid (left). When gently warmed, the CO_2 vapor bubble shrinks (center) until it ultimately disappears (right) as the CO_2 is homogenized into a single phase. Photomicrographs by Nathan Renfro; field of view 1.93 mm.

Complex Fluid Inclusion in Topaz

A blue topaz recently examined by the authors contained an interesting and complex fluid-filled negative crystal that revealed some remarkable behavior when cooled down. The contents of this three-phase fluid inclusion were very small solid phases, and carbon dioxide fluid trapped within an aqueous immiscible liquid, which has been previously documented (E.J. Gübelin and J.I. Koivula, *Photoatlas of Inclusions in Gemstones, Volume 2*, Opinio Verlag, Basel, Switzerland, 2005, p. 731). When the stone was cooled below approximately 31.5°C, the carbon dioxide fluid turned into liquid and gaseous states consisting of a multitude of tiny vapor bubbles nucleating and coalescing into a single larger bubble of gaseous CO_2 within the liquid CO_2 (see the video at www.gia.edu/gems-gemology/spring-2022-microworld-complex-fluid-inclusion-topaz). This type of complex inclusion results in a CO_2 vapor bubble trapped within a liquid CO_2 bubble that is trapped within an aqueous, immiscible liquid (figure 18, left). If the stone is warmed above 31.5°C, the liquid and gaseous CO_2 phases are homogenized into a single-phase fluid, causing the vapor bubble to shrink (figure 18, center) and ultimately disappear (figure 18, right). Similar behavior of CO_2 trapped in negative crystals has been previously documented in sapphire (Spring 2016 *G&G* Micro-World, pp. 78–79). The extraordinary behavior of this fluid inclusion in topaz is a delight for any gemologist.

Nathan Renfro and John I. Koivula
GIA, Carlsbad

Vietnamese Skyline

In the red spinel from Vietnam's Luc Yen district in figure 19, layers of iridescent needles stretch skyward like a futuristic skyline from a science fiction novel. Such hogbomite-filled dislocations are a common sight in red, pink, and blue spinel from Vietnam. According to Gübelin and Koivula (*Photoatlas of Inclusions in Gemstones, Volume 2*, Opinio Verlag, Basel, Switzerland, 2005), hogbomite $(Mg,Fe)_2(Al,Ti)_5O_{10}$ is found in spinel via isomorphous replacement.

Wimon Manorotkul
Lotus Gemology, Bangkok

YAG with Flux-Filled Fingerprints

The author recently examined a 3.58 ct yellowish green yttrium aluminum garnet, a manufactured product known in the trade as "YAG," that contained numerous large flux-filled fractures. The flux material crystallized

Figure 19. Hogbomite-filled dislocations in a Vietnamese spinel. Photo by Wimon Manorotkul; vertical field of view 4 mm.

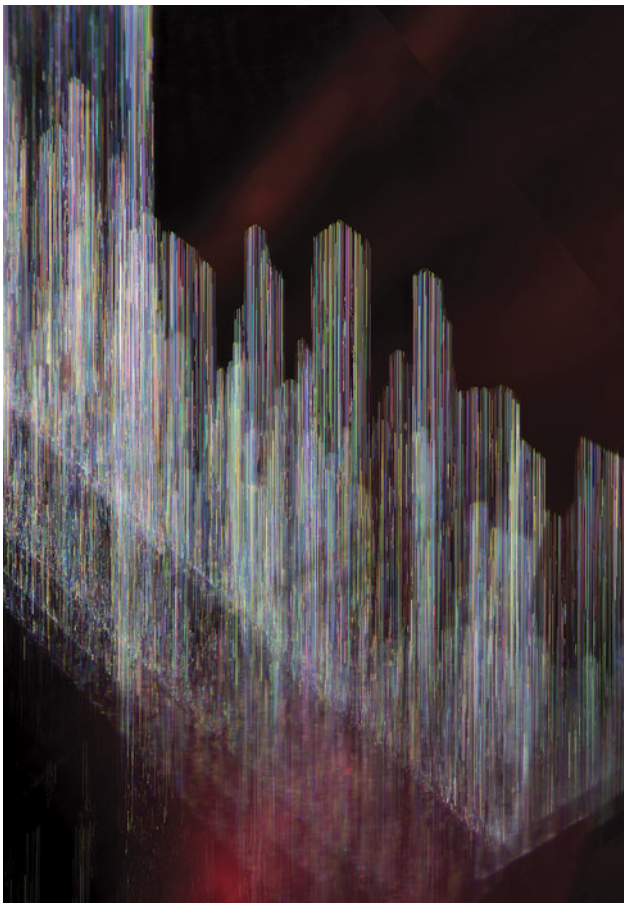

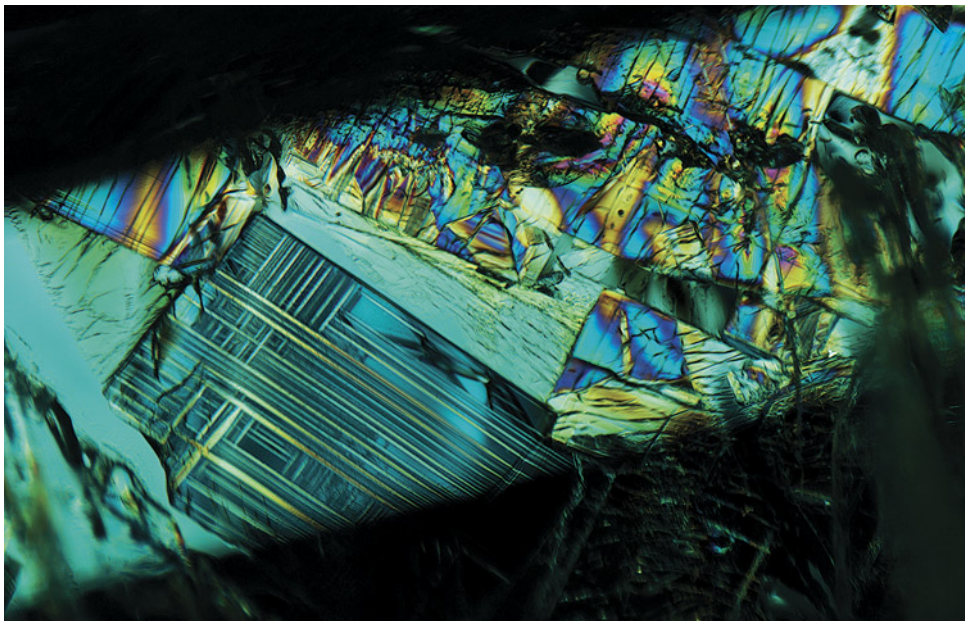

Figure 20. Flux-filled fractures displaying geometric shapes and iridescent colors when viewed through crossed polarizers. Photomicrograph by Michaela Stephan; field of view 2.9 mm.

in the fractures formed interesting geometric shapes that showed birefringent interference colors when viewed between crossed polarizers, reminiscent of stained glass windows (figure 20). It is possible this YAG was intentionally fractured and filled with flux to more convincingly imitate tsavorite grossular garnet. Although the flux inclusions in this example were quite beautiful, such inclusions are not common in this manufactured gem material.

Michaela Stephan
GIA, Carlsbad

Quarterly Crystal: Hillocks on Beryl

Whenever we study natural uncut gem minerals, we carefully examine all outer surfaces for any photogenic etch figures or growth hillocks that might yield interesting and educational photographs. For this issue's Quarterly Crystal, we recently had the opportunity to study a very well-formed, gem-quality aquamarine crystal supplied by Ali Shad of Shad Fine Minerals in Gilgit-Baltistan, Pakistan. The aquamarine, pictured in figure 21, was reportedly from the Qandahar mine, located in the Braldu Valley, Shigar District, Gilgit-Baltistan, Pakistan.

Figure 21. Measuring 22.28 mm in length and weighing 31.06 ct, the outer pinacoidal surface on the termination of this Pakistani aquamarine crystal is decorated with numerous hexagonal growth hillocks. Photo by Nathan Renfro.

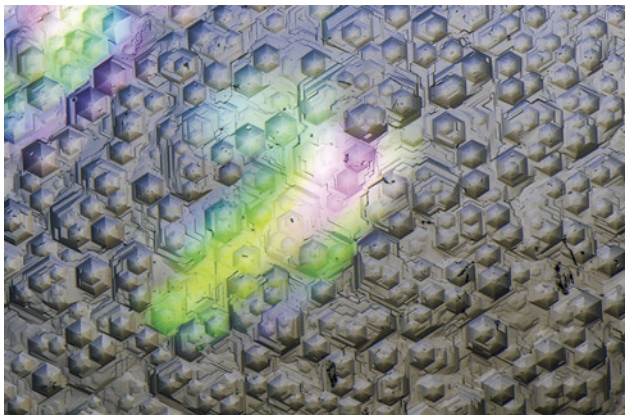

Figure 22. The generally uniform size of the numerous growth hillocks on the terminal pinacoid of the aquamarine is clearly shown in this shadowed reflected light image. The bright colors result from light interacting with thin-film separations in the body of the aquamarine. Photomicrograph by Nathan Renfro; field of view 7.97 mm.

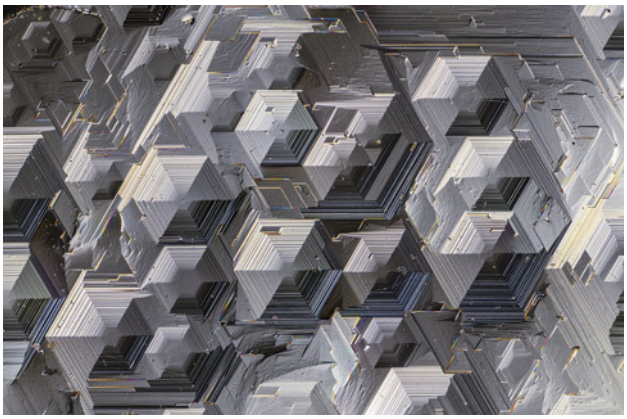

Figure 23. The complexity of some of the hexagonal growth hillocks on the pinacoid of the aquamarine is shown in closer detail in this differential interference contrast image. Photomicrograph by Nathan Renfro; field of view 2.32 mm.

At 31.06 ct with corresponding measurements of 22.28 × 14.50 × 11.24 mm, this aquamarine did not show etch figures on any of its crystal faces, proving that the beryl had not gone through post-growth dissolution. However, examination showed that the pinacoid was completely covered with small hexagonal growth hillocks (figure 22) of the type discussed by John Sinkankas in *Emerald and Other Beryls* (1981) and illustrated on page 273. The hillocks on the terminal pinacoid, which were all generally of the same small size, blanketed the termination completely. Under high magnification, the hexagonal hillocks appeared very complex in form (figure 23). Their sharp, pristine, geometric habit once again illustrated that post-growth dissolution of this crystal had not taken place.

John I. Koivula and Nathan Renfro

Complex Fluid Inclusion in Topaz

To see video of a topaz containing a remarkable complex fluid inclusion, go to www.gia.edu/gems-gemology/spring-2022-microworld-complex-fluid-inclusion-topaz or scan the QR code on the right.

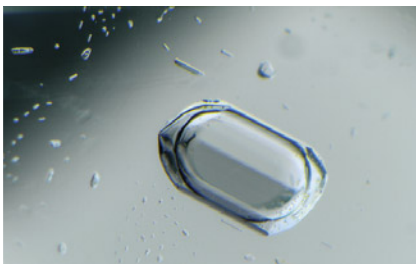

Editor: Evan M. Smith

Deep-Focus Earthquakes: The Heartbeat of a Diamond Factory?

The geological landscape around us evolves so slowly that it can appear static, but the rigid tectonic plates that make up the outer layer of our planet drift across its surface over time. Interactions between plates result in large-scale bumping, grinding, and breaking of rocks that we feel as earthquakes. Some earthquakes originate from *below* the rigid outer layer of plates, even from depths greater than about 300 km where rocks are expected to be under too much confining pressure to break by brittle failure. Instead of being related to multiple plates jostling together, these deep earthquakes are always associated with cold, lone plates that have sunken down into the warmer convecting mantle through the process of subduction. The nature and cause of these so-called deep-focus earthquakes remain poorly understood, but recent research suggests they might have something to do with the growth of top-quality gem diamonds.

As a sinking or subducting plate, also colloquially called a "slab," descends into the mantle, the pressure and temperature increase. Changing conditions can cause some minerals to melt or undergo phase changes that release water. Recent slab modeling shows that the measured depths of deep-focus earthquakes coincide with the depth where melts and fluids should be released from some slabs, especially those that are relatively cold to begin with (Shirey et al., 2021). The release of melts and fluids at depths beyond 300 km potentially serves to trigger these deep-focus earthquakes. Shirey et al. (2021) also linked this earthquake activity to the formation of sublithospheric or super-deep diamonds, which have been connected with subducted material and both carbonatitic melts and hydrous fluids in previous studies (Walter et al., 2008; Harte, 2010; Pearson et al., 2014; Smith et al., 2016, 2018; Thomson et al., 2016b; Smith and Nestola, 2021). Here we will explore the connection between deep-focus earthquakes and the growth of diamonds—specifically the variety known as CLIPPIR diamonds (Cullinan-like, Large, Inclusion-Poor, Pure, Irregular, and Resorbed) that make up many of the type II diamonds in the gem market (Smith et al., 2016, 2017).

Editor's note: Questions or topics of interest should be directed to Evan Smith (evan.smith@gia.edu).

Gems & Gemology, Vol. 58, No. 1, pp. 72–79.

Deep-Focus Earthquakes

An earthquake in the crust is caused by a sudden brittle failure of rock, often along a preexisting, large-scale fracture where two plates meet, called a *fault*. Tectonic plates move at a pace of a few centimeters per year, about the same rate our fingernails grow, but the motion is not smooth and continuous at the boundaries between plates. Friction along faults resists the motion. Stresses build up until they cause sudden brittle failure and movement that can shake Earth's interior and surface. The vibrations or seismic activity can cause serious damage to buildings and infrastructure, or they can be so slight that they are only detected with sensitive instruments called *seismometers*.

Scientists have been recording earthquake activity for more than a century, with increasing degrees of sophistication, accumulating a tremendous amount of data. With multiple seismometers recording the same earthquake, it is possible to calculate where it originated within the earth. The location in the earth where an earthquake starts is called the *hypocenter*, while the location directly above it at the surface is called the *epicenter*. When mapped out over time, earthquakes near the surface trace out faults, marking the boundaries between mobile tectonic plates.

There is also important information conveyed by the depth of earthquake hypocenters. Figure 1A shows a his-

togram of the depth of earthquakes worldwide, revealing two humps or modes in the data. The first and most prominent mode peaks within the uppermost 100 km and drops off exponentially with depth (Frohlich, 2006). These shallower earthquakes are associated with movements along faults between tectonic plates, especially where plates push together, at subduction zones and continental collisions (figure 1B). Deeper earthquakes, plotted all the way down to 700 km in figure 1A, are associated with subducting plates and record their activity as they sink into the mantle.

Initially, earthquake activity coincides with dehydration and the release of fluids from sediment and crust in a subducting slab. Seismicity tapers off sharply down to a depth of 300 km, and it is expected that dehydration and loss of volatiles from the slab are largely complete by this point. There should be no further earthquakes as the slab continues to descend into the mantle. For this reason, the deep-focus earthquakes below about 300 km that peak in a second mode at 500–600 km are anomalous (figure 1A).

Deep-focus earthquakes are a subject of active research. Several ideas have been proposed to explain them. One of the proposed mechanisms is that subducting slabs contain hydrous minerals in their interior from previous interaction with seawater at the surface, which eventually break down as the slab warms up, releasing water and promoting brittle failure within the slab (Omori et al., 2004). This idea is singled out here because it ties in with the modeling work by Shirey et al. (2021), who refined the idea and connected it with recent observations from CLIPPIR (~type IIa) and type IIb diamonds.

A Primer in Plate Tectonics

It is clear that deep-focus earthquakes are linked with subduction, so it is important to clarify some of the concepts of plate tectonics before moving further. The rigid outer layer of the earth that makes up the plates in figure 1B is called the *lithosphere*, and it rides on the weak and plastic (but not molten) rock beneath the lithosphere, shown simply as white space under the plates. The lithosphere is an open-faced sandwich of two components, with the crust on top and a portion of rigid mantle rock beneath it. The bottom of the lithosphere or plate is a mechanical boundary where the mantle rocks transition from rigid and brittle to weak and plastic. The weak and flowing mantle beneath the lithosphere is sometimes specified as the sublithospheric mantle or convecting mantle, which extends all the way down to the outer core at 2900 km.

There are two very different kinds of lithosphere. Continents, including their underwater continental shelf extensions, are made of continental lithosphere, whereas ocean floors are made of oceanic lithosphere (figure 1B). Continental lithosphere is thicker, more buoyant, and relatively stable through geologic time. Oceanic lithosphere is thinner, denser, and has a relatively finite life cycle.

Figure 1. Earthquake depth distribution and overview of plate boundaries. A: Depth distribution of earthquakes worldwide (note the logarithmic scale). Most "regular" earthquakes occur at depths shallower than 200 km, and the frequency decreases with depth. Earthquakes deeper than about 300 km stray from this pattern, and there is an anomalous mode of activity around 500–600 km. The histogram shows magnitude 5 and greater earthquakes for a 40-year period (1964–2004) in the EHB (Engdahl-van der Hilst-Buland) catalog (Engdahl et al., 1998). B: A simplified schematic cross section of the earth, showing interactions between tectonic plates. Most earthquake activity occurs by interactions between these rigid plates near the surface, especially where plates push together, at subduction zones and continental collisions. Deeper earthquakes are spatially associated with subducted plates and must occur by a different mechanism that remains poorly understood.

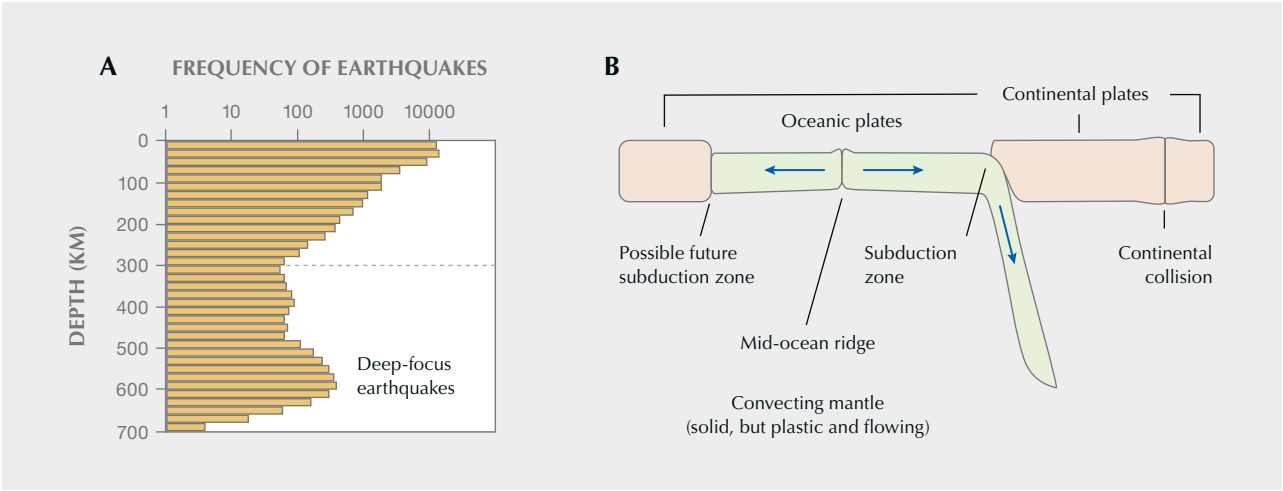

Figure 2. These large type IIa diamonds are good examples of CLIPPIR diamonds, which are the kind of top gem-quality diamonds produced in the sublithospheric mantle, potentially in association with deep earthquakes. The diamonds shown are from the Letšeng mine in Lesotho and range from 14 to 91 ct. Note the irregular morphologies, including surfaces that are both broken and substantially resorbed. Photo by Robert Weldon/GIA; courtesy of Gem Diamonds Ltd.

Oceanic lithosphere is created almost continuously at the spreading centers of mid-ocean ridges. On either side of a ridge, the plates gradually spread apart. Eventually, in 20 to 200 million years, the oceanic lithosphere bends and sinks down into the convecting mantle, a process called *subduction* (figure 1B). The creation and subduction of oceanic lithosphere are ongoing. The rate of spreading at mid-ocean ridges and convergence at subduction zones often differs and is not necessarily balanced in the same ocean basin, so oceans are dynamic regions that can open and grow or shrink and close. The opening of the Atlantic Ocean, for example, is facilitated by the creation of new oceanic lithosphere along the mid-Atlantic ridge. There is currently no subduction of oceanic lithosphere around the Atlantic's perimeter. The Pacific Ocean, however, is almost completely surrounded by subduction zones where oceanic lithosphere is subducting down into the mantle and fueling arc volcanoes that make up the Pacific Ring of Fire.

Nearly all the oceanic lithosphere on Earth is younger than about 200 million years old. Modern-style plate tectonics is thought to have been operating for about the past 3 billion years (Earth is 4.5 billion years old) (Shirey and Richardson, 2011). Over this time, several oceans have opened and closed (Wilson, 1966) along with the assembly and breakup of various continental configurations, such as the supercontinent Pangaea.

Super-Deep Diamond Factories

Hundreds of kilometers down inside the earth, where subducting slabs reach perhaps 360–750 km, there may be blossoming domains of diamond growth. Most mined diamonds are thought to originate from shallower depths within the continental lithosphere at about 150–200 km, but some (estimated to be approximately 2%) originate from below the continental lithosphere. These are known as *sublithospheric* or *super-deep* diamonds. Despite being a relatively rare mineral, diamond can form in multiple different ways. The variables that lead to different kinds of diamond include the host rock type, the composition of the diamond forming fluid, how carbon resides in the fluid and surrounding mantle, and the pressure and temperature conditions. Individual diamond deposits at the surface often contain several distinct populations that can be recognized by studying mineral inclusions or other features, such as their morphology, internal growth history, nitrogen content and aggregation, and carbon isotopic composition (e.g., Stachel and Harris, 2008).

The study of sublithospheric diamonds over the past few decades has been dominated by small (usually <1 ct), generally non-gem quality diamonds from the Juina region of Brazil and various other localities worldwide (see reviews by Stachel et al., 2005; Kaminsky, 2012; Harte and Hudson, 2013; Smith and Nestola, 2021). In the past few years, however, it has been discovered that the prevalence

of sublithospheric diamonds is greater than previously thought and includes some of the largest and highest-quality gem diamonds (Smith et al., 2016, 2017, 2018). Diamonds such as the exquisite type IIa (containing no detectable nitrogen by FTIR) gems from the Letšeng mine (figure 2) are now recognized to belong to the sublithospheric variety termed CLIPPIR diamonds. These are argued to account for most of the type IIa diamonds in the gem marketplace, amounting to about 1% of diamonds (Smith et al., 2017). Similarly, rare type IIb diamonds (boron-bearing), which can be blue in color, have also been shown to be sublithospheric (Smith et al., 2018).

A connection to subducted oceanic lithosphere is an emerging theme common to many sublithospheric diamonds, based mainly on the composition of mineral inclusions (Walter et al., 2008, 2011; Bulanova et al., 2010; Burnham et al., 2015; Ickert et al., 2015; Seitz et al., 2018; Smith et al., 2018; Thomson et al., 2016a). CLIPPIR and type IIb diamonds have also been linked to subducted slabs and to serpentinized peridotite in the mantle portion of slabs in particular. Serpentinization is a complex series of reactions between water and rock, resulting in the formation of hydrous (water-bearing) minerals such as serpentine from normally anhydrous minerals such as olivine. The strongest piece of evidence for this connection between diamonds and serpentinites comes from measurements of iron isotopes in inclusions trapped in CLIPPIR diamonds (Smith et al., 2021). The iron in these inclusions has an isotopic signature produced during serpentinization reactions between seawater and the ocean floor. In order for this signature to be trapped in CLIPPIR diamonds, deeply subducted serpentinized oceanic lithosphere must have contributed to their formation. In a sense, subducting slabs are like conveyor belts feeding raw materials down to hidden super-deep diamond factories at 360–750 km depths. Exactly how these diamonds make their way upward to shallower depths where they can be swept up to the surface in volcanic eruptions of kimberlite magma remains an open question, however (figure 3).

Earthquakes and Diamond-Forming Fluid

Slabs gradually warm up as they subduct into the mantle. The temperature change with depth is called a *geotherm*. About half of Earth's subducting slabs trace out warmer pathways, while the remainder are colder, depending on the

Figure 3. Mantle cross section showing a relatively cool subducting slab, with an inset histogram of earthquake frequency (from figure 1). Profiles on the right show the slab surface and interior temperature during subduction. Where the slab surface temperature intersects the solidus of carbonated mid-ocean ridge basalt (MORB), partial melting may occur (red arrows). At the far right, a cold slab interior remains within the dense hydrous magnesium silicates (DHMS) stability field until the slab stalls and warms up, causing the breakdown of these hydrous phases and the release of hydrous fluid (blue arrows). Large white and smaller brown diamond symbols signify the growth of high-quality gem diamonds (CLIPPIR and type IIb) and low-quality, generally non-gem sublithospheric diamonds, respectively. Poorly understood mechanisms transport some diamonds upward where they can be swept up in kimberlite eruptions and mixed with common lithospheric diamonds (small black diamond symbols). Modified from Smith and Nestola (2021) with carbonated MORB solidus from Thomson et al. (2016b) and DHMS stability field from Harte (2010).

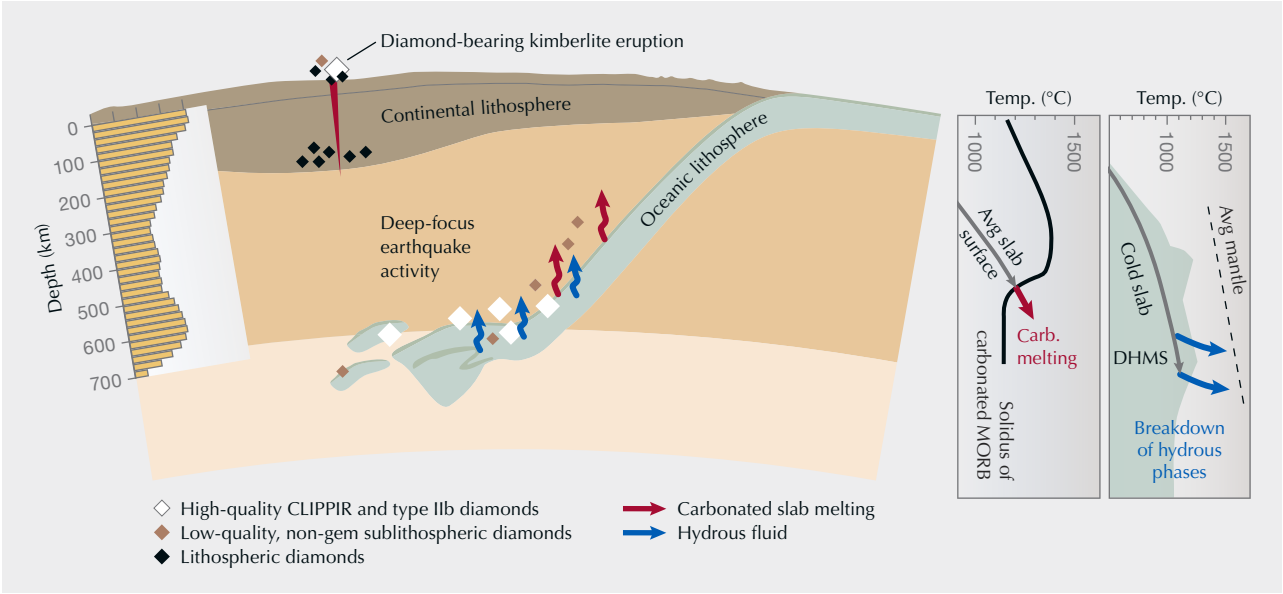

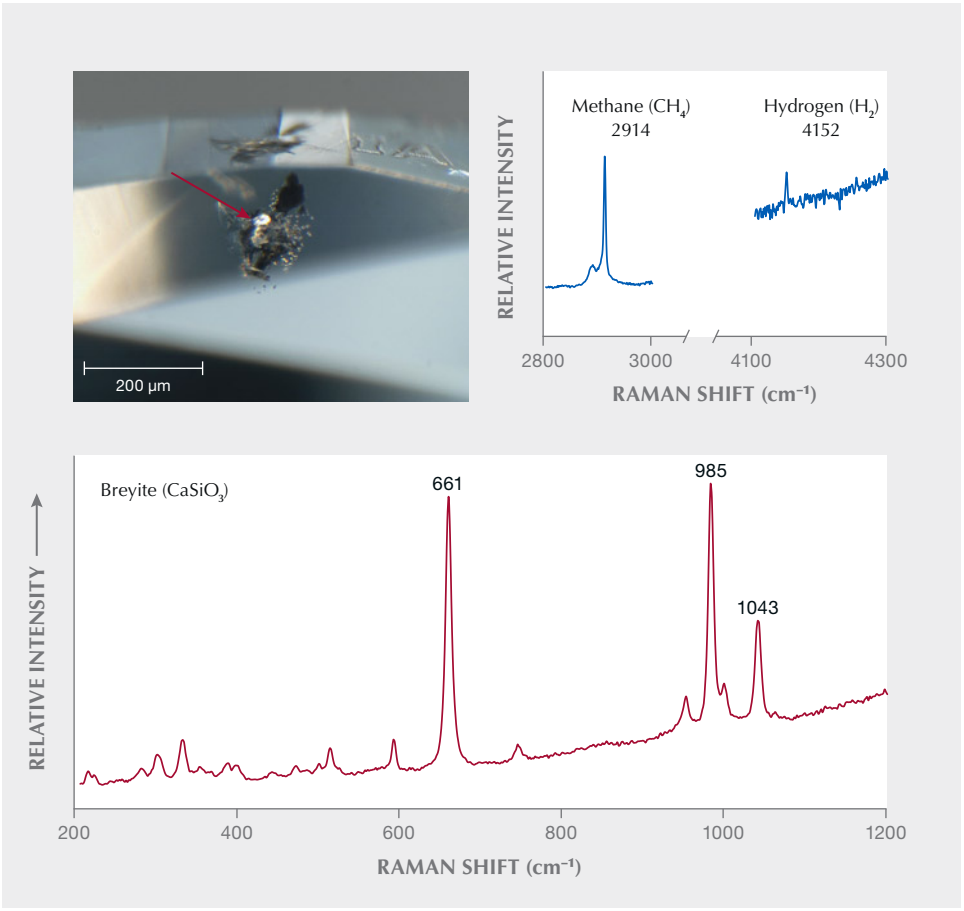

Figure 4. Evidence of hydrous fluid presence during diamond growth. This inclusion of breyite (photomicrograph and bottom Raman spectrum) within a blue type IIb diamond is interpreted to have been trapped as $CaSiO_3$ perovskite, which has inverted to a lower-pressure mineral form during exhumation from the mantle, originating from a depth greater than 360 km. Raman spectroscopy also reveals peaks associated with methane and molecular hydrogen (top right spectrum), which are present as a thin fluid layer trapped at the interface between the solid inclusion and the host diamond. Photomicrograph by E.M. Smith; field of view 0.65 mm.

age of the slab and the speed at which it subducts. Warmer slabs generally lack deep earthquakes, which appear to be unique to colder slabs. Shirey et al. (2021) examined slabs around the world and modeled their temperature change with depth as they heat up during subduction into the mantle. They also made a careful comparison between earthquake locations, slab geotherms, and the expected mineralogy and phase changes within slab rocks. Overlaying the slab geotherms onto phase diagrams helps to illustrate where water-bearing phases break down and release fluid, such as the relatively well-accepted loss of most water from warm slabs at relatively shallow depths (<200 km). This is the activity that generates melt and fuels arc volcanoes such as those of the Pacific Ring of Fire. Cold slabs, however, can partially bypass this shallow dewatering process and transport a budget of carbonate and water to depths beyond 300 km, where its later release can cause deep-focus earthquakes (figure 3).

The cold slabs can be thought of as having a carbonated crust component and a hydrated/serpentinized mantle peridotite component that lies shielded beneath the crust, toward the interior of the slab. The deep release of carbonatitic melt and hydrous fluid from each component, respectively, is shown in the two depth profiles in figure 3. The carbonated crust (mid-ocean ridge basalt, or MORB) of the slab surface will intersect a deep depression in its solidus, the curve describing the beginning of melting, meaning it exceeds the melting temperature. Beyond this point, carbonate melting (red arrows) is expected to occur within the top/crustal portion of the slab.

For hydrated/serpentinized mantle peridotite inside the slab, its stability also depends on temperature. If it remains cool, the serpentine can metamorphose into higher-pressure water-bearing minerals called *dense hydrous magnesium silicates* (DHMS) rather than breaking down. DHMS phases are a good vehicle for transporting water, with some carrying as much as 10% or more water by weight. The geotherm for the interior of cold slabs remains in the DHMS stability field far beyond a depth of 300 km (far right in figure 3). The slab in figure 3 is shown deflecting as it reaches the top of the lower mantle (at 660 km), where there is a change in mantle density and deformability. As the slab stalls and warms up, DHMS phases break down to form minerals that carry much less water, thereby causing water release (blue arrows in figure 3). These are the mechanisms proposed to trigger not only deep-focus earthquakes but also super-deep diamond growth (Shirey et al., 2021).

Inclusions in the smaller, lower-quality varieties of sublithospheric diamonds often show evidence of growth from carbonatitic melts derived from slabs (Walter et al., 2008), but hydrous/aqueous fluids have also been implicated for some samples (Wirth et al., 2007; Pearson et al., 2014; Palot

et al., 2016). Serpentinite in subducting slabs can be relatively enriched in boron, meaning that the eventual breakdown of hydrous minerals from serpentinized peridotite can release boron-bearing hydrous fluid, which has been linked with the formation of type IIb (boron-bearing) diamonds (Smith et al., 2018). Figure 4 shows a calcium silicate (breyite) inclusion with methane and hydrogen in a type IIb diamond. The original mineral inclusion may have been relatively hydrogen-rich upon trapping because it crystallized from, or was exposed to, hydrous fluids. Subducted serpentinized peridotite is also a key ingredient for CLIPPIR diamond growth, on the basis of recent iron isotope measurements (Smith et al., 2021).

Broken Diamonds

Evidence of natural deformation and breakage in diamond is not uncommon. For example, this evidence can be in the form of plastic deformation lines or internally fractured diamond overgrown by new layers of pristine diamond. Features such as these attest to the occasional turbulent conditions in the mantle, even before diamonds are picked up and scrambled by kimberlite eruptions. Little is known about the circumstances responsible for these features.

Sublithospheric diamonds in particular bear evidence of deformation and breakage, typically having irregular morphologies with broken and resorbed surfaces. CLIPPIR diamonds, which can reach thousands of carats (including the 3,106 ct Cullinan), often have surfaces that appear to be broken (figure 2). Some of those broken surfaces on large diamonds have high degrees of resorption or chemical dissolution, to an extent that would consume any small diamonds nearby (Gurney and Helmstaedt, 2012). For this reason, such extreme resorption is unlikely to be associated with volcanic transport in a kimberlite where smaller diamond crystals survive. This indicates that the resorption, and in turn some of the breakage of large CLIPPIR diamonds, occurred early in the diamond's history.

In addition to diamond breakage, some sublithospheric diamonds have internal evidence of more subdued brittle fractures that have healed rather than separated (figure 5). Network-like patterns of dislocations inside these diamonds often conform with the healed fractures rather than being cross-cut by them, suggesting the deformation and fracturing was followed by a protracted period of annealing in the mantle to allow the network pattern to develop. Again, this points to sublithospheric diamond deformation and breakage that is not due to kimberlite activity.

If fluid and melt release from deeply subducted slabs causes both deep-focus earthquakes and diamond growth, it is worth considering how diamonds might be affected by earthquakes. Breakage and other signs of deformation could potentially be related to diamond growth in a dynamic setting punctuated by deep-focus earthquakes. Obviously, more research is needed to decipher the natural deformation history of diamonds. Nevertheless, it is interesting to speculate on a possible connection between diamond breakage and deep-focus earthquakes.

Figure 5. Evidence of the incredibly dynamic setting in which these diamonds form. A: Deep-UV luminescence image of a type IIa diamond with irregular blue lines (see arrows) that may be healed fractures lying within a typical dislocation network pattern. Image by E.M. Smith; field of view 5.92 mm. B: Cathodoluminescence image of a type IIb diamond with an irregular dislocation network pattern that encloses several long straight segments, reaching up to 600 µm, interpreted as healed segments of brittle fracture/cleavage within an otherwise plastically deformed and annealed diamond. Image by E.M. Smith; field of view 2.39 mm.

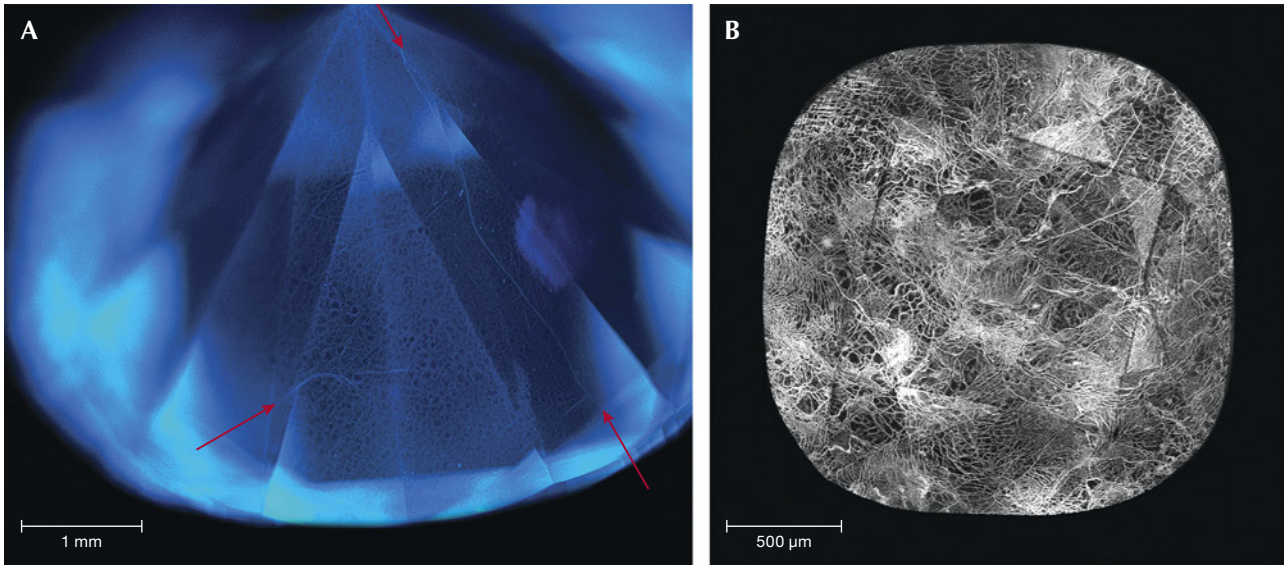

Scientific Significance

Subduction is a fundamental aspect of plate tectonics that is driven by Earth's internal heat engine—the means by which heat escapes from the mantle and core. It forces us to consider plate tectonics not just as a system of plates at Earth's surface but also as a process that involves the exchange of material between the surface and the deeper convecting mantle over time (figure 1B). During its time at the seafloor, oceanic lithosphere interacts with seawater over many millions of years. Water can circulate into fractures and react with the basaltic and peridotitic rocks that make up the oceanic lithosphere. As the aged and modified oceanic plates subduct, they now carry sediments, pore fluids, altered oceanic crust, and serpentinized peridotite along for the ride.

The sediments, water, and carbonate in the upper portion of the slab may be stripped off at shallower depths in the subduction zone (<200 km) where they fuel arc volcanoes, but some carbonated crust and serpentinized peridotite can be transported deeper. Deep-focus earthquakes and diamonds may be a product of some slabs, namely those that have remained cooler during subduction, carrying a budget of carbonate in altered ocean crust and hydrous minerals in serpentinized peridotite down to 300 to 700 km. The deep cycling of carbon and water has a big impact on the behavior of Earth's interior, how it moves and melts.

These large-scale processes are relevant for the evolution of the atmosphere, the distribution of water at the surface, and the formation of continents over geological time. All of these parts of the dynamic earth are connected. Despite the proven 1 to 3 billion-year-old ages of many gem diamonds that come from the lithosphere, there is no reason that diamonds cannot be forming in the present. If diamonds and deep earthquakes are truly related, as described by Shirey et al. (2021), the implication is that modern-day earthquakes herald the formation of new diamonds. In this sense, subduction drives a sort of modern diamond factory—one that has the potential to produce some of the largest and most valuable diamonds known (including type IIa and type IIb diamonds). Diamonds and earthquakes, while fascinating in their own right, are two of the most powerful tools we have to unravel the inner workings of our planet.

ACKNOWLEDGMENT

Many thanks to Dr. Steven B. Shirey for insightful discussion and suggestions that helped to improve this column.

REFERENCES

Bulanova G.P., Walter M.J., Smith C.B., Kohn S.C., Armstrong L.S., Blundy J., Gobbo L. (2010) Mineral inclusions in sublithospheric diamonds from Collier 4 kimberlite pipe, Juina, Brazil: Subducted protoliths, carbonated melts and primary kimberlite magmatism. *Contributions to Mineralogy and Petrology*, Vol. 160, No. 4, pp. 489–510, http://dx.doi.org/10.1007/s00410-010-0490-6

Burnham A.D., Thomson A.R., Bulanova G.P., Kohn S.C., Smith C.B., Walter M.J. (2015) Stable isotope evidence for crustal recycling as recorded by superdeep diamonds. *Earth and Planetary Science Letters*, Vol. 432, pp. 374–380, http://dx.doi.org/10.1016/j.epsl.2015.10.023

Engdahl E.R., van der Hilst R., Buland R. (1998) Global teleseismic earthquake relocation with improved travel times and procedures for depth determination. *Bulletin of the Seismological Society of America*, Vol. 88, No. 3, pp. 722–743, http://dx.doi.org/10.1785/BSSA0880030722

Frohlich C. (2006) *Deep Earthquakes*. Cambridge University Press, Cambridge, UK.

Gurney J.J., Helmstaedt H.H. (2012) The origins of type IIa diamonds and their enhanced economic significance. *10th International Kimberlite Conference*, Extended Abstract No. 10IKC-123, pp. 1–6.

Harte B. (2010) Diamond formation in the deep mantle: The record of mineral inclusions and their distribution in relation to mantle dehydration zones. *Mineralogical Magazine*, Vol. 74, No. 2, pp. 189–215, http://dx.doi.org/10.1180/minmag.2010.074.2.189

Harte B., Hudson N.F.C. (2013) Mineral associations in diamonds from the lowermost upper mantle and uppermost lower mantle. *Proceedings of the 10th International Kimberlite Conference*, Vol. 1, pp. 235–253.

Ickert R.B., Stachel T., Stern R.A., Harris J.W. (2015) Extreme ^{18}O-enrichment in majorite constrains a crustal origin of transition zone diamonds. *Geochemical Perspectives Letters*, Vol. 1, No. 1, pp. 65–74, http://dx.doi.org/10.7185/geochemlet.1507

Kaminsky F. (2012) Mineralogy of the lower mantle: A review of 'super-deep' mineral inclusions in diamond. *Earth-Science Reviews*, Vol. 110, No. 1-4, pp. 127–147, http://dx.doi.org/10.1016/j.earscirev.2011.10.005

Omori S., Komabayashi T., Maruyama S. (2004) Dehydration and earthquakes in the subducting slab: Empirical link in intermediate and deep seismic zones. *Physics of the Earth and Planetary Interiors*, Vol. 146, No. 1-2, pp. 297–311, http://dx.doi.org/10.1016/j.pepi.2003.08.014

Palot M., Jacobsen S.D., Townsend J., Nestola F., Marquardt K., Miyajima N., Harris J., Stachel T., McCammon C., Pearson D.

(2016) Evidence for H_2O-bearing fluids in the lower mantle from diamond inclusion. *Lithos*, Vol. 265, pp. 237–243, http://dx.doi.org/10.1016/j.lithos.2016.06.023
Pearson D.G., Brenker F.E., Nestola F., McNeill J., Nasdala L., Hutchison M.T., Matveev S., Mather K., Silversmit G., Schmitz S., Vekemans B., Vincze L. (2014) Hydrous mantle transition zone indicated by ringwoodite included within diamond. *Nature*, Vol. 507, No. 7491, pp. 221–224, http://dx.doi.org/10.1038/nature13080
Seitz H.-M., Brey G.P., Harris J.W., Durali-Müller S., Ludwig T., Höfer H.E. (2018) Ferropericlase inclusions in ultradeep diamonds from Sao Luiz (Brazil): High Li abundances and diverse Li-isotope and trace element compositions suggest an origin from a subduction mélange. *Mineralogy and Petrology*, Vol. 112, No. S1, pp. 291–300, http://dx.doi.org/10.1007/s00710-018-0572-0
Shirey S.B., Richardson S.H. (2011) Start of the Wilson Cycle at 3 Ga shown by diamonds from subcontinental mantle. *Science*, Vol. 333, No. 6041, pp. 434–436, http://dx.doi.org/10.1126/science.1206275
Shirey S.B., Wagner L.S., Walter M.J., Pearson D.G., van Keken P.E. (2021) Slab transport of fluids to deep focus earthquake depths – Thermal modeling constraints and evidence from diamonds. *AGU Advances*, Vol. 2, No. 2, http://dx.doi.org/10.1029/2020AV000304
Smith E.M., Nestola F. (2021) Super-deep diamonds: Emerging deep mantle insights from the past decade. In H. Marquardt et al., Eds., *Mantle Convection and Surface Expressions*, Geophysical Monograph Series 263, American Geophysical Union, pp. 179–192.
Smith E.M., Shirey S.B., Nestola F., Bullock E.S., Wang J., Richardson S.H., Wang W. (2016) Large gem diamonds from metallic liquid in Earth's deep mantle. *Science*, Vol. 354, No. 6318, pp. 1403–1405, http://dx.doi.org/10.1126/science.aal1303
Smith E.M., Shirey S.B., Wang W. (2017) The very deep origin of the world's biggest diamonds. *G&G*, Vol. 53, No. 4, pp. 388–403, http://dx.doi.org/10.5741/GEMS.53.4.388
Smith E.M., Shirey S.B., Richardson S.H., Nestola F., Bullock E.S., Wang J., Wang W. (2018) Blue boron-bearing diamonds from Earth's lower mantle. *Nature*, Vol. 560, No. 7716, pp. 84–87, http://dx.doi.org/10.1038/s41586-018-0334-5
Smith E.M., Ni P., Shirey S.B., Richardson S.H., Wang W., Shahar A. (2021) Heavy iron in large gem diamonds traces deep subduction of serpentinized ocean floor. *Science Advances*, Vol. 7, No. 14, http://dx.doi.org/10.1126/sciadv.abe9773
Stachel T., Harris J.W. (2008) The origin of cratonic diamonds—Constraints from mineral inclusions. *Ore Geology Reviews*, Vol. 34, pp. 5–32, http://dx.doi.org/10.1016/j.oregeorev.2007.05.002
Stachel T., Brey G., Harris J.W. (2005) Inclusions in sublithospheric diamonds: Glimpses of deep earth. *Elements*, Vol. 1, No. 2, pp. 73–78, http://dx.doi.org/10.2113/gselements.1.2.73
Thomson A.R., Kohn S.C., Bulanova G.P., Smith C.B., Araujo D., Walter M.J. (2016a) Trace element composition of silicate inclusions in sub-lithospheric diamonds from the Juina-5 kimberlite: Evidence for diamond growth from slab melts. *Lithos*, Vol. 265, pp. 108–124, http://dx.doi.org/10.1016/j.lithos.2016.08.035
Thomson A.R., Walter M.J., Kohn S.C., Brooker R.A. (2016b) Slab melting as a barrier to deep carbon subduction. *Nature*, Vol. 529, No. 7584, pp. 76–79, http://dx.doi.org/10.1038/nature16174
Walter M.J., Bulanova G.P., Armstrong L.S., Keshav S., Blundy J.D., Gudfinnsson G., Lord O.T., Lennie, A.R., Clark S.M., Smith C.B., Gobbo L. (2008) Primary carbonatite melt from deeply subducted oceanic crust. *Nature*, Vol. 454, No. 7204, pp. 622–625, http://dx.doi.org/10.1038/nature07132
Walter M.J., Kohn S.C., Araujo D., Bulanova G.P., Smith C.B., Gaillou E., Wang J., Steele A., Shirey S.B. (2011) Deep mantle cycling of oceanic crust: Evidence from diamonds and their mineral inclusions. *Science*, Vol. 334, No. 6052, pp. 54–57, http://dx.doi.org/10.1126/science.1209300
Wilson J.T. (1966) Did the Atlantic close and then re-open? *Nature*, Vol. 211, No. 5050, pp. 676–681, http://dx.doi.org/10.1038/211676a0
Wirth R., Vollmer C., Brenker F., Matsyuk S., Kaminsky F. (2007) Inclusions of nanocrystalline hydrous aluminium silicate "Phase Egg" in superdeep diamonds from Juina (Mato Grosso State, Brazil). *Earth and Planetary Science Letters*, Vol. 259, No. 3-4, pp. 384–399, http://dx.doi.org/10.1016/j.epsl.2007.04.041

GEM NEWS INTERNATIONAL

Contributing Editors
Gagan Choudhary, *Gem Testing Laboratory, Jaipur, India* (gagan@gjepcindia.com)
Christopher M. Breeding, *GIA, Carlsbad* (christopher.breeding@gia.edu)
Guanghai Shi, *School of Gemmology, China University of Geosciences, Beijing* (shigh@cugb.edu.cn)

TUCSON 2022

Sellers and buyers alike were delighted to be back at Tucson for the show season after a two-year absence. As the world enters a new phase of the pandemic, the gem and jewelry industry is also preparing for the post-pandemic era. Attendees embraced precautions such as social distancing and face coverings (figure 1). Although social gatherings were much less crowded than usual, the atmosphere and business at the shows were as strong as before, if not better.

Due to travel restrictions, the international presence was down, but that did not affect vendor attendance at the main AGTA GemFair at the Tucson Convention Center, where the majority of exhibitors had strong U.S. representation. The Gem & Jewelry Exchange (GJX) show was slightly affected, with some booths left empty by foreign dealers who could not make it to Tucson this year. Vendor attendance in the satellite shows outside of the convention center area remained strong, as observed by the authors at

Figure 1. Customers select goods at the AGTA GemFair. Photo by Tao Hsu.

Figure 2. A stone decor dealer's booth at the Kino Gem & Mineral Show. Open to the public, the show saw steady foot traffic. Photo by Tao Hsu.

Editors' note: Interested contributors should send information and illustrations to Stuart Overlin at soverlin@gia.edu or GIA, The Robert Mouawad Campus, 5345 Armada Drive, Carlsbad, CA 92008.

Gems & Gemology, Vol. 58, No. 1, pp. 80–136.


Figure 3. Left: The Pueblo Gem & Mineral Show was an ideal place to source rough gems of all kinds. Right: Cutting services were provided at multiple shows open to the public. Photos by Tao Hsu.

the Pueblo Gem & Mineral Show, the Kino Gem & Mineral Show (figure 2), and the 22nd Street Mineral, Fossil, Gem & Jewelry Show.

Many exhibitors felt that while foot traffic was lighter than usual, buyers were focused on purchasing targeted goods to restock inventory. Meanwhile, the pandemic's influence on the supply side of the value chain was just starting to show. Therefore, this Tucson show season provided a very good opportunity to prepare for a potential shortage in the coming months (figure 3).

The variety of gems and jewelry traded at the shows remained consistent with previous years. The "big three"—ruby, sapphire, and emerald—still dominate the market (figure 4), with the intake at the GIA Show Service Lab reflecting this. Collector minerals and gems such as meteorite, gahnospinel, fluorite of various colors, opalized fossils, cerussite, and colemanite continued to attract a niche market clientele (figure 5). Also in high demand were fantasy cuts, rose cuts, briolettes, and mineral or rock slices. Jewelry designers on a mission to fulfill special orders sourced gems such as Montana sapphire, Oregon sunstone, Arizona turquoise, Washington nephrite jade, and other American gems.

Vendors have never been more creative in terms of their products and business savvy. To fulfill the ever-growing demand for one-of-a-kind creations, gem cutters, carvers, and jewelry manufacturers have put more thought and individuality into their pieces (figure 6). Products manufactured with a high level of sophistication such as inlaid jewelry or gems were prominent at the show (figure 7). Many vendors have shifted more business online over the past two years to combat limited foot traffic in stores. Newly formed companies, meanwhile, have often started completely online or done most of their business online.

Figure 4. An 8.23 ct star ruby cut by David Nassi. Photo by Robert Weldon; courtesy of 100% Natural Ltd.

Figure 5. A 45 ct green fluorite from New Mexico. Dealers carried fluorite of all colors and cutting styles at both the AGTA and GJX shows. Photo by Emily Lane; courtesy of Barker & Co.

Figure 6. Left: Rock and metal wall decor in combination with metal art at the Kino show. Right: A 22.93 ct carved citrine crafted in Jaipur, India; courtesy of Artisav Jaipur. Photos by Tao Hsu.

GIA relished in the much-anticipated return to Tucson this year, enthusiastically gathering the latest from the shows to share in this report. Our coverage includes market updates, interesting and noteworthy finds, and uplifting accounts from dealers, cutters, designers, and more.

The following contributed to this report: Erin Hogarth, Erica Zaidman, Robert Weldon, Albert Salvato, Wim Vertriest, Lisa Neely, and Nathan Renfro.

Tao Hsu and Lisa Kennedy
GIA, Carlsbad

COLORED STONES AND ORGANIC MATERIALS

Large, rare faceted collector gems. Barker & Co. (Scottsdale, Arizona) exhibited remarkable stones at this year's AGTA show, including some extremely fine, rare gemstones for collectors. Two of their collector stones, colemanite and phosphophyllite, stood out for their record-breaking size.

The colorless colemanite in figure 8, a modified triangular brilliant weighing 7.36 ct, is believed to be one of the largest faceted examples of its kind. Colemanite is known

Figure 7. Gemstone-inlaid bangles from David R. Freeland Jr. Designs at the Pueblo Gem & Mineral Show. Photo by Lisa Kennedy.

Figure 8. A 7.36 ct colorless, modified triangular brilliant-cut colemanite displayed at the AGTA show. Photo by Emily Lane; courtesy of Barker & Co.

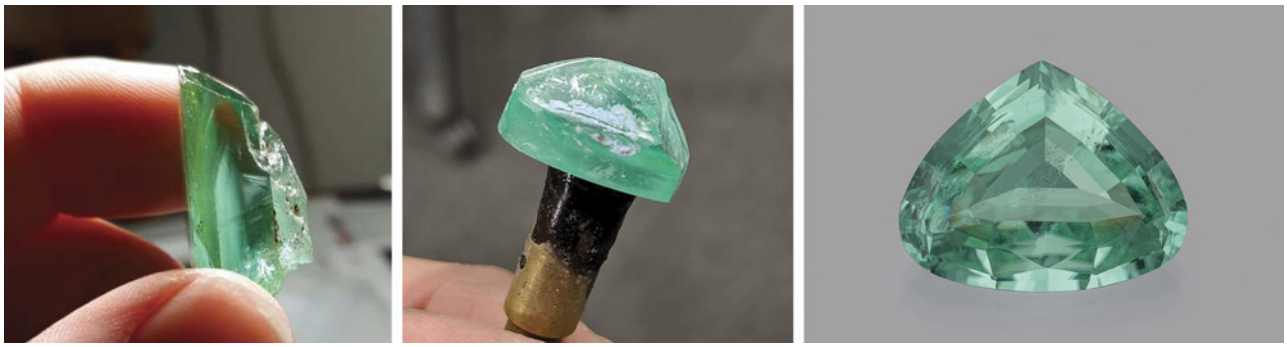

Figure 9. The evolution of a 45.42 ct rough phosphophyllite in the hands of Stacy Whetstone (left). It took four weeks to cut and finish the stone due to its heat sensitivity (center). The finished 17.52 ct bluish green, modified triangular brilliant-cut phosphophyllite was displayed at the AGTA show (right). Left and center photos courtesy of Barker & Co.; right photo by Emily Lane.

to fluoresce a strong yellow under ultraviolet light and phosphoresce green.

The strongly saturated bluish green hue of a 17.52 ct phosphophyllite echoed that of some of the finest hues of Paraíba tourmalines, though the stone is very different both structurally and chemically. Phosphophyllite was named in 1920 as a homage to its phosphate composition and perfect leaf-like cleavage (from the Greek *phyllon*, meaning "leaf"). Ann Barker of Barker & Co. explained that this particular phosphophyllite has a significant provenance. Once owned by author and renowned mineral collector Dr. Peter Bancroft, it was mined in the famed Potosí mine of Bolivia in 1958. Many years later, prize-winning gem cutter Stacy Whetstone took the striking 45.42 ct rough and expertly faceted the material into the finished 17.52 ct rounded trillion (figure 9). Given phosphophyllite's considerable heat sensitivity, the gem took four weeks to cut and finish.

Colemanite and phosphophyllite, like other collector stones, are seldom faceted due to their low hardness (4.5 and 3–3.5, respectively) and durability issues. As collector stones, they hold a unique position in the gem and jewelry industry, valued for expanding private collections. In recent years, with the help of a little luck and a lot of talent, collector stones are being seen more in jewelry.

Lisa Kennedy and Tao Hsu

Custom knives by Loren Feldman. Some of the most interesting discoveries in Tucson came courtesy of Loren Feldman (Feldman Custom Knives, Gold Canyon, Arizona). His knives are works of art constructed from some of the rarest materials on Earth—and other planets. A visit to Feldman's booth is a fascinating walk through history that reveals geological treasures such as *Tyrannosaurus rex* bones, woolly mammoth tusks, and meteorites that fell to the earth millions of years ago.

Remarkably, Feldman has only been making knives for seven years. He describes his introduction to the craft and training as pure luck. Collecting rocks and minerals since he was a young boy, Feldman impressed custom knife maker Robert Stratton with his enthusiasm at the 22nd Street show in Tucson. After a fourth visit to the booth, Stratton generously offered to teach Feldman everything he knew about the craft. At the end of the training, he allocated part of his Tucson booth space to help Feldman get his start in the business. Feldman said that after his apprenticeship, "it took me about two years full-time to consider my work what I considered good. It took me about three years to pay all my bills. And seven years later, it's the happiest I've ever been as far as a profession."

Feldman's knife handles are crafted from minerals, gems, and fossilized dinosaur bone. One of his favorites is a knife made of gem dinosaur bone from nine different dinosaurs (shown on the cover of this issue). He explained that only 1/20 of 1% of all dinosaur bone turns into gem, describing it as a miracle of nature because it is only created under very specific conditions. During this process, the dinosaur bone undergoes a transformation that leaves the bone with a beautiful pattern of color and texture (fig-

Figure 10. Loren Feldman holds a piece of gem dinosaur bone, displaying the variety of colors and textures he can choose for his knives. Photo by Robert Weldon; courtesy of Loren Feldman.

Figure 11. Feldman studies a piece of gem dinosaur bone he cut, contemplating how to incorporate it in the knife handle. Photo by Robert Weldon; courtesy of Loren Feldman.

ure 10). Of all the materials he uses, he gets the most excited about gem dinosaur bone because it's so scarce and highly coveted (figure 11). Feldman also makes his handles from rare gems and minerals from all over the world, such as charoite from Siberia, Ammolite from Alberta, green jade from British Columbia, black jade from Western Australia, dumortierite from Mozambique, lapis lazuli from Afghanistan, labradorite from Madagascar, and agate from Northern Mexico.

Equally impressive are Feldman's blades. Made of fine American Damascus steel, the blades are one of three types: carbon, stainless steel, or mosaic. Feldman also crafts blades from iron meteorites that fell to the earth millions of years ago (figure 12). Feldman noted that while rare and expensive, meteorite has been used to make knives throughout history, adding that at least one meteorite blade was found in King Tut's tomb.

Feldman purchases some of the material he uses but also does his own exploration and digging. Each summer, he visits a friend's ranch in Montana to dig for dinosaur bone, and any bone recovered is sent to a lab for identification. He recently found enough *T. rex* bone to make a knife. Feldman noted that he's never seen another knife maker incorporate *T. rex* bone.

Each knife comes with a sheath made of premium leather or exotic skin such as alligator, snake, or elephant—"all legally obtained," Feldman said. About half of Feldman's customers also purchase stands, which are crafted with the same rare materials, including dinosaur bone, woolly mammoth tusk, and fine gemstones, and are often chosen to coordinate with the materials in the knife.

When asked what he enjoys most about his business, Feldman revealed that his favorite part is attending the shows and talking with customers. "Doing these events and meeting the collectors, the hunters, the scientists, museum curators, and the professors. I love learning more about the products I sell. Just about everything that I share with my customers, I learned here at this very show."

Figure 12. A finished six-inch knife featuring a meteorite blade and gem dinosaur bone handle. Photo by Robert Weldon; courtesy of Loren Feldman.

For Feldman, business is better than ever. The pandemic has increased the demand for his handmade creations. He explained that customers have been treating themselves during a time when they've been deprived of so much. His clientele, which includes collectors, investors, ranchers, hunters, and culinary artists, has kept him busy for the past two years.

Erica Zaidman
GIA, Carlsbad

Social media success for Black Opal Direct. At the GJX show, Justin Thomas (New South Wales, Australia) told us about Black Opal Direct's success on social media during the pandemic, his efforts to share opal knowledge, and a black opal with a special story. Founded in 1961 by Thomas's father, Jurgen, and owned and operated by Thomas and his wife, Ruth, Black Opal Direct specializes in black opal from Lightning Ridge.

Thomas said most of their customers come from YouTube and Instagram. In the last three years, their YouTube subscriber count has increased from 30,000 to 170,000. He said views fluctuate between 500,000 and 3 million a month, averaging about a million. This led to a tripling of sales over the last two years, though their business has now returned to normal. "It was a dream run," Thomas said. "I believe those days are over." He acknowledged that they have been fortunate in a time when many businesses around the world failed due to the pandemic. Without YouTube, he said, they would have weathered the last two years but would not be doing nearly as well.

Black Opal Direct began selling on eBay more than a decade ago. They determined that a million people per month were searching the Internet for the word "opal." Within a few months of starting to sell rough on eBay, sales were strong; then they built their website and brought their eBay customers to it. Thomas created a YouTube channel (figure 13) around the same time as the eBay store, but it was only three years ago that he started posting videos more frequently.

"As the channel grew, it started to morph into more entertainment videos, showing them how fun it is to cut an opal, and my funny side, so they can see my personality," he said. "I think in social media you have to show a lot more and a little bit of vulnerability. If you can connect in that way, in the heartstrings way, people will trust you a lot more and are much more likely to buy from you."

Thomas believes his videos are helping the whole industry because he does not push sales. "I don't even give the link to my website very often," he said. "It's all about the love of opal, how to cut it, how to mine it. It also helps the world understand opal."

According to Thomas, the opal industry is very secretive, and he is probably the first person to share so openly through social media how to cut opal. He said many had thanked him at the show, saying they learned how to cut opal from his videos and in some cases quit their jobs to go into the opal business. "I think it's awesome to be able to share that abundance," he said.

Thomas learned to cut opal from his father, who moved to Australia from East Germany in the '60s and began mining in Lightning Ridge. Jurgen Thomas's tools included a pick, shovel, and candle. When he began cutting, he used a manual Singer sewing machine that he converted by adding a corundum grinding wheel. "He's passed away now, and all that knowledge is only with me," Justin Thomas said. Despite the positive response of those learning from his videos, he said, many cutters are unhappy because he's giving away prized secrets. "That knowledge—if that's gone with my dad, and it goes with me, and my son never takes it up, it's wasted," he said. "Why let it go?"

Thomas emphasizes the quality of social media followers over the number. "Even if you've got a hundred followers, they could be a hundred genuine followers because they genuinely like you," he said. "Say up to five percent of those people may buy. You grow from that."

When Thomas cuts a highly valuable opal from rough on camera, he often does a dance. "They love it," he said. "There's always a comment before they watch a video: 'I

Figure 13. Black Opal Direct's YouTube channel helped dramatically increase sales during the last two years.

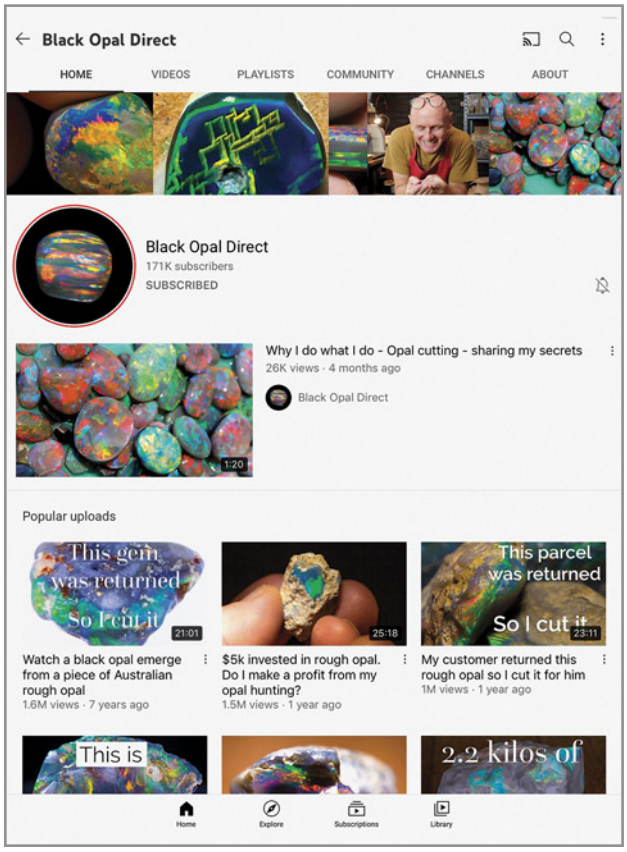

Figure 14. A 10.65 ct black opal found in Lightning Ridge by one of Jurgen Thomas's friends, at a location almost directly under where Jurgen lived nearly 60 years ago. Shown in diffused (left) and direct (right) lighting. Photos by Robert Weldon; courtesy of Black Opal Direct.

hope this one gets a dance!'" He has also been testing TikTok. "I always make jokes so they can see that I'm human, I'm personable, I can make an idiot of myself. I thought TikTok could be a good place for me to concentrate on those parts of my videos. I had a lot of followers quickly, who want to see me dancing."

Some competitors have tried to copy him—unsuccessfully, according to Thomas, because "their heart's not in it." Some also criticize his style. "I get lots of people saying 'You're an idiot' or 'You're a clown' or 'Why are you dancing?' Water off a duck's back. I try to focus on all the people that love me."

After years of working out of their home, the Thomases recently purchased a warehouse and built a cutting workshop there. Thomas said their subscribers have loved watching the small business grow. "I love this industry so much and I love what I do so much that it's addictive," he said. "Giving more and more to the subscribers and to my followers, going to the next level. So watch this space."

Thomas showed us a 10.65 ct black opal (figure 14), which he calls "the ultimate black opal." Its vivid colors, patterns, and strong play-of-color make it extraordinary. One of his father's friends, who mined with him at Lightning Ridge in the '60s, brought it to Thomas two years ago after finding it almost directly under the shed his father lived in back then.

Erin Hogarth
GIA, Carlsbad

Spectacular yellow sapphire from Sri Lanka. A return to the Tucson shows meant the opportunity to see the latest findings and designs from the Kreis family—stunning yellow sapphire from Sri Lanka. As *G&G* has reported in previous Tucson reports from 2014, 2015, and 2017, father Stefan buys the rough, mother Sonja designs the jewelry, and Alexander cuts the gems for the family business (Kreis Jewellery GmbH, Niederworresbach, Germany). Locating the sapphire rough in Sri Lanka required a combination of planning and luck, relying on the family's previously established network while also acting on rumors of possible sources. Two successful trips in 2020 and 2021 yielded five exceptionally large rough stones from five different deposits in the area surrounding Ratnapura, Sri Lanka (figure 15).

Figure 15. This 160 ct yellow sapphire rough was found in a deposit outside of Ratnapura, Sri Lanka. Photo courtesy of Kreis Jewellery GmbH.

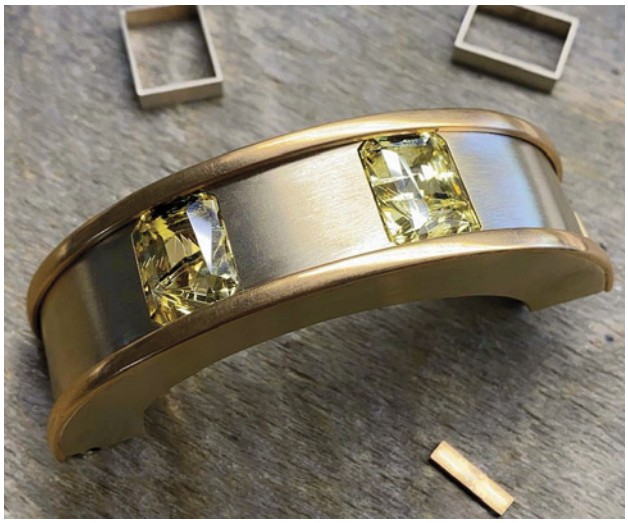

Figure 16. The yellow sapphires faceted by Alexander Kreis were set in a bracelet designed by Sonia Kreis. Photo courtesy of Kreis Jewellery GmbH.

Back in Germany, Alexander cut the five rough stones, and Sonja designed an exquisite bracelet (figures 16 and 17) to complete a suite of jewelry for a private collector. (Her previously designed pieces included a pendant, brooch, ring, necklace, and earrings.) The family aimed to create a harmony between the gems and the materials used, concentrating on gold colors that would not overshadow the sapphires. Alexander opted for a traditional cut for the outer shape but faceted the back to allow for more cross-reflection, mimicking this faceting in the diamonds that appear on the side of the bracelet. The creative combination of faceting and design perfectly captures the sunlight, creating magnificent reflections for the admirer. With an impressive total weight of 168.27 carats (containing 50.33, 32.80, 33.70, 23.98, and 27.46 ct sapphires), the bracelet is truly a breathtaking sight.

Erica Zaidman

Figure 17. The stunning finished bracelet features five yellow sapphires from Sri Lanka with a total weight of 168.27 carats. Photo courtesy of Kreis Jewellery GmbH.

Gray "spinel sisters." At the AGTA show, 100% Natural Ltd. (New York) took center stage with some large, extremely rare gemstones spared of treatments of any kind. Two stones that caught the authors' attention were a pair of exceptionally cut and nearly loupe-clean gray spinels weighing 69.96 ct (figure 18) and 11.78 ct (figure 19). There has been an increase in demand for gray spinel the past few years (Spring 2019 GNI, p. 130). Supply has remained relatively consistent, but larger, fine-quality stones are still quite rare.

Both of the gray spinels were cut from the same rough, weighing just over 220 ct and mined in Myanmar. Though famed for its rubies, Myanmar also produces equally fine red and pink spinel, as well as a range of other colors, including gray.

Master lapidarist and AGTA Spectrum Award winner David Nassi of 100% Natural Ltd. explained that gray spinel can appear lifeless and overly dark if cut poorly. His decision to create two "spinel sisters" from the same rough resulted

Figure 18. David Nassi's 69.96 ct antique cushion-cut, loupe-clean gray spinel. Prized in the trade for its metallic-like sheen, gray spinel of this size, quality, and color is extremely rare. Photo by Robert Weldon.

Figure 19. The finest gray spinel is a pure neutral gray, without a blue or violet secondary color component, as exemplified by this 11.78 ct antique pear shape expertly cut by David Nassi. Photo by Robert Weldon.

from a fissure running through the large piece of rough (figure 20). The 11.78 ct stone provided more of a challenge, as the shape of the rough piece was a bit flat and asymmetrical when sawn from the larger stone. Inspired by a large Mozambique stone he cut many years ago, Nassi expertly fashioned this piece into an antique pear shape, perfectly complementing the larger 69.96 ct antique cushion cut (to watch video of the "sister spinels," visit www.gia.edu/gems-gemology/spring-2022-gemnews-gray-spinel-sisters).

Nassi and the authors agree that gray spinel has been an underappreciated treasure in the trade for a while now. Its presence at the AGTA show gives us hope that gray spinel is gaining the popularity it deserves.

Lisa Kennedy and Tao Hsu

Michael Traurig: An opal dealer's battle with COVID-19. At the AGTA show, Michael Traurig (Jayson Traurig Bros. of Australia—Phoenix, Arizona, and Sydney, Australia) told us about his hospitalization for COVID-19 in Phoenix beginning in June 2020. "I went into shutdown," he said. "Heart, lungs, kidneys. I was on dialysis. I was on a respirator. I became diabetic."

Doctors put him on a life-support machine that acts as the heart and lungs outside the body. He said that up until that time, few people in the world with COVID-19 had survived the procedure. He was taken off and put back on the machine several times and visited by top doctors in the Phoenix area. "The ICU nurses called me magic because they put you on the machine to die basically," he said. After 30 days, he was sent to a rehab facility in order to free the hospital bed. "I coded one more time in rehab and they jumpstarted me," he said. "A few days later, everything started working again." Today he is no longer diabetic.

At a second Phoenix hospital, where Traurig underwent surgery to remove the dialysis tubes, the staff had heard his story. "The head OR nurse looked at me and said, 'Oh, you're the one.' I was the hope shot for the nursing staff because nobody else had lived through it."

Traurig went home in September, more than two months after he was admitted. He had lost 70 pounds. "I couldn't stand up," he said. "I was jelly. I had to learn to walk. So I got a dog. And she walked me every day, twice a day."

"It's worth sharing my story if I can get even one person to put on a mask," he said.

Before contracting COVID-19, Traurig had a successful show in February 2020. But a month later, 85% of the sales hadn't been paid for, and he got the stock back. "Because everybody's business shut down," he said. He had used most of his funds to buy stock for Tucson because his business had changed in recent years due to changes in the industry and in the company. "I ended up mostly broke," he said.

After his hospital stay, people began calling him and finding out what had happened. "They started throwing me a few bones," he said. "And I started getting some business. They've been kind." When he made his first purchase in months, a large batch of loose opals from a supplier in

Figure 20. The large rough gray spinel before (left) and after being sawn (right) because of a fissure in the rough. Not pictured is an additional small chipped-off piece weighing 3.32 ct, leaving open the possibility of a future third spinel sister. Photos courtesy of David Nassi.

Figure 21. A selection of opals at Jayson Traurig Bros. of Australia's booth at the AGTA show. Photo by Erin Hogarth.

Australia, they let him pay it off over time. "There's never credit given normally when you buy opals," he said. They sent him more shortly before this year's show. He had several displays of opal at the booth (figure 21) but said he had not yet been able to buy enough stock to make a living. "But it's okay," he said. "You realize who the friends are."

Figure 22. Cover of the Summer 1988 issue of G&G *featuring the 26 ct "Jason" boulder opal, which has since been sold. Photo © Harold & Erica Van Pelt; opal courtesy of Jayson Traurig Bros. Pty. Ltd.*

Traurig's father, John, and uncle, Tom, began working in the opal business in 1969. Jayson Traurig Bros. was the only non–North American member when AGTA was founded in 1981, the same year Michael bought into the business (Jayson = J's son). In 1988, one of their boulder opals—which was later sold—was featured on the cover of *G&G*'s Summer issue (figure 22).

Traurig and his father are both red-green colorblind. He said they had both learned to compensate and that lighting makes a difference. During GIA's Gem Identification course in the '70s, John was given permission to ask what color a stone was because he couldn't identify alexandrite's color change. "I remember him coming home and laughing," Traurig said. "During the exam he never asked the question. He said, 'If I had to ask, I knew it was alexandrite.'"

Traurig spoke about how the opal business and his business have changed in the last 20 years. More dealers have joined the industry, and older miners have stopped mining. He noted that there are far fewer mining concerns today. In the '80s and '90s, they used to have three people to work the booth. "There were people who were trying to always be next to us because of the overflow. We were the draw. We stopped being the draw. It's okay."

Traurig also visited Tucson last April. "It was my tour of 'I'm alive, I'm here, and I can walk,'" he said. "People were really welcoming and wonderful."

Erin Hogarth

Conversation with True Blue Opals and Gems. At the AGTA show, we spoke with Natassa Patel, who along with her mother, Salma, owns and operates True Blue Opals and Gems (Tucson and Gold Coast, Queensland, Australia). While they typically specialize in black opal from Lightning Ridge (figure 23), the closure of Australia's state bor-

Figure 23. A 13.12 ct black opal from Lightning Ridge, 19.7 × 14.4 × 7 mm. Photo by Robert Weldon; courtesy of True Blue Opals and Gems Inc.

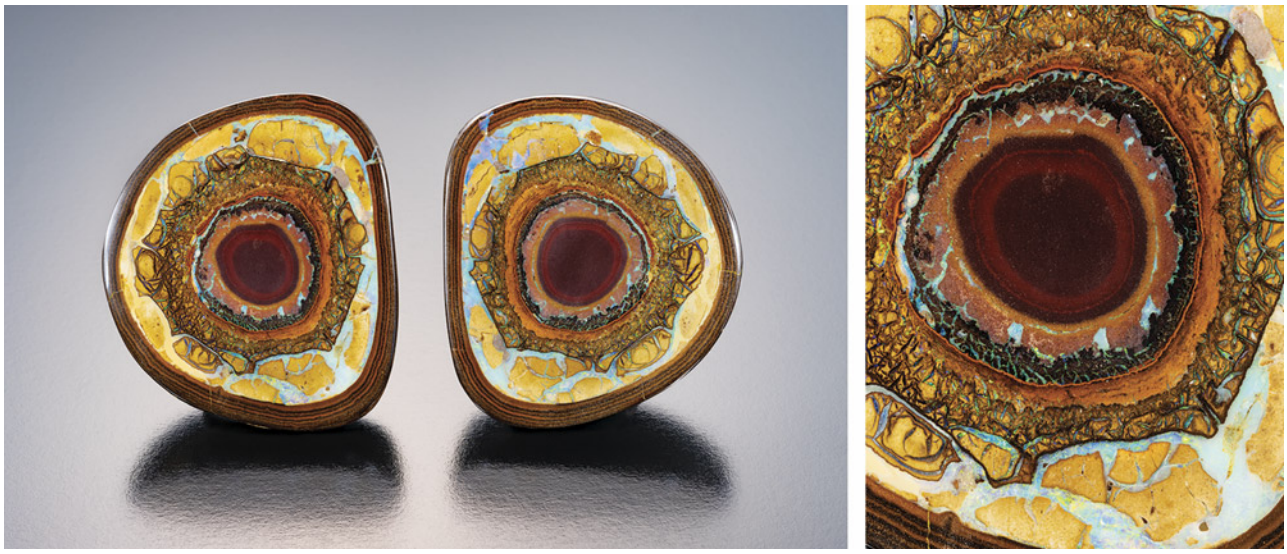

Figure 24. A Yowah boulder opal or "Yowah nut" weighing 312.6 ct and measuring 74.6 × 67.3 × 22.6 mm (detail on the right). Photo by Robert Weldon; courtesy of True Blue Opals and Gems Inc.

ders during the pandemic prevented them from traveling there. Canceled trade shows and the inability to see clients face-to-face also limited business, but their online sales increased and they began sourcing from Queensland's Yowah and Koroit boulder opal fields. The majority of the stones at the booth were Yowah and Koroit boulder opal, with only one showcase of black opal.

"Circumstance made us specialize in Yowah and Koroit," Natassa said. "I think my mom has taught me that, to make the opportunity. We could have just left it at home because everybody's chasing black opal, but we didn't. We believe in it."

According to Natassa, buyers don't want "generic" stones anymore, and opal is "very non-generic." She said boulder opal (figures 24 and 25) is "like a bouquet of flowers" with its immense variety of colors and patterns. "I think it appeals to the uniqueness we all want to feel, with our imaginations running wild in trying to see landscapes and faces and paintings that are so prevalent in the patterns of boulder opals," she said.

Natassa said that despite the common belief that anticipating customer demand is the way to success, it's important to her and her mother "to stay true to ourselves and sell what we like." She added that if you focus on persuading people by sharing knowledge rather than on trends, you can create a trend. "I like to pave the road. I don't like to follow: I want to go first."

When True Blue began exhibiting in Tucson in the early 2000s, they often had to educate customers on black opal. Natassa estimated that the number of opal dealers at the

Figure 25. Boulder opals: "Rainbow Jungle" (left), 73.53 ct and 52 × 25 × 7 mm, and "Red Lantern" (right), 188 ct and 54.8 × 41.4 × 22.0 mm. Photos by Robert Weldon; courtesy of True Blue Opals and Gems Inc.

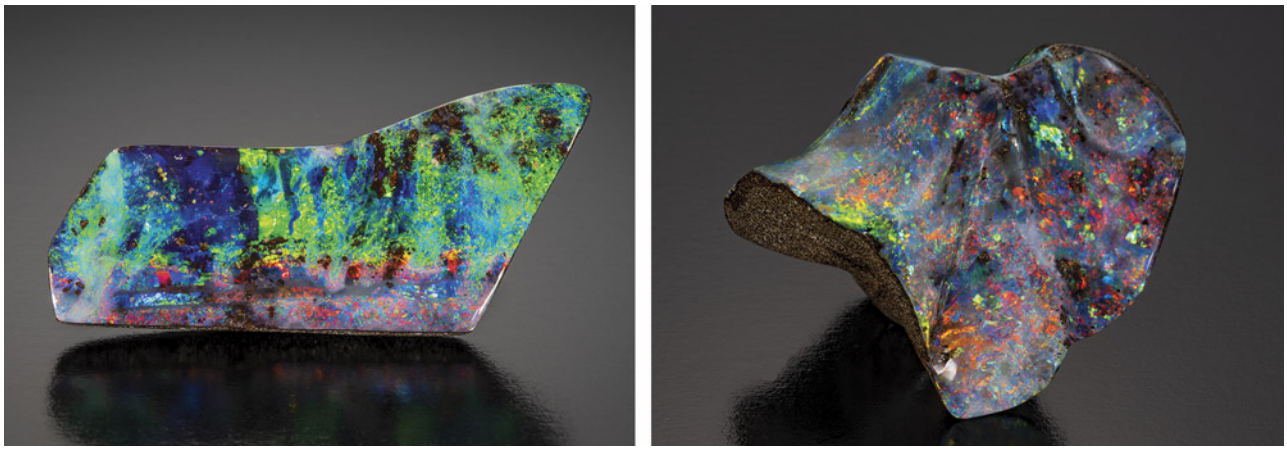

Tucson shows has increased perhaps tenfold since, which has increased customer understanding of the gem. Boulder opal has become more popular, but they still have to inform people about Yowah and Koroit boulder opal.

"No matter if we sell one stone or a hundred stones, the focus, for me, should still be the same," Natassa said. "To bring something new, to educate people. What's the point of doing all this, if people still misunderstand opal or they don't see the value in it?"

Natassa noted that while many more designers use opal now, customers are still coming to terms with pricing. She attributes this to a lack of understanding of opal mining: The cost of opal is difficult to standardize because there are too many variables in its mining. "If you find one pocket in five years, and you've spent half a million dollars in mining, then that parcel is half a million plus," she said. "And sometimes there's a drought—no water to wash the dirt to see if there's opal trace."

True Blue celebrated their 20th anniversary last year, but Salma's passion for opal goes back further. After the Patels moved from Vanuatu to the Gold Coast in 1988, Salma was free to wander the shops while Natassa and her siblings were in school. She became fascinated with the black opals that were so different from the familiar gold and diamonds. After learning they were from Lightning Ridge, she traveled there with an opal dealer friend in the early 1990s. "I think it's something that she was called to," Natassa said. "I think what happened to her was what happened to me."

In 1995, Salma bought a small store on the Gold Coast, initially focusing on small parcels. Natassa helped her mother on nights and weekends while attending university, although she wasn't interested in gemstones at first. "I'm assertive, but I'm not aggressive," she said. "I didn't know how to push them."

Salma's first visit to Tucson was in 1995, and a few years later she exhibited at the Globex Gem and Mineral Show (now held at the Red Lion Inn). In 2002, after Natassa finished her master's degree, she went to live with family in New Jersey and look for a job in finance. Salma asked her to help at that year's show, but Natassa was still reluctant about selling. Salma promised she only had to stand behind the booth and rely on set prices. Natassa made a good salary based on commission over the two-week show. "It took her a while, but she convinced me to join the business," she said.

Soon Natassa started going to the opal fields with Salma and doing the smaller trade shows in Tucson. "I'm a good listener, I think," Natassa said. "And I believe I'm a good observer. So I learned quickly. It just kind of started rolling off my tongue eventually."

Since then, Natassa has only missed the Tucson shows twice, once while completing the Accredited Gemologist program at the Asian Institute of Gemological Sciences (AIGS) in Bangkok. "I felt that opals weren't in the mainstream," she said. "There was so much misinformation." She wanted to be able to explain opal in gemology terms "because it's this mysterious stone to most people." She found she loved gemology and being in the lab. "I love the microscope," she said. "It's pretty cool to see opals under microscopes."

True Blue's first AGTA show was in Las Vegas in 2005. Natassa got a call on opening day offering them the booth of an exhibitor who hadn't showed. "Back then we didn't have any money," she said. "We used to put stuff on credit cards." The cost of the booth was $7,000—the cost of the entire trip. "I'm thinking, how are we going to do these two booths? Is there enough stock to spread around? Plus seven grand. Plus it's already opening. Then we said okay—we'll just do it." Their first big sale that day wasn't an opal but a giant clam (*Tridacna gigas*) pearl they'd bought a few days prior, for which another exhibitor paid $10,000 cash. "So we covered our booth," Natassa said.

"We're blessed, because there have been difficult times for us personally and financially over the last 28 years," Natassa said. "For my mum, even more so because she was on her own before me. All these things I've learned from her, day in, day out."

Natassa recalled that in the early years some customers, expecting a male dealer, would ask where the owner was. "They just assumed that we weren't. A client would say, 'Go ask your boss if I can get a better deal on this.' I'd say, 'Well, I am the boss, and this is the price.' It's easier now."

Natassa and Salma try to find niches in the local market, such as opal beads (figure 26), which they began selling in the late 2000s. The beads use the precious part of the opal as well as the potch. "The really dark potch is jet black," Natassa said. "If you can wear a black spinel strand, you can wear a potch opal strand."

Natassa revealed that she never intended to stay in the opal business this long. "But I think it's God's plan for me," she said. "I don't think I could do anything else." She hopes

Figure 26. Faceted beads of black opal from Lightning Ridge totaling 45.15 carats. Each bead is 4 × 4 × 3 mm. Courtesy of True Blue Opals and Gems Inc.

Figure 27. Salma and Natassa Patel of True Blue Opals and Gems at their AGTA show booth. Photo by Erin Hogarth.

someone in the family will take over and operate True Blue when she and her mother no longer can.

The Patels (figure 27) have been discussing what to do when they return to Australia. They have considered splitting their stock fifty-fifty between black and boulder opal. "Black will always be king of all opal," Natassa said. "That's our favorite. We grew up on black opal, so we can't help ourselves."

Erin Hogarth

Washington Jade update. At the AGTA show, Rod and Nathaniel Cook of Washington Jade (Edmonds, Washington) told us about shifting their focus to cat's-eye blue and bluish green nephrite jade (figure 28). (We first spoke with them in 2019—see Spring 2019 GNI, pp. 124–125.) They initially intended to concentrate on the mid-tier jewelry market, but the non-chatoyant nephrite was not valuable enough to be cost-effective. About two years ago, they saw that two small pieces of chatoyant nephrite were drawing the most attention. This year, they cut 100 chatoyant stones from rough.

"It was a matter of finding something unique to our deposit that was a high enough grade of material that it would have broad market appeal," Nathaniel said. "People seem to really like not necessarily the really sharp eyes, but the really strong eyes, even if it's sort of a broad eye that moves across the stone. They're very charismatic and sort of bold."

Rod said they find better material each year. "The blue sort of validated the whole operation," he said. "We have pretty good demand emerging for the rough. Partially because around the world, supplies are down. We hear rumors that Siberia is not producing like it used to, that the surface material is pretty much gone—and going underground is to be avoided." The host material is also selling very well for high-end lapidary work.

Nathaniel has been cutting the rough since 2019. Orienting it for cutting can be tricky, he said, but understanding how it forms has shown him how to orient and process it. He first locates the line between the two dark sides of the nephrite (the directions where the eye moves back and forth), which he calls the "axis of chatoyance." Then he starts slabbing the stone parallel to this axis. Some adjustment is required within the slabs to ensure correct orientation of the finished stone. To cut cabochons, he pays attention to the direction of the cat's-eye and cuts calibrated sizes and shapes either parallel or perpendicular to that alignment.

Nathaniel explained that the material requires slightly different tools than most lapidaries use because of its variable hardness: The ends of the axis of chatoyance are very hard, but around it is much softer. After some trial and error, he began using inflatable sanding drums for much of the shaping process because they are gentler.

Processing the material also informs how they harvest it with their low-impact mining methods. "Nathaniel is integrating all the way from harvesting to finished stones," Rod said. "With that information, we can go up there and selectively harvest. It's like noninvasive surgery. We can essentially find the critical stuff."

According to Rod, many carvers are accustomed to materials like quartz, which is very hard and uniform in all di-

Figure 28. A chatoyant bluish green nephrite ring: 3.14 ct marquise cabochon (10.92 × 7.65 mm), 0.1 carats of round diamonds, and 14K yellow gold. Photo courtesy of Washington Jade.

rections. He said educating the market on chatoyant nephrite will take a few years. "We've realized in this industry it's not something you can throw money at and make it happen. It's pretty much listening to customer wants."

Rod showed us a piece of rough with a striking banded chatoyant pattern that resembles New Zealand's rarest, most prized jade. The New Zealand material has cultural significance and is often called *pīpīwharauroa* jade because its pattern is reminiscent of the breast feathers of the pīpīwharauroa (shining bronze cuckoo) bird. The claim contains a lot of the material, but they have not yet processed much of it. So far most of what they have found is unstable due to fractures, but they are looking into stabilization and may still find larger quantities of stable material. Rod expects to have more at next year's show.

"Our strategy is organic growth over the next few years using AGTA as the high end, and it appears that's enough to get people showing up and buying rough," he said. "So stay tuned."

[Editor's note: The term "cat's-eye jade" is a trade term and a misnomer. Although this material falls within the mineral series that constitutes nephrite jade, nephrite is characterized by its fibrous, interlocking felted structure, which gives it the toughness that is so important to jade. The cat's-eye material is made up of parallel fibers, which is why it has an eye. However, this structure does not possess the toughness required for a jade. The GIA laboratory would refer to this material as "cat's-eye actinolite."]

Erin Hogarth

Many faces of wavellite. A well-known collector mineral, wavellite ($Al_3(PO_4)_2(OH)_3 \cdot 5H_2O$), is named after its discoverer, British surgeon Dr. William Wavell. Wavellite mineral specimens seen on the market often occur as botryoidal aggregates. The crystal clusters are usually spherical in appearance. When the spheres are broken open, the cross sections show their signature radiating pattern formed by acicular-shaped crystals (figure 29).

Figure 29. This specimen of wavellite in matrix shows the mineral's characteristic radiating pattern. Photo by GIA.

Wavellite is not a gem material renowned for its brilliance or breathtaking colors, but its unique appearance does trigger curiosity and creativity. At the AGTA show, James Carpenter of Unconventional Lapidarist (Hot Springs, Arkansas) showed the authors a variety of wavellite cabochons and slabs and shared how he stabilizes the material for jewelry use.

All wavellite carried by Unconventional Lapidarist is sourced from Arkansas, one of the well-known sources for this gem. When used in jewelry, wavellite must be stabilized (figure 30) to make the piece durable. This is due to both the relatively low hardness of the material (3.5–4) and

Figure 30. Left to right: Wavellite rough before treatment, stabilized rough, a slab of stabilized rough with all the waste host rock trimmed off, and two pieces of polished stabilized wavellite cabochons (89 and 405 ct, respectively). Photo by Tao Hsu; courtesy of Unconventional Lapidarist.

Figure 31. This wavellite cabochon is of high quality. Some of the spheres were sliced open to show the radiating pattern, while others were left untouched. Wrapped in gold-plated wires, the cabochon weighs 150 ct, with a blue apatite mounted at the top. Photo by Tao Hsu; courtesy of Unconventional Lapidarist.

its occurrence in the host rock. Arkansas wavellite formed in veins cementing together brecciated sandstone/chert host rock. Therefore, the majority of wavellite specimens occur as very thin slabs or small spherical bodies.

Carpenter noted that 99% of the production needs stabilization for the materials to withstand further processing. He developed his own resin for this stabilization process. This resin is hydrophobic, meaning it is water resistant, and environmentally and biologically friendly. The material is impregnated with this resin in a vacuum under very high pressure and then cured and sliced. Slicing helps reveal where the wavellite is embedded in the host rock. Host rock that bears no wavellite is trimmed off before further polishing. Restabilization is sometimes necessary, especially when cabochons are to be made, to ensure the finished product is durable when set in jewelry. The yield of this process is only about 15%, with 85% waste.

Stabilized wavellite can then be polished to cabochons (figure 31) and mounted in jewelry, with high-quality material revealing an attractive botryoidal structure of rounded segments and/or radiating patterns with beautiful colors. The slab can also be utilized without much polishing (figure 32, left). The latter option works perfectly for stones showing the botryoidal exterior. When one turns this type of cabochon on its side, some of the broken spheres clearly show the radiating pattern, adding appeal to the jewelry piece (figure 32, right). Wavellite can be collected as mineral specimens or used as decor and jewelry material.

Tao Hsu and Lisa Kennedy

CUTS AND CUTTING

Stephen M. Avery: Celebrating half a century in gem cutting. Approaching his 50th anniversary in the business, Stephen M. Avery (Lakewood, Colorado) reflected on his journey to becoming an award-winning lapidary artist, detailing his signature cuts and gem sets and offering advice to up-and-coming gemstone cutters. Since starting his career at the age of 17, Avery has accumulated a remarkable amount of cutting experience. But even after all this time, the part he enjoys most is continuing to find new challenges.

Figure 32. Left: This piece of wavellite slab kept the original look of the rock with its botryoidal habit. Right: The view from the side reveals the radiating pattern on the cross sections of sliced-open spheres. Photos by Tao Hsu; courtesy of Unconventional Lapidarist.

Figure 33. With names like "Flaming Comet" and "It's a Zoisite Party," Avery's gem sets have enchanted for decades. This three-piece set consists of a 6.22 ct golden tourmaline flanked by two aquamarines, 5.14 carats total. Photo by Sara Rey; courtesy of Stephen M. Avery.

Figure 34. When skill and experimentation combine, something as brilliant as Avery's signature Triopp cut is born. This stunning example is a 9.79 ct chrome tourmaline measuring 14.5 mm. Photo by Sara Rey; courtesy of Stephen M. Avery.

Avery was not born into the business and began his career by enrolling in the American School of Diamond Cutting. He learned the foundations of diamond cutting from the prestigious diamond cutter Leonard Ludel. A few years later, he found himself working for Stradley Lapidary in Colorado, where he made the instinctual move from diamonds to colored stones. He describes this as a moment of clarity, as he was bored with the lack of creativity in cutting standard round brilliant diamonds. Avery noted that at the beginning of his career in the late 1970s, he was "bringing something unknown to the colored stones business: diamond cutting quality to colored gemstones."

Avery started to create gem sets—suites of intricately cut gemstones that fit perfectly together (figure 33)—about 40 years ago. He describes them as something that started experimentally and has exploded in popularity. When it comes to creating his gem sets and sourcing the right stones, he has learned that patience pays off. He explained that some colors will negatively impact other colors, and some colors when paired will read neutral. The most gratifying outcome occurs when all the gemstones used look better when they're together.

Throughout his career, Avery has fashioned numerous signature cuts. His very first signature cut was a Portuguese-cut trilliant, which took three years to design. Another early signature cut was the Triopp cut (figure 34), a triangular cut born out of anger when the perfect trillion preform had an inclusion in the corner. He ground it out, only to discover a completely new concept in faceting. He then went on to create the OVOB cut, an oval opposed bar cut, and most recently the Diamondback, a recreation of the checkerboard cut to fit elongated pieces of gem rough (figure 35).

His exquisite attention to detail and understanding of color and light enable Avery to cut award-winning, one-of-a-kind faceted gemstones. The majority of his pieces require designers to create custom settings. He has relationships with several skillful designers who allow him to share his

Figure 35. Avery's Diamondback cut is a blessing to stones longer than 50 mm. This 73.22 ct tourmaline measures 11.1 × 79.3 mm. Photo by Sara Rey; courtesy of Stephen M. Avery.

Figure 36. 2019 AGTA Spectrum Award–winning earrings designed by Adam Neeley with a pair of indicolite tourmalines cut by Stephen Avery, weighing 41.45 carats total. Other stones are tsavorite garnets (3.34 carats total) and diamonds (2.42 carats total) set in purple titanium, 14K white gold, and green VeraGold. Photo by Sara Rey; courtesy of Stephen M. Avery.

vision for the piece and then take it from there. His talent, in combination with the talent of these designers, has earned him many "Best Of" titles in the AGTA Spectrum Awards. Avery cut a matching pair of Afghanistan indicolite tourmalines that were 2018 AGTA Cutting Edge Awards first-place winners in Pairs and Suites. The following year, those same tourmalines won yet again in the Spectrum Awards, in earrings designed by Adam Neeley (figure 36).

Avery shared his advice for emerging gem cutters: "Learn all the techniques, then challenge the rules. If you want to do something and you don't have the technique, you're going to have to invent it. And that's okay—it just hasn't been done because you didn't do it yet."

To see an interview with Avery, visit www.gia.edu/gems-gemology/spring-2022-gemnews-stephen-avery.

Lisa Kennedy and Tao Hsu

Skull carved of meteorite. At the AGTA show, Nature's Geometry (Tucson) had on display a life-sized skull carved of meteorite (figure 37). The skull, "Gaia," was a collaboration between Lee Downey of Artifactual Studios (Tucson and Bali, Indonesia) and Balinese artist Ida Bagus Alit. It was carved from two pieces of the Gibeon iron meteorite, which landed in prehistoric times after bursting into pieces upon coming through the atmosphere. Its fragments are scattered over a large area in Namibia. Based on radiometric dating, the meteorite is estimated to be around four billion years old. Long before Westerners documented it in the early 1800s, the Nama people used pieces of it as weapons and tools.

Downey and Alit worked on the carving from March 2015 to January 2020 in the workshop Downey shares with Ratu Pedanda Manuaba, a high priest of Bali. In Balinese culture, meteorites are seen as powerful, and meteorite iron is used to make traditional *keris* (daggers) for ceremonial use.

The Gibeon meteorite's makeup is about 90% iron and 8% nickel, with small amounts of cobalt and phosphorus. Downey said the material is somewhat soft and sticky. The critical aspects were maintaining the proportions and watching for potential imperfections in the material. "Cracks and pockets of odd space junk can pop up," he said. "Luckily Gaia was basically flawless. She was difficult but forgiving."

The work was done using hacksaws, steel grinders, and rotary carving setups. Protective gear was required when using cutting burrs because the tiny shards coming off the skull were "like little razor blades flying around." Based on models of the human skull, a sphere-shaped piece of the meteorite was carved for the upper cranium and a block for the jaw, which is articulated and removable. Roughly 159 lbs. (72 kg) of material were cut and ground away to form the 39 lb. (18 kg) skull. After carving, the skull was fully polished to a chrome-like finish.

The final step was etching with a weak acid to reveal the meteorite's fine octahedrite structure, visible in the pattern on the skull's surface. The pattern, known as a Widmanstätten pattern or Thomson structure, is composed of interwoven bands of kamacite and taenite (iron-nickel alloys) and develops over millions of years of very slow cooling. It is revealed only through cutting, polishing, and etching.

The brown line on top of the skull is an inclusion of tridymite, a silica polymorph. Tridymite is also found on Earth, the moon, and Mars, and in planet-forming disks of dust and gas around stars.

Downey has previously described the human skull as "undeniably sure to register emotions in all of us. It has all the fear of death, the reminder of being alive, and the possibility of something greater in store…out there in the mysterious beyond."

Figure 37. A skull carved from the Gibeon meteorite, which landed in Namibia in prehistoric times. The brown line is a tridymite inclusion. Exhibited by Nature's Geometry at the 2022 AGTA show in Tucson. Photo by Robert Weldon; courtesy of Lee Downey.

"The intense gravity of this extraterrestrial metal is itself a mystery of life," he said. "Four billion years old and counting, the long travel to arrive on Earth, the rare beauty of the crystal patterns that can only form in the vacuum of space. The symmetry of the entire tale is beyond human comprehension."

Erin Hogarth

Puzzle-like gemstone designs. At the AGTA show, Rare Earth Mining Co. (Trumbull, Connecticut) offered a vast array of fine and unusual gem materials unavailable anywhere else in the trade. Among the opalized wood, Tiffany stone, honeycomb petrified wood, and many other varieties was one of the most expansive Steve Walters collections seen at Tucson (figure 38).

While Walters himself did not attend the show this year, Rare Earth Mining Co. was eager to detail his work for us. A master gemstone carver specializing in one-of-a-kind gemstone designs in Utah, Walters has been in the business for more than 50 years. He creates his carvings for jewelry designers, to help them achieve a unique look.

Walters's designs feature a perfect mix of traditional and exotic gemstones, expertly paired and carved to create a dramatic shape and color story. All done by hand, Walters uses titanium to bridge together and inlay the different gemstones.

Among the wide variety of gemstones used in Walters's carvings were onyx; chrysocolla; tourmalinated and rutilated quartz; amethyst, citrine, and ametrine with striking color zones; rock crystal quartz backed with onyx and gold foil; lapis lazuli; various agates; Australian and pink opals;

Figure 38. Trays of Steve Walters's unique gemstone carvings displayed at the 2022 AGTA show in Tucson. Photo by Tao Hsu; courtesy of Rare Earth Mining Co.

Figure 39. Left: This citrine "flame" top is connected to a chrysoprase "main body." Next to the chrysoprase is a portion made of a black chalcedony backing, covered by 24K gold leaf and capped by rock crystal quartz. The piece is completed with a freeform ametrine. Right: All pieces have a mother-of-pearl backing with Steve Walters's signature. Photos by Kevin Schumacher.

and meteorite. Every piece is finished with a mother-of-pearl backing with his signature (figure 39), ready to be set into a showstopping piece of jewelry.

Lisa Kennedy and Tao Hsu

JEWELRY DESIGN

One-of-a-kind designs from Zoltan David. 2022 marks the 42nd year in the industry for iconic jewelry designer Zoltan David (figure 40). At the AGTA show, the authors had an opportunity to converse with David about his passion, career, and inspired jewelry creations.

Curiosity and the drive to create led David to his career in metalsmithing. For David, creativity can be furthered by an in-depth understanding of the materials and skillful maneuvers. While modern technology allows for efficient jewelry sketching and design, the lack of knowledge about metals—base or precious—limits the execution of a great design or even the creativity of the design itself. David's jewelry pieces reflect this philosophy. Each of his creations is a three-dimensional "architecture," which must be viewed from multiple directions to fully appreciate its beauty.

The "Time" pendant (figure 41) is David's most recent award-winning design. In 2020, this piece won second place in the Business/Day Wear category of the AGTA Spectrum Awards. This pendant features a 19.54 ct fantasy-cut citrine as the center stone, surrounded by eight suspended metal elements forming two circles. The metal elements are made of iridescent blue and purple steel with

Figure 40. Zoltan David working at the bench in his studio, located in his store in Austin, Texas. Photo by Patti David.

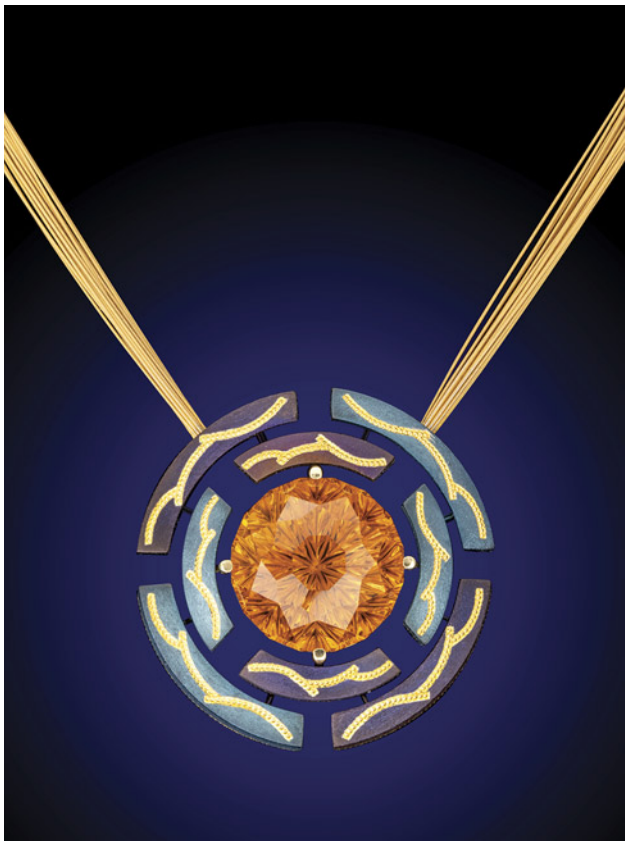

Figure 41. Exotic metals such as the iridescent blue and purple steel in the "Time" pendant are Zoltan David's signature. 24K gold inlay is also a Zoltan David distinction. This piece features a 19.54 ct citrine. Photo by Robert Weldon; courtesy of Zoltan David.

Figure 42. Zoltan David's "Mirror Mirror" pendant combines multiple innovative techniques and materials. The piece features platinum inlays in the mother-of-pearl surrounding the pink opal center stone, highly polished surgical steel as the base frame (left), a leaf wreath made of green gold wrapping around the outer edge of the whole piece, and diamonds mounted in the steel base (right). Photos by Robert Weldon; courtesy of Zoltan David.

24K textured yellow gold inlays, a signature patented technique invented by David. In addition, all these metal elements are suspended and well connected with each other. David wanted to create a sense of rotation with this design: All elements rotate around the center of the universe, trying to find the perfect balance.

More than four decades of knowledge building and practice have made David's jewelry pieces the perfect combination of metal art and architectural construction. The "Mirror Mirror" pendant (figure 42) represents the continuous exploration and technique refinement by the master designer. To fully understand this piece, one needs to carry out a jewelry "anatomy." Starting from the center of the pendant, an elongated oval pink opal is encased by a cut piece of mother-of-pearl, which was carved and inlaid with beaded pure platinum. The mother-of-pearl is surrounded by polished surgical steel and inlaid with 24K engraved and shaped rose gold. All of these elements are nestled in a framework of green gold leaves. From the side view, diamonds mounted in the surgical steel layer are exposed through the space between the green gold leaves (figure 42, right).

Although renowned for his metalsmithing, David is also drawn to spectacular colored stones. The "Ruby Flight" ring (figure 43), a piece from the Duchess collection, features a 2.45 ct Burmese ruby. The ruby is held by 18K gold prongs between two platinum wings inlaid with 24K gold. The engraved and shaped gold inlays form patterns on both sides of the wings. The interior walls of the wings are set with melee diamonds in between the gold inlays, while the exterior walls are set with melee rubies along the inlaid lines. More than 300 melee rubies also decorate the edges of the wings. The shank of the ring is also one of a kind, made up of three components: a melee diamond stud band sandwiched by the bottom of the two wings.

Figure 43. The "Ruby Flight" ring is representative of Zoltan David's stone selection and construction of a complex jewelry piece. Photo by Robert Weldon; courtesy of Zoltan David.

From the start, David has been an eager learner and has never stopped his exploration of the metalsmith profession. He is involved in all aspects of his business: designing, crafting, and trading each one of his creations. As David said, he would like to keep traveling along this journey by continuously surpassing himself.

To see interviews with David, visit www.gia.edu/gems-gemology/spring-2022-gemnews-zoltan-david.

Tao Hsu and Lisa Kennedy

Old techniques reimagined: *Maki-e* pearls. At the AGTA show, Eliko Pearl (New York) exhibited a series of unusual cultured pearls, many of which were worked after culturing to create unique pieces of art. Among these, *maki-e* pearls caught the authors' attention.

Maki-e is an ancient Japanese lacquer technique that translates to "sprinkled picture" and is said to have originated more than 1,200 years ago. A fine brush is used to paint a design with lacquer, which is then sprinkled with gold powder before the lacquer dries. More lacquer may then be painted again over the design and polished. For centuries, the meticulous technique has been used to decorate screens, *inrō* (a type of small case worn in traditional Japanese culture; figure 44), Japanese letter boxes, and other vessels, and it has now been adapted for use on pearls.

Figure 44. An inrō *dating back to eighteenth-century Japan with gold* maki-e *and mother-of-pearl inlay. Courtesy of Getty Images.*

A representative from Eliko Pearl explained that each pearl is decorated by hand using a combination of *urushi* lacquer and 24K gold powder overlay, with abalone shell inlay (figure 45). The natural lacquer is derived from the sap of the urushi tree, which is native to Japan, China, Vietnam, and Southeast Asia. Sap can be harvested from a single tree for 14 to 15 years, during which the tree only yields about 200 grams of material. The sap also goes through a lengthy treatment process before it can be used as a lacquer. After application, the urushi lacquer must cure in a high-humidity environment (70–90%) in a series of thin layers. The time-consuming and laborious process of harvesting, processing, and applying the lacquer on pearls makes urushi lacquer a costly material, but the finished maki-e pearl is a treasured piece of art.

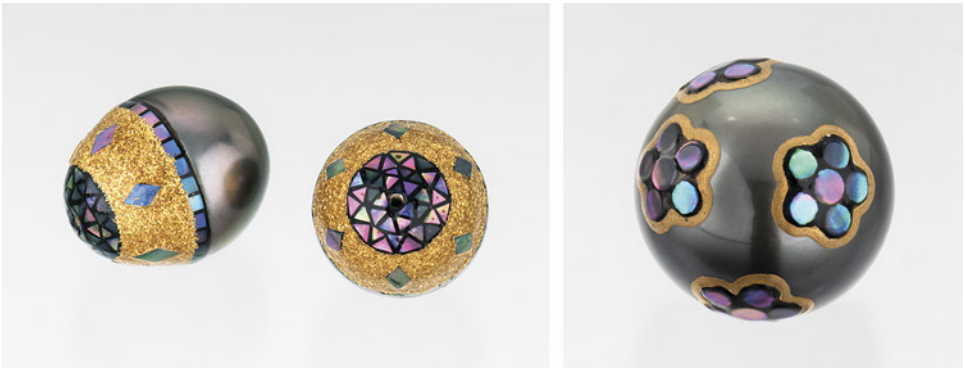

Figure 45. A pair of Tahitian pearls decorated with 24K gold maki-e and abalone shell inlay (left). A single near-round Tahitian pearl, decorated by the same technique in a flower motif (right). Photos by Emily Lane; courtesy of Eliko Pearl.

The décor adorns Tahitian pearls predominantly and can be found on matching pairs as well as single pieces. Prices vary from piece to piece based on the detail of the design and the size and shape of the pearl, with the most expensive shape being round (figure 46).

Lisa Kennedy and Tao Hsu

Blue sapphire *Lord of the Rings* pendant. At the AGTA show, Jeffrey Bilgore of New York exhibited a sapphire, diamond, and platinum pendant (figure 47) inspired by *The Lord of the Rings*. From initial inspiration to delivery of the just-finished pendant midweek at the show, the piece was 15 years in the making.

"I read it in high school," Bilgore said of the beloved trilogy. "I read it again in college. Then I read it to my son when he was little, and when he was older he read it to me."

The 19.30 ct unheated light blue Sri Lankan sapphire briolette rotates within the platinum setting, accented by 177 round Flawless to VVS round brilliant diamonds (0.86 carats total). The pendant is modeled after the Phial (vial) of Galadriel, which the elf queen Lady Galadriel gives to hobbit Frodo Baggins for light and protection during his journey to Mordor. The vial contains water from her fountain, which holds the light and power of the elves' cherished star Eärendil.

"The Star of Eärendil is the North Star at night and the star you see in the dawn," Bilgore said. "It gives you hope in the darkness and brings you strength." He said the pendant

Figure 46. Trays of Tahitian maki-e pearls offered by Eliko Pearl at the 2022 AGTA show in Tucson. Available in a range of sizes in matching pairs and single pieces. Photo by Lisa Kennedy; courtesy of Eliko Pearl.

Figure 47. Platinum pendant with a 19.30 ct unheated light blue Sri Lankan sapphire briolette and 177 round brilliant diamonds, 0.86 carats total. Photo by Robert Weldon; courtesy of Jeffrey Bilgore.

"symbolizes all the good energies of hope and faith that add light to the world and protect those that it shines on."

The concept for the pendant came to Bilgore when he bought a diamond briolette in 2004, a year after establishing his own business. Prior to that, he spent 16 years as the primary gem buyer for Oscar Heyman. He began sketching the design but then sold the diamond. Over the next decade, he continued to refine the design. He eventually acquired a pair of light blue sapphires and began developing the piece with a jeweler about five months before the AGTA show.

"*The Lord of the Rings* is a story about our world, the power of faith, and good vs. evil," Bilgore said after the show. "Today, with all that is going on in Ukraine, it seems even more meaningful. The story shows how wars destroy everything and put groups against groups for no good reason. That only trust and faith in each other and in the positive powers of love and respect can conquer all." He added that the story—with its elves, dwarves, hobbits, and other beings—is also about diversity. "No matter your size, shape, color, or type, everyone has value and strengths."

"Others have attempted to replicate the Phial of Galadriel, but not quite like this," he said. "If you have anything going on in your life, put it around your neck and you'll be protected. You'll get through it."

Erin Hogarth

Figure 48. Sapphire ring designed by Rachel Chalchinsky: 5.18 ct heated mixed-cut pink sapphire (11.0 × 9.4 mm), 1.24 carats of diamonds, 0.36 carats of no-heat padparadscha sapphires, and 0.65 carats of orange sapphires, set in 18K rose gold. Photo by Robert Weldon; courtesy of Color Source Gems.

A pink sapphire ring with a message. At the AGTA show, Rachel Chalchinsky (Color Source Gems, New York) showed us a triple-halo ring (figure 48) designed to commemorate surviving breast cancer. "It's hard to live with it and go on," she said, "but once you do, you feel powerful." After her diagnosis in August 2018 and finishing chemotherapy in January 2019, she wanted to "replace" the tumor with "something good and positive."

Chalchinsky had three requirements for the center stone: that it be pink, for breast cancer awareness; the same size as the tumor (11 mm); and heated, to symbolize the radiation treatments she received in March 2019. After nearly three years of searching, she found a 5.18 ct heated mixed-cut pink sapphire measuring 11.0 × 9.4 mm.

"I used to have very big curly red hair, and I wanted to represent that in the ring," she said. "Now I have grayish hair. So I put orange sapphire around the outside. Then on the inside, I used white diamonds to represent gray hair. And on the side of the ring, I used the breast cancer ribbon. I had that graduated to fit on the sides of the band and set it all in rose gold."

When people admire the ring, Chalchinsky often tells them the story behind it "to bring awareness that people need to get their diagnostic tests and not wait." She noted that delaying or avoiding her annual mammogram and ultrasound could have resulted in a more serious prognosis. Chalchinsky said her story compels people to share their experiences with cancer. "It becomes almost like a bonding because we've all been through these emotional journeys."

Chalchinsky also uses Instagram to share the message. During Breast Cancer Awareness Month in October, she posts photos of pink stones, sometimes in pairs, asking people to get checked and make sure their loved ones do so as well. "I'll say, 'Ask your mom. Ask your loved ones. Nag them—take them by the hand to go with them.'"

Chalchinsky recognizes she is fortunate to have had excellent healthcare and supportive family and friends—and that many women undergo more invasive surgery or have a worse outcome. In 2021, Color Source Gems donated funds to White Plains Hospital in Westchester County, New York, to cover 10 mammograms for uninsured women.

"In Judaism they say that if you can rescue one person, you're saving the world," Chalchinsky said. "I really feel that is extremely important—that we all help each other."

Erin Hogarth

MARKETING

Market reaction to the pandemic: Insights from exhibitors. When COVID-19 evolved from a regional crisis to a global pandemic, the gem and jewelry trade abruptly paused for a short period and then gradually recovered to the pre-pandemic level. To investigate the trade's reaction, the impact on business, and market trends over the past two years, the authors took advantage of the Tucson show to survey the exhibitors.

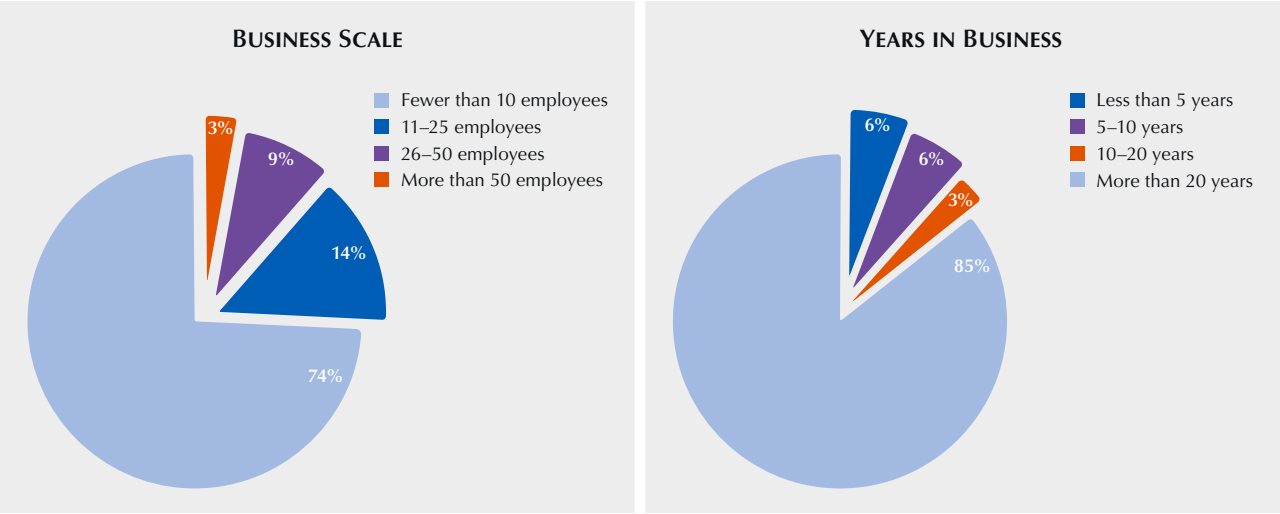

Figure 49. The majority of the 35 exhibitors surveyed have a small-scale business and more than 20 years in the industry.

This brief report presents outcomes from written surveys conducted with 35 randomly selected AGTA and GJX show exhibitors. The survey consists of two portions: general information about the business, and six pandemic- and market trend-related questions. All 35 exhibitors based their responses on their own experiences, with a very limited number of "not applicable" answers that were not included in the findings.

Nearly all respondents identified themselves as wholesalers, with a couple of exceptions as designers or miners. The authors noticed that some exhibitors played multiple roles: wholesaler, retailer, and sometimes even designer. While traditional roles in the gem and jewelry industry still carry on, the boundaries between them have become blurred. More than 70% of the exhibitors surveyed have fewer than 10 employees, and 85% of them are industry veterans with more than 20 years' experience in the trade (figure 49). Although the pool is small, it aptly reflects the nature of the gem and jewelry business in general, with small-scale business as the majority, but often with generations of commitment to the industry.

When asked about the impact of the pandemic on their business, most responded that it was most impactful at the beginning of the crisis, but recovery has been quite smooth since then. Some did express concern about the post-pandemic supply issues. Two-thirds of the interviewees stated that more business shifted online over the past two years, resulting in marketing and selling strategy changes (figure 50).

Figure 50. Due to mobility restrictions caused by the pandemic, most companies have shifted at least some business online to adapt to the new normal. This often required changes in sourcing, marketing, and selling strategies.

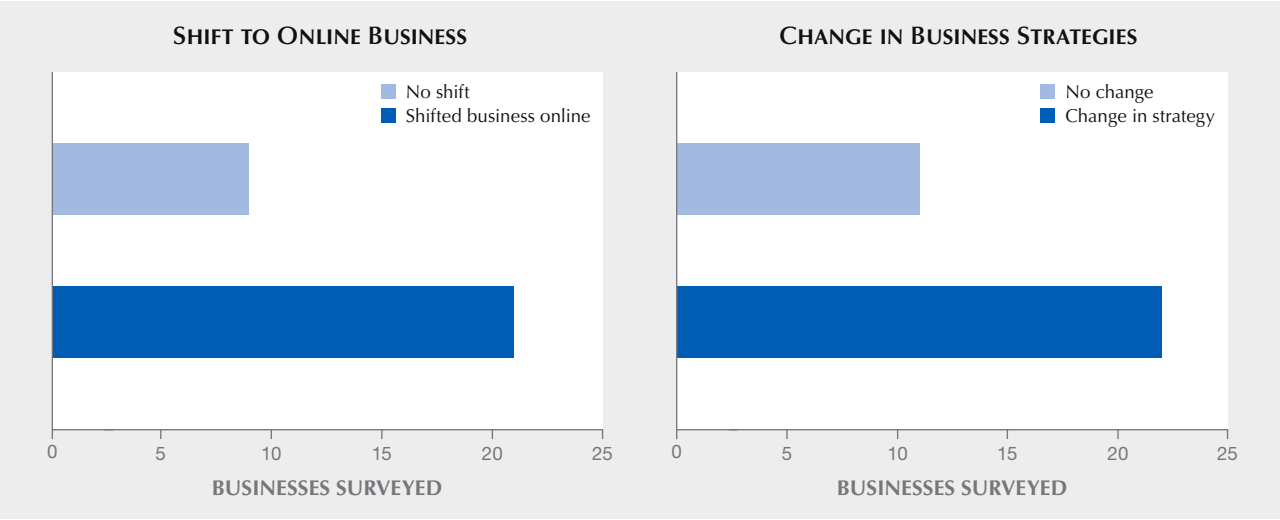

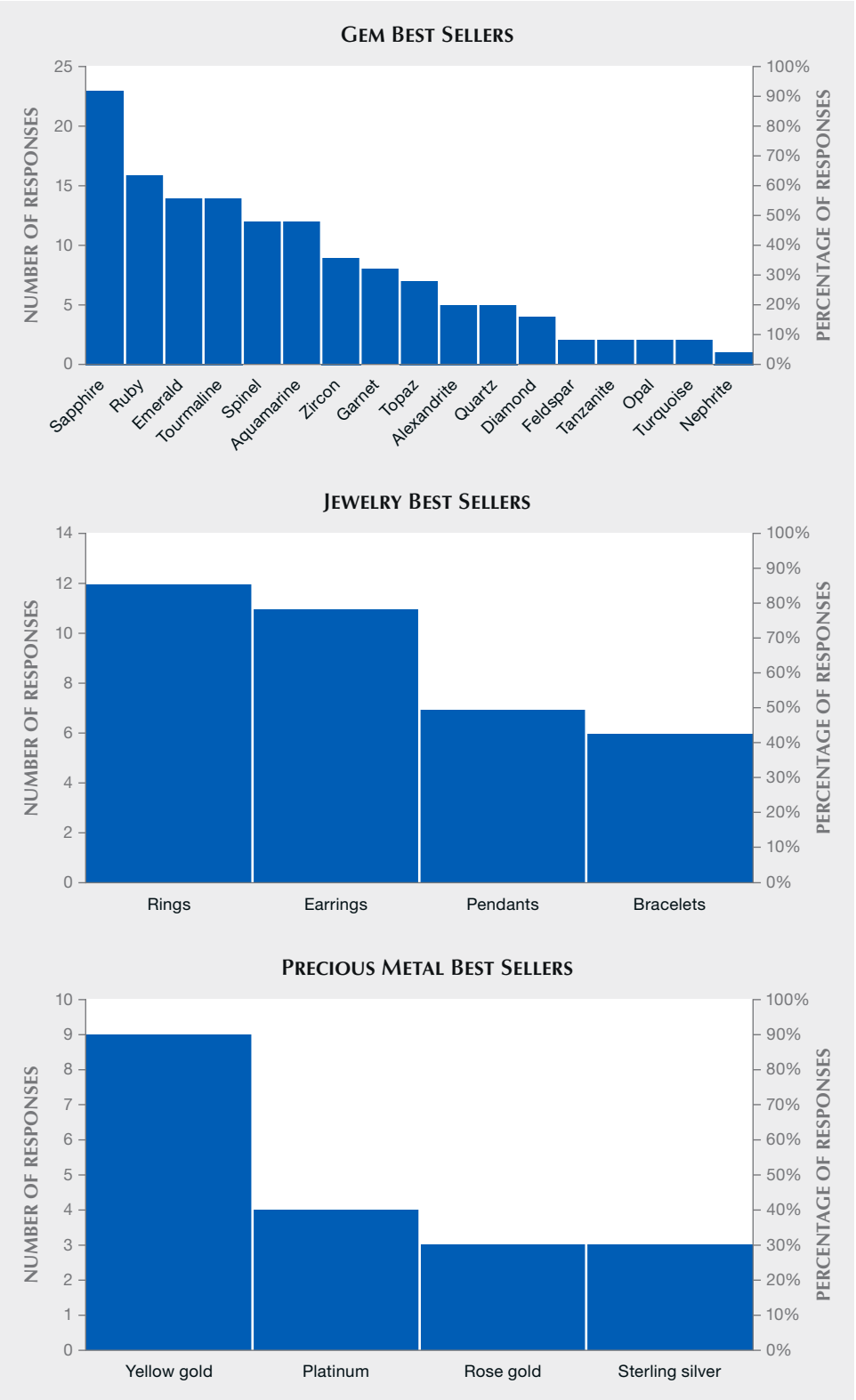

Figure 51. The best sellers over the past two years during the pandemic, according to gemstone species, jewelry type, and precious metal type.

Notably, the relatively new businesses, many with less than five years in the trade, often started with more business online than offline. Though sellers mostly embraced online trading of gems and jewelry, some had difficulties capitalizing on it, particularly with colored stones since buyers still prefer to check the quality in person.

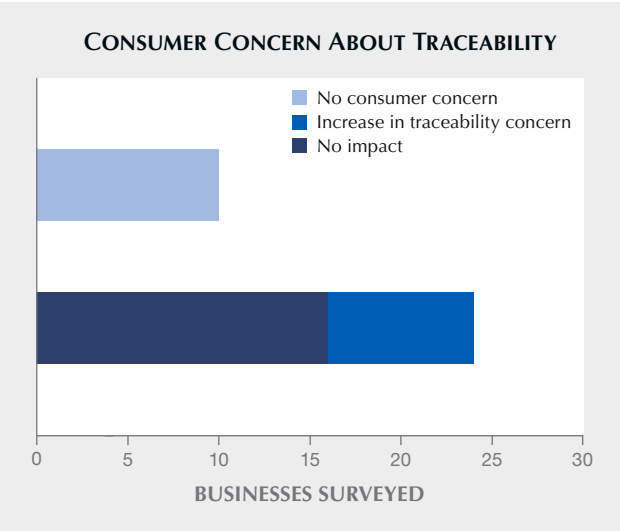

Figure 52. Many of the exhibitors surveyed noticed an increase in consumer concern about traceability, but the majority of them said it does not impact their business.

To investigate the types of stone and jewelry sales over the past two years, the authors asked the selected exhibitors to circle the corresponding items, with many circling multiple answers in each category. These questions covered gemstone species, jewelry, precious metal, and pearl types, with the understanding that while diamond sales continue to dominate the market, they are not the focus for the exhibitors surveyed. Not surprisingly, the "big three" still dominate sales, with sapphire leading the trend (figure 51, top), and tourmaline and spinel immediately following the big three. As for jewelry types, rings and earrings lead the way (figure 51, middle). Yellow gold still sells the best, with platinum as the second best seller (figure 51, bottom). Several pearl dealers circled their best sellers, but the authors found that overall sales were quite evenly distributed among the four major cultured pearl types.

As traceability is a hot topic in the trade, the authors also asked two related questions about whether respondents noticed increased consumer concern on traceability. If they answered yes, they were asked whether it affected how they do business. The result shows that about two-thirds of them noticed the concern, and two-thirds of those who noticed the concern did not feel that it affected their business (figure 52).

As the world enters the post-pandemic era, it is worthwhile to continue monitoring how the market reacts to the changes and how tradespeople adapt to the new normal.

Tao Hsu and Lisa Kennedy

RESPONSIBLE PRACTICES

Mercury Free Mining pilot program. In late 2021, Mercury Free Mining (MFM), the Alliance for Responsible Mining (ARM), and GIA joined with Peruvian artisanal and small-scale gold miners (ASGM) to launch a new program intended to find alternatives to mercury in gold mining. The partners are bound in recognizing the reliance on artisanal and small-scale gold mining to produce major quantities of an extremely valuable commodity. This situation unfortunately perpetuates the leading cause of anthropogenic mercury pollution. The pilot program aims to proactively develop mercury alternatives in two gold mines, increasing their sustainability, building a traceable ASGM gold supply, and acting as a major leap in the MFM research team's understanding of how we can ultimately eradicate mercury in gold mining.

Mercury Free Mining, the program lead, is a nonprofit organization founded by Toby Pomeroy, a lifelong goldsmith, jeweler, and passionate advocate for responsible sourcing. Founded in 2019 with the mission of eradicating mercury, MFM has been building a community of jewelers supporting efforts to provide the nearly 20 million ASGM with efficient and nontoxic mercury alternatives where presently unavailable.

MFM's research and deployment team, led by the author, a geometallurgist, fosters novel sociotechnical solutions to address the issues facing ASGM with a focus on finding suitable mercury alternatives. This is a challenge. Gold is nonreactive to most chemicals (mercury being one of the only exceptions) and coincides with dense black sands that are difficult to mechanically separate (figure 53).

Figure 53. Gold and dense black sands in a traditional wooden batea, shown by a Colombian miner at Oro Verde. Typically, mercury is used to separate the two materials. Photo courtesy of Toby Pomeroy.

Figure 54. In this photo from November 2020, Kenyan miners in Kakamega County press amalgam in a pan to remove excess water. Amalgam is a mixture of mercury and gold produced by adding mercury to concentrated gold ores. This method puts miners in direct contact with mercury, a potent neurotoxin that can be absorbed through the skin. Photo courtesy of Ruth Epwoka.

The team's methodologies rely upon the miners' desire to maximize earnings by recovering more gold from the raw ores while also minimizing harmful social, health, and environmental side effects. Currently, reliable information about implementing mercury alternatives that are more effective and less harmful is scarce. Without this, miners have no choice but to rely upon a multi-generational neurotoxin in order to earn an income (figure 54).

Figure 55. Miners wash the gold ores and use a sluice to collect gold within the slurry. Sluices are one of the most common tools used in artisanal and small-scale mining to concentrate gold. This simple configuration can capture ~20–70% of gold based on ore type, water flow, feed rate, and other specifications geometallurgists determine through research. Photo courtesy of Ruth Epwoka.

GIA granted $50,000 to jumpstart the pilot. Since then, MFM has collaborated with ARM engineers and Peruvian miners to collect representative mineral samples for use in testing a suite of innovative gold concentrators. MFM is partnering with six mineral processing experts to evaluate their respective technologies based on key performance indicators such as throughput, gold recovery, and concentration ratio. Spread across three continents, the testing will evaluate a large swath of potential mercury alternatives, helping to gather critical information on how different processors are suited for various gold ores (figure 55). This stage of the project will draw from advanced engineering and science to perform thorough analyses in an accurate and timely manner.

Following the testing, the results will be holistically synthesized by the MFM research team with respect to the many complexities of the miners' unique situations. This will include a mercury comparison to understand the true viability for the miners to adopt an alternative. Stakeholder discussions will then determine whether the miners ultimately decide to adopt one of the mercury-free technologies. If so, the team will help implement the transition to mercury-free methods and conduct observational research to better define the impact on the health of miners and their communities.

The completion of this pilot program in 2022 will mark a turning point in MFM's ability to minimize the global impacts of mercury by having a tested and verified framework that can translate to additional mercury elimination projects as MFM expands. Following the pilot, the MFM team will publicly release the first report documenting the research process and results in complete detail. This and future reports can be used freely by miners and organizations to enhance the ability to safely source gold. For those interested in learning more, collaborating, or using these methods elsewhere, please contact the author.

Caelen Burand (caelen@mercuryfreemining.org)
Mercury Free Mining
Tucson

TREATMENTS

Sugar/heat-treated opal. Treatments can cause harm when they are not disclosed properly, but without treatments, fewer gem resources would find their usage in the jewelry trade. At the AGTA show, the authors had the rare opportunity to talk with James Carpenter from Arkansas-based Unconventional Lapidarist about sugar/heat treatment on porous rough opal.

Sugar and acid treatment is one of the most commonly used methods to enhance opal. In the trade, this treatment is usually applied to matrix opal from Andamooka, Australia, a particularly porous material. The finished product is often referred to as "Andamooka matrix opal" or "Andamooka rainbow matrix opal" by the trade. This treatment was presented as a hot sugar bath followed by a hot acid bath (G. Brown, "Treated Andamooka matrix opal," Summer 1991 *G&G*, pp. 100–106). The chemical reaction between sugar and acid then deposits carbon to the porous structure of the opal as black dots. The treatment darkens the background color of the opal and therefore makes the play-of-color stand out more.

Carpenter revealed that he treated the opal without using acid to gain a similar result. The opals, either slices

Figure 56. From left to right: rough Andamooka matrix opal, a slice after treatment, and a 72 ct finished freeform cabochon. Photo by Tao Hsu; courtesy of Unconventional Lapidarist.

Figure 57. The winning design from the 2021 Gianmaria Buccellati Foundation Award for Excellence in Jewelry Design, created by Meghan Simmons, a Carlsbad graduate of the GIA Jewelry Design program.

or cabochons, were first soaked in a hot 50% sugary water solution for 6 to 9 hours. After cooling down from the hot sugar bath, the pieces were patted dry and then tightly wrapped in aluminum foil. Carpenter emphasized that tight wrapping is especially important because a loose wrap causes the sugar to sweat out and possibly generate more cracks in the material. The well-wrapped materials were then heated in a toaster oven at 450–500°F for about 4 hours. After the final cooling, the materials were polished to finished products or retreated if necessary, revealing a dramatic change from start to finish (figure 56).

Tao Hsu and Lisa Kennedy

ANNOUNCEMENTS

Fifth annual Gianmaria Buccellati Foundation Award winner. Meghan Simmons, a graduate of GIA's Jewelry Design program at the Carlsbad campus, received the fifth annual Gianmaria Buccellati Foundation Award for Excellence in Jewelry Design. The award was presented at the GIA Alumni Collective's "Night at the Museum" event held during the AGTA GemFair Tucson. One of 11 finalists, Simmons competed against more than 80 students from GIA's seven campuses. Her winning earring design (figure 57), inspired by the abstract artist Wassily Kandinsky, emphasizes the use of line and shape with gold, diamonds, and blue sapphires.

Simmons will spend a week in Italy, traveling from Florence to Venice to Milan, and will meet with a representative from the foundation.

Larry French, chief officer of North American strategies for the foundation, said, "This competition was born out of the life and work of Gianmaria Buccellati. We congratulate not only all the students who participated in this year's design competition but also the talented instructors from GIA who guided the students on this beautiful art."

The 2022 Gianmaria Buccellati Foundation Award for Excellence in Jewelry Design competition is underway and open to students in GIA's Jewelry Design courses who meet the eligibility requirements. For more information, visit gia.edu/buccellati-foundation-award-jewelry-design.

2022 Tucson Photo Gallery

Helen Serras-Herman's "Pluto & Persephone—Rulers of the Underworld" carving features a 59.98 ct Oregon sunstone from the Dust Devil mine and a 280 ct gem-quality silica chrysocolla and quartz with malachite. The piece is 110 × 55 × 38 mm, with a base carved in wax and cast in sterling silver. The silver faces depicted represent the spirits of the underworld, with the Greek gods Pluto and Persephone sitting above them. Courtesy of Helen Serras-Herman.

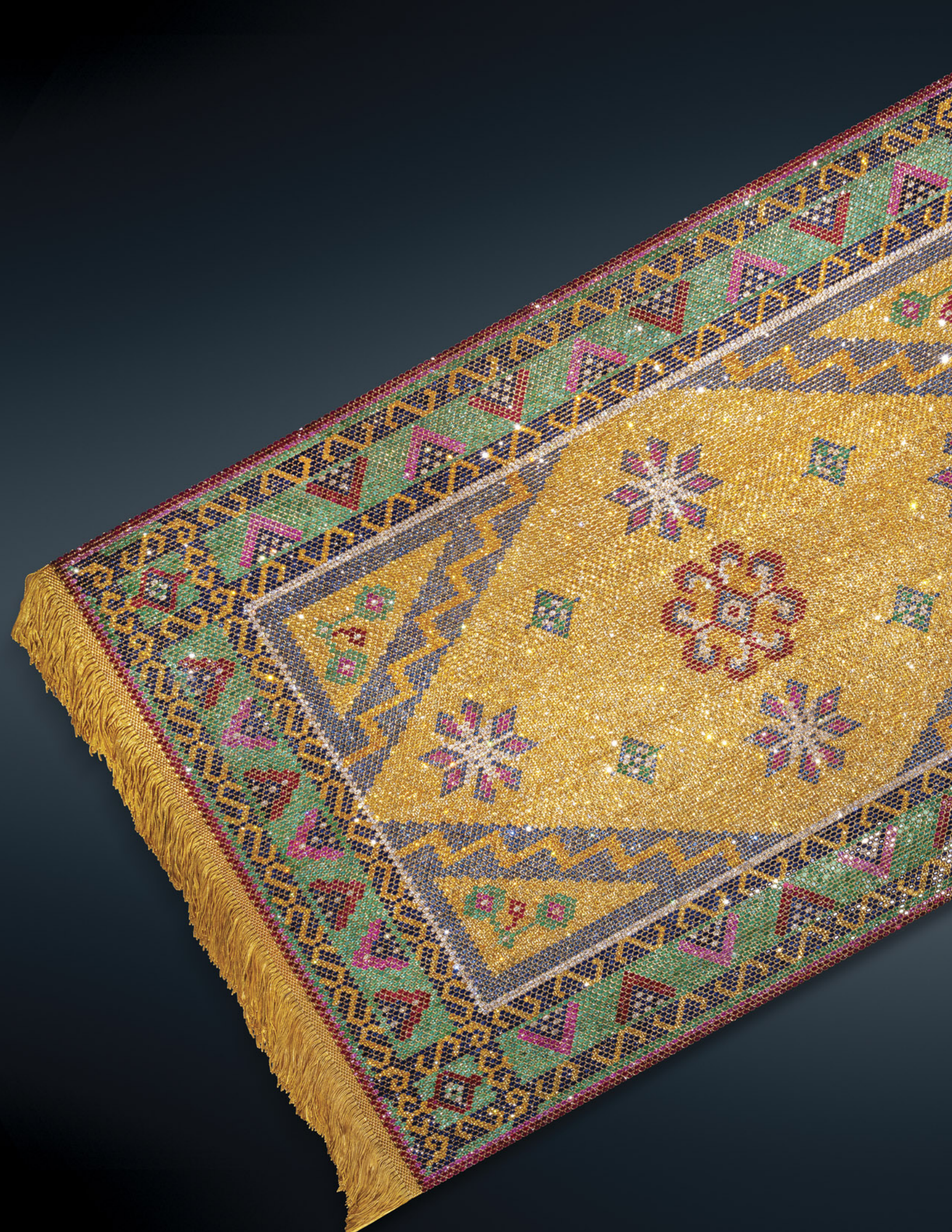

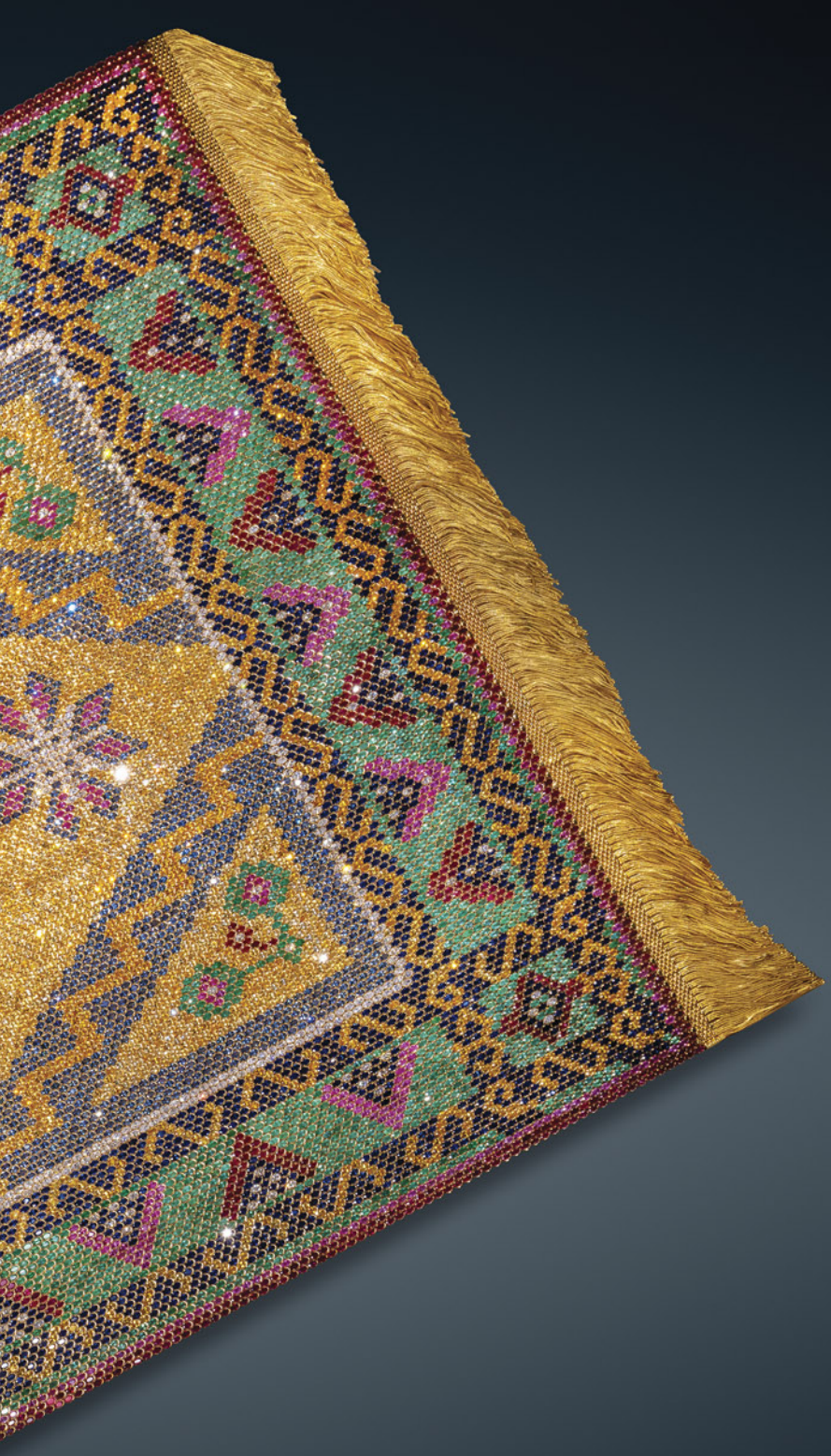

"The Royal Tapestry," created by Parisian jeweler Cristofol, contains 26,649 individual gems—emerald, ruby, sapphire, and diamond—set in 18K gold. A team of more than 10 artisans spent more than 16,000 hours to complete it, in addition to the five years needed to source, cut, and calibrate the gems. The 122 × 71 cm tapestry has more than 100,000 gold prongs and weighs over 40 lbs. Owned by a private collector, this piece is on display at the new Alfie Norville Gem and Mineral Museum in Tucson.

Corundum crystals often exhibit growth features such as these eye-visible trigons. Helen Serras-Herman, best known for her carving expertise, left these crystals intact to emphasize the natural growth features as design elements, with simple gold wire turning them into pendants. Courtesy of Helen Serras-Herman.

These sugarloaf cut gems, a 5.62 ct sapphire and a 9.00 ct emerald, are of excellent color and clarity. Courtesy of Crown Color.

A 234 ct cat's-eye topaz from Mozambique. Courtesy of Meg Berry.

Inspired by the beautiful geometry of the Art Deco era, Zoltan David's "Deco Drama" pendant features a 4.30 ct tourmaline along with 24K gold inlay and diamonds totaling 0.44 carats. Courtesy of Zoltan David.

Zoltan David's "Twilight" pendant is inspired by the colors of the evening sky. It features a 24.06 ct Ethiopian opal set in titanium, inlaid with 24K gold, and accented with diamonds, blue sapphires, pink sapphires, tsavorite garnets, and spessartine garnets on a multi-strand steel chain. Courtesy of Zoltan David.

This functioning compact powder box and lipstick set, with a hand-engraved floral motif, is encrusted with emeralds, rubies, sapphires, and diamonds. Fashioned in gilded silver, the set was made in Russia circa 1930. Courtesy of Jewelerette & Co.

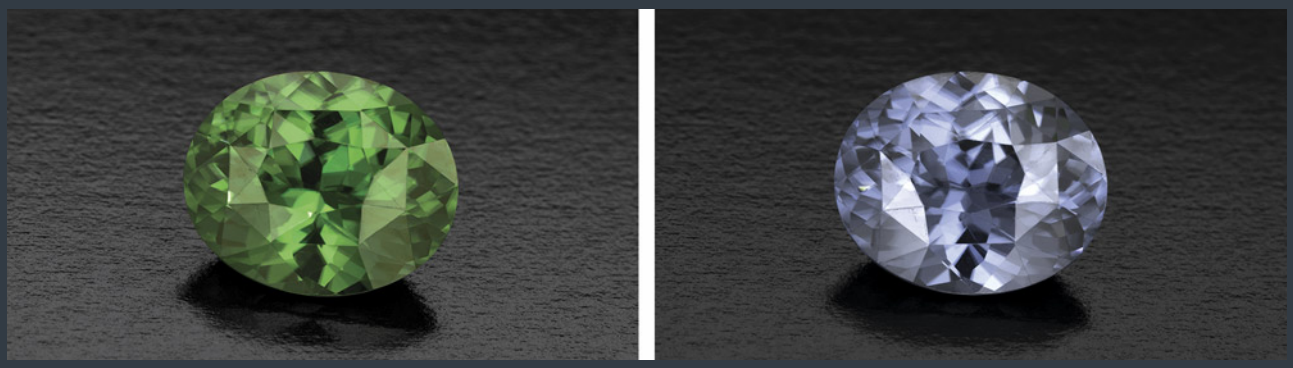

This 14.62 ct color-change zircon (believed to be from Sri Lanka or Myanmar) was fashioned in Thailand. The gem appears bright green in incandescent light, changing to violet in daylight. Courtesy of Bryan Lichtenstein, 30/90.

Although cerussite is rarely faceted due to its softness (3–3.5 on the Mohs scale) and distinct cleavage, this 2.65 ct faceted gem exhibits remarkable dispersion. Courtesy of Gembridge.

Opals are generally one-of-a-kind gemstones and rarely found as a matching pair, even as doublets. These 7 cm Australian opal doublets, set in 18K recycled rose gold earrings, were inspired in form and texture by the Azores island chain. Courtesy of Eve Streicker, Original Eve.

This fully terminated rhodonite crystal from the Conselhero region of Minas Gerais, Brazil, weighs 133.5 g and measures 52 × 33.9 × 29.4 mm. The 46.19 ct oval gem is of remarkable clarity and quality for rhodonite, which is generally used for ornamental carvings and cabochons. Courtesy of Jean Claude Nydegger.

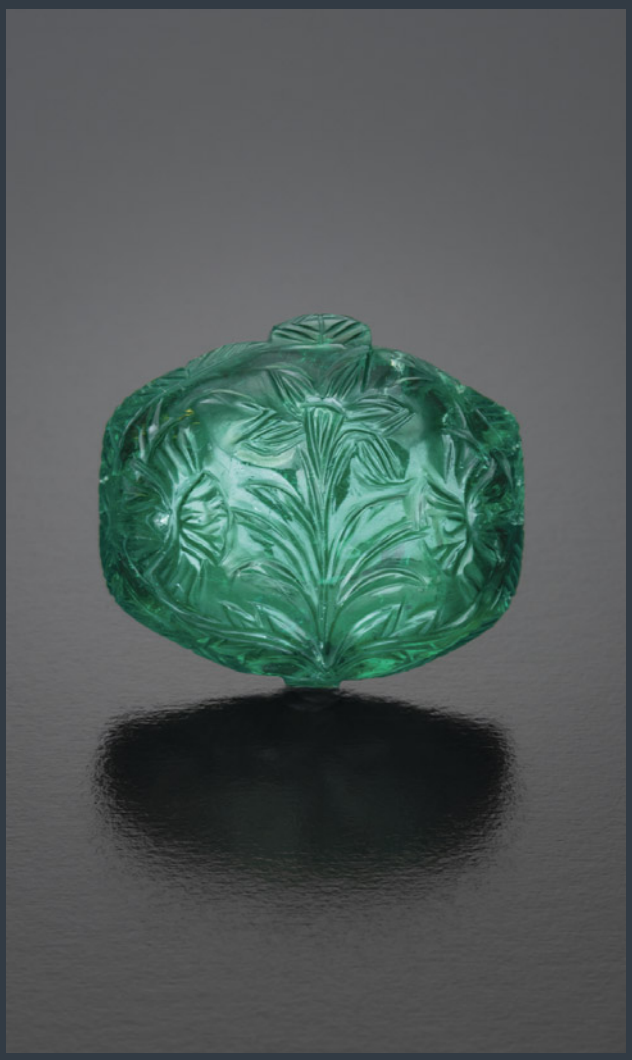

Coveted by the Indian Mughal emperors during the seventeenth and eighteenth centuries, Colombian emeralds were often allowed to retain their hexagonal outline and then carved and fashioned using Golconda diamond tools. This 49.08 ct emerald exhibits a floral motif. Courtesy of a private collection.

This superb 50.09 ct color-change sapphire from Sri Lanka goes from purple to blue in incandescent and daylight, respectively. Courtesy of Pioneer Gems.

Jewelry clients increasingly seek gold that is equitably mined and not harmful to the environment. This 18K yellow gold "Oasis Medallion" pendant uses recycled gold and features F-color, VS_2 diamonds (0.17 carats total) and a 2.41 ct blue sapphire from Sheehan Sapphires, Sri Lanka. Made of Fairmined 18K yellow gold, the ring contains 0.09 carats of diamonds and a 2.19 ct pink sapphire. Courtesy of Lester Oehler and Juleia Dooley of Toby Pomeroy.

All photos by Robert Weldon.

REGULAR FEATURES

COLORED STONES AND ORGANIC MATERIALS

Cuprite and malachite in agate from the Yanyuan region, Sichuan. The Yanyuan region in China's Sichuan Province is rich in agates known for their vibrant colors, including pink, purple, and green. Dendritic inclusions are common in agates from many areas but rarely seen in agates from Yanyuan. Recently, our interest was drawn to a 9.40 g gray-purple carved pendant submitted for identification (figure 58) that displayed peculiar dendritic inclusions. The piece was reported by the client to be from Yanyuan.

Standard gemological testing of the pendant yielded a spot refractive index of 1.54, and Fourier-transform infrared (FTIR) spectroscopy was used to confirm the identity of the pendant. Microscopic observation revealed a blue-green spherical mineral surrounded by copper-red dendritic inclusions (figure 59), which appeared to have a metallic luster under reflected light.

The red inclusions in the exposed surface and the blue-green inclusion nearby were analyzed with Raman spectroscopy. The analyses showed that the red inclusions were cuprite (Cu_2O) and the blue-green sphere was malachite ($Cu_2(CO_3)OH_2$), both of which were confirmed by energy-dispersive X-ray fluorescence (EDXRF) testing (figure 60). In the Raman spectra of the inclusions, the peak at 464 cm^{-1} was assigned to the agate host (figure 60).

Figure 58. This 9.40 g gray-purple pendant was identified as agate. Photo by Su Xu.

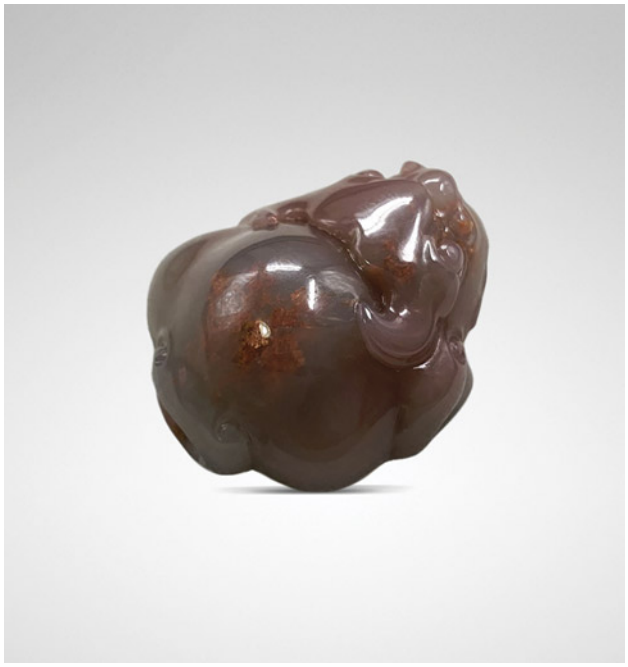

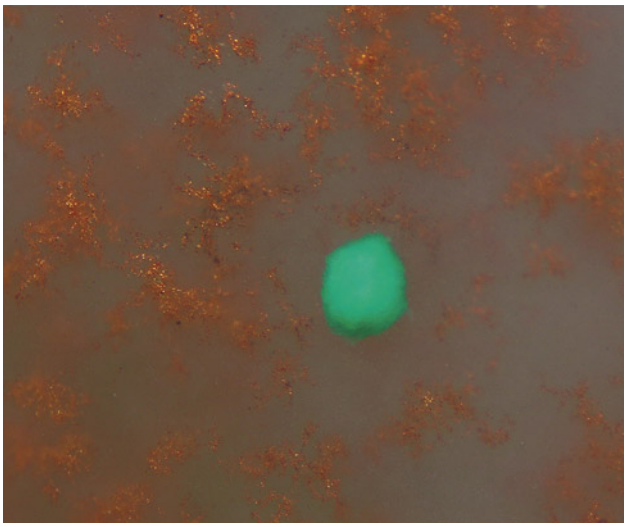

Figure 59. Microscopic observation of the pendant revealed copper-red dendritic inclusions and a blue-green spherical inclusion. Photomicrograph by Su Xu; field of view 1.5 mm.

While copper inclusions have been previously reported in purple chalcedony (Spring 2019 *G&G* Micro-World, p. 111) and chrysocolla chalcedony (M. Ye and A.H. Shen, "Gemmological and mineralogical characteristics of chrysocolla chalcedony from Taiwan, Indonesia and the USA, and their separation," *Journal of Gemmology*, Vol. 37, No. 3, 2020, pp. 262–280), this is the first time we have identified two kinds of copper-bearing inclusions in agate from Yanyuan.

Su Xu and Dapeng Chen
National Gold-Silver Gem & Jewelry Quality Supervision & Inspection Center, Sichuan

Unusual repair of a natural emerald. A 5.24 ct bluish green emerald (figure 61) was presented to the State Gemmological Centre of Ukraine for identification and determination of the presence of treatment. The client reported that this stone was mined in Colombia. The stone exhibited a refractive index of 1.566–1.571, birefringence of 0.005, hydrostatic specific gravity of 2.67, moderate pleochroism with bluish green to green colors, and a very weak pink fluorescence to long-wave and short-wave UV. Qualitative analysis using EDXRF spectroscopy showed major amounts of vanadium, chromium, and iron and minor amounts of gallium.

Magnification with a gemological microscope revealed an abundance of fluid growth tubes, as well as two-phase and three-phase inclusions. Thick masses of gray matter were revealed inside the cracks of the emerald. Infrared spectroscopy (FTIR) was subsequently performed to ana-

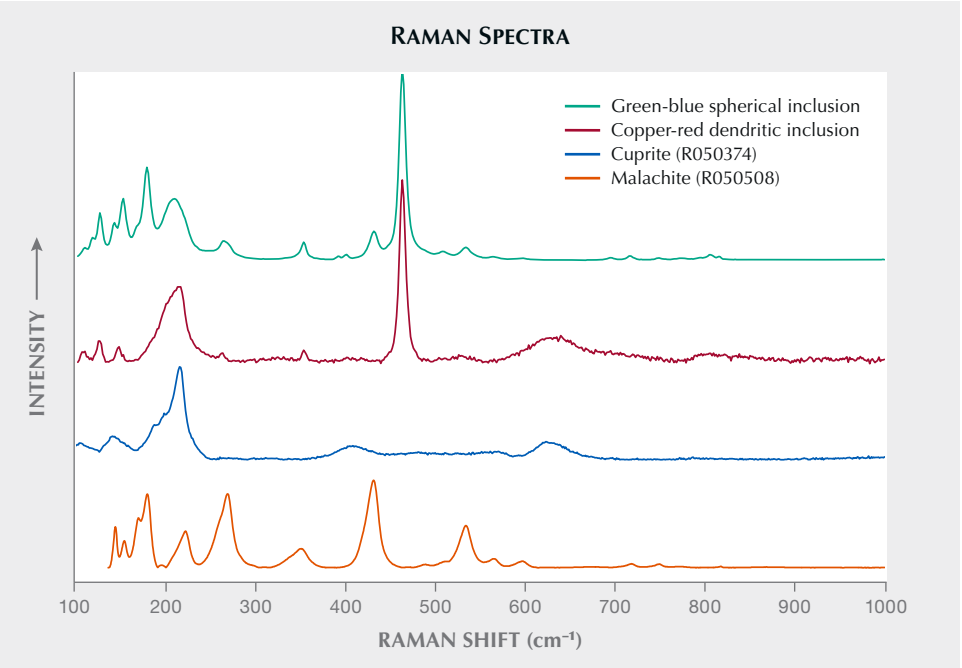

Figure 60. Comparison between the Raman spectra obtained for the two kinds of inclusions found in the agate and reference spectra for cuprite and malachite from the RRUFF database. Spectra are offset for clarity.

lyze this gray substance. Epoxy resin peaks at 3060, 3035, 3000, 2964, 2932, and 2871 cm^{-1} confirmed an epoxy resin treatment (M.L. Johnson et al., "On the identification of various emerald filling substances," Summer 1999 *G&G*, pp. 82–107).

DiamondView imaging clearly revealed the epoxy resin filler within the fissures as a series of blue lines extending over the entire surface against the emerald's red-fluorescing bodycolor (apparently due to the presence of the Cr^{3+} impurity). Additionally, careful examination from all sides of the stone revealed a patch in one of the corners. This patch was covered with rounded pits and glowed strong blue in the DiamondView (figure 62). In daylight, there was a clear, even border between the patch and the emerald (figure 63). EDXRF analysis showed additional admixtures of potas-

Figure 61. Examination of this 5.24 ct clarity-enhanced emerald revealed unusual repair work. Photo by Iurii Gaievskyi.

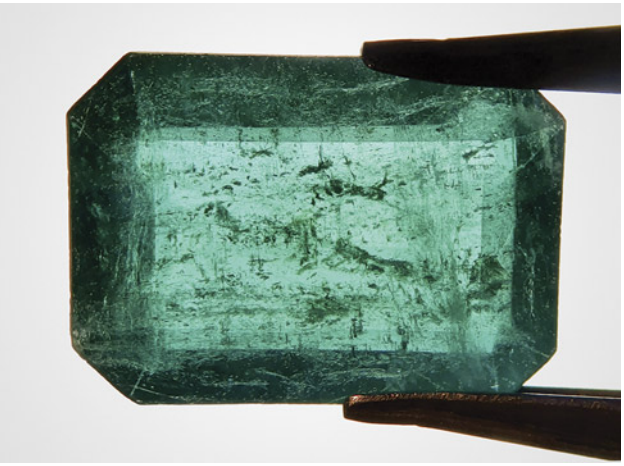

Figure 62. DiamondView imaging of a patch applied to a corner of the emerald. Image by Iurii Gaievskyi.

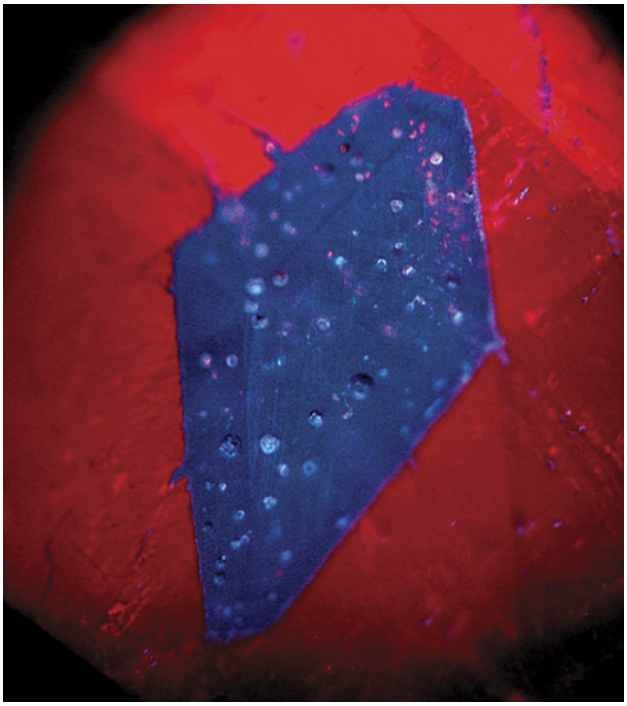

Figure 63. The clear, even border between the patch and the emerald, shown in daylight. Photomicrograph by Iurii Gaievskyi; field of view 4.0 mm.

sium and calcium on the side of the patch. All of these properties suggest that glass was the raw material for this patch, which was presumably used to conceal a damaged part of the cut emerald. This kind of repair is extremely unusual for cut stones.

Iurii Gaievskyi (gaevsky@hotmail.com)
State Gemmological Centre of Ukraine, Kyiv

Inclusions and spectroscopic features of yellowish green enstatite. Gem-quality enstatite is the magnesium end member of the enstatite-ferrosilite series in the clinopyroxene subgroup of the pyroxene group. While the most common color is brown, it can also be colorless, green, or gray. Myanmar, Tanzania, and Sri Lanka are the main sources of gem-quality stones currently in the market. Enstatite can yield clean faceted gems but can also display four-, six-, or eight-rayed asterism.

Enstatites have been documented many times from various sources. Six-rayed star brown enstatite was reported from India (W. Eppler, "Star-diopside and star-enstatite," *Journal of Gemmology*, Vol. 10, No. 6, 1967, pp. 185–188). Sri Lankan samples were reported in U. Henn and H. Bank, "Sternbronzit aus Sri Lanka," *Zeitschrift der Deutschen Gemmologischen Gesellschaft*, Vol. 40, No. 2–3, pp. 145–148. Star enstatite from Madagascar was described in T. Cathelineau, "Six-rayed star enstatite from Madagascar," *Journal of Gemmology*, Vol. 36, No. 8, 2019, pp. 688–690. Four-rayed star brown enstatites from Sri Lanka were documented in E.J. Gübelin and J.I. Koivula, *Photoatlas of Inclusions in Gemstones, Volume 3*, Opinio Publishers, Basel, Switzerland, 2008. Faceted brown enstatite was reported in Koivula et al., "Gemmological investigation of a large faceted East African enstatite," *Journal of Gemmology*, Vol. 21, No. 2, 1988, pp. 92–94. Yellowish green enstatites from Africa were discussed in K. Schmetzer and H. Krupp, "Enstatite from Mairimba Hill, Kenya," *Journal of Gemmology*, Vol. 18, No. 2, 1982, pp. 118–120, as well as in B.M. Laurs et al., "Yellowish green enstatite (and star enstatite) from Tanzania," *Journal of Gemmology*, Vol. 36, No. 8, 2019, pp. 691–693. Norwegian stones were documented in F. Schmitz et al., "Polymer-filled star enstatite from Norway," *Journal of Gemmology*, Vol. 35, No. 2, 2016, pp. 98–101.

Recently, GIT Gem Testing Laboratory (GIT-GTL) received six bright yellowish green enstatite samples weighing 0.65 to 2.78 ct (figure 64) that were reported by author SD to be from Africa. The stones appeared fairly similar to the previously documented four-rayed star yellowish green

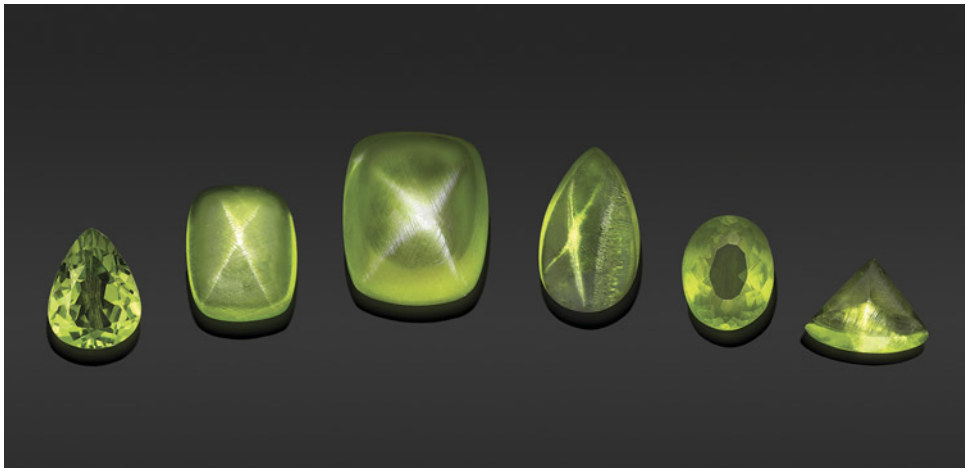

Figure 64. Two faceted and four cabochon bright yellowish green enstatites. Left to right: a 1.02 ct pear (sample no. e102), 1.32 ct cushion (e132), 2.78 ct cushion (e278), 1.44 ct pear (e144), 0.65 ct oval (e065), and 0.67 ct modified triangle (e067). Photo by C. Kamemakanon; courtesy of American-Thai Trading.

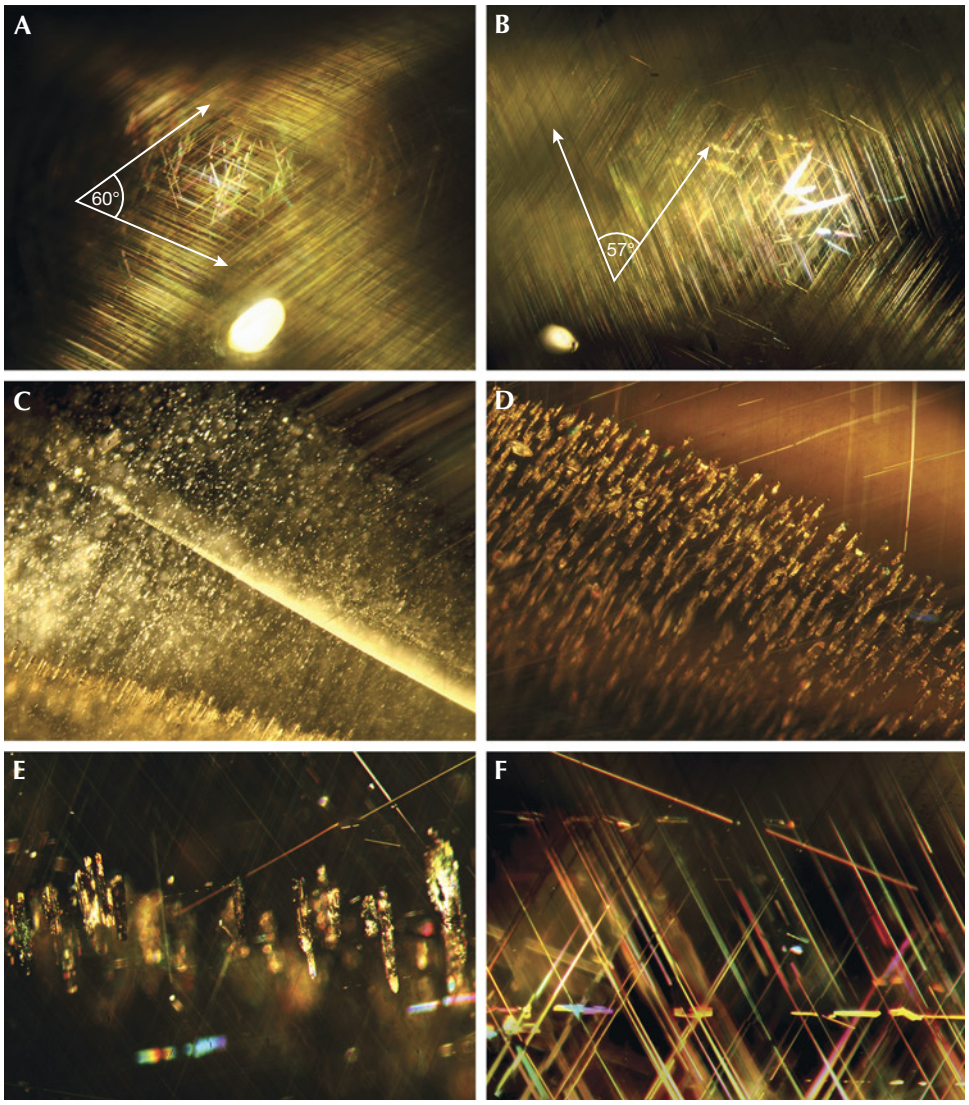

Figure 65. A and B: Using oblique fiber-optic lighting, the four-rayed star enstatite cabochons reveal two sets of densely and regularly oriented fine needle-like inclusions intersecting at approximately 57° to 60°. C–E: The pear cabochon shows patches of densely oriented minute white particles (C), a plane of oriented tubes partially filled with small brownish white to colorless magnesite crystals (D), and oriented tubes filled with magnesite (E). F: Rectangular platelets and needle inclusions with bright interference colors in the modified triangle. Photomicrographs by S. Promwongnan; fields of view 3.6 mm (A–D) and 1.5 mm (E–F).

enstatite from Tanzania documented by Laurs et al. (2019). In that article, needle-like inclusions were found to be the cause of the four-rayed asterism, but their mineralogical identity was not reported.

Of the six stones examined in this study, four were cabochons displaying a four-rayed star effect while two were faceted (figure 64). The five stones with at least one polished flat surface gave refractive indices of α = 1.655–1.660, β = 1.661–1.665, and γ = 1.668–1.669, with a birefringence of 0.009–0.014, and are therefore biaxial positive. The spot RI reading of one cabochon without a flat surface was ~1.66. The hydrostatic specific gravity of all samples was 3.22–3.25. All these values fall well within the range of enstatite. The stones appeared weak orange under the Chelsea color filter and showed moderate yellow and yellowish green pleochroism. All were inert to both long-wave and short-wave UV.

The main diagnostic internal features were the two sets of dense and regularly oriented needle-like inclusions (figure 65, A and B). The two sets measured on the same plane at the top of three cabochons (e278, e132, and e144) were found to intersect at an approximate angle of 57° to 60°, producing the four-rayed star effect seen on the cabochon surface (figure 64). While the two faceted stones also contained fine needle-like inclusions, they were not cut to display a star.

Close examination also uncovered two sets of needles that did not produce asterism. In addition, patches of densely oriented minute white particles (figure 65C) and a plane of oriented short tubes (figure 65, D and E) were found in one stone (e144). These tubes were partially filled with tiny brownish white to colorless crystals identified by Raman spectroscopy as magnesite (figure 66). The presence of epigenetic magnesite ($MgCO_3$) could have resulted from alteration of the host enstatite. The other feature consisted of sparse rectangular platelet inclusions occurring in various directions within the dense mesh of needle inclusions (e067, figure 65F).

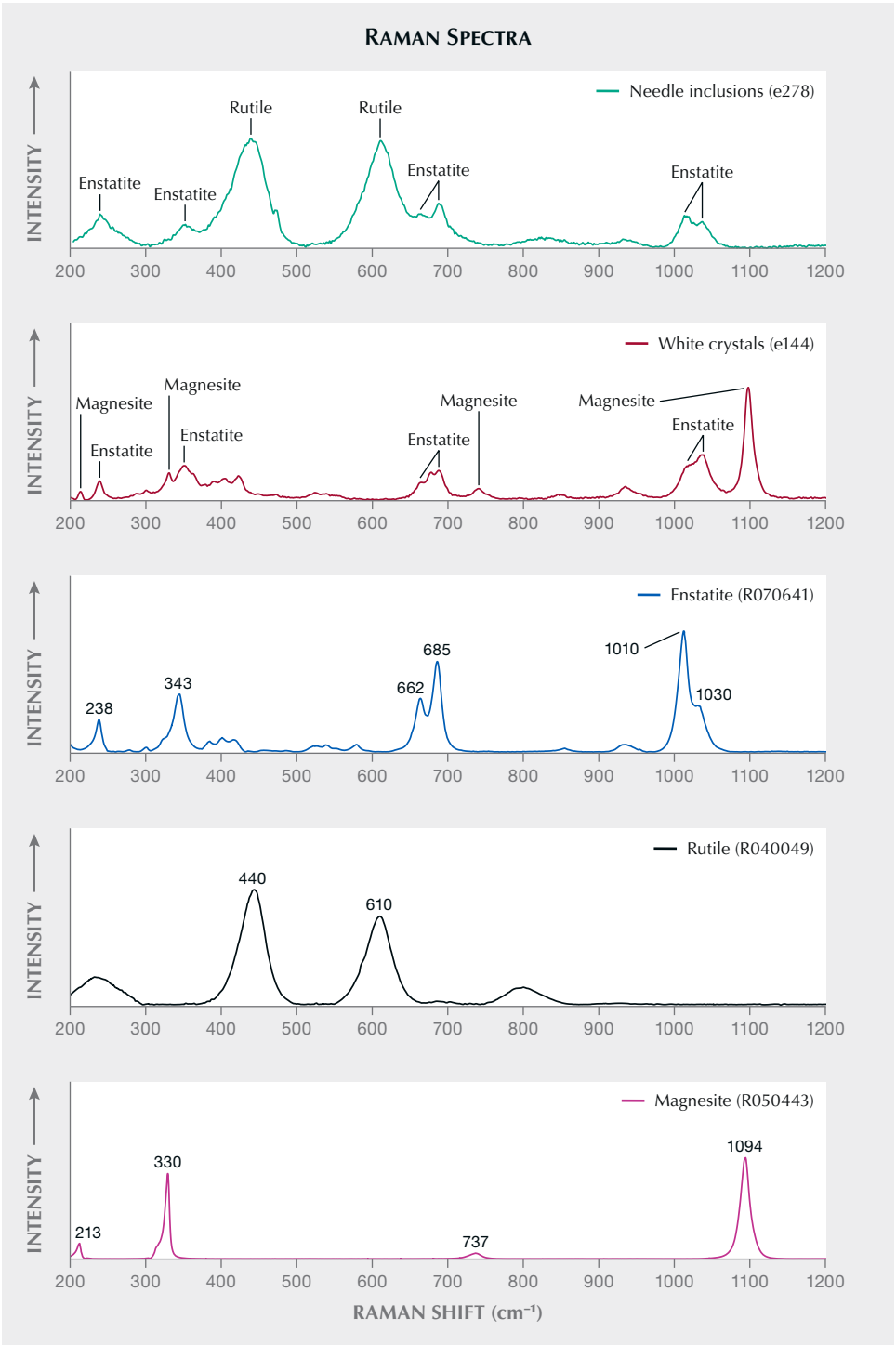

Figure 66. Raman spectra of the exposed fine needle inclusions plus host mineral (green line) show the superimposed peaks of rutile and enstatite that match with the RRUFF reference spectra (black and blue lines, respectively). Similarly, the spectra of exposed white to colorless crystals in short tubes plus host mineral (red line) display peaks of magnesite and enstatite that match with the RRUFF reference spectra (pink and blue lines, respectively).

The Raman spectra of all host mineral samples, recorded using 532 nm laser excitation, similarly showed dominant peaks that matched the enstatite reference spectrum from the RRUFF database (not shown here). Moreover, the Raman spectrum of the exposed fine needle inclusions plus host mineral in one sample (e078) gave the superimposed peaks of rutile (440 and 610 cm^{-1}) and enstatite (238, 343, 662, 685, 1010, and 1030 cm^{-1}), consistent with the RRUFF reference spectra in figure 66. Similarly, the Raman spectrum of exposed white to colorless crystals in short tubes plus the host in a sample (e144) showed overlapping peaks of magnesite (213, 330, 737, and 1094 cm^{-1}) and enstatite, also consistent with the RRUFF reference spectra. The identity of the rectangular platelet inclusions, however, could not be resolved due to their sparsity and their depth below the surface.

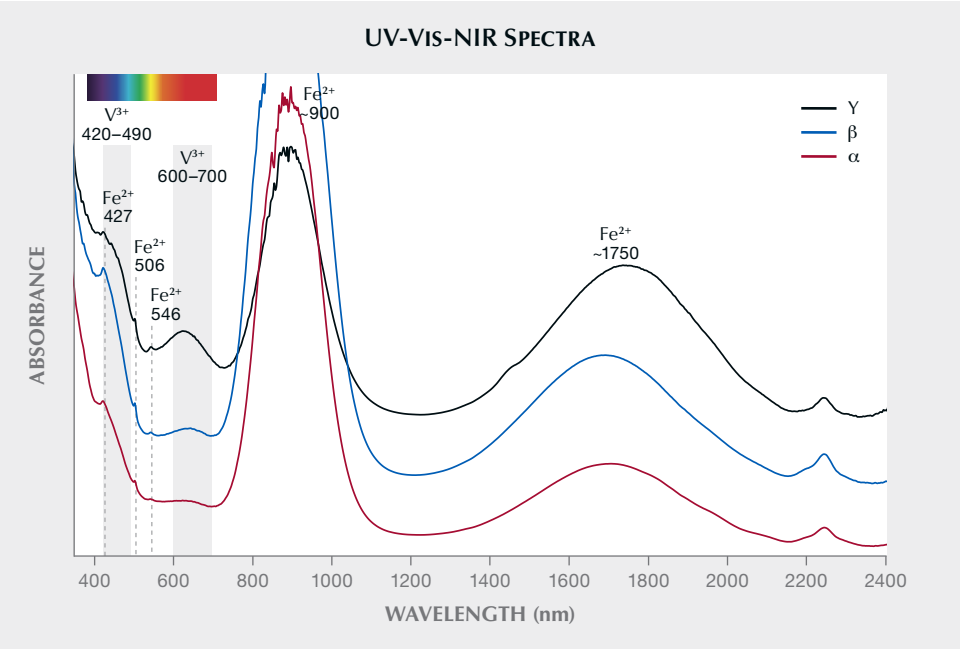

Figure 67. Polarized UV-Vis-NIR absorption spectra of an enstatite (e132) showing a dominant Fe^{2+}-related broad band around 900 nm and additional Fe^{2+}-related absorptions at 1750 nm in addition to a continuous rise from ~700 nm toward the UV with smaller absorptions at 427, 506, and 546 nm. The iron absorptions are superimposed by two broad bands around 420–490 nm and 600–700 nm due to the presence of V^{3+} plus trace Cr^{3+} in the stone lattice (see table 1). Spectra are offset for clarity.

Polarized ultraviolet/visible/near-infrared (UV-Vis-NIR) spectra of a sample (e132) showed features dominated by broad absorption bands of Fe^{2+} in the NIR region centered at ~900 and ~1750 nm (figure 67). The spectra rise continuously from ~700 nm toward the UV with small Fe^{2+} peaks at 427, 506, and 546 nm in the visible range (Cathelineau,

TABLE 1. Chemical contents of the six enstatite samples measured by EDXRF in this study and those of previously reported yellowish green enstatites from Africa.

Sample no./locality	Element oxides (wt.%)									
	MgO	Al_2O_3	SiO_2	CaO	TiO_2	V_2O_5	Cr_2O_3	MnO	Fe_2O_3	ZnO
e278	31.53	7.65	58.92	0.08	0.07	0.07	0.02	0.32	1.28	0.05
e065	31.10	7.34	58.05	0.14	0.13	0.13	0.04	0.55	2.41	0.11
e067	31.16	7.14	58.24	0.12	0.13	0.15	0.06	0.59	2.30	0.10
e102	31.05	6.29	59.19	0.14	0.11	0.11	0.04	0.70	2.24	0.13
e132	30.88	7.34	58.19	0.12	0.14	0.13	0.03	0.56	2.50	0.12
e144	26.49	8.09	59.15	0.21	0.23	0.22	0.07	1.04	4.26	0.24
Kenya (Schmetzer and Krupp, 1982)[a]	38.27	3.60	55.57	n.a.[c]	n.a.	n.a.	0.22	n.a.	1.62	n.a.
Tanzania (Laurs et al., 2019)[b]	n.r.[d]	n.r.	n.r.	n.r.	0.12	0.14	0.01	0.52	2.00	n.r.

[a]*Electron microprobe*
[b]*EDXRF*
[c]*n.a. = not analyzed*
[d]*n.r. = not reported*
Detection limits: ~0.01 wt.% for all elements.

TABLE 2. Comparison of the localities and physical properties of gem enstatites from this study and those reported previously.

Locality	Color	Asterism	Inclusion features	Properties	Color-causing ions	References
Tanzania (probable locality)	Yellowish green	4 rays	Rutile needles, 57°–60°	RI α = 1.655–1.660 β = 1.661–1.665 γ = 1.668–1.669 SG = 3.22–3.25	Fe^{2+}, V^{3+}, Cr^{3+}	**This study**
Tanzania	Yellowish green	4 rays	Needles	RI = 1.660–1.669 SG = 3.25	V^{3+}	**Laurs et al. (2019)**
Kenya	Yellowish green	None (faceted)	—	RI=1.652–1.662 SG = 3.23	Fe^{2+}, Cr^{3+}	Schmetzer and Krupp (1982)
Tanzania	Brown	None (faceted)	Parallel needles	α = 1.662 β = 1.667 γ = 1.673 SG = 3.33–3.41	—	Koivula et al. (1988)
Sri Lanka	Brown	6 rays	Hollow channels, 57° and 61°	—	—	Henn and Bank (1991)
Sri Lanka	Brown	4 rays	Rutile or sillimanite	—	—	Gübelin and Koivula (2008)
India	Brown	6 rays	Possible rutile needles, 57° and 64°	—	—	Eppler (1967)
Norway	Brown	4 rays	Ilmenite, 64°	RI n_α = 1.685 n_β = 1.693 n_γ = 1.697 SG = 3.35	Fe^{2+}	Schmitz et al. (2016)
Madagascar	Brown	6 rays	Needles, 57° and 62°	—	Fe^{2+}	Cathelineau (2019)

2019). In addition, these iron absorption features were superimposed by absorption bands around 420–490 nm and 600–700 nm due to the presence of V^{3+} with trace Cr^{3+} (see table 1). These two bands cause the absorption of the violet-blue and orange-red ends of the visible spectrum. Such overlapping absorption features allow the transmission window in the green to the yellow region, giving rise to the bright yellowish green color (Laurs et al., 2019). The origin of the absorption band at ~2220 nm, however, could not be resolved.

Semi-quantitative EDXRF chemical analyses revealed enriched contents of silicon (58.1–59.2 wt.% SiO_2), magnesium (26.5–31.5 wt.% MgO), and aluminum (6.3–8.1 wt.% Al_2O_3), with trace amounts of iron, calcium, titanium, vanadium, chromium, manganese, and zinc (table 1). Furthermore, the end-member compositions were calculated and appeared close to the enstatite end members (92.0–96.2% enstatite, 3.5–7.5% ferrosilite, and 0.3–0.5% wollastonite) of the enstatite-ferrosilite series.

In summary, the attractive bright yellowish green colors of these enstatites are caused by the combination of significant iron and vanadium with a trace of chromium substituting magnesium in the crystal lattice. The four-rayed asterism phenomenon is caused by light reflection

Figure 68. The 271.76 ct topaz was very light blue and transparent under daylight (A). Directing the flashlight as reflected light on the dome caused an eight-rayed star effect. Because of the wide light zone, the ray extending along the stone was blurred when the light was directed at the dome (B) and became more defined as the stone was moved (C and D). Photos by Le Ngoc Nang.

from two sets of very dense fine rutile needle inclusions intersecting one another at approximately 57° to 60°. The similarity of these stones and those reported by Laurs et al. (2019) (tables 1 and 2) leads us to conclude these stones could also be from Tanzania.

Supparat Promwongnan, Visut Pisutha-Arnond, Wilawan Atichat, Thanong Leelawathanasuk, and Cheewaporn Suphanan
Gem and Jewelry Institute of Thailand (GIT), Bangkok

Scott Davies
American-Thai Trading, Bangkok

Star topaz from Vietnam. In addition to ruby, sapphire, spinel, tourmaline, garnet, and aquamarine, Vietnam is a source of topaz, discovered in many mining areas of several northern and Central Highlands provinces. These crystals are mainly colorless or very light to light blue. In 2020, we purchased a star topaz, reported to be from Lam Dong, Vietnam (figure 68). It was cut and sold by a gem setter in Ho Chi Minh City.

This transparent oval cabochon weighed 271.76 ct and measured 43.98 × 32.16 mm and 19.12 mm tall. Observed with the unaided eye under a spotlight, it had a visible eight-rayed star effect. Testing at Liu Gemological Research and Application Center revealed the following standard gemological properties: refractive index—1.620–1.627 (measured on the flat polished bottom); hydrostatic specific gravity—3.56; biaxial optic figure under the polariscope; inert to long- and short-wave UV radiation; very weak pleochroism (colorless to light blue); and two-phase inclusions and needle-like inclusions. These characteristics confirmed a natural topaz.

We directed a flashlight as reflected light on the top of the stone, keeping the background dark to accentuate the phenomenon. An eight-rayed asterism appeared, caused by a strong band of light that extended along the length of the stone. This band of light formed the two main arms of the star. Six sharper arms extended from the main band. These six arms were formed by three bands—one perpendicular to the main light band and the other two inclined to it. Depending on the stone's orientation, the arms of the inclined light bands were split into two parts or crossed the intersection of the main light band and the light band perpendicular to it. Each pair of inclined arms formed an angle of ~98° (i.e., the single light band was inclined at ~49° to the main light band). The length and width of the rays changed when we directed the light at different angles (figure 68). See video of this effect at www.gia.edu/gems-gemology/spring-2022-gemnews-star-topaz-from-Vietnam.

Under the microscope, we recorded white needle-like inclusions but could not identify them. They were oriented in four directions, and this was responsible for the eight-rayed star effect. These inclusions did not form long nee-

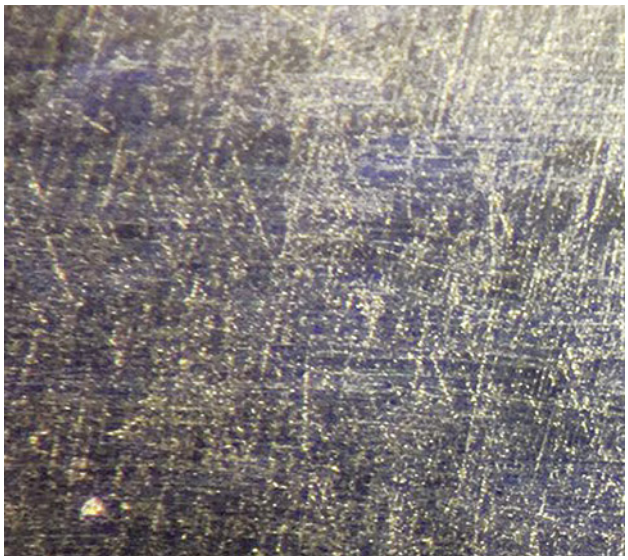

Figure 69. Needle-like inclusions arranged in four directions, viewed here from the top of the stone, created the asterism effect in the Vietnam topaz. Photomicrograph by Le Ngoc Nang.

dles but slightly elongated dashes that were unevenly distributed in the stone (figure 69). This uneven distribution of inclusions explains why some rays became blurred or vanished while others were continuous and sharp.

Topaz has been documented to have chatoyancy, four-rayed asterism (Spring 2007 GNI, p. 73; Summer 2008 GNI, pp. 182–183), and six-rayed asterism (M. Steinbach, *Asterism—Gems with a Star*, MPS Publishing and Media, Idar-Oberstein, Germany, 2016). However, there have been no reports of topaz with eight-rayed asterism. The orthorhombic system has four Bravais lattices: primitive, base-centered, body-centered, and face-centered. When the topaz crystal has a base-centered lattice, the needle-like inclusion will align to four directions on the (001) plane: two perpendicular directions of *a* and *b*, and two diagonal directions intersected at the center of the top and bottom faces of the lattice. These directions are perpendicular to the c-axis (figure 70). When the light reflects off these inclusions, an eight-rayed asterism will appear. A typical example of an orthorhombic mineral with an eight-rayed asterism was bronzite, introduced by Steinbach (2016). Nevertheless, this eight-rayed star topaz was a rare and intriguing case.

Le Ngoc Nang
Liu Gemological Research and Application Center and University of Science, Vietnam National University Ho Chi Minh City

Pham Minh Tien
Liu Gemological Research and Application Center Ho Chi Minh City

Figure 70. Bravais lattice with base-centered orthorhombic system (left). On the (001) plane, the needle-like inclusions aligned in four directions to form an eight-rayed asterism (right).

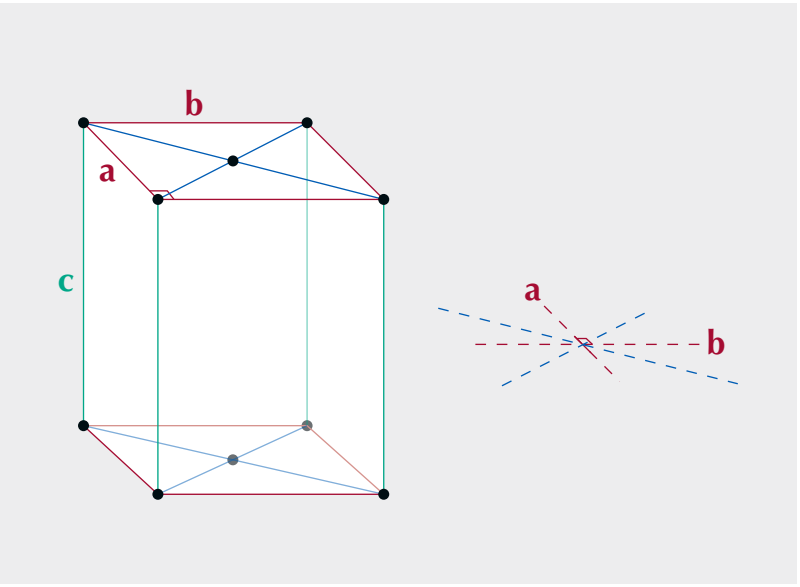

DIAMONDS

The discovery of davemaoite, the $CaSiO_3$ perovskite, in a diamond from Earth's lower mantle. Common silicate minerals such as olivine and garnet convert to other phases when brought to great depths in the planet, where they are subjected to extreme pressures. It has long been thought that two of the most common phases at depth in Earth have the perovskite structure. They have long been known from experimental studies in which they have been called magnesium silicate perovskite ($MgSiO_3$) and calcium silicate perovskite ($CaSiO_3$). Only recently has the magnesium silicate perovskite been found in nature, in a meteorite, where it was characterized and named bridgmanite (O. Tschauner et al., "Discovery of bridgmanite, the most abundant mineral in Earth, in a shocked meteorite," *Science*, Vol. 346, 2014, pp. 1100–1102). More recently, the calcium silicate perovskite has been found in a diamond and sufficiently characterized to be given a mineral species name (O. Tschauner et al., "Discovery of davemaoite, $CaSiO_3$-perovskite, as a mineral from the lower mantle," *Science*, Vol. 374, 2021, pp. 891–894).

Diamonds are one of the few minerals that bring us samples of the minerals found in the deep earth. Diamonds serve as chemically inert and nearly volume-conserving hosts for these minerals, thereby allowing them to retain

Figure 71. A typical coated diamond from Orapa. This is not the stone studied, but rather one from the same batch and locality with approximately the same color and size. Photo by George Rossman.

Figure 72. The polished slab of the diamond containing davemaoite showing the round spots where the grains were excavated for LA-ICP-MS analysis. Photo by Aaron Celestian.

their composition and in some cases even their original structure. The examination of the inclusions in an 81 mg (~0.405 ct) octahedral diamond from Orapa, Botswana, has resulted in the discovery of the high-pressure form of $CaSiO_3$ in the perovskite structure occurring as a natural mineral in the diamond (figure 71). This phase has been approved by the International Mineralogical Association with the name davemaoite, named in honor of Dave (Hokwang) Mao, for his contributions to understanding the deep-mantle geophysics and petrology of our planet.

Experimental studies in the laboratory have indicated that $CaSiO_3$ assumes the perovskite structure at depths between 420 and ~2700 km. This phase, first synthesized in 1975 (L. Liu and T. Ringwood, "Synthesis of a perovskite-type polymorph of $CaSiO_3$," *Earth and Planetary Science Letters*, Vol. 28, 1975, pp. 209–211), is only thermodynamically stable at pressures greater than 200,000 atmospheres (20 GPa). Furthermore, the rate of back-conversion to low-pressure polymorphs is rapid if the pressure is lowered. Consequently, the natural mineral is unlikely to survive transport from the deep earth to the surface.

Davemaoite was first identified and characterized within a diamond studied at the Advanced Photon Source at Argonne National Laboratory in Illinois, where an X-ray beam was focused to a 0.5 × 0.5 µm spot. Calcium-rich inclusions in the diamond were first located. Two inclusions, 4 × 6 µm and 4 × 16 µm in size, were examined with X-ray diffraction. They both produced a perovskite pattern. Their identity was further confirmed by infrared spectroscopy. Theoretically, a cubic perovskite has no Raman pattern, and none was obtained from these inclusions. The inclusions were next excavated from the surrounding diamond and analyzed with laser ablation–inductively coupled plasma–mass spectrometry (LA-ICP-MS) (figure 72). Their composition corresponded to the calcium silicate perovskite.

Davemaoite is significant in Earth's deep mantle because it acts as a host to many elements that are incompatible with upper-mantle minerals, fulfilling a role that garnet plays in the upper mantle. Davemaoite may be the most geochemically important phase in the lower mantle because it will act as a repository in which the radioactive, heat-generating elements thorium and uranium become concen-

trated. Calculations suggested that davemaoite was entrapped in the host diamond at pressures of at least 290,000 atmospheres and temperatures of at least 1400 K. These diamonds from Orapa are also noteworthy because in addition to davemaoite, a high-pressure form of ice was found as a solid inclusion within them where the diamond's internal pressure was great enough to maintain the ice in the solid form, allowing it to be characterized as the new mineral species ice-VII (O. Tschauner et al., "Ice-VII inclusions in diamonds: Evidence for aqueous fluid in Earth's deep mantle," *Science*, Vol. 359, 2018, No. 6380, pp. 1136–1139).

George R. Rossman
Division of Geological and Planetary Sciences
California Institute of Technology

Oliver Tschauner
Department of Geoscience
University of Nevada, Las Vegas

Natural near-colorless type IIb diamond. While colorless to near-colorless HPHT laboratory-grown diamonds usually contain detectable boron impurities (classified as type IIb; see S. Eaton-Magaña et al., "Observations on HPHT-grown synthetic diamonds: A review," Fall 2017 *G&G*, pp. 262–284), it is uncommon to encounter a boron-bearing diamond of natural origin due to its rarity (0.02% of natural gem diamonds; E.M. Smith et al., "Blue boron-bearing diamonds from Earth's lower mantle," *Nature*, Vol. 560, No. 7716, 2018, pp. 84–87). The boron concentrations in natural diamonds are generally low (typically <1 ppm), but boron is such an efficient coloring agent that it imparts a blue color to most type IIb diamonds. However, exceptions still exist. For example, when boron absorption is accompanied by absorptions from plastic deformation, the combined effects may give rise to other colors (e.g., yellowish green; Spring 2012 Lab Notes, pp. 47–48; see also Summer 2009 Lab Notes, p. 136). Occasionally, some type IIb diamonds are near-colorless because their boron concentrations are too low to cause a blue color (e.g., E. Fritsch and K. Scarratt, "Natural-color nonconductive gray-to-blue diamonds," Spring 1992 *G&G*, pp. 35–42), but they are far from common. Therefore, any near-colorless type IIb diamond submitted to a gem laboratory should be given particular attention to determine its possible lab-grown origin.

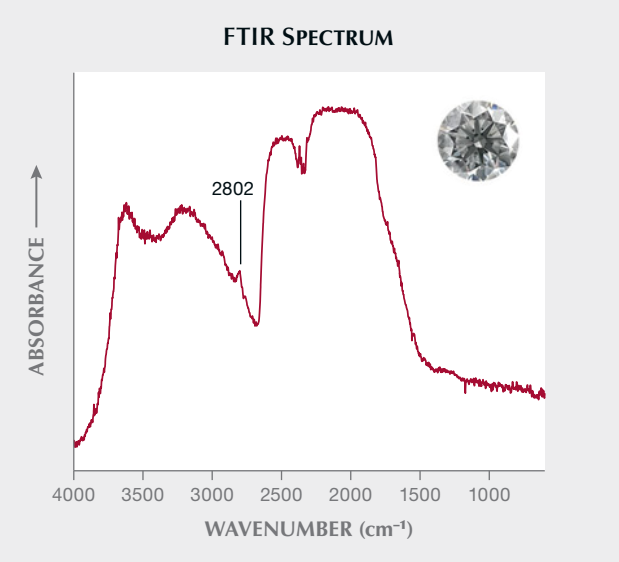

Figure 73. FTIR spectrum of the sample showing a band (2802 cm^{-1}) characteristic of type IIb diamond.

Recently, we had the opportunity to examine such an example. This 0.24 ct round brilliant cut had an I color grade due to its grayish component, usually seen in natural type IIb diamond. Fourier-transform infrared (FTIR) absorption spectroscopy detected a weak band at 2802 cm^{-1} (figure 73), characteristic of uncompensated boron, and identified the sample as type IIb. The diamond was inert to both long- and short-wave ultraviolet radiation. When observed with the DiamondView, it exhibited blue fluorescence and moderate blue-green phosphorescence (figure 74). The dislocation net-

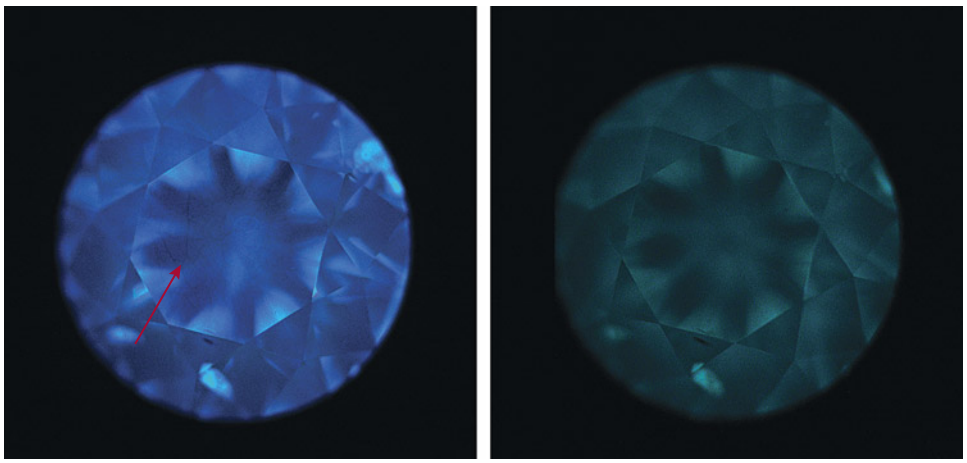

Figure 74. DiamondView imaging of the 0.24 ct diamond revealed blue fluorescence (left) and moderate blue-green phosphorescence (right). Subtle dislocation networks on the table (red arrow) that resulted from plastic deformation, typically observed in type IIa and IIb diamond, are consistent with a sublithospheric origin. Images by Wenqing Huang.

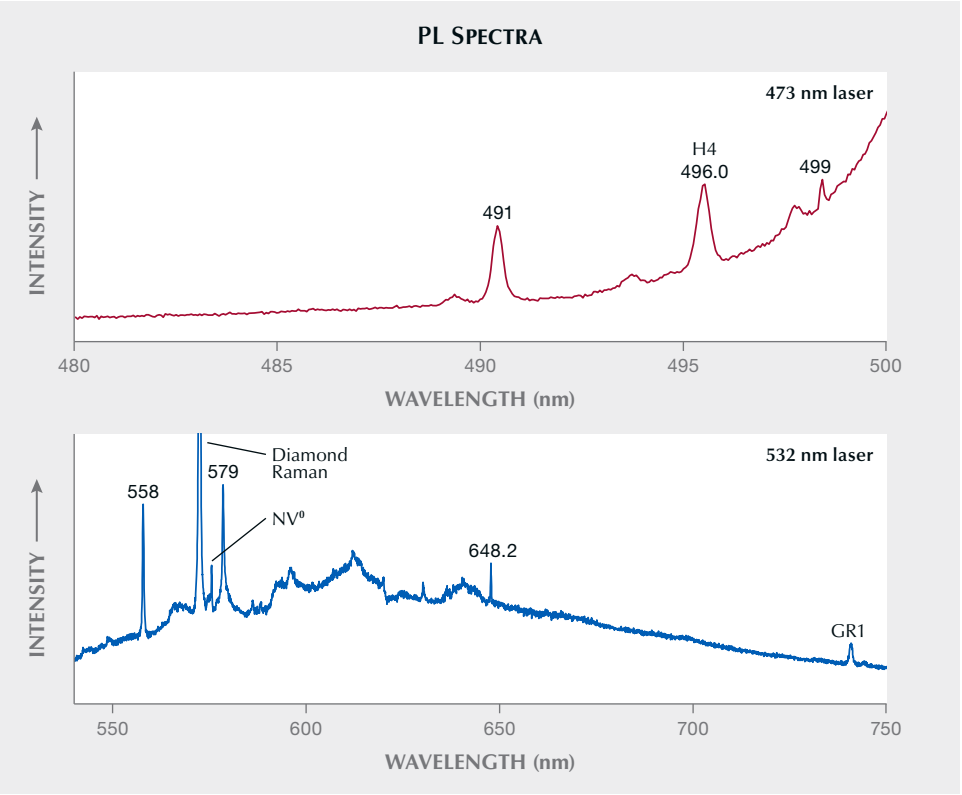

Figure 75. Photoluminescence spectra from the type IIb diamond under 473 nm and 532 nm laser excitations. Nitrogen-related defects such as H4 (top) and NV^0 (bottom) were observed, along with GR1 (bottom).

works observed on the table (figure 74, left), typically seen in some natural type IIa and IIb diamonds but not previously described for lab-grown diamonds, suggest a natural origin. Further evidence of natural origin came from photoluminescence (PL) spectroscopy and inclusion analysis.

Multiple laser excitations (473, 532, and 633 nm) were used to characterize its photoluminescence features at liquid nitrogen temperatures. The PL spectrum measured with a 473 nm excitation revealed the presence of nitrogen-related defect H4 (496.0 nm) (figure 75, top). PL spectroscopy using a 532 nm laser (figure 75, bottom) revealed the occurrence of GR1, NV^0, and a sharp peak at 648.2 nm that is probably related to interstitial boron, all of which have been documented previously in type IIb diamonds (S. Eaton-Magaña et al., "Natural-color blue, gray, and violet diamonds: Allure of the deep," Summer 2018 *G&G*, pp. 112–131). Nickel defect-related peaks (883/884 nm), a common feature in HPHT laboratory-grown diamonds of various colors, were not detected with any of these excitations.

Magnification indicated several solid inclusions (figure 76), mostly in the crown, that resulted in its SI_1 clarity grade. The inclusion scenes were consistent with those described in natural type IIb blue diamonds (Smith et al., 2018). Namely, they tended to show a tiny satellite-like appearance composed of the main inclusion and accompanying decompression cracks. Raman spectra using a 532 nm laser revealed that two of these inclusions were coesite (figure 77). This feature confirmed the diamond's natural origin. Coesite is a relatively common inclusion in lithospheric diamonds that formed at depths of ~150–200

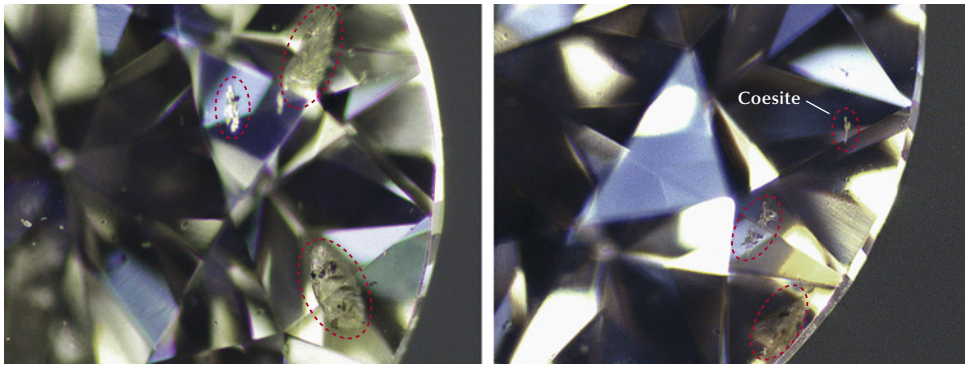

Figure 76. Inclusions (outlined in red circles) observed in the type IIb diamond tended to show a satellite-like appearance. Fields of view are 2.5 mm (left) and 2 mm (right), respectively. Photomicrographs by Wenqing Huang.

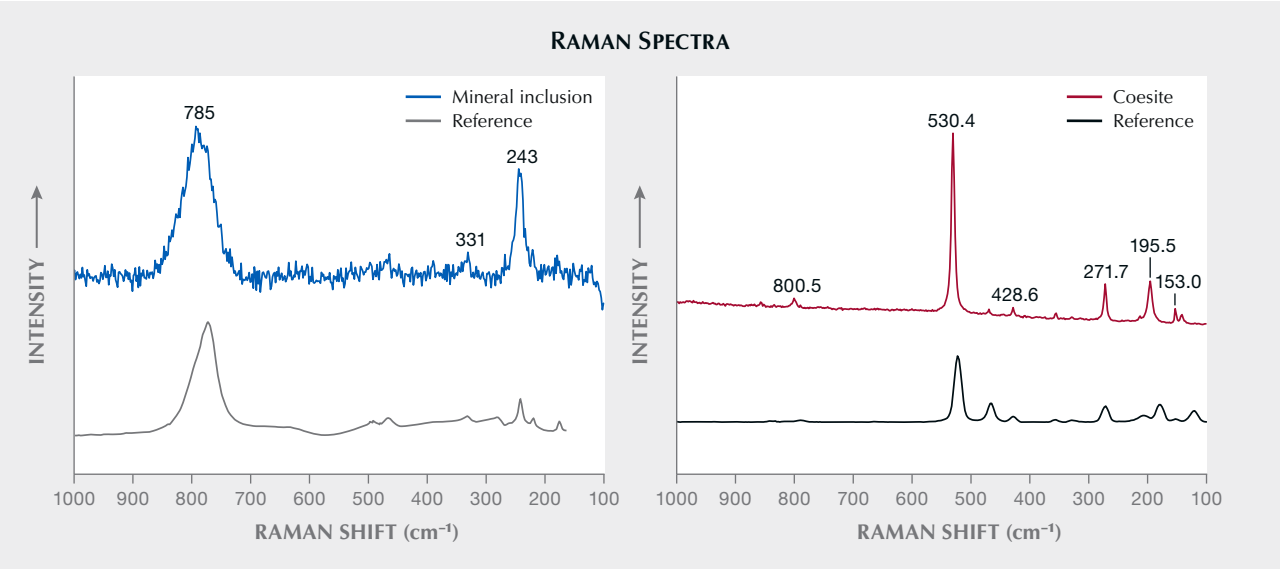

Figure 77. Raman spectra of mineral inclusions in the type IIb diamond. Left: Baseline-corrected Raman spectra of a mineral inclusion (blue line) match the $CaTiO_3$ perovskite reference spectrum (light gray line) from Nestola et al. (2018). The included mineral could be perovskite or $CaSiO_3$ perovskite, since their Raman spectra are almost indistinguishable. Right: Baseline-uncorrected Raman spectrum of a coesite inclusion inverted from the presumed stishovite, showing main bands at approximately 530, 272, and 195 cm^{-1}. Reference spectrum is from RRUFF-X050094.

km. However, recent studies show that type IIb diamonds have a sublithospheric origin and are formed in the upper part of the lower mantle (Smith et al., 2018). For type IIb diamond formed at such depths, the coesite inclusion has not been considered to be in its original pristine form, but rather the back-transformation product from stishovite. Another inclusion showed bands matching roughly with perovskite ($CaTiO_3$) (figure 77), but its precise mineralogy was difficult to determine. This is because the Raman spectra of perovskite and $CaSiO_3$ perovskite, both of which have been described in sublithospheric diamonds, are very similar (F. Nestola et al., "$CaSiO_3$ perovskite in diamond indicates the recycling of oceanic crust into the lower mantle," *Nature*, Vol. 555, No. 7695, 2018, pp. 237–241). No matter what exact mineral this inclusion corresponds to, its occurrence implies a sublithospheric origin for the host diamond. Other mineral inclusions could not be identified, probably because of their depth within the diamond.

Due to the scarcity of natural type IIb diamonds, any near-colorless diamond that contains boron detectable by FTIR spectroscopy should be given close attention to determine its origin. The near-colorless type IIb diamond examined here, though rarely encountered, was identified as natural on the basis of its gemological and spectroscopic characteristics.

Ting Shui
China Geological Survey, Nanjing
Wenqing Huang
National Center of Inspection and Testing on Quality of Gold and Silver Products
Nanjing Institute of Product Quality Inspection

SYNTHETICS AND SIMULANTS

Barite-calcite composite as imitation "Wulanhua" turquoise from Hubei Province, China. "Wulanhua" turquoise is well known in the Taiwan and mainland China market. It has also been called "Ulan flower" turquoise in previous publications (L. Liu et al., "Unique raindrop pattern of turquoise from Hubei, China," Fall

Figure 78. The bracelet submitted as "Wulanhua" turquoise. Photo by Shu-Hong Lin.

2020 *G&G*, pp. 380–400). The term "Wulanhua" is a Chinese transliteration that means black orchid, and it usually refers to turquoise of medium dark to very dark blue color with a black spiderweb pattern found in Hubei Province.

A bracelet recently submitted to Taiwan Union Lab of Gem Research (TULAB) as Wulanhua turquoise (figure 78) contained dark blue opaque beads with a black spiderweb pattern on the surface. The spot refractive index of these beads was about 1.62–1.63, close to that of turquoise. EDXRF analysis determined that the composition of the beads was inconsistent with that of turquoise ($CuAl_6(PO_4)_4(OH)_8 \cdot 4H_2O$). Instead, it was composed mainly of barium (Ba) and calcium (Ca).

To further identify the composition, Raman spectra (785 nm laser) were analyzed and compared with those from the RRUFF database. The beads displayed mixed spectra of barite, calcite, and other unknown materials. With the consent of the client, a bead was cut into two halves and polished for more testing. One half was immersed in 95% ethanol for 72 hours to extract the dark blue dye (figure 79). After the ethanol volatilized, the blue precipitate was analyzed with Raman spectroscopy and the spectrum was compared with that of the bead and the spectra from the RRUFF database. Raman analysis and the extraction experiment revealed that this material was composed of barite and calcite with an unidentified blue dye (figure 80). Microscopic observation of the cross section suggested that the beads were made of irregularly shaped barite and barite with minor calcite particles with an unknown black filling as a bonding material (figure 81).

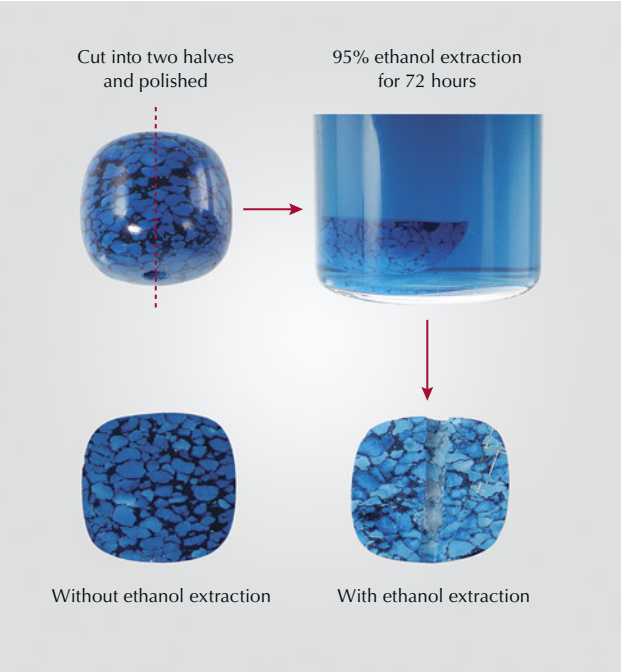

Figure 79. A bead from the bracelet was cut into two halves. One half was immersed in 95% ethanol for 72 hours, clearly extracting the blue dye. Photos by Yu-Ho Li.

The beads could be defined as a composite material made of barite ($BaSO_4$), calcite ($CaCO_3$), and blue dye.

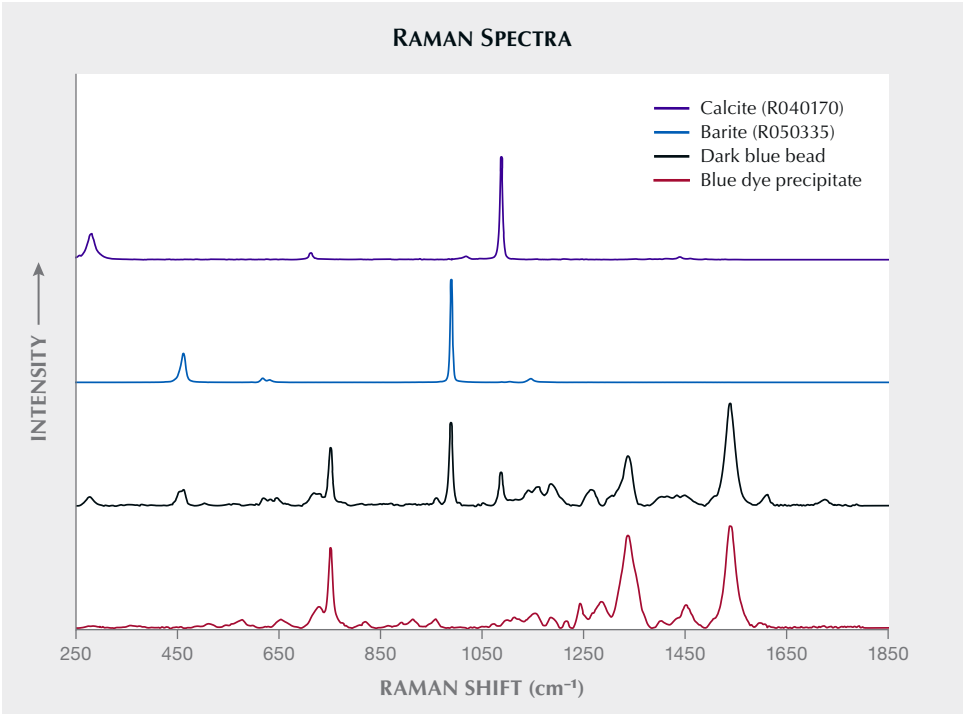

Figure 80. Raman spectra comparisons between the bead, the blue dye precipitate, and those of barite and calcite from the RRUFF database suggest that the bead consisted of barite, calcite, and blue dye. The stacked spectra are baseline-corrected and normalized.

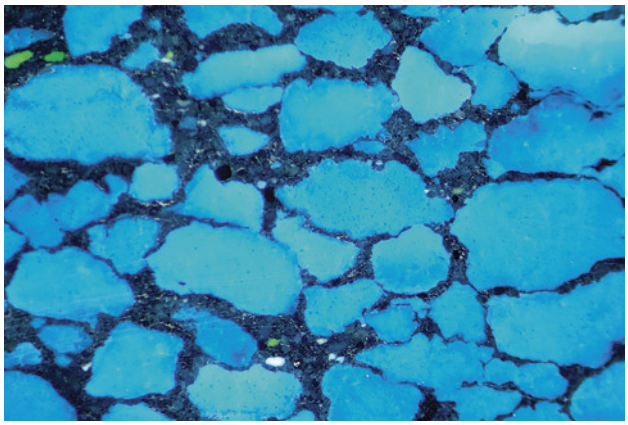

Figure 81. The cross section of one bead showed irregularly shaped barite and barite with minor calcite particles, along with a black filling that could be some unknown bonding material. Photomicrograph by Shu-Hong Lin; field of view 8.56 mm.

While visual observation and refractive index might not be enough to distinguish these beads from true Wulanhua turquoise, Raman spectroscopy and EDXRF analysis were able to reveal their true identity.

Shu-Hong Lin
Institute of Earth Sciences,
National Taiwan Ocean University
Taiwan Union Lab of Gem Research, Taipei

Yu-Ho Li
Institute of Earth Sciences,
National Taiwan Ocean University

Huei-Fen Chen
Institute of Earth Sciences,
National Taiwan Ocean University
Center of Excellence for Oceans,
National Taiwan Ocean University, Keelung

TREATMENTS

Amber filled with epoxy resin. Amber prayer beads are very popular in the Gulf countries. Due to this high demand, the Dubai Central Laboratory receives many of them for identification. Recently we noticed that a majority of the amber rosary samples received for identification contain an epoxy resin filling. These fillings are seen in cavities of different sizes but sometimes show up in tiny veins.

The fillings are not always easy to detect without magnification because of the nearly identical luster of both amber and epoxy, but sometimes they are obvious, as shown in figure 82. Occasionally gas bubbles can be observed in epoxy fillings by microscope. Fillings may show a mixed reaction under both long-wave and short-wave UV radiation, and the fluorescence is more intense in long-wave UV. Filled beads can be inert under UV or show weak to strong white or blue fluorescence (figure 83).

Figure 82. Epoxy resin is easily detected in the amber of this rosary. Photo by Nazar Ahmed Ambalathveettil.

To identify the fillings, we observed the rosary under the microscope, marked the suspected areas or spots, and analyzed them by Raman spectroscopy to confirm the presence of fillings. The spectra were compared with those of amber and epoxy reported previously in *G&G* (figure 84;

Figure 83. When exposed to long-wave UV radiation, the epoxy resin displayed weak to moderate white fluorescence. Photo by Nazar Ahmed Ambalathveettil.

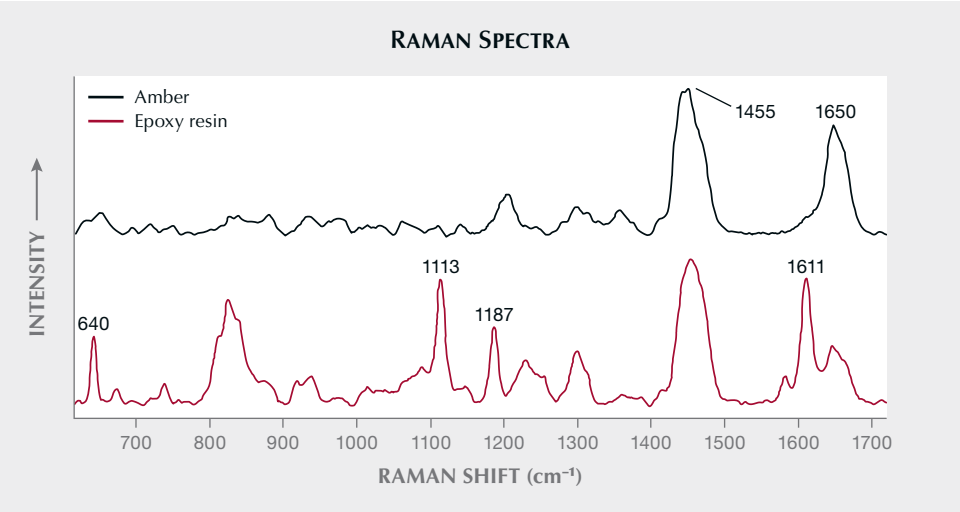

Figure 84. The Raman spectra of the bead and the cavity filling shown here matched with spectra previously reported in G&G *for amber and epoxy resin.*

see Fall 2013 GNI, pp. 181; Summer 2021 GNI, pp. 179–180). Nowadays, having an amber rosary tested by a gemstone laboratory before buying can avoid a costly mistake.

Nazar Ahmed Ambalathveettil (nanezar@dm.gov.ae), Nahla Yaqub Al Muhari, and Sameera Mohammed Ali
Gemstone Unit, Dubai Central Laboratory

Characteristics of amber with irradiation treatment. The organic gem amber is particularly popular in China, Europe, the Middle East, and South Asia. With strong demand for rarer colors, some enterprises use electron accelerator–charged particles or ^{60}Co gamma-ray radiation to irradiate amber and enhance its color from light yellow to orange-yellow and orange-red.

As early as 2012, foreign suppliers tried to introduce irradiation-treated amber into the Chinese market. Due to the booming demand for natural golden and beeswax amber in the Chinese market, amber manufacturers had little interest in the irradiated products. After the market cooled in late 2015, irradiated amber emerged as a new variety (figure 85). Some irradiated amber (containing microstructure defects in the original material before treatment) was accompanied by dendritic inclusions with

Figure 85. A: Rough amber material after irradiation treatment. B: Irradiated amber products with dendritic inclusions. C: Irradiated amber pendants without root-like inclusions and irradiated amber with a red-white alternating pattern (far right). D: The current irradiated amber products have much more natural color. Photos by Yamei Wang.

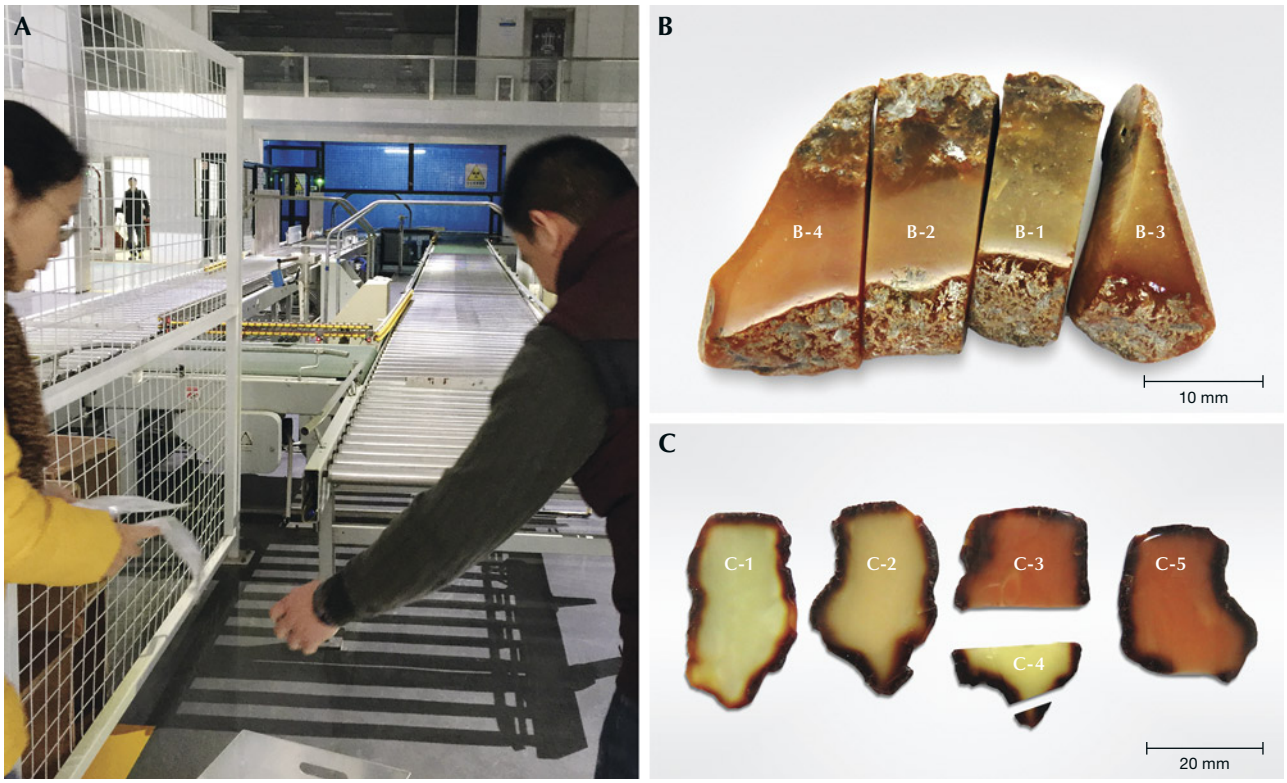

Figure 86. A: The irradiation treatment of amber via an IBA Rhodotron TT200 accelerator. B: The color improvement of sample 1 at different irradiation doses: before irradiation (B-1) and after irradiation doses of 10 kGy (B-2), 150 kGy (B-3), and 200 kGy (B-4). C: Color enhancement and annealing of sample 2 with different irradiation doses: before irradiation (C-1) and after irradiation doses of 10 kGy (C-2), 170 kGy (C-3), and 200 kGy (C-5). C-4 shows discoloration after heat treatment (10 minutes, 100°C) after cutting. Photos by Yamei Wang.

color enhancement or change (figure 85B). The amber materials used for irradiation treatment were selected from Baltic amber. After irradiation, the red color was usually internally uniform when the weathered skin was polished. Due to differences in original bodycolor and flow pattern, the irradiated amber with the superimposed red color can be red, orange-red, orange-yellow, or yellow-brown, or have a red-white alternating pattern (figure 85C, far right). Early irradiated amber from the end of 2015 was easy to identify due to the presence of dendritic inclusions. Recently, the generation of dendritic inclusions has been suppressed and the quality of the samples has improved (figure 85C). The dendritic inclusions are basically inhibited, and the irradiated amber will not produce them as long as there are no cracks or defects on the surface that can be broken down by the irradiation source. Moreover, the enhanced color via irradiation treatment is much more natural (figure 85D).

The authors selected 13 Baltic rough amber samples for irradiation treatment via an IBA Rhodotron TT200 electron accelerator to investigate the effects of different irradiation doses on the color enhancement of amber (figure 86A), considering that the utilization of high-energy gamma-ray could change its color into red, possibly accompanied by the introduction of dendritic inclusions.

Since the irradiated amber on the market consists of Baltic amber, 12 of the 13 sample groups were Baltic amber (including transparent, translucent, and opaque yellow polished double-sided wafers and round beads), and one group was Burmese amber. The irradiation dose ranged from 10 to 200 kGy (1 kGy = 1000 J/kg), accumulated multiple times, and the samples began to display a red color at 150 kGy. When the irradiation dose reached 200 kGy, the samples turned obvious red, and the irradiation effect showed most clearly. The color changes of representative samples (1 and 2) under different radiation doses were selected; only sample 1 with surface cracks produced dendritic inclusions. When the irradiation dose exceeded 200 kGy, the samples turned varying degrees of red (figure 86B); sample 2 most clearly showed the effect (figure 86C).

The dendritic inclusions are triggered by microstructure defects (physically weak points) and extend like microfractures (figure 87). The roots usually start from the micro defects of amber and form a structural deterioration zone with microcracks. Under the high-energy electron beam,

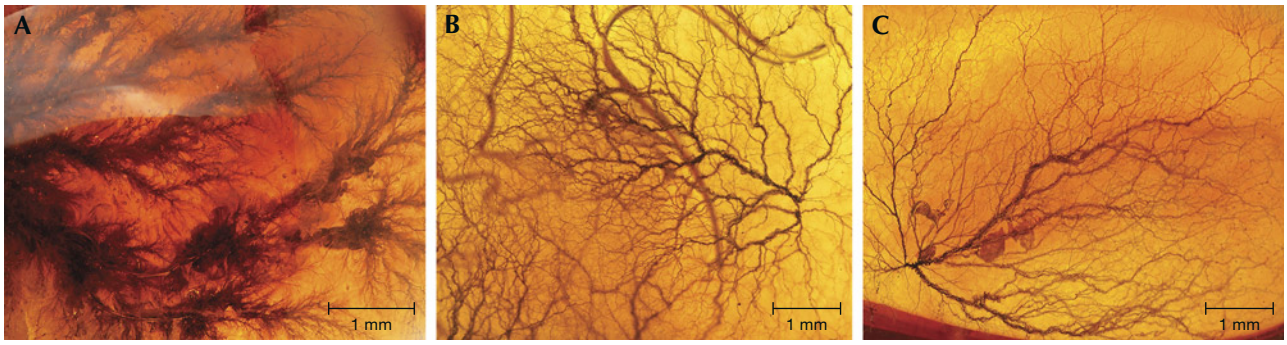

Figure 87. Various appearances of the dendritic inclusions. Photomicrographs by Yamei Wang.

the microcracks in the degradation zone expand rapidly and connect to form a submicroscopic "tree." The continuous development of the submicroscopic tree forms the root-like whisker region with a macro fractal structure. The growth of dendrites can be regarded as a random growth process of fractal clusters composed of discontinuous microcracks.

If the irradiated amber undergoes heat treatment at 100ºC for 10 minutes in an oven, its original color will be restored (figure 88A and figure 85, C-4); the treated color can also fade and return to its original yellow after heating in a pressure furnace. But once the dendritic inclusion is formed, it is irreversible (figure 88B). After about a year in a natural environment, the induced color from irradiation will automatically fade (figure 88C). Along with a significant reduction in brightness, the color will no longer be uniform (figure 88D) and color spots will appear (figure

Figure 88. Discoloration of irradiated amber. A: Two irradiated round beads cut into halves (top). Bottom left: the half bead heated in an oven at 90°C for 10 minutes fades to yellow; on the bottom right, the internal color is uniform after irradiation. B: Heating the bead in the pressure furnace restores the original color but does not heal the root pattern. C: The irradiated color gradually fades after natural storage for 12 months. D: The color of irradiated amber becomes uneven after natural fading. E: Red spots appear at weak points of the dendrites. F: Red dots remain at the site of irradiation. Photos by Yamei Wang.

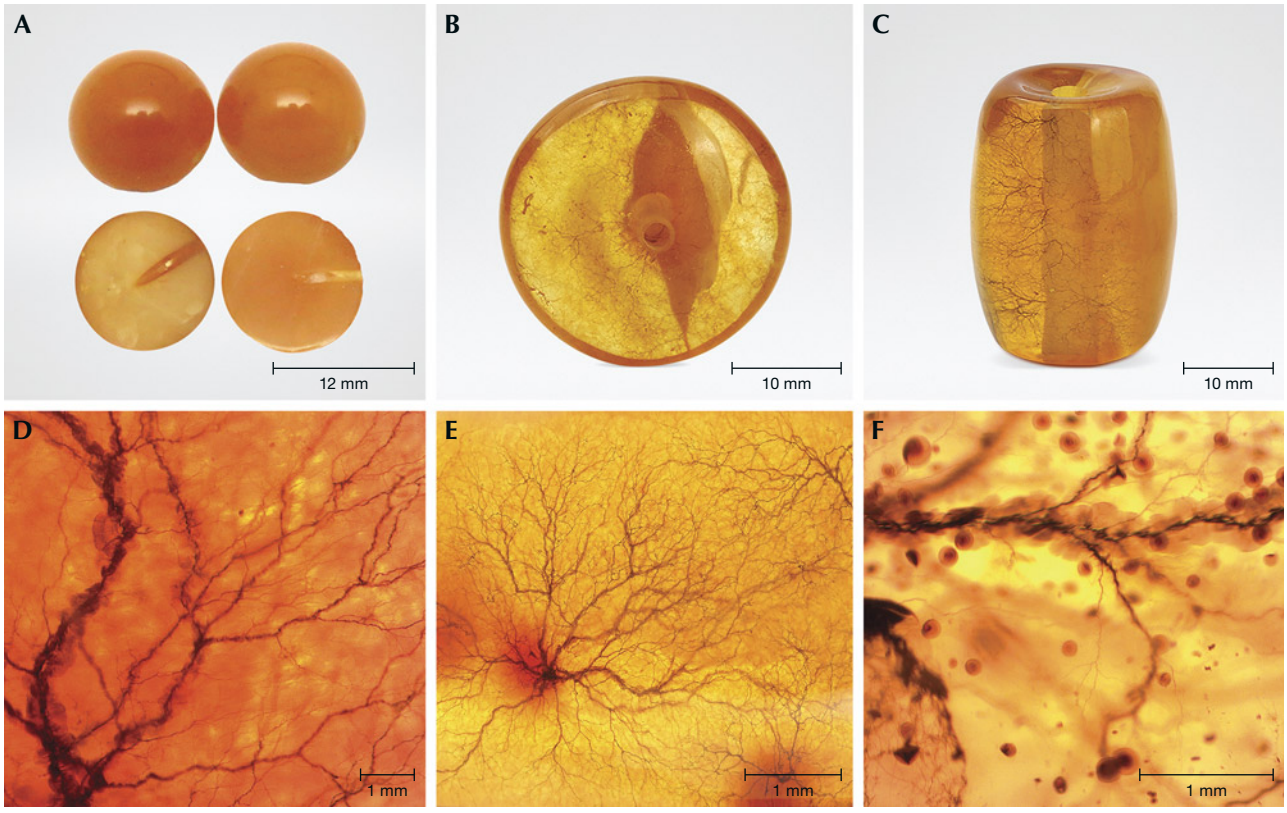

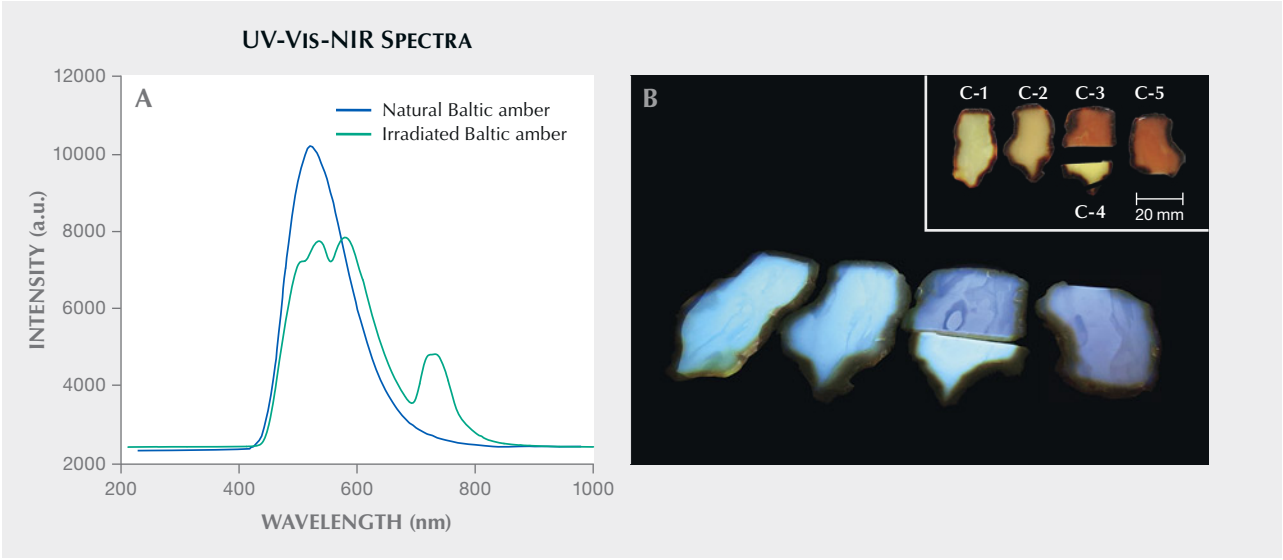

Figure 89. A: The UV-Vis-NIR spectra of natural and irradiated Baltic amber. B: The fluorescence characteristics of irradiated amber under a 365 nm UV lamp. Sample C-2 with a small irradiation dose of 10 kGy; sample C-4 shows discoloration after heat treatment at 100°C for 10 minutes. Photo by Yamei Wang.

88E). Even the original irradiation points are clearly displayed as color spots after fading (figure 88F), indicating that the irradiated color is not stable.

Some irradiated ambers with bright color and high transparency that lack the dendritic inclusions can be distinguished using a conventional 365 nm ultraviolet lamp, but the treatment of lighter-colored amber is not as easy to distinguish. The non-irradiated natural Baltic amber showed a strong absorption peak at 521 nm. The irradiated Baltic amber (orange-red) showed three characteristic peaks at 535, 578, and 728 nm (figure 89A). Dendritic inclusions are common in the earlier versions of irradiated amber. In addition, as the irradiation dose increases, the fluorescence intensity of the amber weakens. Under the 365 nm UV lamp, irradiated amber (samples C-3 and C-5 with irradiation doses higher than 150 kGy) has weaker fluorescence intensity than natural amber. Furthermore, the weaker florescence is superimposed on the darker bodycolor of orange-red (C-3, C-5). The fluorescence of amber with heat treatment (C-4) is the same as that of unirradiated natural sample (C-1).

Yan Li, Yamei Wang, and Quanli Chen
Gemological Institute, China University of Geosciences Wuhan

ANNOUNCEMENTS

18th Annual Sinkankas Symposium. The 2022 Sinkankas Symposium, an annual event featuring presentations by specialists in gem-related disciplines, will follow a virtual format once again this year with pre-recorded sessions available on-demand. Sponsored by the Gemological Society of San Diego, the Geo-Literary Society, and GIA, the symposium will include 10 pre-recorded 30-minute presentations available to view from April 25 through June 6, highlighting alexandrite and other color-change gemstones (figure 90).

Speakers will include Evan Caplan, William Larson, Cigdem Lüle, Sally Eaton-Magaña, Niveet Nagpal, Nathan Renfro, Stuart Robertson, Aaron Palke, George Rossman, Wim Vertriest, and Robert Weldon. The presentations will cover a variety of topics regarding alexandrite and other color-change gemstones, from characteristics and sources to market trends and photography.

Registration closes June 1. The registration cost of $25 includes a PDF of the symposium volume, available June 23. Visit https://sinkankassymposium.net for more details.

Figure 90. A 32.35 mm alexandrite twinned crystal and a 2.61 ct faceted alexandrite, both from Russia, shown in daylight (left) and incandescent light (right). Photos by Robert Weldon; courtesy of William Larson.